Modelling the atmospheric chemistry of volcanic plumes

A thesis submitted to the School of Environmental Sciences
of the University of East Anglia in partial fulfilment
of the requirements for the degree of Doctor of Philosophy

Luke Surl

June 2016

Abstract

Volcanoes are the principal way by which volatiles are transferred from the solid Earth to the atmosphere-hydrosphere system. Once released into the atmosphere, volcanic emissions rapidly undergo a complex series of chemical reactions. This thesis seeks to further the understanding of such processes by both observation and numerical modelling.

I have adapted WRF-Chem to model passive degassing from Mount Etna, the chemistry of its plume, and its influence on the wider atmosphere. This investigation considers model plumes from the point of emission up to a day's travel from the vent and is able to reproduce observed phenomena of BrO formation and O_3 depletion within volcanic plumes.

The model plume influences several atmospheric chemistry systems, including reactive nitrogen and organic chemistry. Plume chemistry is driven by sunlight, and I examine how the modelled phenomena identified in this investigation vary with the diurnal cycle.

In the modelled plume all of the bromine is involved in O_3-destructive cycling. When HBr is exhausted, volcanic HCl sustains the cycling. The rate-limiting factor of this cycling, and therefore the rate of O_3 destruction, is sunlight.

I find qualitative differences between the chemistry of low and high intensity plumes, with the bromine chemistry in the latter case being limited by O_3 depletion.

This modelling investigation is complemented by an observational study of O_3 in a young Etnean plume from which I estimate the rate of in-plume O_3 destruction within seconds to minutes after emission.

These investigations demonstrate that volcanic plumes can be included in complex, 3D atmospheric chemistry models, and that the output from these can be used to observe and quantify influences of volcanic plumes on the wider atmosphere.

Acronyms and chemical symbols

ASL	Above sea level
KPP	The Kinetic Pre-Processor
mASL	Metres above sea level
PBL	Planetary Boundary Layer
ppm	parts per million (by volume)
ppb	parts per billion (by volume)
ppt	parts per trillion (by volume)
NWP	Numerical Weather Prediction
WRF	Weather Research and Forecasting model

SO_2	sulfur dioxide
H_2SO_4	sulfuric acid
HNO_3	nitric acid
NO	nitric oxide
NO_2	nitrogen dioxide
NO_3	nitrate radical
N_2O_5	nitrogen pentoxide
HONO	nitrous acid
O_3	ozone
O^1D	oxygen atom singlet D (higher energy state)
O^3P	oxygen atom triplet P (lower energy state)
OH	hydroxyl radical
HO_2	hydroperoxyl radical
H_2O_2	hydrogen peroxide
Br	bromine atom
Br_2	bromine molecule
BrO	bromine oxide
HBr	hydrogen bromide
HOBr	hypobromous acid
$BrNO_2$	bromine nitrite
$BrNO_3$	bromine nitrate
BRCl	bromine monochloride
HCl	hydrochloric acid
Cl	chlorine atom
ClO	chlorine monoxide
OClO	chlorine dioxide
Cl_2	chlorine dimer
$ClNO_2$	nitryl chloride
$ClNO_3$	chlorine nitrate
HOCl	hypochlorous acid
CH_4	methane
CO	carbon monoxide
C_2H_6	ethane
CH_3O_2	methylperoxy radical
HCHO	formaldehyde
CH_3OOH	methyl hydrogen peroxide

Dedication

This thesis is dedicated to the memory of Professor Roland von Glasow, who died after a sudden illness on 6 September 2015.

I have been incredibly fortunate to have had Roland as a supervisor for this PhD. A brilliant and dedicated scientist, Roland's advice and guidance was always intelligent and insightful, and always delivered with kindness and understanding. Over the last four years, on too many times to count, I have knocked on Roland's door and he would stop what he was doing and help me sort out my latest misunderstanding or bug in the code. As with everything he did, Roland approached this role with imagination, enthusiasm, and humour.

Both academically and pastorally, Roland was the model of a PhD supervisor. Quite literally, this thesis would not have existed without his vision and drive. With Roland's death, we have lost a brilliant colleague, a dedicated and caring mentor, and a dear friend.

The research in this thesis was carried out on the High Performance Computing Cluster supported by the Research and Specialist Computing Support service at the University of East Anglia.

Contents

List of figures

List of tables

Chapter 1

Introduction

Volcanic plumes present a unique challenge to atmospheric chemists, venting concentrated and potent cocktails of gases and aerosol into the atmosphere. Due to their hostility and remoteness, the chemistry of volcanoes' plumes are hard to study directly, and the uniqueness of plumes' chemical environments renders most models used to investigate atmospheric chemistry inadequate, at least without substantial modification.

In this document I describe and present results from an investigation into the atmospheric chemistry of volcanic plumes, using Mount Etna as my primary case study. This documents presents both an analysis of observations made at Mount Etna and analysis of model simulations of its plume.

In this Chapter I introduce the science upon which the research in the later chapters of this thesis is based. This begins with an overview of relevant atmospheric chemistry (Section 1.1), and then details the current understanding of volcanic emissions (Section 1.2) and the chemistry which occurs within plumes (Section 1.3). In Section 1.4 I discuss the literature concerning atmospheric chemistry modelling.

I also delineate the scope of this investigation and describe how it has been divided into chapters within this document; this is done in Section 1.5.

1.1 Overview of atmospheric chemistry

1.1.1 Basic atmospheric physics

It is necessary here to introduce some elements of atmospheric physics prior to discussing the chemistry of the atmosphere.

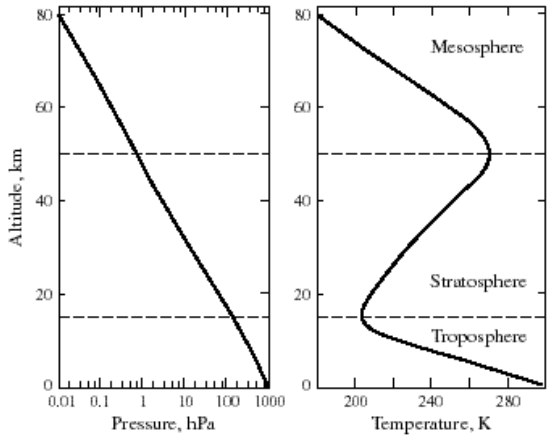

Figure 1.1: Pressure and temperature profiles of the atmosphere. From Jacob (1999).

Atmospheric scientists divide the atmosphere into distinct levels, as show in Figure 1.1. The lower two layers, the troposphere and the stratosphere contain 99.9% of the atmosphere's mass (Jacob, 1999). While atmospheric pressure's relationship with altitude is relatively simple, the temperature-altitude relationship is more complex.

The heat source in the troposphere is, predominantly, the ground, which adsorbs solar radiation and transfers heat to the air. This air cools as it rises and expands (adiabatic cooling), leading to a decrease in temperature with altitude. However in the stratosphere, gases are heated by adsorbing solar radiation at certain wavelengths. The lower levels of the stratosphere receive less of this radiation, and thus are cooler. These two phenomena give rise to a temperature minimum, the tropopause, which divides these two layers. The height of the tropopause varies with time and location within a range of roughly 8–18 km. Different chemical systems dominate the troposphere and stratosphere. This investigation only concerns air in the troposphere.

Specifically, this investigation is concerned with the *free troposphere*, which is the troposphere above a thin (approx. 1–2 km) layer in contact with the Earth's surface. This lowest layer, the *planetary boundary layer* (PBL), is where

the motion of the air is impacted by frictional surface effects. Although not as impermeable as the tropopause, mixing of air between the PBL and the free troposphere is restricted. Surface-emitted pollutants tend to accumulate within the PBL, leaving the free troposphere comparatively clean.

All motion of air and water in the atmosphere on earth (i.e. all weather), is ultimately powered by the sun. Wind occurs due to pressure and temperature differences within the atmosphere, and the motion of air is also impacted by the Coriolis effect. The dynamics of the atmosphere are highly complex, as indicated by the vast computational power devoted to making numerical weather predictions.

On smaller scales, plumes in the atmosphere disperse over time, mixing with the surrounding air. This happens faster than would occur via only molecular diffusion effects. Air is mixed by turbulence processes, small vortices of a variety of length scales promote the dissipation of plumes. Such processes are important for numerical weather predictions models (such as the WRF model used in this investigation), but are often too small to be resolved explicitly. As such, turbulent mixing is often incorporated into models by means of parametrisation.

1.1.2 Atmospheric composition

One of the defining aspects of the chemical revolution of the 17th and 18th centuries was the discovery that distinct gases with differing properties could be isolated from air. Early chemists discovered that there was a component of air which supported combustion and respiration (oxygen), and another that did not (the remaining gases of air, mostly nitrogen). Transformation processes of oxygen were simple to demonstrate, a candle sealed within a bell-jar would eventually exhaust all of the combustion-supporting gas and extinguish. At around the same period, “fixed air” (carbon dioxide) was isolated from limestone, and was found to exhibit different properties from either of the components isolated from the ambient atmosphere.

With the major components of the atmosphere now described within chemical theory, atmospheric chemistry could begin in earnest in the nineteenth century as investigations isolated, evaluated and quantified trace gases. For example, the curious smell that followed lightning strikes was discovered to be caused by a gas (ozone) that could be isolated in the laboratory.

The modern understanding of the atmosphere is that it consists of a mixture of countless different gases in various proportions. Almost all of the dry atmosphere consists of three gases, nitrogen (N_2), oxygen (O_2), and argon (Ar). To the nearest %, these species respectively compose 78%, 21%, and 1% of the atmosphere by volume (Seinfeld and Pandis, 2006). The variations in their proportions are minimal enough that these values can generally be used without qualification for any consideration of the Earth's current atmosphere.

Modern atmospheric chemistry generally studies *trace species*, species which by volume compose minute fractions of the atmosphere—often measured with the units parts-per-million (ppm), parts-per-billion (ppb), or parts-per-trillion (ppt)[1]. Despite these small values, several of these species can have impacts on animal and plant health, as well as influencing climate.

As well as gas species, particles of solid and liquid matter are suspended within the atmosphere. These are known as aerosol particles. The size of these particles can cover a great range, from a few nanometers to tens of micrometers. The chemical composition of these particles also varies. Gases and aerosol can interchange: aerosol can be formed from gases, and matter from aerosol particles can transfer to the gas phase.

There are four different ways by which the chemical composition at a given location can change:

- **Transport** Atmospheric motion can bring air with a different composition to the point of interest.
- **Emissions** Gases and aerosol can be added into the atmosphere, for example volcanic emissions add SO_2, ash particles and many other species.
- **Deposition** Gases and aerosol can be removed from the atmosphere, for example rain (wet deposition) can "wash" species out of the atmosphere, transferring them to the ground.
- **Chemistry** Species can react and transform into other species. Atmospheric chemistry reactions decrease the concentrations of the reactants, and increase the concentrations of the products.

The above four factors can be expressed mathematically as the continuity equation (Equation 1.1), which expresses the rate change in concentration of a

[1] All units of this type in this document refer to volume fractions (sometimes written ppmv etc.).

species (n) with respect to time (t) in a volume in terms of transport in and out of the volume ($-\bigtriangledown\cdot\mathbf{F}$), the net production ($P$, emissions minus deposition) and the chemical flux of the species ($-L$) (Jacob, 1999):

$$\frac{dn}{dt} = -\bigtriangledown\cdot\mathbf{F} + P - L \tag{1.1}$$

Although the modelling of this investigation considers all factors impacting the concentration of species, this investigation is primarily concerned with questions regarding the reactive chemistry.

A note on units — mixing ratios and concentrations

ppm, *ppb* and *ppt* are all "mixing ratio" units, describing the proportion of the atmosphere that exists as a specific gas. For example, a mixing ratio of O_3 of 30 ppb indicates that, at the point of measurement, 30 out of every billion gas molecules are O_3 molecules. This can also be expressed as a molar ratio, 3×10^{-8} mol mol^{-1} or 30 nmol mol^{-1}.

Because the ideal gas law holds at the temperatures and pressures considered in this investigation, it can be considered that the volume of space per molecule in the atmosphere is the same for all species. Thus in the example, it is also true that O_3 occupies 30 billionths of the atmospheric volume (at the point of measurement). Terms such as "ppbv" (parts per billion per volume) are equivalent to ppb, ppm to ppmv etc..

Atmospheric compositions are also expressed as *concentrations*, the number of molecules of a species per volume. In this document I use the standard units of molecules per cubic cm (molec cm^{-3}). Atmospheric concentrations are products of the mixing ratio of the species in question and the total concentration of air. This latter concentration varies with altitude — a species which has the same mixing ratio throughout the atmosphere will be more *concentrated* at ground level than in the free troposphere.

1.1.3 Chemical reactions

Throughout this document I write chemical reactions in the form:

$$\mathrm{A} + \mathrm{B} \longrightarrow 2\,\mathrm{C} \tag{R1}$$

which means that a molecule of A and a molecule of B react to form two molecules of C.

With the exception of noble gases, all species in the atmosphere undergo some degree of chemical transformation, being created and destroyed by chemical reactions. The relative importance of such reactions varies between species. For example, CO_2 is effectively inert within the atmosphere, and its concentration is far more strongly dependent on the balance of emissions and deposition, whereas OH is chemically produced and destroyed rapidly within the atmosphere with emission and deposition processes being negligible in comparison.

The speed of processing of a species in a chemical reaction, in terms of how many molecules are processed in a given volume in a time period, is known as its *rate*. This is normally expressed in units of molecules cm^{-3} s^{-1}. Rates of atmospheric chemical reactions depend upon the concentrations of the reactants and other factors and therefore vary both temporally and spatially. Most gas-phase chemical reaction rates can be calculated as the product of the concentrations of the reactants multiplied by a *reaction constant*. The values of these reaction constants depend on various variable factors, most commonly temperature, as well as fixed factors. For example, the rate (k) of the $Br + O_3 \longrightarrow BrO$ reaction can be expressed as:

$$k = [Br][O_3]Ae^{\frac{E_a}{RT}} \tag{1.2}$$

where [Br] and [O_3] refer to the concentration of bromine atoms and ozone. $Ae^{\frac{E_a}{RT}}$ is the reaction constant, which depends on temperature (T) and fixed coefficients.[2] The form of these equations, and the values of the coefficients within these, are determined empirically.

The reaction described above is a *second-order* reaction, meaning that its rate depends on the concentration of two species. First- and third- order reactions are also relevant to atmospheric chemistry. Where a reaction rate is proportional to the square of the concentration of one species (for example the $BrO + BrO$ reaction) this is considered a second-order reaction.

The reactions of interest to this investigation can be divided into three classes:

[2]Specifically in this case A is the Arrhenius pre-exponential factor, E_a is the activation energy and R is the gas constant (a universal constant). For details on the physical meaning of these values see Keeler and Wothers (2003).

Photolysis reactions Photolysis reactions involve a molecule adsorbing a photon of light, which provides the energy to split into two or more products. This only occurs for some species, these are known as *photolysable* species. The wavelengths of light adsorbed (described by the *photolysis cross-section* of the molecule) and the likelihood of a reaction occurring given such an adsorption (described by the *quantum yield*) vary between photolysable species. Photolysis rate constants are always first-order, however they tend to be written in the form:

$$reactant + h\nu \rightarrow products \tag{R2}$$

where $h\nu$ represents a photon.

Photolysis rates vary with the intensity of sunlight, being greatest at solar noon, reduced in the morning and evening, and nil at night. Photolysis rates can also be perturbed by adsorption of light by gases, aerosol, and clouds above a given point. For example solar radiation at the wavelength required to photolyse O_2 molecules is almost completely adsorbed in the upper atmosphere (producing the ozone layer), and the photolysis of O_2 in the lower atmosphere is consequently very small.

Gas-phase reactions Technically photolysis reactions are gas-phase reactions, however the below discussion concerns all *other* reactions that occur exclusively in the gas phase.

These reactions are described by collision theory (and more sophisticated developments thereof), which holds that reactions occur when two or more reactants collide with sufficient energy to instigate a reaction. Because molecules move faster and collide more often at warmer temperatures, most of these reactions have a rate constant that increases with temperature. The factors that determine whether a collision results in a reaction or not are complex, coefficients of these rate equations are determined empirically.

The Arrhenius equation, as described for the $Br + O_3 \longrightarrow BrO$ reaction above, is useful for describing many reaction rates. For other reactions, equations of different forms better fit the empirical data.

Heterogeneous reactions Heterogeneous reactions are reactions whereby the reactants are in different phases. In terms of atmospheric chemistry, these are generally reactions between gas-phase species and species within atmospheric aerosol. The reaction may occur on the interface between the phases, or the

gas-phase species may be adsorbed into aerosol particles, where it undergoes a reaction. A heterogeneous reaction of relevance to this investigation is the reaction of gas-phase HOBr with HCl which proceeds as follows:

- Having adsorbed it from the gas phase, an aerosol particle is rich in HCl, which is dissolved and present as H^+ and Cl^- ions.
- A HOBr molecule collides with the particle and is adsorbed.
- On the particle surface HOBr reacts with the ions:

$$HOBr + H^+ + Cl^- \longrightarrow BrCl + H_2O \tag{R3}$$

- The H_2O remains with the aerosol, while the insoluble BrCl is expelled back to the gas phase.

Thus the overall reaction is:

$$HOBr + HCl \longrightarrow BrCl + H_2O \tag{R4}$$

If the rate-limiting-step of this reaction is the collision and adsorption of HOBr then the rate of this reaction will be proportional to both the concentration of HOBr (molec cm^{-3}) and the "concentration" of aerosol surface area available for reactions (cm^2 cm^{-3}). In general heterogeneous reactions are complex and less well understood than gas-phase reactions.

1.1.4 Steady states

A species is considered to be in a *steady state* if, for the volume considered, the rate of destruction of the molecule is approximately equal to the rate of production. This phenomena often occurs because the rate of destruction of a species is proportional to its concentration, whereas the rate of production of a species is fixed. Thus the concentration of the species rises or falls to the *steady-state concentration* and these fluxes balance. Should the production or destruction rate change, the steady-state concentration will alter accordingly.

A species' *lifetime* is the average time that a molecule of a species exists for before being destroyed chemically. This can vary between species by several orders of magnitude. Species with short lifetimes achieve steady states rapidly,

with these systems quickly adjusting to any perturbation in the production or destruction rates.

An example in the atmosphere is the NO and NO_2 steady state. During the daytime, NO_2 photolyses to produce NO, while NO is oxidised to produce NO_2. Due to the relative speed of the two reactions, the equilibrium "favours" NO_2 and this species has a greater concentration. Changes in the rates of interconversion reactions perturb such states, altering the balance between the species.

1.1.5 Significant chemical systems in the troposphere

The following is a brief overview of the major chemical systems that dominate the chemistry of the troposphere.

1.1.5.1 HO_x cycling

The OH radical[3] is generated by the photolysis of ozone. This species is a powerful oxidising agent and reacts rapidly with many different species. Its atmospheric lifetime is very short, of the order of seconds; during the day its atmospheric concentration is only of the order of a few 10^6 molec cm^{-3}.

Despite this, OH is considered the "detergent of the atmosphere" because it is involved in the removal of many species, including pollutants, from the reactive systems of the atmosphere (Riedel and Lassey, 2008). These processes include:

- The conversion of carbon-containing species to simpler forms, ultimately converting them to CO_2.
- The conversion of nitrogen-containing species to HNO_3, which is mostly inert to further gas-phase chemistry and is removed from the atmosphere by rainout.
- The conversion of sulphur-containing species to H_2SO_4, which forms and is taken up by aerosol particles and is removed from the atmosphere by rainout.

[3]The term "radical" indicates the molecule contains an unpaired electron. Such molecules are highly reactive.

Most of these reactions do not eliminate the radical, but rather convert it to a HO_2 radical. HO_2 is also involved in various chemical systems, although it is generally less reactive than OH and thus has a greater steady-state concentration. HO_2 is converted back to OH by various reactions, of which

$$HO_2 + NO \longrightarrow OH + NO_2 \tag{R5}$$

is typically the most important. Collectively these radicals are known as HO_x radicals.

As HO_x radicals are generated by photolysis and react quickly, their concentrations follows diurnal cycles; concentrations of OH and, in most environments HO_2, are effectively nil at night. H_2O_2 acts as a reservoir of HO_x.

1.1.5.2 NO_x and NO_y chemistry

N_2 comprises approximately 80% of the atmosphere, and N_2O has mixing ratios of a few hundred parts per billion (ppb). However these species are highly unreactive in the troposphere, and it is other, less abundant, oxidised nitrogen species that undergo significant reactive chemical cycles. These species are known collectively as NO_y. The two most reactive of these species, NO and NO_2, are known as NO_x. Processes that produce such species occur naturally and as a result of human activity (Nakicenovic et al., 2000). NO_x concentrations vary substantially depending on whether a location is downwind of a pollution source; NO_x mixing ratios in polluted areas may be several ppb, whereas those in remote areas may be just 10s of ppt. Because most such sources are within the boundary layer, and the time taken for air to travel from the boundary layer to the free troposphere is of the same order as typical NO_x atmospheric residence times, NO_x mixing ratios within the free troposphere are lower than in the boundary layer.

NO_x interacts with other chemical systems. Significantly, it interacts with the HO_x cycling and CO and organic species oxidations resulting in processes which form O_3.

Other forms of oxidised nitrogen can exist. N_2O_5 and NO_3 can accumulate at night, but are unstable during the day. HNO_3 is produced by the oxidation of NO_2 by OH; this species is effectively inert and its formation represents a sink of NO_x.

1.1.5.3 Organic chemistry

A very large number of different volatile organic carbon (VOC) species exist within the atmosphere. The most abundant of these is CH_4, which is well mixed in the atmosphere at a mixing ratio of about 1.8 ppm (2011 value from Myhre et al., 2013). Compared to other organic species, CH_4 is relatively inert; reactive organic chemistry in the troposphere is, except for very clean areas, dominated by chemistry of biogenic and anthropogenic non-methane VOC emissions and their products. Such reaction chains are complex, have multiple branches and often involve NO_x. The fate of VOCs in the troposphere is either to be decomposed to simpler species (ultimately CO_2) or to be transformed to species which are removed from the gas-phase; this includes the formation and growth of aerosol (*secondary organic aerosol*).

However, for this investigation it is oxidation of CH_4 which is the dominant initialisation step of reactive organic chemistry. This is partly because the region of interest (Mount Etna) is remote and elevated above the altitudes immediately affected by pollution, and partly because the modelling employed does not include biogenic emissions. Like other VOC-degradation pathways, the reactant is successively attacked by HO_x and NO_x oxidants and sunlight, eventually forming either deposited products or CO_2. Figure 1.2 is a diagram of CH_4 degradation taken from Seinfeld and Pandis (2006) which shows the pathways common in the troposphere. This mechanism is greatly perturbed by plume chemistry, this is discussed in section 5.4.

1.1.5.4 Atmospheric aerosol

"Aerosol" describes all particulates that are suspended within the atmosphere, both solid and liquid (and multi-phase). These range in sizes from a few nm in diameter to 10s of μm. The majority of aerosol particles are smaller than 0.1 μm in diameter (the *Aitken mode*), the majority of aerosol surface area is contributed by particles with diameters between 0.1 μm and 2.5 μm (the *accumulation mode*), and the majority of the aerosol mass is contributed by larger particles (the *coarse mode*).

Aerosol particles can be emitted directly into the atmosphere, physical processes such as ash emissions from a volcano produce *primary* aerosol. Aerosol particles can also form from gases (such as H_2SO_4, which is an important source of aerosol in this investigation), such aerosol is known as

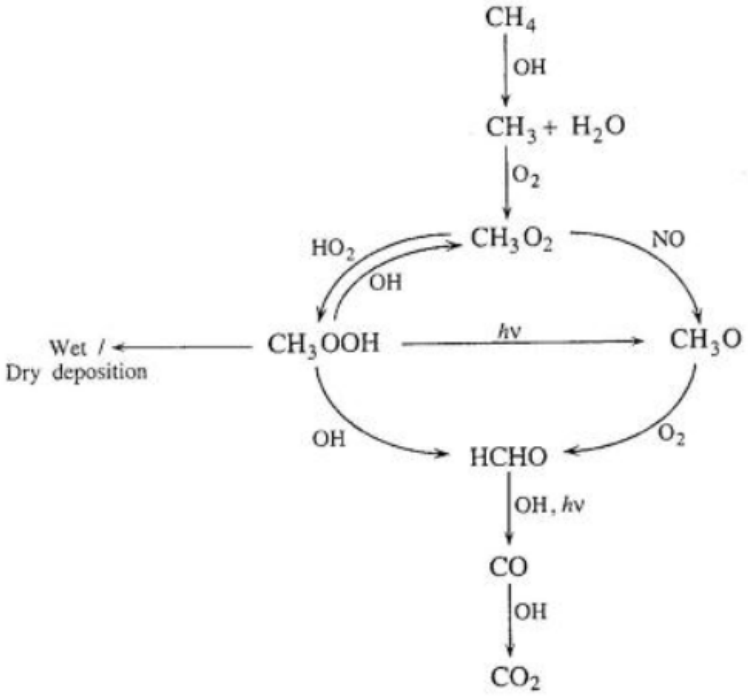

Figure 1.2: Atmospheric methane oxidation chain, figure from Seinfeld and Pandis (2006)

secondary aerosol. As is the case for gas species, aerosol emissions into the atmosphere occur by geogenic, biogenic and anthropogenic processes, and the relative importance of these different processes varies with both location and time.

Once in the atmosphere, aerosol particles can transform, coagulating and growing by taking in matter from the gas phase. The growth of particles via the uptake of water vapour is strongly dependant upon both the chemical composition of the aerosol and the humidity of its environment —a soluble aerosol composition and humid environment makes such growth likely. The dynamics of aerosol liquid water content are complex, and hysteresis phenomena can occur at moderate humidities.

Like trace gases, aerosols can be removed from the atmosphere by wet- and dry-deposition processes. Large particles are prone to being too heavy to remain suspended in atmosphere and being removed by gravitational settling.

The chemical composition of aerosol particles are, mostly, products of their mechanisms of formation and growth, although gas-particle exchange and chemical processes can alter the composition of particles.

Understanding aerosol in the atmosphere is important for various reasons.

These include high concentrations of aerosol particles causing health problems, aerosol's ability to act as cloud condensation nuclei, both positive and negative radiative forcing effects from aerosol which influence climate, and the fact that aerosol can facilitate heterogeneous chemical reactions.

For this investigation, it is this latter effect, discussed in Section 1.1.3, which is of interest.

1.1.5.5 Halogen chemistry and the bromine explosion

For the purposes of this investigation, the reader should interpret "halogens" to mean chlorine and bromine. Although technically the term refers to all group 17 elements, only chlorine and bromine species are simultaneously abundant and reactive enough in the volcanic environments considered to have significant chemistry

Halogen chemistry is a relatively minor component of the general chemistry of the troposphere, however it is central to this investigation.

The most well-known impact of halogens on the chemistry of the atmosphere is O_3 depletion in the stratosphere—the famous "hole" over the Antarctic. Within the troposphere, halogens, particularly bromine, can also deplete O_3 and have other effects on atmospheric chemistry. The modelling of von Glasow et al. (2004) suggests that on a global scale, active bromine chemistry can have a sizeable impact on O_3 and dimethyl sulfide. However the majority of research into tropospheric bromine chemistry, including this investigation, considers more localised phenomena.

The "bromine explosion" is a name given to a chemical process of the troposphere that converts bromine from HBr (an unreactive form) to other, more reactive species. It was first described by Wennberg (1999), with the critical heterogeneous step described earlier by Vogt et al. (1996). The review of Saiz-Lopez and von Glasow (2012) is a good overview of the current scientific understanding of this process.

The process is described as an "explosion" because it is auto-catalytic; the reactive bromine generated facilitates the release of further bromine. The process involves multiple steps, including heterogeneous and photolysis reactions (von Glasow and Crutzen, 2007). I describe the process below.

Step 1: Aerosol particles contain dissolved HBr, either due to their method of

formation, or by having absorbed it from the gas phase.

$$HBr_{(g)} \longrightarrow HBr_{(aq)} \longrightarrow H^+ + Br^- \tag{R6}$$

Step 2: In the gas phase, a BrO molecule reacts with HO_2, forming HOBr

$$BrO_{(g)} + HO_{2\,(g)} \longrightarrow HOBr_{(g)} + O_{2\,(g)} \tag{R7}$$

Step 3: This HOBr is absorbed by or adsorbed at the surface of the aerosol particles

$$HOBr_{(g)} \longrightarrow HOBr_{(aq)} \tag{R8}$$

Step 4: In the aqueous phase, the bromine species react

$$HOBr_{(aq)} + H^+ + Br^- \longrightarrow H_2O_{(l)} + Br_{2\,(aq)} \tag{R9}$$

Step 5: The insoluble Br_2 is expelled from the particles

$$Br_{2\,(aq)} \longrightarrow Br_{2\,(g)} \tag{R10}$$

Step 6: Br_2 is photolysed

$$Br_{2\,(g)} + h\nu \longrightarrow 2\,Br_{(g)} \tag{R11}$$

Step 7: The radicals produced react with O_3

$$2\,Br_{(g)} + 2\,O_{3\,(g)} \longrightarrow 2\,BrO_{(g)} + 2\,O_{2\,(g)} \tag{R12}$$

The "sum" of the above cycle is:

$$HBr + HO_2 + 2\,O_3 \longrightarrow BrO + H_2O + 3\,O_2 \tag{R13}$$

Thus the process creates BrO from HBr, and consumes HO_2 and O_3. This process requires aerosol in order to facilitate the aqueous chemistry. It also requires sunlight, both for the Br_2 photolysis and to produce HO_2 (HO_2 is a daytime-only species, see Section 1.1.5.1).

The cycle described above is a simplified version of the bromine system, which is shown in more detail in Figure 1.3. The varying significance of these different pathways within the plume are discussed in Section 5.6.

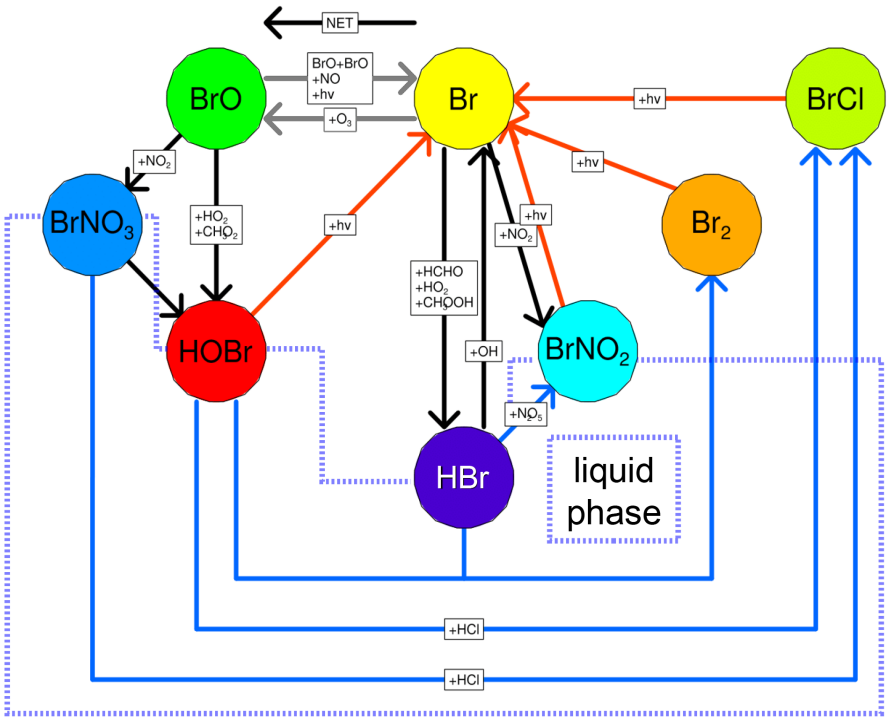

Figure 1.3: Diagram of the major reactive pathways of the bromine cycle within the plume.

There are a few variations to the above 7-step process that are of particular significance in this investigation:

- In step 2, instead of HO_2, BrO can react with CH_3O_2, producing HOBr and HCHO.[4]
- The photolysis of HOBr and the self-reaction of BrO can recycle bromine. von Glasow and Crutzen (2007) and others consider such reactions to be separate phenomena to the bromine cycling, however in this investigation I consider these as "bypass reactions" within the context of the main cycling. This is discussed in Section 5.7.1.
- HCl can take the place of HBr in the above cycle, with BrCl being produced rather than Br_2. This reaction will only by favoured when the chloride concentration of the liquid phase is of the order of 10^4 times greater than that of bromide (Fickert et al., 1999). Such cycles do not add extra bromine to the gas phase. The fate of the Cl radical produced by the photolysis of BrCl is, predominately, reconversion back to HCl via reaction with

[4]The yield of HOBr from this reaction is less than unity (Shallcross et al., 2015). The consequences of this are discussed in Section 5.7.1.

hydrocarbons (Saiz-Lopez and von Glasow, 2012; Simpson et al., 2007, , see also section 5.4); a self-sustaining "chlorine explosion" (without further contribution from bromine chemistry) is not theorised to occur. Because this chlorine radical does not typically destroy an O_3 molecule, the per-cycle O_3 loss in this case is one molecule, i.e. equal to the number of bromine atoms cycled.

- Instead of continuing the cycling, a Br radical can be converted back to HBr via reaction with HCHO or HO_2. As the cycle HBr $\longrightarrow$ Br_2 $\longrightarrow$ Br $\longrightarrow$ HBr does not destroy ozone, the reformation of HBr effectively reduces the O_3-destruction efficiency of the cycling.

The bromine explosion has been identified from measurements of elevated reactive bromine (typically BrO) in various environments where bromine/bromide is emitted into the atmosphere. Such environments include polar regions (where fresh sea ice is the bromine source), the marine boundary layer and salt lakes (salt), and volcanic plumes (direct emission of bromine species from the volcano). As well as measurements of elevated reactive bromine, O_3 depletion events (ODEs) have been observed in these environments. These ODEs are attributed to destruction of O_3 by halogen chemistry (von Glasow and Crutzen, 2007; Simpson et al., 2007).

Reactive halogens are also cited as the cause of mercury depletion events. Elemental mercury, the dominant long-range mercury transport species, is oxidised by reactive bromine species, and these oxidised species deposit rapidly to the ground, resulting in a depletion of mercury in the atmosphere. In a global context, this acts as a mercury sink (assuming the deposited mercury is not re-volatilised), however this deposited mercury is a localised health hazard in the areas where this phenomena occurs (Simpson et al., 2007). Part of the motivation behind this investigation is that an understanding of bromine chemistry within plumes may help to predict the fate of mercury emitted by volcanoes, helping to determine whether mercury deposition is a potential hazard in the locale of volcanoes.

1.2 Overview of volcanic emissions

Volcanoes are locations where where heat, magma and gas from deep in the Earth are discharged to the surface. Some volcanoes erupt continuously, while

others release material in short-lived but intense explosive eruptions. The intensity of volcanic eruptions can vary by many orders of magnitude, with the most intense eruptions ejecting material into the stratosphere, impacting the global climate.

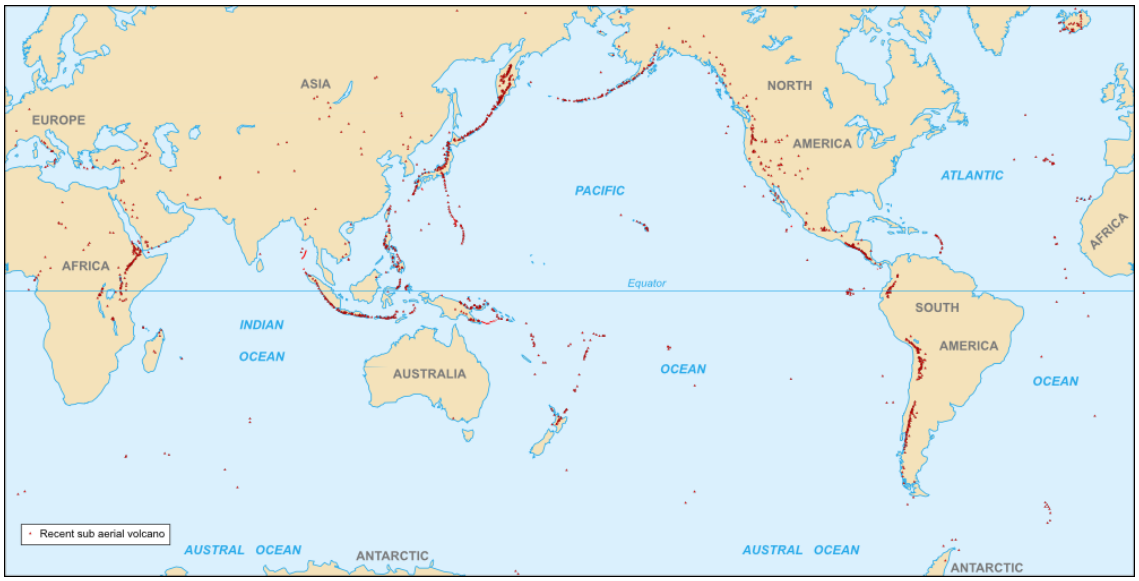

Figure 1.4: Locations of sub-aerial volcanoes which have erupted in the last 10,000 years. Adapted from an image created by Eric Gaba, published on Wikimedia Commons, and released under a Creative Commons Attribution-Share Alike 2.5 Generic license.

Figure 1.4 shows the location of sub-aerial[5] volcanoes which have erupted in the last 10,000 years.

The study of volcanoes (volcanology) is a large and varied field covering all aspects of volcanoes and their activity. This investigation, and this introduction, focuses on a small subset of this field: volcanoes' emissions of aerosol and gas into the atmosphere. Specifically, this investigation is concerned with the influence of these emissions on the atmospheric chemistry of the troposphere, and does not address geological factors that determine the timing, volume, or composition of these emissions. The viability of using volcanic gas observation as a predictor of future activity is an area of current active research (Aiuppa et al., 2007), however this investigation does not directly address this topic.

Once emitted, volcanic plumes are carried by winds. Plumes disperse; this can either be considered as plume components spreading over a large volume, or plumes taking in background air. Over time plume components

[5]"sub-aerial" volcanoes are volcanoes which emit matter into the atmosphere, i.e. have vents that are not underwater. Undersea volcanism is not relevant to this investigation.

will either be removed from the atmosphere (by a combination of physical and chemical processes), or the plume will disperse to a point where species are not significantly elevated above background levels.

Seinfeld and Pandis (2006) discuss analytical solutions to atmospheric dispersion equations, and show that, given various assumptions, the profile of plumes emitted from point sources can be described with Gaussian diffusion equations. Tiesi et al. (2006) studies the dispersion of an Etnean plume based upon satellite observations, and finds that a lateral cross-section of the plume approximately fits a Gaussian profile, with the variance (square of the standard deviation) of this profile rising linearly with time since emission.

This investigation is primarily concerned with gaseous emissions from continuously emitting vents (quiescent degassing), using such behaviour of Mount Etna as a case study. Emissions of this type are not propelled great distances above the vent, and remain within the troposphere at approximately the altitude they are emitted. Volcanoes emit large volumes of gases ("volcanic volatiles") as well as aerosol particles.

1.2.1 Sulphur, water and carbon dioxide

Passive degassing emissions are estimated by Halmer et al. (2002) to account for $6.0 - 8.4 \times 10^{12}$ g of SO_2 emissions per year, approximately 40% of the global total from volcanism (SO_2 emissions are a commonly used measure of volcanic activity).
By volume, the most substantial volatile is H_2O, however, especially for quiescent degassing, this is of relatively little impact on the troposphere's H_2O, as the H_2O content of the troposphere is already substantial in comparison to the emissions. Similarly, volcanic CO_2 emissions, although a substantial fraction of volcanic volatiles by volume, are relatively unimportant. Globally, volcanic CO_2 emissions amount to only a fraction of those from human activities — Gerlach (2011) notes that typical annual emissions of all the world's volcanoes combined are roughly equal to anthropogenic emissions of the U.S. state of Ohio.

Based primarily on measurements from fumaroles, H_2 and H_2S are predicted to be emitted from volcanic vents in significant quantities (Halmer et al., 2002). For primary volcanic vents, it is calculated that these species are oxidised almost immediately upon contact with air in the high temperature "effective source region", producing H_2O and SO_2 (Martin et al., 2006), however some

observations of reduced species in plumes have led to a reassessment of these calculations (Martin et al., 2009). The effective source region is discussed further in Section 1.2.4 below.

1.2.2 Halogens

Volcanoes emit halogen species, principally as halogen halides. HCl is ubiquitous in volcanic plumes, and is often a very substantial component. Although the proportions are low and vary substantially between volcanoes, at least some bromine appears to be present whenever the composition of volcanic volatiles are quantified (Gerlach, 2004).

Bromine is a naturally rarer element and is much less abundant than chlorine in magmas, Bromine's behaviour in volcanic systems is qualitatively similar to that of chlorine, however bromine's fluid/melt partitioning ratio is greater, meaning that the bromine present in a volcano's system is more likely to be emitted in a degassing event (Bureau et al., 2000).

Volcanogenic halides are known to present environmental hazards upon deposition to soils (e.g. Delmelle et al., 2003). Estimates of the magnitudes of these emissions are less well-constrained than those of SO_2, Halmer et al. (2002) for example estimates annual global volcanic inputs to the atmosphere of $1.2 - 170 \times 10^{12}$ g HCl, $0.7 - 8.6 \times 10^{12}$ g HF, and $2.6 - 43.2 \times 10^{9}$ g HBr. HF is considered to be too stable for there to be significant in-plume chemistry (von Glasow et al., 2009). However there exists a large number of observations of elevated levels of BrO within plumes (Donovan et al., 2014; Hörmann et al., 2013) showing that some or all of the HBr emissions are converted to other forms of bromine. This, and observations of O_3 depletion in volcanic plumes are attributed to the bromine explosion (see Section 1.1.5.5). There is also a smaller dataset of OClO observations within volcanic plumes (Donovan et al., 2014; Theys et al., 2014), indicting some reactive chlorine chemistry.

1.2.3 Mercury

Among other toxic trace metals, volcanoes are known to emit mercury (Pyle and Mather, 2003). Although the quantities of emission are comparatively small (for example Pyle and Mather (2003) estimate a global average mercury flux of

7×10^8 g, with about a tenth from continuously erupting/degassing volcanoes), the high toxicity of mercury and its potential for interaction with bromine chemistry (see Section 1.1.5.5) makes these emissions a subject of interest to researchers.

1.2.4 High temperature effective-source region

For practical reasons, most inventories of volcanic volatiles come from measurements of low-temperature gases (often fumarole measurements). However at the point of emission to the atmosphere from primary vents, volcanic volatiles are extremely hot (of the order of 1000°C). These magmatic volatiles will mix with atmospheric air and the extreme temperatures of the of volatiles-air mixtures will be sufficient to atomise many of the gases in the mix, re-equilibrating them to a lower energy composition (Gerlach, 2004; Martin et al., 2006). Critically, the inclusion of oxygen from the background atmosphere in this high-temperature mix produces oxidised species. This phenomenon is considered to produce an "effective source region" (von Glasow, 2010), the output of which will depend upon the composition of the volatiles, the temperature of the mix, and the ratio of volcanic volatiles to background air (V_A/V_M) within the mixture.

In its simplest form, this approach considers only the thermodynamics of the mixture. Developments within this field consider also the kinetics of the re-equilibration process; some thermodynamically-permitted processes may not have time to occur in the few seconds duration of the effective source region (Martin et al., 2009).

1.2.4.1 Reactive nitrogen

A significant unknown with regards to this is the generation (or lack thereof) of NO_x within this region. Direct emissions of fixed nitrogen from volcanoes are expected to be negligible (Mather et al., 2004b), however NO_x generation may occur due to some atmospheric N_2 being consumed within the high-temperature effective source region by the Zeldovich mechanism ($N_2 + O_2 \longrightarrow 2\,NO$ (Zeldovich, 1946)). Such generation would be thermodynamically viable (given sufficient O_2 and heat (Martin et al., 2009)) but analyses of the kinetics of this mechanism (Kaschka, 2007; Martin et al., 2012) suggests that the amount of NO_x generated in the short-lived effective source region would be

small.

Complicating this assessment are inconsistent measurements of reactive nitrogen species in volcanic plumes. The literature contains some reports of detections of NO or NO_2 within volcanic plumes (Bandy et al., 1982; Hobbs et al., 1982, 1991; Huebert et al., 1999; Mather et al., 2004a), however there are also several reports of non-detections (Hobbs et al., 1982; Hubler et al., 1992; Oppenheimer et al., 2010; Boichu et al., 2011)[6]. All of these positive detections used chemiluminescence as the detection method, which may be subject to interference (Weinheimer, 2006).

More consistent are detections of HNO_3 within volcanic plumes (positive results reported in Allen et al., 2000; Mather et al., 2004a,b; Oppenheimer et al., 2010; Sawyer et al., 2011).
A discussion of potential mechanisms which could explain these phenomena can be found in Mather et al. (2004b) however, at present, there is no universally-agreed theory which resolves these observations and model results.

If generated, volcanic NO_x could significantly interfere with the bromine chemistry. This is discussed in Roberts et al. (2014b) and in Section 3.4. In the WRF-Chem modelling of this investigation I have chosen not to model any nitrogen-containing species being emitted from the volcano. This is partly for simplicity, and partly because the modelling results of Section 3.4 showed better agreement with observations when volcanogenic NO_x was not included in the MISTRA model.

1.3 Reactive chemistry within tropospheric volcanic plumes

1.3.1 Observations

As mentioned in Section 1.1.5.5, volcanic plumes are one of the environments where the bromine explosion has been observed. The first such observation was reported by Bobrowski et al. (2003), who observed elevated BrO in the plume of Soufrière Hills volcano, Montserrat by means of a Differential Optical Absorption Spectroscopy (DOAS) instrument. Since then, elevated BrO has been

[6]The results of Oppenheimer et al. (2005) were originally reported as a positive detection of NO_2 in the Erebus plume, however re-analysis of these data by Boichu et al. (2011) revised this to a non-detection

detected in the plumes of over 20 volcanoes, via both ground-based observations and satellite measurements. The phenomenon appears to be common to all plumes.

A good overview of the ground-based observations of BrO in volcanic plumes can be found in Donovan et al. (2014), whilst the systematic study of Hörmann et al. (2013) greatly expanded the dataset of observations from space. In general, practical and safety considerations mean that ground-based observations tend to observe plumes from low-intensity eruptions within a few km of the vents, whereas the limited resolution of satellite observations means they are only able to observe BrO columns from large eruptions but can observe such plumes over a regional scale.

In order to compare eruptions of different magnitude, it has become standard practice to report spectroscopic BrO observations as a ratio of the corresponding SO_2 column (these two species being measured simultaneously). In both satellite and ground-based studies, in-plume ratios of BrO to SO_2 have been found to be of the order of 10^{-5}–several 10^{-4} once the plume has been transported a few km from the source (e.g. Bobrowski et al., 2007; Boichu et al., 2011; Hörmann et al., 2013). Measurements and modelling studies of in-plume BrO / SO_2 ratios have shown BrO to be either present at low levels or undetectable within 1 km of volcanic vents whilst the BrO / SO_2 ratio a few km downwind of the same vent is measured as up to several 10^{-4} (e.g. Bobrowski et al., 2007; Kern et al., 2009). This suggests the formation of BrO is occurring within the time taken for this downwind transport. SO_2 is widely used as a tracer for volcanic emissions due to its high concentration in volcanic plumes, low reactivity, and easily detectable spectroscopic signal (McGonigle et al., 2004).

There is also a smaller dataset of OClO observations within volcanic plumes. Measurements of oxidised Cl in volcanic plumes are varied, having been observed at Sakurajima (Lee et al., 2005), Etna (Bobrowski et al., 2007; General et al., 2015), Puyehue-Cordòn Caulle (Theys et al., 2014), and Soufière Hills (Donovan et al., 2014). However a DOAS investigation by Kern et al. (2009) specifically looking for oxidised Cl did not detect any in the plume of Masaya Volcano. It is unknown whether this reflects natural variability or measurement issues. A discussion of reactive chlorine formation in volcanic plumes can be found in Roberts et al. (2009).

The reactive chemistry of volcanic plumes have also been measured via observations of O_3 destruction. Compared to the BrO observations, the current

Table 1.1: Table of reported depletions of O_3 in tropospheric volcanic plumes.

Volcano	Measurement platform	Reference
Augustine	airborne	Vance et al. (2010)
Erebus	airborne	Oppenheimer et al. (2010) Boichu et al. (2011)
Etna	ground-based	Vance et al. (2010) Chapter 3/Surl et al. (2015)
Eyjafjallajökull	airborne	Vance et al. (2010) Schumann et al. (2011)
St. Helens	airborne	Hobbs et al. (1982)
Redoubt	airborne	Kelly et al. (2013)
Sakurajima	ground-based	Lee et al. (2005)

dataset of O_3 depletions within volcanic plumes, tabulated in Table 1.1 is small.

The ozone depletion observed via aircraft discussed in Section 4.5.3 may be considered an addition to this list, however I have elected not to include it in Table 1.1 as it has not been previously published.

This smaller dataset reflects the difficulty of making O_3 observations within a volcanic plume. While BrO can be measured remotely using passive spectroscopic techniques, direct measurements of O_3 depletion within volcanic plumes have to be made in situ due to the large atmospheric O_3 column. Active DOAS measurement of O_3 at a volcano is possible, however it presents significant difficulties in distinguishing the plume from background air. To my knowledge the only published active DOAS O_3 measurement at a volcano is Kern et al. (2009). In this investigation, no O_3 depletion could be determined — the authors of this publication attribute this to the difficulties of isolating a plume O_3 signal from that of the background air.

The magnitude of ozone destruction in the different plumes vary considerably, from a few % points to almost complete destruction. For example, Vance et al. (2010) report results from an aircraft campaign making interceptions of the April–May 2010 Eyjafjallajökull plume where peak O_3 depletion ranged from 4 to 84%. While O_3 destruction seems to be common, possibly ubiquitous, in volcanic plumes, it is not possible to define with any precision an expected magnitude from the available global data.

It should be noted that some of the plumes listed in Table 1.1 are ash-containing plumes. O_3 take-up to ash particles is a potential additional

O_3 loss mechanism, though presently poorly understood (Vance et al., 2010). However, in their results, Vance et al. (2010) show little-to-no relationship of the amounts of O_3 loss to particulate emissions, suggesting that this effect is weak or not present. In this study I will not consider this potential effect — the Etna eruption investigated is mostly ash-poor. This effect is not included in my modelling.

1.3.2 Modelling

Complimenting these observational studies, a small number of modelling studies have attempted to replicate the chemical processes occurring within volcanic plumes.

Two dedicated models investigating volcanic plume chemistry have been discussed in the literature to date: *MISTRA* and *PlumeChem*.

MISTRA is a 1-dimensional (vertical column) Lagrangian model. It was first discussed in von Glasow et al. (2002) where it was used to investigate marine halogens in a marine environment. Its first implementation in modelling a volcanic plume was in Bobrowski et al. (2007). The model, as a tool for investigating volcanic plumes, is described in detail in von Glasow (2010) and has also, with some developments and customisation, been used to complement observational results in Surl et al. (2015) (these results are also presented in Section 3.4 of this document) and Bobrowski et al. (2015).

PlumeChem has both single- and multi-box modes (i.e. 0 and 1D models). It was first described in Roberts et al. (2009) and was used to complement observational results in Kelly et al. (2013). Further *PlumeChem* modelling was published in Roberts et al. (2014b).

These models consider the chemical evolution of a portion of volcanic plume as it travels downwind. The physical dispersion in both models assumes a Gaussian, cone-like plume. The plume chemistry in both models involves the repeated calculation of rates of reaction and the resulting change in species' concentration over short, discrete time steps.

Both models are able to reproduce approximately plume BrO/SO_2 measurements, including the rise in the ratio in the first few km of plume travel. Roberts et al. (2009) found that the model did not reproduce these ratios if either sunlight or aerosol was absent, and that if the model was initialised without considering the oxidation of volcanic volatiles in the high temperature effective

source region, the modelled rise of the BrO/SO_2 takes longer than observations indicate occurs in real plumes.

Similarly, *MISTRA* reproduces observed plume $BrO:SO_2$ ratios better when initialised with volcanic emissions that consider the high temperature effective source region. The downwind phenomena are shown to vary substantially with variations in the ratio of air and volcanic volatiles within the high temperature effective source region (Bobrowski et al., 2007). Results from both models show that the downwind plume halogen chemistry is sensitive to the composition of the initial emissions. Roberts et al. (2009) showed variations in modelled downwind phenomena when the volcanic volatile composition was varied to represent different types of volcanoes.

In both models, O_3 is considered to be depleted within volcanic plumes. In von Glasow (2010) *MISTRA* models O_3 losses of near 100% are modelled within the core of the plume, however in Surl et al. (2015) *MISTRA*, with different settings, reproduces more moderate O_3 loss observed in the plume of Mount Etna. *PlumeChem*'s modelled O_3 depletions are also variable.

Broadly, the chemical reaction schemes used by *MISTRA* and *PlumeChem* are similar, both using the same collations of reactions and their rates. One significant difference in the latest iterations of these models is the treatment of nitrogen-containing bromine species, a factor which may be significant in plume if reactive nitrogen is emmitted from the high temperature effective volcanic source region (see Section 1.2.4.1). In the base run of *MISTRA* in von Glasow (2010), which included such emissions, $BrNO_2$ was the dominant bromine species for most of the first hour of modelled plume evolution. In the *MISTRA* model output of Surl et al. (2015) significant differences in the chemistry of the early plume were found between model runs that did and those that did not include volcanogenic NO_x. However Roberts et al. (2014b) presents a development of *PlumeChem* that includes a more complicated reaction scheme regarding $BrNO_2$ which results in a more rapid formation of HNO_3 and a substantially smaller fraction of plume bromine being present as $BrNO_2$.

Although the models are able to reproduce observations of BrO in the plume, the distribution of the rest of the bromine between different forms varies substantially between different model output. For example, figures 3 and 5 in Roberts et al. (2014b) shows that *PlumeChem*'s modelled bromine distribution in the first hour of plume evolution varies significantly with variations in the modelled volcanic flux of bromine.

In general, the 'parameter space' of plausible inputs to a volcanic plume model is large, and even when trying to reproduce a real-world case study there are still a large number of unknowns. In most cases BrO and SO_2 measurements are the only results against which a model's outputs can be verified. This situation means that even when model output reproduces observational results, there is still uncertainty in any conclusions inferred about in-plume processes from the model output.

Although the understanding of the chemistry of volcanic plumes within the last decade has been substantially improved by use of models, it is not yet possible to determine fully the meaning of variations between model outputs, and discrepancies between model outputs and observations. Some such variability may represent real differences between volcanic plumes, but at least some will be the result of errors (in model initialisation or processes, or in the observations themselves).

The WRF-Chem modelling discussed in this document represents a significantly different approach to modelling a volcanic plume to either *MISTRA* or *PlumeChem* and is therefore a valuable compliment to the existing plume modelling literature. In Section 5.8 I compare WRF's results pertaining to the base case model run to similar results from these models.

1.4 Atmospheric chemistry modelling

Section 1.3.2 discusses previous results from one-dimensional Lagrangian models. One of these models is used in Section 3.4, however the majority of the modelling results discussed in this document are from the WRF-Chem model, which is a more complicated and computationally demanding model designed to simulate real atmospheric chemistry and physics on a regional scale. WRF-Chem is discussed in detail in Chapter 2, in this section I present a brief overview of these sorts of chemical models.

Fundamentally, numeric atmospheric chemistry models model the concentration of species within the atmosphere by dividing the atmosphere into discreet "boxes" each representing a specific volume. Then, for each box and each chemical species, the model solves Equation 1.1, computing each of the transport, production, loss and chemistry terms.

Calculating transport between grid boxes is a complicated task. In the

Lagrangian models discussed in Section 1.3.2, this task is simplified by considering grid boxes that effectively move with the plume. However for *Eularian* models such as WRF-Chem, the locations of the grid boxes relative to the earth's surface are fixed. In such cases, prediction of the motion of air becomes equivalent to the science of meteorology. Although the WRF-Chem model calculates both meteorology and chemistry simultaneously, I consider the modelling of meteorology to be mostly outside of the domain of this chemistry-focussed investigation. The model's skill in terms of meteorology is briefly assessed in Section 4.3 and is found to be mostly adequate for this investigation; no modification of WRF-Chem's meteorological modelling is attempted.

Such a decoupling of meteorological and chemical modelling is even more explicit in *off-line* models such as GEOS-Chem (Bey et al., 2001), which drive a chemical model with pre-calculated meteorological fields.

The Lagrangian models discussed in Section 1.3.2 necessarily include a volcanic emissions source. Otherwise these models, being concerned with an elevated portion of air, do not need to include other trace gas emissions. Regional and global models however need to consider both natural and anthropogenic emissions.

Such emissions predominantly happen at the surface. Some processes, such as the generation of sea-spray aerosol, may be predicted from the model's meteorology. However for the majority of processes, models such as WRF predict the magnitude and composition of such emissions by reading inventories. These inventories incorporate a large volume of data and give values, in terms of flux per ground surface area, for grids covering large regions or the entire globe. For example, the EDGAR inventory (JRC & PBL, 2010) provides a global $0.1° \times 0.1°$ grid of emissions relating to human activities, and data products from the National Emissions Inventory (NEI) are even higher resolution but are only available for the United States. Such inventories are generally not merely sums of reported emissions, they also incorporate expert judgement to synthesise useful data products. Inventories are also used for biogenic emissions, such as the widely-used MEGAN inventory (Guenther et al., 2006).

Numerical weather models have been used to trace the motion of volcanic emissions, however, to my knowledge, no prior model regional or global model of tropospheric chemistry has included a detailed representation of emissions

from volcanic plumes. One of the purposes of this investigation is as a proof-of-concept exercise, showing that volcanic emissions can be incorporated into a regional model and that the model output can produce useful scientific output.

The models discussed in Section 1.3.2 do not need to include depositional processes, as they consider air elevated above the ground (thus making dry deposition redundant) that is free of clouds and precipitation (thus no wet deposition occurs). More complete models require routines to estimate these depositional fluxes from the simulated meteorology.

Computing the rates of chemical reactions in the atmosphere requires having a list of chemical reactions, and for each the values of various constants describing the rate of the reaction and its dependence upon temperature and other meteorological parameters. These reaction equations are based on empirical studies and are compiled in compilations such as (Atkinson et al., 2004). A numerical model is required to construct, and then solve, a set of differential equations for each timestep (Jacobson, 2005).

More chemical reactions are known than can be used in large-scale model. For example the Master Chemical Mechanism (http://mcm.leeds.ac.uk/MCM) models hundreds of reactants and thousands of reactions, but employing this in WRF-Chem (where the calculation would need to be repeated for every grid cell for each time step) would be too computationally demanding. Modelling studies such as this one need to construct a *reduced mechanism* using a subset of these known reactions. A challenge for modellers is to produce a workable mechanism without significantly compromising the accuracy of the model's simulation of species of interest. The "*CBMZ_MOSAIC_8bins*" scheme (Zaveri and Peters, 1999; Zaveri et al., 2008) is an example of a reduced mechanism that aims to remain reasonably accurate for the major trace gases of the atmosphere.

1.4.1 "The modeller's advantage"

An inherent advantage of modelling, as opposed to direct observation of physical phenomena, is that the modeller is able to observe all parts of the simulation, including information for which the real-world equivalents are impractical or impossible to observe. Additionally, in an open-source model such as WRF-Chem/KPP, the algorithms that determine all modelled chemical and physical processes that occur are known. As such an experimentalist using

WRF-Chem can, in theory, know entirely the reasons why a simulation evolves between states over the time steps.

In practice de-constructing an entire model in this manner would be an impossibly large task for a human operator, and would effectively negate the purpose of using powerful computers to do the processing. Thus, the challenge in analysing model output is in choosing, visualising, and understanding a selection of the available output in order to build a meaningful and understandable picture of the modelled system.

1.5 Overview of this document

This document is an investigation into the chemistry of volcanic plumes. Specifically, the modelling and observations relate to a quiescent degassing episode of Mount Etna, however it is intended that this investigation improves the understanding of similar plumes from other volcanoes.

- The main tool I have used for this investigation is an extensively modified version of the atmospheric chemistry model WRF-Chem. This model, and the amendments made to it in order to facilitate this investigation, are described in Chapter 2.
- Chapter 3 discusses a near-vent field campaign conducted on Mount Etna in 2012 and analyses the results from this. These are complimented with analysis of runs of the 1D model *MISTRA*. This Chapter is an edited version of the previous published peer-reviewed paper Surl et al. (2015).
- Chapter 4 evaluates the skill of the WRF-Chem model by comparing its output to available measurements. I assess to what extent the model can be expected to reproduce real-world phenomena.
- Chapter 5 is the main results chapter of this document. In it I discuss in detail the output from running the model with the "base" settings, and evaluate what chemical processes these results suggest occurs within volcanic plumes.
- While the previous chapter considers phenomena modelled to occur in plumes emitted from the volcano during the day, Chapter 6 evaluates the model results concerning plumes emitted at night. Because the plume

chemistry is highly influenced by photolysis, there are significant potential differences between these cases.

- Chapter 7 considers modelled plumes with significantly greater volcanic emission fluxes, and evaluates how the plume chemistry changes with this variation.
- Chapter 8 considers various modelled plumes whereby a parameter of the model has been changed from the base case. In evaluating the output from these model runs, I assess the plume chemistry's sensitivity to these parameters.
- Chapter 9 summarises my conclusions from this investigation.

This document also has appendices containing additional information.

Chapter 2

Model description

In this chapter I will discuss the modelling system which I have used to produce the results presented in Chapters 4, 5, 6, 7, and 8.

Section 2.1 of this chapter gives an overview of the modelling system, insomuch as is useful for the reader to know in terms of this investigation. This is, necessarily, not a comprehensive description of what is a very complicated model. Although in the rest of this document I refer to the entire modelling system as "WRF-Chem" for brevity, in this Chapter I distinguish between the the different elements of the modelling system, with WRF-Chem "proper" being one of a series of utilities. WRF-Chem is the largest and most complex of these utilities, and is the utility which actually does the main modelling calculations. I also discuss here the other utilities which are auxiliary to WRF-Chem but are necessary for my modelling.

In Section 2.2 I discuss how I have modified WRF-Chem and auxiliary programs in order to perform the modelling necessary for this investigation. This is intended to be comprehensive, although this does not extend to line-by-line commentary on the modifications to the code.

Section 2.3 discusses the options I have chosen within the inputs to the modelling system for the runs. These runtime options include both the time and locations modelled, and the composition of the modelled volcanic emissions.

Attribution of this work: The preparation of the model for this and related investigations was begun before I started my PhD by Dr. Deanna Donohoue. Between 2011 and 2013 Dr. Donohoue and I worked together on model development, and from 2013 I have worked on model development

independently. Throughout this process I have been supported from my supervisory team, primarily Prof. Roland von Glasow. The chemical mechanism we have developed is a direct development from an earlier mechanism created by Prof. von Glasow and uses much of the same code. In this Chapter I do not attempt to distinguish between the work of my colleagues and myself.

2.1 Overview of the modelling system

In this investigation I model the atmospheric chemistry of the central Mediterranean and environs in which the plume of Mount Etna is modelled as occurring. The modelling system used has at its core the "Weather Research and Forecasting model with coupled Chemistry" (WRF-Chem), version 3.4.1. In order to provide the required input into WRF-Chem several auxiliary programs have been run, processing information from external sources such that these can be read by WRF-Chem.

The modelling system works on a grid basis, with the modelled space divided three dimensionally into cuboidal grid boxes. The model computes processes occurring within and between these grid boxes, evaluating how various parameters representing physical and chemical entities evolve over time. Like space, time is divided into discreet time steps.

The flow of information through this system is shown in Figure 2.1. This ultimately cumulates in the model output, which is then analysed. In this Section I discuss each of the different utilities and the sources of external data used for this investigation. The discussion of WRF-Chem itself (Section 2.1.4) is necessarily subdivided into several further subsections; WRF-Chem is a complicated, modular system and it is useful to discuss how information is passed between these modules.

This section is subdivided as follows:

1. **2.1.1:** WRF Pre-processing system (WPS)
2. **2.1.2:** Initial and boundary conditions
3. **2.1.3:** Emissions
4. **2.1.4:** WRF-Chem

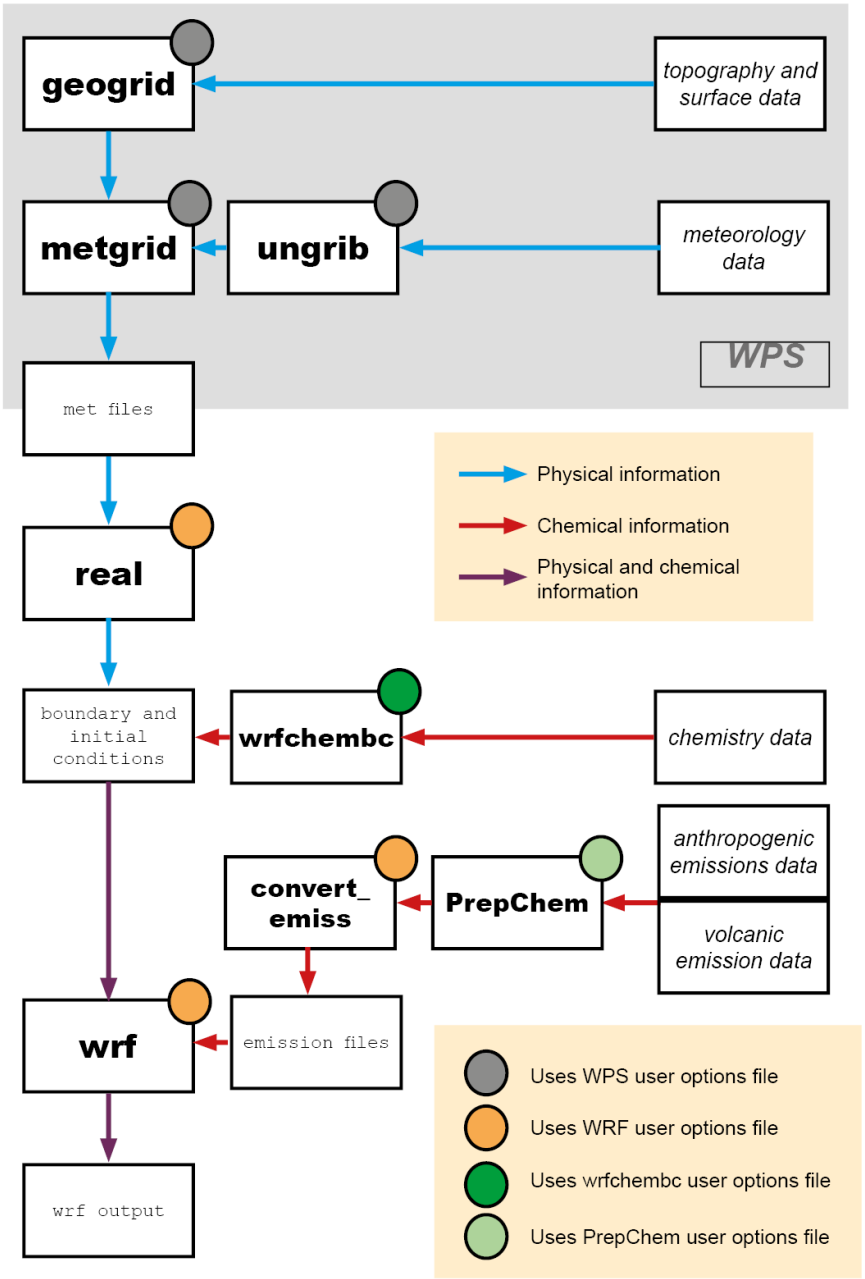

Figure 2.1: A diagram of the components of the WRF-Chem modelling system as used in this investigation, and the flow of information through this system.

2.1.1 WRF Pre-processing system (WPS)

WPS is a collection of three utilities (*geogrid, ungrib* and *metgrid*) that, collectively, produce the files used by the *real* utility (see Section 2.1.2) to produce the initial and boundary conditions for the WRF simulation. WPS processes data regarding the physical situation, it does not process any chemical information. All three utilities use the same user-input file, `namelist.wps`, which defines the location and dimensions of the modelled area, the nesting (see Section 2.1.4.1), and time duration of the model.

Where nested domains are used, WPS processes the data for each, producing separate output.

Geogrid defines domains according to the user's choices in `namelist.wps`, calculating the latitude and longitude of each grid point. It also processes and interpolates geographic information relating to the topography of the area modelled and information about the surface. The source of this information in this investigation is the Global 30 Arc-Second Elevation (GTOPO30), a global digital elevation model (data available from the U.S. Geological Survey). *Geogrid* produces files which are read and processed by *metgrid*.

WRF requires meteorological information from an external source to determine the initial and boundary conditions. In general, such information is extracted from low-resolution global models. For this investigation, this information is sourced from the NCEP dataset (NCEP, 2000) which has a $1° \times 1°$ spatial resolution and 6-hour temporal resolution (NCEP Reanalysis data provided by the NOAA/OAR/ESRL PSD, Boulder, Colorado, USA, from their web site at http://www.esrl.noaa.gov/psd/). The *ungrib* utility extracts the necessary data from the global model output and writes files in a format that can be read by *metgrid*.

Metgid interpolates the meteorological information prepared by *ungrib* onto the grid as defined by geogrid. The meteorological and geographic information are combined in the output of *metgrid* ("`met`" files).

2.1.2 Initial and boundary conditions

The non-chemical initial and boundary conditions are set by the utility *real*, using the output from WPS. Supplementing this with adequate chemical initial and boundary conditions requires use of an additional utility, *wrfchembc*.

2.1.2.1 Physical initial and boundary conditions

The utility *real* reads the `met` files and produces files defining the initial conditions for each domain of the WRF run (a `wrf_input` file corresponding to the start time of the model) and boundary conditions for the outermost domain (`wrf_bdy` files corresponding to regular time intervals, 6 hours in this investigation). During the model runs information is taken from the appropriate `wrf_bdy` file when there is a need for information relating to outside of the model domain, i.e. when air is advected into the domain from outside its boundaries.

This process is controlled by a namelist file containing various user options. By design, the *real* utility uses the same namelists as the WRF utility. Using the exact same namelist means that the files produced by *real* are compatible with the later processing of WRF.

2.1.2.2 Chemical initial and boundary conditions

For investigations concerned only with the physical atmosphere, an adequate WRF simulation can be run following the preparatory steps discussed above. However in order to adequately model atmospheric chemistry using WRF-Chem it is necessary to use additional information to set the chemical initial and boundary conditions. To do this we use a utility called *wrfchembc*.

In a similar manner to how WPS reads meteorological information from a low-resolution global model to obtain the initial and boundary meteorological conditions, *wrfchembc* has the capability to read information from a global chemistry model and use this to define the initial and boundary conditions in regard to the mixing ratios of gases and the concentrations of aerosol. The global chemistry model we have used has been RAQMS[1] (Pierce et al., 2007), chosen because it is the only such model we are aware of that provides estimations for the mixing ratios of halogens and has output that can be easily adapted for WRF-Chem use.

The RAQMS model does not use the exact same set of species as the chemical mechanism used in this investigation. For the gas phase species we have set the model to assume a mixing ratio of 0 for the species not defined in RAQMS—these are all relatively minor species in the atmosphere,

[1]RAQMS is a collaboration between the NOAA Satellite and Information Service (NESDIS), Center for Satellite Applications and Research (STAR) and the University of Wisconsin-Madison Space Science and Engineering Center (SSEC).

thus this assumption is predicted to not introduce a major error in the modelling. RAQMS uses a different aerosol scheme to the MOSAIC_8_bins scheme used in WRF-Chem. The conversion from RAQMS to MOSAIC uses the recommendations of the developers of RAQMS. Because there is not a 1:1 equivalence between the two aerosol schemes the conversion necessarily introduces additional uncertainty into the initial and boundary conditions.

2.1.3 Emissions

Incorporating emissions of gases and aerosol from anthropogenic and volcanic sources requires additional input for WRF. These files define the location, composition and magnitude of these emissions. The procedure for preparing these files used in this investigation requires two ultities. The first, *PrepChem* (Freitas et al., 2011) is a utility which has been developed independently of WRF-Chem, although it has been designed for compatibility. The second, *convert_emiss*, is part of the main WRF-Chem package, although at runtime it is executed separately from the WRF program.

In this investigation we use these utilities to model only anthropogenic and volcanic emissions.[2]. The utilities discussed in this section are capable of also preparing similar WRF input for biogenic emissions and fires. Neither of these have implemented in this investigation.

2.1.3.1 PrepChem

In this investigation we have used PrepChem SRC version 1.1 (Freitas et al., 2011), a utility for reading emissions from external databases and interpolating them to a grid. PrepChem is designed to produce files that can be used as input for atmospheric chemistry models, and some scripts are specifically written for compatibility with WRF-Chem.

PrepChem requires an input file of user options. As well as determining the emissions to be gridded, this file also defines the grids themselves. In order for the PrepChem output to be compatible with the rest of the modelling system, it was necessary in this investigation to define an identical grid to the one defined in WPS.

[2]Sea-salt emissions are included directly in the WRF-Chem code. These are discussed in Section 2.2.1.6. These emissions are not expected to be of significance as this investigation is mostly concerned with the atmosphere a few km above the sea surface.

For the anthropogenic emissions, PrepChem is directed to a database of global emissions, specifically the EDGAR database (JRC & PBL, 2010). PrepChem extracts from this database the ground-level emissions estimates corresponding to the modelled time and area. The information in this database is interpolated onto the model grid and these output are written to files which can be read by the *convert_emiss* utility.

The approach used for volcanic emissions is different, and has been subject to substantial modification for the purposes of this investigation (see Section 2.2.5). Rather than consult an external database, the system is now such that the user defines in the input file the magnitude of (SO_2 and primary aerosol flux) and chemical composition (ratios of the emission fluxes of various species to that of SO_2). Some information about the volcanic emission (the location and the relative size distribution of the primary aerosol emission) is, effectively, hard-coded into the PrepChem script—these are parameters which are not varied between the different runs of this investigation.

As for anthropogenic emissions, PrepChem interpolates the volcanic emissions onto the model grid. The volcano is considered to be a point source, and this investigation only models one active volcano. Consequently the output regarding volcanic emissions is a grid of zero values, with a single grid cell representing the volcanic emission.

The modelling system considers volcanic emission fluxes to be invariant and continuous throughout the modelled period. In the modified set-up used in this investigation, PrepChem does not define the height of the volcanic emission.

2.1.3.2 *convert_emiss*

The files produced by PrepChem cannot be read directly by the main WRF process. The primary purpose of the *convert_emiss* utility is to convert these files into a readable format, and makes sure that these files are compatible with the main WRF processing.

This utility uses the same type of namelist as the real and WRF executables. It also requires the initial conditions file (see Section 2.1.2) to have been already generated.

In our modified setup, is the *convert_emiss* utility which sets the modelled height at which the volcanic emissions are released, the utility reads a user option from the namelist file (see Section 2.2.3.1).

Convert_emiss produces, for each domain of the model, two netcdf format files: one for the gridded anthropogenic emissions, and another for the volcanic emissions. These files are read during the model runs.

2.1.4 WRF-Chem

The main WRF-Chem executable can be run once all of the pre-processing is complete.

The WRF-Chem process is controlled by the same namelist file that was used for the *real* and *convert_emiss* processes. This namelist file contains many options and most are only relevant for the main WRF executable. Section 2.3.4 contains a discussion of the options used in the model runs of this investigation.

In order to maximise the use of the available computational resources, WRF-Chem was run in a parallel processing mode, making simultaneous use of 128 processors.

WRF (without the coupled chemistry) is an advanced meteorology modelling system which is used in many investigations into the dynamics and meteorology of the atmosphere. The physical modelling core used in this investigation is Advanced Research WRF (ARW)[3]. Fundamentally, it approximates the solutions to the equations of fluid dynamics, heat transfer and moisture which are known to govern the dynamics of the atmosphere (Skamarock et al., 2008). In order to produce a representative model of the atmosphere with limited computational resources it is necessary for many physical phenomena to be modelled by means of parametrisation.

WRF is a modular system, with subroutines for different atmospheric processes which are executed in succession; for example the chemistry part of the code has separate subroutines for dry deposition and photolysis. Some user namelist options decide which subroutines are called.

As well as considering discreet grid boxes, WRF calculates the model evolving through discreet timesteps, fundamentally the model is an algorithm for determining how the state of the modelled atmosphere changes from one timestep to the next. The fundamental timestep considered by the model is 60 seconds, however it would consume too much memory to write a permanent record of the model state at the end of every timestep. Instead a model

[3]Other core systems exist, such as the Nonhydrostatic Mesoscale Model (NMM), however only ARW is compatible with the coupled chemistry

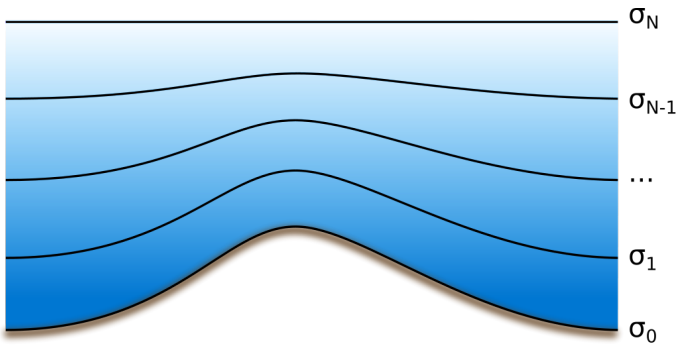

Figure 2.2: Terrain-following σ co-ordinate system. *Public domain image from Wikimedia Commons.*

output file is written at hourly intervals (of model time). This interval allows the evolution of the model state to be observed in the model output, whilst remaining within the limits of the computational resources available. Also for the purposes of conserving disk space, not every parameter that describes the model state is written to these output files, only those which are potentially useful for the analysis.

Vertically, the modelling system divides the modelled volume vertically into 28 levels, using a terrain-following σ co-ordinate system (Skamarock et al., 2008). For all locations, the atmosphere between ground level and 20 km ASL is modelled — ground topography is handled as illustrated in Figure 2.2.

2.1.4.1 Nested domains

WRF is able to consider nested domains, and this capability is exploited for all runs of this investigation. For the outermost domain (domain 1) a large area is considered, with grid cells of dimension 30×30 km. At the edges of the domain, where necessary information is sourced from the external boundary conditions (see Section 2.1.2).

Domain 2 is a *nested domain* which covers a section of domain 1. This area is divided into smaller grid boxes (10×10 km in this investigation). This effectively runs as a separate model, which uses, where necessary, information from domain 1 at its boundary in the same manner that external information is used as the boundary conditions of domain 1. This process can be iterated, with nested domains within domains which are themselves nests (and so on).

We employ two-way nesting in this investigation; the nested domains calculations are fed back to the solution for the larger domain.

As well as a finer spatial resolution, the nested domains also have greater temporal resolution.

Nesting domains allows a small area of particular interest (in this investigation the area of emission) to be modelled in a level of detail which would be prohibitively expensive (in terms of computational resources) to do for the entire area.

2.1.4.2 Modelled physics

The model's treatment of the physics of the atmosphere is complex. However for the purposes of this investigation, which is focussed on the chemistry, it is only necessary that the model provides a reasonable framework for the modelled chemical processes to occur within. In Section 4.3 the model's skill regarding meteorology is assessed and found to generally be sufficient for the purposes of the investigation.

2.1.4.3 Modelled chemistry

The processing of the chemistry uses information determined by the physical model of WRF. Most directly, the calculated motion of air masses govern the transport of the species. Additionally, other parameters, such as temperature and humidity influence reaction rates and other physiochemical processes. WRF-Chem is an *online* chemical model, the chemical processes are calculated continuously as the model progresses. By default, WRF-Chem models chemical processes at a third of the temporal resolution than the corresponding physical timestep. This behaviour has not been modified.

As well as the chemical reactions, discussed below, WRF-Chem also models a number of physiochemical processes which impact the concentrations of both gas phase species and aerosol. For each chemical timestep, WRF-Chem models (where appropriate), dry and wet deposition, in-cloud chemical processes, and aerosol processes.

The most significant choice the user makes when running WRF-Chem is the choice of chemical mechanism. This determines which species are modelled, and the set of reactions between them that are modelled. We created a new chemical mechanism for this investigation, *uea01_hg3*, which is an expanded version of the *CBMZ_MOSAIC_8bins* scheme (Zaveri and Peters, 1999; Zaveri et al., 2008). This has been expanded to include reactive bromine, mercury, and

chlorine chemistry. Every chemical species and reaction modelled is listed, as it appears in the code, in Appendix D.

For the gas phase chemistry, the rates of reaction are calculated by the *Kinetic Pre-Processor (KPP)* (Damian et al., 2002). This is a software tool which is found in many chemical models, and has been incorporated into the WRF-Chem system. For each grid cell and chemical timestep KPP calculates the net destruction/creation of each gas-phase chemical species. Part of the setup of the model involves defining for the chemical mechanism a list of all the reactions to be modelled, and the algorithms for calculating the rates of these —this includes defining the dependence of the rates on physical parameters such as temperature, and also defining coefficients.

For photolysis reactions, the rate constants are calculated outside of KPP. These values, which are calculated from the modelled actinic flux, the composition of the atmosphere, and the photolysis cross sections of the molecules, are then passed to KPP.

The aerosol module used by WRF-Chem implements MADE and SORGAM (Modal Aerosol Dynamics Model for Europe, Secondary Organic Aerosol Model) (Schell et al., 2001). This module can compute the formation of secondary organic aerosol from gas-phase organics, as well as considering the transfer of material both to and from the aqueous aerosol phase (such as the re-volatilisation of nitrate when sulphate is taken up into aerosol).

A development made by us for this investigation is for the aerosol scheme to estimate the aerosol surface area concentration, and then for this information to be passed to KPP in order to calculate the rate of some inorganic heterogeneous reactions. This is described in Section 2.2.2.4.

2.2 Modifications made for this investigation

Although a powerful tool for modelling atmospheric chemistry and physics, WRF-Chem version 3.4.1. in its unmodified state was not adequate for the purposes of this investigation. The same was true of the axillary program *PrepChem*. Thus it was necessary to modify the code of these.

The majority of edits have been made in order to incorporate new chemical species (including tracers) and the new chemical mechanism. The parts of WRF which relate to dynamics and meteorology have been mostly untouched. Some

modifications were solely for the purposes of making WRF compatible with the architecture of the UEA supercomputing system; these purely technical edits have not been discussed here.

This section is divided into sub-sections as follows:

2.2.1: Modifications to the core chemistry code, as found in the *chem* folder of the WRF-Chem code.

2.2.2: Details of the new chemical mechanism that was developed for this investigation.

2.2.3: Modifications to the emissions-related code.

2.2.4: Modifications made to the *Registry* system of WRF.

2.2.5: Modifications made to the code of *PrepChem*, an auxiliary program which processes emissions data for WRF-Chem.

2.2.1 Modifications to the core chemistry code of WRF-Chem

The hierarchy of the code relating to chemistry in WRF-Chem has the chemistry driver at its top, which successively calls a variety of subroutines which relate to processes which can perturb concentrations of chemicals. The most significant of these is the Kinetic Pre-Processor (KPP), which computes chemical reactions. Modifications to the KPP are discussed in subsection 2.2.2. The rest of the chemistry code, which is discussed in this subsection, computes other physiochemical processes which can perturb chemical concentrations (emissions, deposition, aerosol and cloud processes). There are also subroutines that make computations of photolysis rates, which are then used by KPP.

2.2.1.1 Bug fixes and hard-coded options

- A bug identified by the global WRF-Chem community in the file `module_mosaic_therm.F` was addressed. A call to a problematic subroutine was commented out.
- By default WRF-Chem uses data from Texas in 2004 for the initial and boundary conditions of aerosol. In order to change these to those values proscribed by input files from an external data source (see Section 2.1.2.2) a hard-coded option was changed in the file `module_mosaic_initmixrats.F`.

2.2.1.2 Compatibility of new chemical species and new chemical mechanism

We added to the model a new chemical mechanism *uea01_hg3*. This mechanism is an expansion on an existing mechanism, *CBMZ_MOSAIC_8bins* (Zaveri and Peters, 1999; Zaveri et al., 2008). The expansion involved adding 20 new gas-phase bromine, chlorine and mercury species, which are listed in Table 2.1.

Table 2.1: New chemical species added in the modifications to WRF-Chem

Br	Cl
BrO	ClO
	OClO
Br_2	Cl_2
BrCl	
HOBr	HOCl
$BrNO_2$	$ClNO_2$
$BrNO_3$	$ClNO_3$
HBr	
Hg	
HgBr	HgCl
$HgBr_2$	$HgCl_2$

There are two apparent "gaps" in Table 2.1:

- OBrO has not been modelled, as, unlike its chlorine analogue, it decomposes at 0°C (Weast, 1988).
- HCl *is* modelled, this species was already present in the *CBMZ_MOSAIC_8bins* mechanism.

The mercury species and associated reactions, though added to the mechanism, are not relevant to this investigation—they were added to allow the model to be used for a future investigation into volcanic mercury chemistry. Mercury levels within the simulation are too small to significantly perturb either the modelled bromine or chlorine chemistry. These mercury compounds and their chemistry are not discussed in detail in this document.

In many cases within the WRF-Chem code references to individual chemical species and chemical mechanisms are hard-coded. Several edits were made to expand these references to include the new chemical species and the new mechanism. Within the code, different subroutines and options are used for different chemical mechanisms—in almost all cases the same procedures

were used for *uea01_hg3* as were already called for the *CBMZ_MOSAIC_8bins* mechanism. Such edits are made to the following:

- The top-level chemistry driver (`chem_driver.F`)
- The aerosol driver (`aerosol_driver.f`)
- Scripts handling initial and boundary conditions (`chemics_init.F`, `module_input_chem _data.F`)
- The cloud chemistry driver (`cloudchem_driver.F`)
- The dry deposition driver (`dry_dep_driver.F`)
- The emissions driver (`emissions_driver.F`)
- The MEGAN biogenic emissions script (`module_bioemi_megan2.F`)
  - Biogenic emissions are not implemented in this investigation. This edit was made for compatibility with potential future investigations.
- The cumulus convection wet deposition script (`module_ctrans_grell.F`)
- The script for calculating dry deposition using the Wesely scheme (Wesely, 1989) (`module_dep_simple.F`)
- A script for computing aerosol optical properties (`module_optical_averaging.F`)
- The FastJ photolysis scheme (`module_phot_fastj.F`)
- The wet scavenging driver (`module_wetscav_driver.F`)
- The optical driver (`optical_driver.F`)

2.2.1.3 Dry deposition

In this investigation we have used the Wesely dry deposition scheme (Wesely, 1989). It is a widely used scheme in atmospheric modelling. It is compatible with the *CBMZ_MOSAIC_8bins* mechanism, and, therefore, with the modifications I detail below, it is compatible with *uea01_hg3*.

The scheme calculates the dry deposition for each species to each grid cell at each time step by considering the following three factors:

1. The chemical and physical properties of the species
2. The nature of the surface
3. The local meteorology

Factors 2 and 3 are read from the input land use and the meteorology/dynamics calculation respectively. There are four parameters which govern the deposition behaviour of the species. For species in the *CBMZ_MOSAIC_8bins* mechanism the pre-existing values were used. For the new species it was necessary to add these parameters into the code. These parameters are:

hstar The effective Henry's Law constant (H*) at pH 7 in units mol L^{-1} atm^{-1}. The *effective* Henry's law constant accounts for reversible transformations which occur after uptake to the aqueous phase. The source for these data for these new species is the compilation of Henry's law data in Sander (1999)—this is version 3.0 of Rolf Sander's compilations. Where multiple values are reported a representative mid-range value has been chosen.
For extremely soluble species a precise numerical value of H* is neither obtainable or necessary. An arbitrarily large H* value is coded, meaning that the dry deposition is modelled to be not limited by the solubility of the species. The reverse is true for very insoluble species, where an arbitrarily small H* value is used to model this deposition pathway is completely unavailable. In Table 2.2 these two extreme cases are denoted as "large" and "small" respectively.
Sander (1999) does not estimate values for halogenated mercury compounds, but these have been assigned as "large" as they are known to be soluble.

dhr The temperature dependence of the effective Henry's law constant, equal to $-\frac{d \ln k_H}{d \frac{1}{T}}$ in equations 4 and 5 of Sander (1999). The units of these values are K. The source of these data are the same as for H*. For many H* values, the temperature dependence is unknown; in want of better information these have been coded as having no temperature dependence ($-\frac{d \ln k_H}{d \frac{1}{T}} = 0$). For the "large" and "small" H* values, the temperature dependence is irrelevant and these have been coded as $-\frac{d \ln k_H}{d \frac{1}{T}} = 0$.

f0 The reactivity factor. A unitless value representing the propensity of the species to deposit to ground surfaces via the alternative pathway of reaction rather than dissolution. This is a semi-qualitative measure.

The approach of the Wesely scheme is to use three bands. Unreactive species are assigned values of 0, reactive species are assigned values of 1, and intermediate species are assigned values of 0.1. No useful data sources were found for these values, so these assignments are educated guesses based on the known activity of the species and the assignment of species to these three categories in Wesely (1989). For species with "large" effective Henry's law constants this pathway is of negligable importance, and therefore the reactivity factor has been set to 0 for simplicity.

dvj The molecular diffusivity of the species. Units are cm^{-2} s^{-1}. The approach used in table 2 of Wesely (1989), and followed here, is to use the square root of the relative molecular mass of the species as the estimate of the diffusivity value.

The values of these parameters assigned for the new species are tabulated in Table 2.2. Primarily for debugging purposes, code was also added to these files

Table 2.2: Parameters relating to dry deposition assigned to the new gas phase species in the *uea01_hg3* mechanism

Species	**hstar** (mol L^{-1} atm^{-1})	**dhr** (K)	**f0** (unitless)	**dvj** (cm^{-2} s^{-1})
Br	0.034	1800	1	0.11
Br_2	0.8	4000	0	0.079
BrO	small	0	0.1	0.10
HBr	large	0	0	0.11
HOBr	1000	0	0	0.10
$BrNO_2$	0.3	0	0	0.089
$BrNO_3$	large	0	0	0.058
Cl	0.015	1500	1	0.17
ClO	small	0	0.1	0.14
OClO	1.0	3300	0.1	0.12
Cl_2	0.094	2000	0	0.12
$ClNO_2$	0.035	0	0	0.11
$ClNO_3$	large	0	0	0.10
HOCl	660	5900	0	0.14
BrCl	0.94	5600	0	0.093
Hg	0.093	0	0	0.071
HgBr	large	0	0	0.058
$HgBr_2$	large	0	0	0.053
HgCl	large	0	0	0.065
$HgCl_2$	large	0	0	0.061

to make the dry deposition velocities prognostic variables that can be written into the model output.

Code was added to the dry deposition script to set the deposition velocities of the tracer species to zero.

2.2.1.4 Wet deposition

WRF-Chem makes two separate calculations of wet deposition, one for deposition via cumulus convection and the second for below-cloud scavenging. The relevant meteorological information is taken from the output of the meteorological modelling of WRF-Chem.

The physiochemical assumptions in these subroutines are very crude. Wet deposition processes are already coded for sulphate, nitrate, and a few other species, and these were replicated for the new species which are soluble. This is done by hard-coding an aqueous fraction, the proportion of the species in a grid cell which partitions to the aqueous phase if a cumulus or rain event occurs in the grid box. For H_2SO_4 and HNO_3 this fraction was set to 1.0 (100%) for both wet deposition mechanisms. For simplicity, this loss approach has been replicated for the soluble bromine and chlorine species, which are HBr, $BrNO_3$, HCl, $ClNO_3$ and HOCl. All other new species are coded to have no wet deposition.

The exclusion of HOBr from this list of scavenged species is an error. However, no wet deposition events occur in the area of the plume during the simulated time, so this is has not perturbed the results.

Primarily for debugging purposes, code was also added to these files to make the wet deposition amounts (cumulative quantities and instantaneous fluxes) for each of the new species prognostic variables that can be written into the model output. This also required edits to the top-level chemical driver script.

2.2.1.5 Photolysis

This investigation uses the Fast-J photolysis scheme (Wild et al., 2000) to calculate the coefficients of the various photolysis reactions.

Of the newly-added species, BrO, Br_2, HOBr, $BrNO_3$, Cl_2, OClO, $ClNO_2$, HOCl, and BrCl are all considered to be photolysable; additions to the photoylsis-related code has been made to calculate these photolysis rates. Technically a photolysis rate is also calculated for HBr, however the input used means that this rate is 0 at all times. $BrNO_2$ is considered a photolysable species.

The new code added for these species replicates the pre-existing processes used for other photolysable species (such as NO_2). Various parts of the photolysis scripts require the numbers of photolysable species and photolysis reactions to be precisely defined; these values have been increased accordingly.

The subroutine requires that the adsorption cross-sections of the species are written directly into the code. These data were converted into the uniformly wavelength-banded cross-sections (required by Fast-J) by the Fast-J utility of Oliver Wild. All of these data were taken from Atkinson et al. (2006).

The script allows cross-sections at two different temperatures to be inserted, such that the temperature dependence of the photolysis rate can be interpolated and/or extrapolated. Where such data was available, this functionality was used. For species where cross-section data were available at two different temperatures, this functionality was used. Where data for only one temperature exist, these were coded twice, at nominal temperatures of 297 and 298 K, which caused Fast-J to model cross-sections with no temperature variation.

It is useful, both for debugging and analysis, to have the photolysis rates of species written as prognostic variables in the model output. Edits have been made to the code of the photolysis-related scripts, and the top-level chemistry driver, in order for this to occur.

2.2.1.6 Sea salt emissions of bromine

There are pre-existing subroutines within the model which model the emission of chloride and sodium aerosol emission from ocean surfaces to the atmosphere. As a simple method of representing bromine emission from ocean surfaces, code was added such that, in the model, Br_2 is emitted at a fixed ratio of the sodium aerosol emission from ocean surfaces. Specifically, this code uses the seawater Na/Br ratio of Sander et al. (2003), and assumes an efficiency of bromine release into the gas phase to be half that of sodium's release into the aerosol phase. Numerically, this translates to a situation whereby for every 1 μg per kg air Na aerosol is increased by, the corresponding mixing ratio of Br_2 is increased by 0.56 ppt. This is a very crude representation of a complex process.

Sea salt emissions, and the accurate representation thereof, are largely irrelevant for this investigation, which is concerned with processes occurring several km above the sea surface. The main purpose of implementing these emission was in preparation for a different investigation.

2.2.1.7 Aerosol surface area and volume calculations

A major development from the *CBMZ_MOSAIC_8bins* mechanism to the *uea01_hg3* mechanism is the addition of heterogeneous reactions.

CBMZ_MOSAIC_8bins includes routines for the transfer of matter between the aerosol phase and the gas phase (for example, the formation of sulphate aerosol from H_2SO_4 created in the gas phase), and these routines have not been changed in *uea01_hg3*. However *uea01_hg3* differs from *CBMZ_MOSAIC_8bins* by including reactions of gas-phase species, most importantly bromine species, which occur on or within aerosol particles. Most of the details of these are discussed in Section 2.2.2, which details the additions to the code of the Kinetic Pre-Processor (KPP). Discussed in this sub-section are the calculations of the aerosol surface area density and volume density, the former of which is read by the KPP in order to compute heterogeneous reaction rates.

Although the *CBMZ_MOSAIC_8bins* mechanism records the number density of aerosol in 8 different bin sizes, it does not compute the surface area or volume density. A new subroutine added in our modifications to the code estimates the total aerosol surface area density and volume density by assuming spherical particles with, for each bin, diameters of equal to the mid-point of the range of diameters in each bin.

These newly-created variables for aerosol surface area density (`surf_dcen`, units cm^2 cm^{-3}) and volume density (`vol_dcen`, units cm^3 cm^{-3}) are made prognostic variables that are written to the model output.

2.2.2 The Kinetic Pre-Processor (KPP)

The *uea01_hg3* mechanism is defined as a new mechanism in the code on the KPP. This is an expanded version of the *CBMZ_MOSAIC_8bins* mechanism.

The additions to the code of the Kinetic Pre-Processor involve the addition of the new species (as listed in 2.1) and the tracer species. This expansion also includes the reactions of these species. I have subdivided this section into discussions of the different types of reaction: photolysis, gas-phase, and heterogeneous reactions.

The coefficients coded into the KPP `.eqn` file, used to calculate the rate constants, are taken from the recommendations of compilations of chemical kinetic data.

For the same reasons as discussed in Section 2.2.1, although mercury chemistry has been coded into the system, this is not detailed in this subsection as this is not of interest to this investigation and the modelled mercury amounts are insufficient to significantly perturb other chemical systems.

All equations in this section are written as they are coded in KPP. These often assume instantaneous subsequent reactions of short-lived products immediately after formation, and omit species of very high atmospheric concentration (such as O_2 and CO_2) which are not modelled by KPP. For example, the photolysis of BrO produces a Br radical and an O radical. The O radical rapidly reacts with O_2 to create O_3. Although these are two distinct reactions, the second of which destroys an O_2 molecule, this is considered by KPP to have equation

$$BrO + h\nu ->_ Br + O_3 \tag{R14}$$

Where there are different pathways a reaction can take, or multiple reactions with similar rates which have the same reactants, this is often treated by KPP as a single reaction with non-integer stoichiometry in regards to the products. For example, self reaction of BrO ($BrO + BrO$) normally produces two Br radicals, but a less common pathway produces Br_2. This is resolved in KPP by weighting these two pathways to produce

$$BrO + BrO \longrightarrow 1.62Br + 0.19Br_2 \tag{R15}$$

This addition to the mechanism is a development on the modelled halogen chemistry mechanism of von Glasow (2010), which has shown good performance in 1D simulations. These additions are a simplified model of bromine and chlorine inorganic chemistry within the troposphere. Computing a "complete" model which involves every such reaction currently known would be too computationally expensive for this investigation. The model includes all the reactions we expect to be necessary to model the major halogen chemistry phenomena.

tracer species: The tracer species have been included in the KPP equations. None are reactants in any reaction involving "real" species, therefore they will not perturb the modelled chemistry.

The decay of tracer2 is coded with an arbitrary first order loss rate. It is a technical requirement of the KPP system that every species must be included in at least one reaction, in order to circumvent this for the fully inert tracer1 species a tracer1 $\rightarrow$ tracer1 "reaction" is defined with an arbitrary rate constant.

2.2.2.1 Photolysis reactions

The calculations of the photolysis constants are made outside the KPP, and are instead made in the main chemistry code (see Section 2.2.1.5). KPP reads these constants and applies them to calculate the photolysis rates.

The following photolysis reactions have been added.

$$BrO + h\nu \longrightarrow Br + O_3 \quad \text{(R16)}$$
$$Br_2 + h\nu \longrightarrow 2\,Br \quad \text{(R17)}$$
$$HOBr + h\nu \longrightarrow Br + OH \quad \text{(R18)}$$
$$BrNO_2 + h\nu \longrightarrow Br + NO_2 \quad \text{(R19)}$$
$$BrNO_3 + h\nu \longrightarrow Br + NO_3 \quad \text{(R20)}$$
$$OClO + h\nu \longrightarrow O_3 + ClO \quad \text{(R21)}$$
$$Cl_2 + h\nu \longrightarrow 2\,Cl \quad \text{(R22)}$$
$$HOCl + h\nu \longrightarrow Cl + OH \quad \text{(R23)}$$
$$ClNO_2 + h\nu \longrightarrow Cl + NO_3 \quad \text{(R24)}$$
$$BrCl + h\nu \longrightarrow Br + Cl \quad \text{(R25)}$$

The photolysis rate constant of $BrNO_2$ is not calculated independently, but is rather considered to be 2.5$\times$ the rate constant of HOBr. This is a minor error in the model, an unnecessary simplification as photolysis cross-section data are available for $BrNO_2$. At most wavelengths, the cross-sections of both isomers of $BrNO_2$ are sufficiently in excess of that of HOBr that this simplification underestimates the photolysis rate of $BrNO_2$. This is unlikely to be a significant error however, as it is found that $BrNO_2$ is an insignificant species in terms of the modelled bromine cycling (see results in Chapter 4).

2.2.2.2 Gas-phase reactions

In this section, the reference "IUPAC online" refers to IUPAC's compilation of chemical kinetic data, which is published both online at http://iupac.pole-ether.fr/ and as a special issue of the Atmospheric Chemistry and Physics journal. This special issue consists of the articles Atkinson et al. (2004), Atkinson et al. (2006), Atkinson et al. (2007), Atkinson et al. (2008), Crowley et al. (2010), and Ammann et al. (2013).

Already coded for the *CBMZ_MOSAIC_8bins* mechanism are various procedures for calculating rate constants from a few inputs. In most cases this includes the temperature, which is computed for each grid cell by the meteorological modelling of WRF-Chem. Other inputs are rate coefficients, which are required to be coded in the equation file of the mechanism. No new procedures for calculating gas-phase reaction rates were required.

The information required to expand the equation file of the mechanism were taken from a variety of compilations of reaction rates; no one compilation was found to contain all the necessary information. Table 2.3 lists the new gas-phase reactions and, for each, the providence of the reaction information (including coefficients) used. The large and highly-regarded compilations of Sander et al. (2011) and IUPAC were the first consulted, with the former preferred for the bromine reactions, and the latter preferred for chlorine reactions (these sections being more complete than the other for each), with a few other sources used for other reactions.

2.2.2.3 Organic bromine source

The model only considers inorganic bromine chemistry. However organic bromine exists within the troposphere, and its degradation by reaction with OH radicals is a significant source of inorganic bromine (von Glasow et al., 2004) in the background troposphere.

In order to assimilate this without requiring modelling of organic bromine species (which would unnecessarily increase the model's complexity), we have assumed a uniform background mixing ratio of organic bromine, resulting in the modelled source being proportional to the modelled concentration of OH in the grid box. This is rendered in KPP as $\mathrm{OH} \longrightarrow \mathrm{Br}$, a (pseudo) first-order reaction. The method and values which determine the rate constant of this reaction are from Parrella et al. (2012).

Table 2.3: Gas-phase reactions added to the chemical mechanism

Reaction	Source of information
$Br + O_3 \longrightarrow BrO$	Sander et al. (2011)
$Br + HO_2 \longrightarrow HBr$	Sander et al. (2011)
$Br + HCHO \longrightarrow HBr + CO + HO_2$	Sander et al. (2011)
$Br + CH_3OOH \longrightarrow CH_3O_2 + HBr$	von Glasow et al. (2004)
$BrO + HO_2 \longrightarrow HOBr$	Sander et al. (2011)
$BrO + CH_3O_2 \longrightarrow 0.72HOBr + 0.28Br + 0.28HO_2 + HCHO$	von Glasow et al. (2004)
$BrO + NO \longrightarrow Br + NO_2$	Sander et al. (2011)
$BrO + NO_2 \longrightarrow BrNO_3$	Sander et al. (2011)
$BrO + BrO \longrightarrow 1.62Br + 0.19Br_2$	Sander et al. (2011)
$HBr + OH \longrightarrow Br + H_2O$	Sander et al. (2011)
$Br + NO_2 \longrightarrow BrNO_2$	Sander et al. (2011)
$BrNO_3 \longrightarrow BrO + NO_2$	von Glasow et al. (2004)
$Cl + O_3 \longrightarrow ClO$	IUPAC online
$Cl + HO_2 \longrightarrow 0.8HCl + 0.2ClO + 0.2OH$	Sander et al. (2011)
$Cl + RO_2 \longrightarrow 0.5ClO + 0.5HCHO + 0.5HO_2 + HCl$	Sander et al. (2011)
$Cl + CH_4 \longrightarrow HCl + CH_3O_2$	IUPAC online
$Cl + C_2H_6 \longrightarrow HCl + RO_2$	IUPAC online
$Cl + HCHO \longrightarrow HCl + HO_2 + CO$	Sander et al. (2011)
$Cl + ClNO_3 \longrightarrow Cl_2 + NO_3$	IUPAC online
$ClO + HO_2 \longrightarrow HOCl$	IUPAC online
$ClO + ClO \longrightarrow Cl_2$	IUPAC online
$ClO + ClO \longrightarrow OClO + Cl$	IUPAC online
$CLO + CH_3O_2 \longrightarrow CL + HCHO + HO_2$	IUPAC online
$CLO + NO \longrightarrow Cl + NO_2$	IUPAC online
$CLO + NO_2 \longrightarrow ClNO_3$	IUPAC online
$HCl + OH \longrightarrow H_2O + Cl$	IUPAC online
$ClNO_2 + OH \longrightarrow HOCl + NO_2$	IUPAC online
$ClNO_3 + OH \longrightarrow 0.5ClO + 0.5HNO_3 + 0.5HOCl + 0.5NO_3$	IUPAC online
$BrO + ClO \longrightarrow 0.93Br + 0.5OClO + 0.43Cl + 0.07BrCl$	IUPAC online

Specifically the first-order rate constant of this reaction is calculated as:

$$rate = W(X_{CH_3Br}C_M)(A_0 * e^{\frac{-B}{T}}) \tag{2.1}$$

The contents of the right brackets in Equation 2.1 are a standard temperature-dependant Arrhenius expression for the rate of the $OH + CH_3Br$ reaction, where A and B are constants defining the rate and its temperature dependence. X_{CH_3Br} is the mixing ratio of CH_3Br, which is coded as a uniform 8.5 ppt value (Northern Hemisphere value from Parrella et al. (2012)). C_M is the modelled local air number density, meaning that $X_{CH_3Br}C_M$ is equal to the expected concentration of CH_3Br.

Without the W factor, this process would model the expected Br source from the $CH_3Br + OH$ reaction. However, table 1 of Parrella et al. (2012) shows that CH_3Br is responsible for only a fraction of the organic to inorganic bromine flux. In order to represent all sources with one equation, the multiplication factor (W in Equation 2.1) is set to 8.5.

This parametrisation is simplistic. However it is adequate for the purposes of this investigation.

2.2.2.4 Heterogeneous chemistry

In order to accurately represent bromine chemistry within the model, it is necessary to include heterogeneous chemical reactions. These are reactions which do not occur purely in the gas phase. Rather, gas-phase species are taken up onto or into aerosol particles. Reactions occur and then the products are released back into the gas phase. Prior to our additions discussed in this section, KPP did not include any such reactions.

Volcanic plumes are high aerosol-loading environments. Plumes contain liquid particles of condensed acids suspended in air, and, in some cases, solid ash particles also suspended in air.

Although WRF-Chem does include a representation of the aerosol phase, it is not a framework onto which a representation of such chemistry can be easily applied. Such a development of WRF-Chem would be a substantial project. The approach used here does not require the explicit modelling of activity within the aerosol phase. The heterogeneous chemistry we have added does not distinguish between different types of aerosol. This is an acceptable simplification as, although the nature of aerosol particles will differ, almost all particles in a volcanic plume (ash and acid) should provide an acidic environment where the reactions of interest can occur — the ash particles being hydrophilic and likely to acquire a liquid coating which will be acidic in the high SO_2 plume environment.

We use a relatively simple parametrisation based upon the collision rate of gas molecules and aerosol surfaces. Although this omits a significant amount of the likely complexity of the system (e.g. that discussed in Roberts et al., 2014a), this "fixed gamma" approach has been shown to produce reasonable results in other modelling studies (e.g. Macintyre and Evans, 2010) and is reasonably computationally inexpensive.

This collision-based method computes that the rate of the reaction is equal to the rate of collision between molecules of a particular species and the surface of aerosol multiplied by a reaction probability (γ). The collision rate calculation uses collision theory and the surface area concentration computed by WRF-Chem (see Section 2.2.1.7). γ is set to 0.1; which is the "standard" value used in modelling studies that utilise this approach. It is assumed that the process of uptake, reaction and emission back to the gas phase happens rapidly, and that the γ value reasonably encapsulates other factors impacting the effective rate of reaction.

For the bimolecular reactions involving HOBr, it is assumed that the concentration of acids with which HOBr reacts are always greatly in excess of the HOBr; i.e. when a HOBr molecule is taken into an aerosol particle there is always acid for it to react with. Therefore the rate of such reactions are computed as above, i.e as if they are unimolecular reactions of HOBr. Again, γ is set to 0.1. The justification for this approach is that in the volcanic plume (which is the domain of interest), the HCl emissions are sufficiently strong that HCl will be always greatly in excess of HOBr, regardless of the partitioning of bromine between its forms.

The model computes the relative yields of the $HOBr + HBr \longrightarrow Br_2$ and the $HOBr + HCl \longrightarrow BrCl$ reactions based upon the relative concentrations of HBr and HCl and the relative activity of each. The chemistry is such that the $HOBr + HBr$ pathway is preferred unless HCl is vastly in excess of HBr. Practically, this means that HBr must be exhausted within the plume before the $HOBr + HCl$ reaction can take over.

The same approach is used for the $BrNO_3 + HBr$ and $BrNO_3 + HCl$ reactions and the $N_2O_5 + HBr$ and $N_2O_5 + HCl$, with $BrNO_3$ and N_2O_5 taking the role of HOBr.

R26–R38 is a list of the heterogeneous reactions we have added to the model:

$$N_2O_5 \longrightarrow 2\,HNO_3 \tag{R26}$$
$$N_2O_5 + HCl \longrightarrow ClNO_2 + HNO_3 \tag{R27}$$
$$N_2O_5 + HBr \longrightarrow BrNO_2 + HNO_3 \tag{R28}$$
$$ClNO_3 + H_2O \longrightarrow HOCl + HNO_3 \tag{R29}$$
$$ClNO_3 + HCl \longrightarrow Cl_2 + HNO_3 \tag{R30}$$
$$ClNO_3 + HBr \longrightarrow BrCl + HNO_3 \tag{R31}$$
$$BrNO_3 + H_2O \longrightarrow HOBr + HNO_3 \tag{R32}$$
$$BrNO_3 \longrightarrow HOBr \tag{R33}$$
$$BrNO_3 + HCl \longrightarrow BrCl + HNO_3 \tag{R34}$$
$$BrNO_3 + HBr \longrightarrow Br_2 + HNO_3 \tag{R35}$$
$$HOBr + HBr \longrightarrow Br_2 \tag{R36}$$
$$HOBr + HCl \longrightarrow BrCl \tag{R37}$$
$$HOCl + HBr \longrightarrow BrCl \tag{R38}$$

Compared to the gas-phase chemistry, the current level of scientific understanding of heterogeneous chemistry is poor, and this representation does not even incorporate all of this understanding. As such, my discussion of approaches that could be made to advance the work of this investigation in Chapter 9.8 includes a discussion of developments that could be made to the representation of heterogeneous chemistry.

In order to investigate the sensitivity of the model results to the speed of the heterogeneous chemistry (and any errors of the representation thereof) in Section 8.1 I consider model runs with varying γ values.

2.2.2.5 Bug in chlorine chemistry

Following the completion of the model runs used for this investigation, a bug was identified in the code which would have affected the calculation of various chlorine-related reactions. This bug, and the impact this is likely to have had on the results, is discussed in Appendix C. Where results presented are likely to have been influenced by the bug to a noteworthy extent this has been noted in text.

2.2.3 Volcanic emissions in core chemistry code

The file `convert_emiss.f` compiles to form the `convert_emiss.exe` executable, which is a utility that converts the output of PrepChem (see section 2.1.3.1 into netcdf-format files which can be read by WRF-Chem during model runs. This utility is capable of processing files relating to antropogenic, biogenic, fire and volcanic emissions.

Additionally, the emissions driver, which is part of the core chemistry code of WRF that operates at runtime, has been modified to incorporate the volcanic emissions, and these changes are also discussed in this subsection.

2.2.3.1 The `convert_emiss` utility

In this investigation biogenic and fire emissions have not been considered. Anthropogenic emissions are implemented, however it has not been necessary to make any alterations to the code relating to this for this investigation. Therefore the edits discussed in this section refer to the `convert_emiss` utility's handling of volcanic emissions. Substantial edits to this code were required.

In the WRF-Chem namelist file the user has an option `emiss_opt_vol` which decides how volcanic emissions are handled. The new code written specifically for this investigation is set to be implemented when `emiss_opt_vol=5`. This new code duplicates some of the pre-existing script, but also contains substantial wholly original code.

The code is designed to allow volcanic emission of many different species, including tracers and all of the new species listed in Table 2.1. Two-dimensional information (north-south and east-west) for the emission amounts of each species is read from the PrepChem output. In the case of this investigation which considers a single volcano assumed to be a point source, these are arrays of 0 values, with a "dot" of emission at the location of the volcano. The total amount of ash emitted is contained within one of these arrays, with the relative distribution of that ash into the different aerosol size bins is contained within a different variable (`size_dist`), also read from the PrepChem output.

Although the PrepChem output contains a variable, `ash_height`, which denotes the height above the vent to which volcanic emissions are ejected, we do not use this value in the implementation of `convert_emiss` (except as a flag to check whether or not a volcano exists in particular cell). Instead the height of emission is effectively controlled by a new namelist variable, `volc_vent_elev` and emission is set to be an injection within only a single 3D grid cell, either at ground level or elevated.

The primary aerosol emissions are divided between the 8 different size bins according to the `size_dist` variable.

2.2.3.2 Emissions driver

Like the `convert_emiss` utility, although the emissions driver handles various forms of emissions within the model, the only modifications required related to its handling of volcanic emissions.

This code reads the files prepared by the `convert_emiss` utility, and converts the flux values in those files into changes of species' mixing ratios caused by the volcano, factoring in the vertical size of the grid cells being emitted into and the local air densities.

For the emissions of primary aerosol from the volcano, this script hard-codes a 70:30 split of the aerosol mass between the "other inorganics" (ash) and sulphate aerosol species. These proportions are an an estimate—there exists

no direct measurement to base this split upon. Watson and Oppenheimer (2000) measured sulphate being a minority of Etna's particulate emissions, of the order of 10%, however visual observations of the plume during the field campaign suggested a relatively ash-poor plume, so a slightly higher proportion of sulphate was used. Regardless, this is unlikely to be an important parameter for the plume chemistry, as the aerosol surface area script does not distinguish between aerosol types.

2.2.4 The Registry

WRF-Chem uses a Registry system, which is a list of all the variables that either are or could be contained in an initial, boundary, emissions, history, or restart file, or otherwise need to be shared at a "top level" between modules within WRF-Chem. Although WRF-Chem has several registry files, the only one which required modification was the registry file relating to chemistry variables, `registry.chem`. In the registry file each variable is assigned a few properties, including those regarding its dimensionality and to which files produced by WRF said variable is written.

Table 2.4 details the additions that have been made to this file. In the tabulated variable names, "`xxx`" is a placeholder for the names of multiple chemical species. The registry defines variables for all possible options of WRF-Chem. In order to conserve computing resources, the variables which are used only with some options are assigned to packages, which are activated if the relevant option is chosen.

A new package was defined, associated with the *uea01_hg3* chemistry option. This listed all the chemicals, aerosol species (subdivided into bins) and tracers that are modelled by this mechanism. This list is a duplication of the list for the the *CBMZ_MOSAIC_8bins* mechanism, with the addition of the new chemical species, tracers, `surf_dcen` and `vol_dcen`.

A new package was also defined for all the `dvel` variables, set to be active if the namelist variable `diagnostic_chem` is set to 2. This means that the option of whether or not to write these diagnostic values to the model output can be made at model runtime.

A new package was defined for the new volcanic emissions option, which contains all of the emissions variables that can be defined in the volcanic emissions file created by the `convert_emiss` utility.

Table 2.4: Additions made to the WRF-Chem chemistry registry

Name	Description	Notes
e_vXXX	Volcanic emissions flux of species	Entries for each species that can be emitted. Includes tracers. Same characteristics as pre-existing e_vso2 varaible.
dvel_XXX	Dry desposition velocities	Entries for every new species. Same characteristics as pre-existing dvel variables.
wd_XXX_sc	Wet deposition amount of species via below cloud scavanging, cumulative	Entries for every new species. Same characteristics as pre-existing wd/wdi variables.
wdi_XXX_sc	Wet deposition rates of species via below cloud scavanging, instantaneous	
wd_XXX_cu	Wet deposition amount of species via cumulus convection, cumulative	
wdi_XXX_cu	Wet deposition rates of species via cumulus convection, instantanous	
ph_XXX	Photolysis rates	Entries for each new photolysable species. Same characteristics as pre-existing ph variables.
XXX	Mixing ratios of species	Entries for every new species. Same characteristics as pre-existing chemical mixing ratios variables.
surf_dcen	Aerosol surface area concentration	Assigned the same characteristics as variables for pre-existing chemical mixing ratio variables.
vol_dcen	Aerosol volume concentration	

The new namelist option, volc_vent_elev (see Section 2.2.3) is also defined in the registry.

In order to conserve memory the properties of several variables which are not of interest to this investigation were set so that these variables were not written to the model output.

2.2.5 PrepChem

The emissions pre-processor, PREP-CHEM-SRC (Freitas et al., 2011), referred to here as *PrepChem*, has been used as an auxillary program to WRF-Chem.

PrepChem processes information regarding emissions, preparing files which can be processed by the `convert_emiss` utility. We have extensively modified version 1.3.2. of *PrepChem* for this investigation. Apart from bug fixes, all of the edits have involved modelling volcanic emissions.

This release version of *PrepChem* contained two different processes for treating volcanic emissions, one designed for explosive eruptions and one for passively degassing volcanoes. Neither of these routines was found to be immediately functional. We found that, despite this investigation concerning a passively degassing volcano, it was the explosive eruptions code that was more easily adapted for the purposes of this investigation.
For volcanic emissions, *PrepChem* does not read an external database, but rather all of the relevant volcano data was contained hard-coded within the script. One of the outcomes of the modifications were to move many of the options regarding the volcanic output to the runtime input file. The eruptive flux of the different species, including bromine and chlorine species, are now specified directly in the input file, allowing them to be varied without requiring the recompilation of PrepChem.

The nature of the communication between PrepChem and WRF-Chem means that this expansion of PrepChem would be incompatible with WRF-Chem without the modifications discussed in Section 2.2.3, and vice-versa.

This Section does not address edits which were made purely for compatibility with the UEA GRACE system's architecture.

2.2.5.1 Bug fixes

After the release of *PrepChem* 1.3.2. the developers published details of how to fix two bugs which were identified by the community. These were implemented in our build.
We also independently identified and fixed a previously unreported bug where in nested domains emissions were slightly misplaced. This was reported to the *PrepChem* developers.

2.2.5.2 Additional chemical species

The code of *PrepChem* includes a file which serves a similar function to WRF-Chem's registry; a list of all the chemical species considered by the program. This is expanded to include all of the new species added in this

expansion. For some species which can be part of both anthropogenic and volcanic emissions (e.g. SO_2), two distinct "species" are defined to avoid confusion within the code. These are resolved later when files relating to both types of emission are read by WRF-Chem.

Table 2.5 lists all of the species which the modified version of *PrepChem* allows to be set as emissions from the volcano, subdivided into those which have been modelled as being emitted in the model runs of this investigation, and those which have not. See section 2.3.2 for a discussion of the magnitude of these emissions used in this investigation.

Table 2.5: Species which can be emitted from *PrepChem*-modelled volcanoes

Used in this investigation	Set to 0 in this investigation
SO_2	NO
Primary aerosol ("ash")	NO_2
CO	NO_3
OH	HONO
HCl	HNO_3
BrO	NH_3
Br	H_2SO_4
HBr	$BrNO_3$
Br_2	OClO
Hg	$ClNO_2$
$HgBr_2$	$ClNO_3$
HOCl	BrCl
Cl_2	HgCl
ClO	$HgCl_2$
Tracer 1	
Tracer 2	

Many of the edits to the files `volc_emissions.f90` and `wrf_fim_utils` involved expanding the capacity of these scripts to handle emissions of all of these species, including reading the additional input file options and writing the additional variables to the output.

2.2.5.3 User choices

A capability which has been added to *PrepChem*, but not implemented in this investigation, is the simultaneous modelling of multiple volcanoes. A new variable which is defined by the user in the input file `numberofvolcanoes` has been added, and the pre-existing variable `volcano_index` has been made into an array which can hold up to 99 values.

The volcanic SO_2 and primary aerosol (referred to in the *PrepChem* code as "ash") emission fluxes can be defined by the user in the input file. The fluxes of other species are also defined in the input file, and are specified in terms of their molar ratio to the SO_2 flux.

2.2.5.4 Amendments to the volcanic emissions code

The code of the file `volc_emissions.f90`, which does most of the processing regarding the modelled volcanic emissions, and that of the file `wrf_fim_utils`, which does processing regarding writing the output, have been extensively modified in order to have the functionality discussed. A full line-by-line discussion is not necessary for this document. Only the details of these edits which are useful for understanding the relationship between the model input and output are discussed here.

Some information about the volcano remains hard-coded in the script. The file `volc_emissions.f90` contains a large lookup table of over 1500 volcanoes, each associated with a location and an "eruption type". Etna is the 15th entry on this table, therefore `volcano_index` has been set to 15. The eruption type chosen decides the values of various parameters, however as much of the control of the emission has been moved to the namelist many of these variables no longer have any impact. The latitude (37.745994 N) and longitude (14.996819 E) of Etna are hard-coded, as is the division of the primary aerosol emission among the MOSAIC aerosol bins. This is tabulated in Table 2.6 The proportions

Table 2.6: Proportion, by mass, of volcanic primary aerosol emitted in each of the 8 aerosol bins

Aerosol size bin	Diameter range / µm	% by mass
1	0.04–0.08	9
2	0.08–0.16	8
3	0.16–0.31	7
4	0.31–0.63	7
5	0.63–1.25	9
6	1.25–2.5	28
7	2.5–5	20
8	5–10	12

tabulated in Table 2.6 were determined by analysis of data collected during the field campaign. This analysis is discussed in Appendix B.

The magnitude of the primary aerosol emissions and all of the gas-phase

chemical emissions are defined by the input file. The code renders a two-dimensional grid, with a point source of flux of the species where the volcano is located. The code has the capability to render multiple volcanoes, each with different fluxes, but this capability has not been exploited in this investigation.

2.3 Runtime options

In Section 2.1 I have described the modelling system used in this investigation, and in Section 2.2 I have described how the system has been modified, at the level of the source code, in order to facilitate this investigation. In this section, I discuss the specific options that have been chosen for the runs of this investigation. These are "runtime options" meaning that they are options made in the namelists and other control files, rather than within the underlying code.

This section describes the "default" setup. For the perturbation runs, discussed in Section 8, some of these settings are varied—these variations are discussed in that section.

2.3.1 Location and time modelled

The geographical focus of this investigation is Mount Etna. This volcano was chosen because its typical activity is of the type that is of interest to this investigation. It is also one of the most accessible and best studied volcanoes (c.f. the field campaign discussed in Chapter 3), meaning that there is more data available to determine the model input and assess the model output.

The modelled area is therefore centred around the island of Sicily. This run is conducted with 4 domains, nested as shown in Figure 2.3. Other information pertaining to the domains is tabulated in Table 2.7.

Table 2.7: Details of the domains used in this investigation

Domain	Spatial resolution / km	Temporal resolution / s	
		Physics	Chemistry
1	30	60	180
2	10	20	60
3	3.33	6.66	20
4	1.11	2.22	6.66

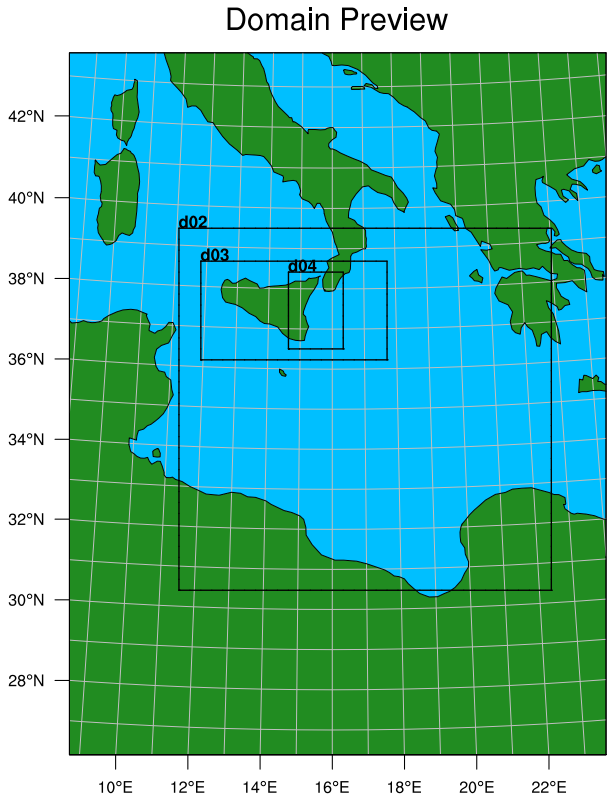

Figure 2.3: Area modelled in this investigation, including the successively nested sub-domains of higher resolution.

Although the temporal resolution varies, for all domains the solar flux (for photolysis) is updated every 10 minutes.

The modelled time is 2012-07-30 00:00:00 to 2012-08-02 00:00:00 UTC, which coincides with the dates of the field campaign of Chapter 3 and additional measurements by other groups (see Chapter 4). In addition this time period has the advantage of having "simple" meteorology with no clouds or precipitation perturbing the plume.

As Mount Etna is at almost exactly 15°E longitude, the UTC time can be near-precisely converted to local solar time by adding one hour.

2.3.2 Volcanic emissions

The simulations of Mount Etna are intended to represent a strong but not abnormal quiescent degassing of the volcano. The emission rate of SO_2 is set to 60 kg/s (5200 tonnes/day). This is above, but within one standard deviation of, the average degassing rate observed for Mt. Etna in Salerno et al. (2009) in the period 2005–2008.

The fluxes of the various gases emitted are listed in Table 2.8. The molar ratio of the flux of the gaseous volatiles to that of SO_2 is same as that for the "low Br/S" modelling study described in Chapter 3 (and also in Surl et al., 2015), these are based on field observations and a model which estimates the rapid high-temperature chemistry predicted to occur in the seconds after emission; see Section 3.4 for a discussion. As in the modelling studies of Section 3.4, the volcanic source modelled is the *effective source region* of the volcano, rather than the actual flux of volatiles from the vents.

It is important to note that we have not included any significant flux of fixed (oxidised) nitrogen in the default WRF-Chem volcanic emissions. Section 3.4 discusses the issues regarding the question of whether volcanoes fix nitrogen from the atmosphere, and presents results from a 1D model showing the effect NO_x emissions can have on the plume evolution. Because it is uncertain whether it would be realistic to include reactive nitrogen emissions or not, and because these would add additional complication to the model, the default case was chosen to be the simpler option (no reactive nitrogen emissions).

The primary aerosol emission flux was based upon analysis of field data from Mount Etna. This is discussed in Appendix B.

The model has a single volcanic source. Modelling distinct emission sources for Etna's different vents has not been attempted —they are geographically too close to be resolved even in the highest-resolution domain of this model. In addition, multiple sources are a complication which would make the results more difficult to interpret and harder to draw conclusions from which may have applicability to other volcanoes.

It is modelled that the volcanic emissions have negligible buoyancy and there is no explosive thrust propelling the emitted gases higher into the atmosphere. In 4-domain runs of this investigation, the model injects all volcanic emissions into model layer 0 (the layer immediately above the ground) at the mountain peak, which in the model is 3065 mASL. This is smaller than the height of Mt.

Table 2.8: Mass flux of the modelled volcanic emissions

Species	Mass flux / kg s^{-1}
SO_2	60
Aerosol	2.4
CO	8.4×10^{-4}
OH	6.2×10^{-2}
HCl	14
BrO	1.7×10^{-6}
Br	1.1×10^{-2}
HBr	3.5×10^{-2}
HOBr	1.1×10^{-6}
Br_2	3.0×10^{-5}
HOCl	4.8×10^{-4}
Cl_2	1.5×10^{-3}
ClO	5.3×10^{-5}

Etna in the physical world (approx. 3330 mASL). It is a known phenomenon that the smoothing of topography to fit the grids of numerical models can fail to resolve features of a smaller scale than the model grid (Jiménez and Dudhia, 2012). As illustrated in Figure 2.4, modelled ground elevation of a grid cell containing a mountain peak will be the average elevation of an area containing the peak and surrounding (lower-lying) terrain and will consequently be less than the peak height. The magnitude of this effect decreases as the model resolution of the highest domain increases.

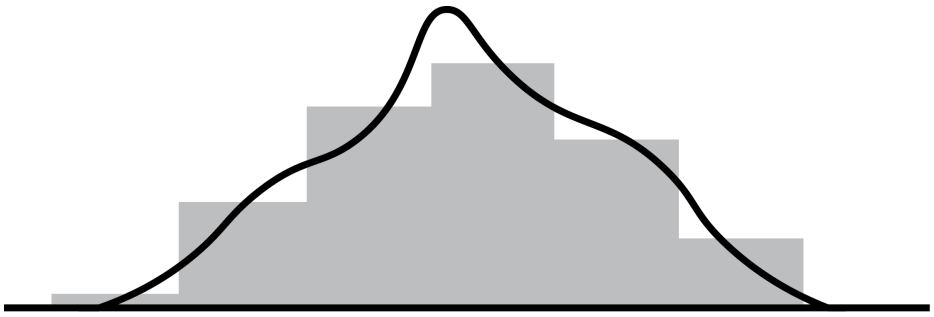

Figure 2.4: Diagram illustrating the representation of topography (black line) in a gridded model (grey polygon). Inevitably, the model will smooth the terrain and therefore "underestimate" the peak height.

The 1×1 km resolution in the 4^{th} domain of WRF approaches the resolution of the topographic data used (Global 30 Arc-Second Elevation (GTOPO30)), thus any attempt to improve the resolution of topographic features would require the acquisition of a higher resolution dataset.

For the purposes of this investigation, the 4th domain's resolution of Etna is adequate. There is no reason to expect a plume which is emitted to a height of approximately 3.0 km to have significantly different behaviour than one emitted at 3.3 kmASL. The 300 m elevation difference will result in changes in temperature and pressure, but these will be too small to make a substantial impact on the phenomena the model is being constructed to investigate. These elevations can both be easily classified as being in the free troposphere (Seinfeld and Pandis, 2006), and are therefore above the influence of planetary boundary layer and its more polluted chemistry.

In order to save computational resources, for some of the runs of this investigation only two domains have been used; the highest spatial resolution is 10 $\times$ 10 km. In these cases inserting the volcanic emissions at "ground" level would not be adequate as the mountain flattening effect is significant. Instead the emissions are injected at 3 km altitude in these model runs.

2.3.3 Anthropogenic emissions

Anthropogenic emissions are less important to this investigation than the volcanic emissions, both because the focus of this investigation is volcanic plume chemistry, and because the plume is emitted into the free troposphere, whilst anthropogenic pollution is almost exclusively emitted into the planetary boundary layer.

Nevertheless, anthropogenic emissions are, in general, important for trace gas chemistry and are relatively simple to incorporate into the model framework, therefore they have been included in this investigation.

The PrepChem utility reads anthropogenic emissions from the EDGAR v4.1 database, which has 0.1° $\times$ 0.1° resolution. This is the highest resolution database PrepChem is, by default, set up to read. It contains inventories of emissions of SO_2, NO, NO_2, CO and a number of non-methane volatile organic species. This database only contains inventories for up to 2005, so data for this year has been applied to 2012 in the model.

The resolution of the databases used for anthropogenic emissions is lower than that of the highest resolution domains. Therefore it is possible for emissions which are intended to represent specific human settlements to be spread out over larger areas. In particular, it is possible for some of the emissions relating to settlements on the slopes of Etna to be assigned to grid cells representing

terrain higher up the mountain. Critically, this can mean that the anthropogenic emissions can be erroneously assigned to locations at or very near the point of volcanic emissions, causing them to mix and interact chemically. In reality, there are negligible anthropogenic emissions within 7-8 km of Etna's peak and such mixing is likely a non-physical phenomenon.

As such, in these runs a circular "exclusion zone" has been set up around the peak of Mt. Etna with a radius of 7.5 km in which the anthropogenic emissions are forced to zero. This prevents this non-physical mixing phenomena from occurring in the model.

2.3.4 Namelist options

The processing of the model physics, dynamics, and chemistry are controlled by a the options chosen in the WRF namelist file. Aside from the newly-created chemical mechanism (see Section 2.2.2) for most options we used the default option. Not all options are mutually compatible, especially for chemistry where the use of a CMBZ and MOSAIC-based mechanism restricted the variety of options that could be used.

During the early stages of model development, before chemistry was implemented, a variety of different physics parametrisation options were tested for mutual compatibility and computational expense. The results of these tests informed the choice used in the final model setup—options were chosen that were sufficiently sophisticated but did not cause the model to consume undue resources.

For almost all namelist options, I have not investigated the impact which variations have on the model output. The potential parameter space would be exceedingly large, with most options unlikely to be of significance for the chemistry of the free-troposphere. For physics, such exercises would be outside of the scope of this chemically-focussed investigation. For chemistry, the perturbations discussed in Section 8 are all that there was sufficient time to execute and analyse in this investigation.

A future investigation which develops from this one could experiment further with the namelist options available. It should also be noted that due to the length of this project, the version of WRF used in this investigation (3.4.1) has been superseded by further versions. As of the time of writing the most recent version of WRF is version 3.7. An investigation using this, or a future

version of WRF, would likely be able to use options which were not available in WRF 3.4.1.

Chapter 3

Field campaign and MISTRA modelling

3.0.5 Attribution of this work

This chapter is a reworked version of *Quantification of the depletion of ozone in the plume of Mount Etna* (Surl et al., 2015), a paper published in Atmospheric Chemistry and Physics in 2015. This was a multi-author paper (Luke Surl, Deanna Donohoue, Alessandro Aiuppa, Nicole Bobrowski, Roland von Glasow) of which I was the lead author. The text of the manuscript was prepared by myself in a process which had continuous review from Dr. Donohoue and Prof. von Glasow from the outset and input from Prof. Aiuppa and Dr. Bobrowski on the final drafts. The published version of this paper also incorporated comments from two anonymous reviewers.

Prof. von Glasow was the PI for this project.

The collection of in-situ data at the mountain top, and the preparation of the equipment for this, was performed by myself, Dr. Donohoue and Prof. von Glasow. The measurement of SO_2 used a MULTIGAS device built by Prof. Aiuppa. Collection of spectroscopic data was performed by Dr. Bobrowski.

The modelling study in this chapter uses the MISTRA model created by Prof. von Glasow. Runs were set up and performed by Prof. von Glasow.

The first stage of data processing involved converting the instrument data to meaningful values. For the SO_2 data this was performed by Prof. Aiuppa. For the rest of the in-situ observations this was performed by Dr. Donohoue with assistance from myself. For the spectroscopic observations this was performed

by Dr. Bobrowski.

Further analysis of the data and model output was undertaken by myself in consultation with Dr. Donohoue and Prof. von Glasow.

3.1 Introduction

The majority of the introduction section in Surl et al. (2015) has been adapted into Chapter 1

We conducted a campaign of ground-based in situ O_3, SO_2 and meteorology measurements at the summit of Mount Etna volcano in July/August 2012. At the same time, we made spectroscopic measurements of BrO and SO_2 columns in the plume downwind.

Depletions of ozone were seen at all in-plume measurement locations, with average O_3 depletions ranging from 11–35 nmol mol^{-1} (15–45 %). Atmospheric processing times of the plume were estimated to be between 1 and 4 min. A 1-D numerical model of early plume evolution was also used (this model, MISTRA is different to the WRF-Chem model used in the other Chapters). It was found that in the early plume O_3 was destroyed at an approximately constant rate relative to an inert plume tracer. This is ascribed to reactive halogen chemistry, and the data suggests the majority of the reactive halogen that destroys O_3 in the early plume is generated within the crater, including a substantial proportion generated in a high-temperature "effective source region" immediately after emission. The model could approximately reproduce the main measured features of the ozone chemistry. Model results show a strong dependence of the near-vent bromine chemistry on the presence or absence of volcanic NO_x emissions and suggest that near-vent ozone measurements can be used as a qualitative indicator of NO_x emission.

The investigation of this chapter examines the bromine chemistry which occurs within the very early plume. The most direct method of doing this is to measure BrO within plumes; BrO is a species which is generated by reactive bromine chemistry. This can be done spectroscopically. Such spectroscopic observations of BrO in volcanic plumes were first published in 2003 (Bobrowski et al., 2003) and since then there have been a large number of similar results published. The spectroscopic observations discussed in this Chapter add to this dataset.

This investigation also examined the plume bromine chemistry in an alternative manner, by measuring in-plume O_3 depletion, a consequence of bromine chemistry. The current dataset of O_3 depletion observations is discussed in Section 1.3.

This study expands this small collection of O_3 observations. In addition, the O_3 depletion data collected are associated with simultaneous measurements of an inert plume tracer (SO_2). To the authors' knowledge, no prior data set exists of simultaneous measurements of O_3 depletion and a tracer species within 1 km of volcanic vents. Wind speeds have also been measured, such that processing time can be determined for every datapoint.

Although this is effectively an indirect measure of the bromine chemistry within the plume, as in-plume halogen and O_3 chemistry are closely linked, from these data we can investigate both qualitatively and quantitatively the fast chemical processes occurring within the early plume.

3.2 Campaign and data processing

3.2.1 Location

The measurement campaign was conducted at Mount Etna, Sicily, Italy (37.7° N, 15.0° E) with the majority of measurements being taken between 24 July and 2 August 2012. Mount Etna is an active stratovolcano with a peak elevation of about 3300 m. At the time of measurement, the volcano was in a passively degassing phase with three active vents (North-East, Voragine and Bocca Nuova) within our survey area. Small Strombolian eruptions and an inner-crateric lava flow were observed at Bocca Nuova but explosive ejecta only rarely surpassed the crater rim. Due to the vicinity of the Voragine and Bocca Nuova craters it was not possible to distinguish between their plumes. Therefore in this analysis we have considered them to be a single source, which we define as the "central craters".

Most of the measurements were taken near the crater rim at elevations significantly above the planetary boundary layer. Due to logistical constraints we took these measurements between 08:40 and 12:00 UTC (10:40–14:00 local time). The sky was cloud-free on all days of measurement. The ground-based remote sensing measurements of the plume were taken from locations further downwind with plume ages of up to 30 min.

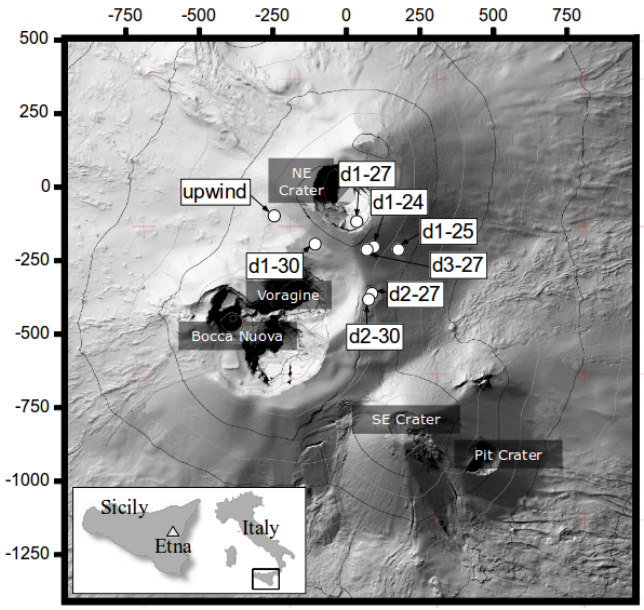

Figure 3.1: Map of the sampling sites and summit craters. Terrain from Neri et al. (2009). Coordinates are metres displacement from the NE crater.

On all days of near-crater measurements we took measurements at a fixed site that was upwind of all summit craters and at 1–3 sites in the plume at varying distances from the craters (Figure 3.1). This was done to sample plumes at different processing times. Sampling times at the sites varied between 20 and 60 min (see Table 3.2).

The names given to the near-crater measurement sites in the figures and in Table 3.2 indicate the day on which the measurements were taken and the order in which they were measured. For example, site "d2-27" was the second downwind site measured on 27 July. All upwind measurements were taken at the same location. In Table 3.2, the upwind site data sets collected on each day have been treated separately. For example, "up-30" is the set of measurements taken at the upwind site on 30 July.

Not all of the measurements taken during this campaign have been used in this Chapter's analysis. Downwind measurements taken on 26 and 28 July did not have an associated upwind measurements and therefore were not useful for this investigation and the attempted downwind measurement on 1 August failed to sufficiently intersect the plume to be useful for this investigation.

3.2.2 Instrumentation

O_3 mixing ratios were measured via UV adsorption with a 2B Technologies

instrument, model 202. A particle filter was placed on the inlet to prevent aerosols from influencing data or damaging the instrument. Because of the overlap of the O_3 and SO_2 adsorption spectra (e.g. Vance et al., 2010) we also fitted the inlet with two SO_2 scrubbers in series to prevent interference in the O_3 measurements. The scrubbers were packed with CrO_3-coated microfibre filter paper. We tested the endurance of the scrubbers prior to the campaign. Air with a SO_2 mixing ratio of 700 μmol mol^{-1} was passed through the setup at a flow rate of 0.58 L min^{-1}. No SO_2-related signal could be detected on the O_3 monitor for 2.25 h, a removal of approximately 15 mg of SO_2. This greatly exceeds the expected SO_2 exposure of the scrubbers in the field.

New scrubbers and particulate filters were used daily. We calibrated the ozone monitor and inlet setup daily with a 2B Technologies model 306 O_3 calibration source. Linear losses of O_3 in the inlet/scrubber system were detected, the field results each day were corrected using the results from the calibration. We determined a measurement error of $\pm$3 nmol mol^{-1} from the calibration results, which incorporates both random error of the instrument and uncertainties in the calibration correction.

We measured several gases' mixing ratios with a portable version of the INGV-type multi-component gas analyser system (MULTIGAS) (Aiuppa et al., 2011, 2012), though only the SO_2 measurements have been used in this analysis. The SO_2 measurement used an electrochemical sensor (0–200 μmol mol^{-1}; 3ST/F electrochemical sensor, City Technology Ltd.). A protective particulate filter was included on the instrument inlet. Data were recorded on an on-board data-logger and stored internally. The instrument's sensors and data-logger were housed in a water-proof box with a 1.2 L min^{-1} pump and a 12V battery. The sensors were calibrated before and after fieldwork with standard calibration gases; the instrument's accuracy and precision were determined to both be about 20 %. The MULTIGAS was not used for the first 2 days of the campaign (24 and 25 July).

Temperature, humidity and wind vector were measured with a Kestrel 4500 commercial weather station, mounted on a tripod. Prior to the campaign, the device's relative humidity measurement was calibrated with standardised salt solutions.

Each instrument recorded data at a different frequency. Table 3.1 shows the instruments' measurement intervals and precision errors.

At the measurement sites we set up the ozone monitor and MULTIGAS on

Table 3.1: Instruments used at the near crater sites.

Name	Parameter	Precision	Sampling interval
Kestel 4500	Temperature	± 1 °C	30 s
	Humidity	± 3 % RH	
	Wind speed	± 3 % or ± 1 m s^{-1} (whichever larger)	
MULTIGAS	SO_2	± 20 %	2 s
2B Technologies Model 202	O_3	± 3 nmol mol^{-1}	10 s

the same tripod, with the inlet tubes positioned closely together. The weather station tripod was positioned within 5 m of the tripod supporting the in situ instruments. The locations of the sites were determined by hand-held GPS. The source of the plume at each downwind site was determined visually.

At the same time as the measurements described above, an optical particle counter was deployed to measure aerosol. These measurements were not used in the analysis described in this chapter, but have been used elsewhere in this document, see Section 3.5.

Remote sensing measurements of the downwind evolution of the volcanic plume with two Mini-MAXDOAS (multi-axis differential optical absorption spectroscopy) instruments were carried out (see Bobrowski et al., 2007, for an instrument description). Scans approximately perpendicular to the plume axis were made at distances between 6 and 16.6 km from the craters, corresponding to plume ages between about 8 and 30 min.

3.2.3 Data processing

The instruments listed in Table 3.1 each had independent internal clocks which could only be roughly synchronised in the field. The MULTIGAS' internal clock does not record absolute time, but only time since the device was switched on. In the field, we turned the device on at the same time as the other instruments, however it is probable some de-synchronisation of the data sets has occurred because of this. Inspection of the O_3 and SO_2 signal suggests that this de-synchronisation may have been up to 25 s.

We used the upwind site data sets as reference values of the background air. For each downwind site, the O_3 concentration time-series was converted to a time-series of O_3 change (ΔO_3) using the average O_3 mixing ratio measured at

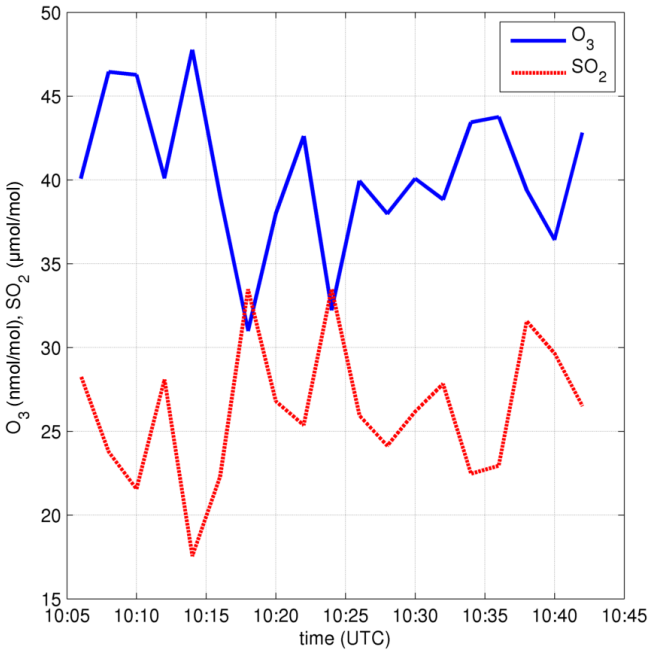

Figure 3.2: An example time series of measurements: O_3 and SO_2 mixing ratios measured in the plume at site d1-27. Data have been averaged into 120 s bins as described in the text.

the upwind reference site on that day.

As the collection frequency of the instruments differed, the data were binned into 120 s bins. Each 120 s bin therefore covered several measurements from each instrument and for each parameter a mean value was calculated. The use of 120 s bins reduced the precision error on the resulting data points. Additionally, the use of 120 s bins is expected to reduce the impact of any potential asynchronisation resulting from either the problem discussed above or from different instrument response times.

Inspection of the signals (e.g. Figure 3.2) showed clear anticorrelation between the O_3 and SO_2 mixing ratios.

SO_2 is used as the inert plume tracer, a measure of plume strength for the bin. Measured background levels of SO_2 were negligible in comparison to in-plume measurements, and SO_2 is expected to be effectively chemically inert. For each 120s measurement bin a ratio ΔO_3 / SO_2 (change in molecules O_3 per molecule inert plume tracer) was calculated, this is a measure of O_3 change that is attributable to chemical and not physical processes (a proof of this can be found in Appendix A). It should be noted that SO_2 *formation* in the plume is possible, it being formed from the oxidation of H_2S. However, the results of Aiuppa et al. (2007) suggest that H_2S chemistry can be ignored on the timescales

considered in this investigation.

Transport times between the craters and the downwind sites were determined from the distances between the sites and the vents, and the measured wind speeds. A single representative transport time was calculated for each 120 s bin from the average wind speed and the known distance from the site to the vent.

Uncertainties

For each bin, the uncertainty in the average wind speed is calculated by combining the known measurement error of the Kestrel instrument and the variance of the individual values of the wind speed used to calculate this average. These were considered independent uncertainties, and the total uncertainty in average wind speed was calculated as the square-root of the sum of the squares of the individual uncertainties. The uncertainty in transport time was calculated from this, assuming that there was no error in the vent-to-site distance number. This error can be seen in the x-axis error bars on Figures 3.3, 3.4, and 3.5.

For the gas measurements the uncertainty in each bin's value is a combination of the errors of the instruments and the variance of the individual measurements comprising that bin. Instrument errors in these individual measurements are assumed to be independent, and thus the combined fractional instrument error on these mean values are assumed to be $\frac{1}{\sqrt{N}}$ of the error on each instrument, where N is the number of measurements being combined. As N is large for both SO_2 and O_3 measurements, it is the variance term which dominates the overall uncertainty in most cases.

Where ΔO_3 values are calculated, the variance in the associated background O_3 measurement is added in quadrature to the error in the downwind O_3 measurement to determine the overall uncertainty. The uncertainty in background SO_2 is assumed to be negligible. These uncertainties are manifested in the y axis error bars of Figures 3.3 and 3.4, and are combined to give the y axis error bars of Figure 3.5.

Mercury considerations

Gaseous elemental mercury is known to be emitted by Etna (Bagnato et al., 2007) and has the potential to cause interference with UV-based ozone monitors

(EPA, 1999), giving false O_3 signal when in the sampled air. The inlet and CrO_3 scrubbers were not tested against mercury interference. If elemental mercury was entering the monitor in the mixing ratios observed by Bagnato et al. (2007), and causing interference of the magnitudes seen by EPA (1999), it would have caused us to make underestimations of the depletion of O_3 on the order of 10 nmol mol^{-1}. However, this would assume that all the mercury emitted from the volcano was primarily in the elemental form. This is unlikely as modelling studies (von Glasow, 2010) indicated that much of the mercury is oxidised within the plume. In addition, mercury measurements at Etna contemporaneous with our campaign (T. A. Mather and M. L. Witt, personal communication, 2014) indicate that the mercury loading of the craters' plumes were significantly less than that which was measured by Bagnato et al. (2007) in 2004–2007 and confirmed that much of the observed mercury was in an oxidised or particulate form. It is also probable that the two CrO_3 scrubbers scavenged or oxidised much of the elemental mercury in the sampled air, as the system is not heated and the scrubbers are changed daily it is unlikely that mercury scavenged by the scrubber would be re-volatilised as elemental mercury. No compensation for this potential effect was made in the post-processing as we believe that the potential for this interference is very low and because the observed anti-correlation of the O_3 and SO_2 signals is the inverse of what would be expected from such interference.

MAXDOAS

The MAXDOAS data were evaluated for BrO and SO_2 with the WinDOAS V2.10 software package (van Roozendael and Fayt, 2001) which uses a nonlinear least-square method (Stutz and Platt, 1996). A BrO / SO_2 ratio was calculated for each measurement day by a correlation plot of the daily data set. The plume ages at the point of measurement were calculated from the wind speed and lateral distance from the craters. In the absence of wind speed data at Etna, speeds from soundings taken at Trapani (37.91° N, 12.50° E, data from http://weather.uwyo.edu/upperair/sounding.html) were used. The 220 km distance between the location of the soundings and the volcano means that there is a relatively large and unquantifiable uncertainty in the calculated plume ages.

Table 3.2: Overview of results from Etna summit measurement campaign.

Site	Upwind/ Downwind	Plume Source	Distance to source/m	Date	Time (UTC)	Average Values				
						Temp./ °C	Humidity/ %	$[SO_2]$/ μmol mol^{-1}	$[O_3]$/ nmol mol^{-1}	$\Delta[O_3]$ / nmol mol^{-1}
up-24	Upwind	–	–	2012-07-24	09:10–09:35	3	49	n.m.	86	–
d1-24	Downwind	Central	300	2012-07-24	10:05–11:30	7	64	n.m.	69	−18
up-25	Upwind	–	–	2012-07-25	11:05–11:30	7	63	n.m.	83	–
d1-25	Downwind	Central	440	2012-07-25	09:52–10:30	11	60	n.m.	58	−25
up-27	Upwind	–	–	2012-07-27	08:41–09:02	9	59	0	77	–
d1-27	Downwind	NEC	150	2012-07-27	09:26–10:16	11	49	34	46	−31
d2-27	Downwind	NEC	380	2012-07-27	10:34–11:06	13	42	11	50	−26
d3-27	Downwind	NEC	240	2012-07-27	11:20–11:50	13	34	17	41	−35
up-30	Upwind	–	–	2012-07-30	09:12–09:34	12	<5	1 0	73	–
d1-30	Downwind	Central	240	2012-07-30	10:05–10:43	16	6	26	40	−32
d2-30	Downwind	Central	300	2012-07-30	11:07–11:41	15	5	9	62	−11

n.m. SO_2 was not measured on these days.

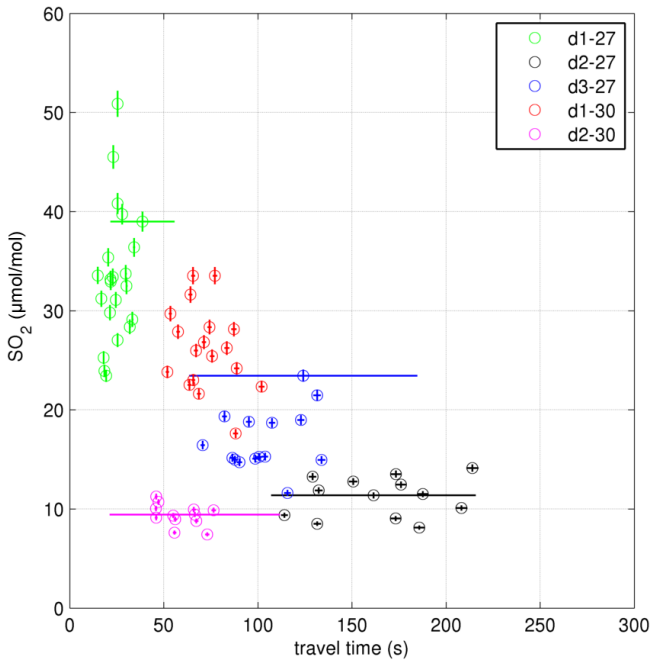

Figure 3.3: SO_2 mixing ratios against calculated processing time at the in-plume measurement sites. Error bars are 1 standard deviation, accounting for both variance in the values over the 120 s of each bin and known errors of the instruments.

3.3 Results

An overview of the near-crater results from this campaign can be seen in Table 3.2. Calculated plume ages were found to be of the order 1–4 min.

The plume was observed to be grounded at all downwind sites, enabling measurement. As both O_3 and SO_2 are known to exhibit deposition to the ground, there is the potential for the mixing ratios of these species at the elevation of the instruments to be perturbed by this physical process. However the ground at the peak of Etna is rocky and devoid of vegetation and could be classed in the scheme of Wesely (1989) as “barren land”. The bulk surface

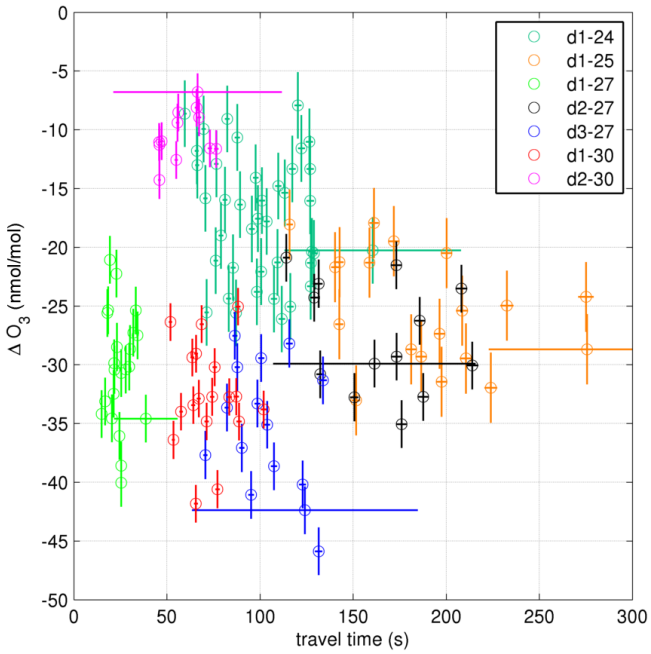

Figure 3.4: ΔO_3 against calculated processing time at the in-plume measurement sites. Error bars are 1 standard deviation, accounting for both variance in the values over the 120 s of each bin and known errors of the instruments.

resistance of this category is sufficiently high that, even if the aerodynamic and sublayer resistances are low, the deposition velocity will be too low to cause a significant perturbation during the transport from crater rim to the measurement sites.[1] SO_2's solubility may result in a slightly increased deposition velocity at high humidity (Wesely, 1989), but the magnitude of SO_2 dry deposition would likely remain at insignificant levels.

Ozone depletion of up to 45 % was observed at all seven downwind sites. SO_2 decreases with transport time (Figure 3.3), as would be expected due to dilution. The low SO_2 mixing ratios at site d2-30 suggest this site was at the plume edge, this is consistent with visual observations of the plume. A plot of ΔO_3 against transport time (Figure 3.4) shows no comparable trend as chemical destruction of O_3 and dilution with background air occur simultaneously.

In Figure 3.5, $\Delta[O_3]$ / $[SO_2]$ vs. transport time is plotted. The negative values increasing in magnitude with transport t are indicative of chemical destruction of O_3 occurring within the first few minutes of plume transport (see Appendix A).

The data in Figure 3.5 appear to fit a linear trend. This indicates, that as a

[1] Specifically, computing Wesely (1989)'s values for "barren land", and assuming nil aerodynamic and sublayer resistances, the deposition velocities for SO_2 and O_3 are 1 and 2.5 mm s^{-1} respectively.

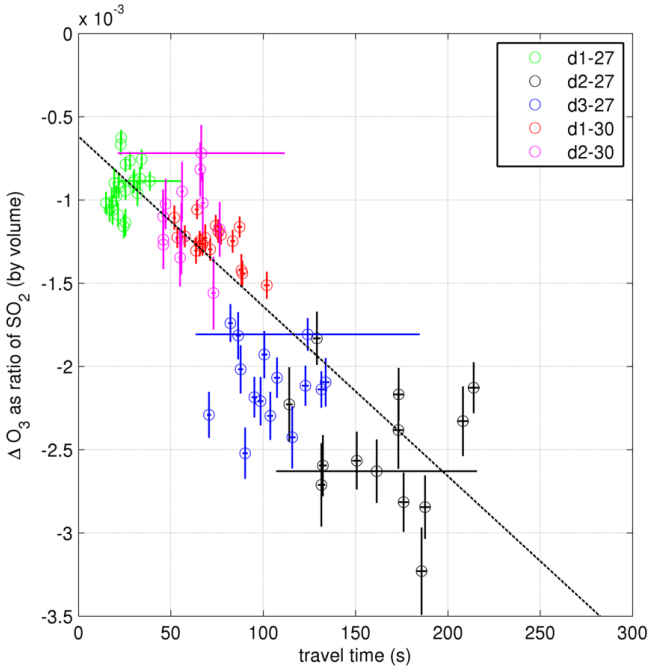

Figure 3.5: ΔO_3 / SO_2 against calculated processing time at the in-plume measurement sites. The gradient of the linear line of best fit is $-(1.02 \pm 0.07) \times 10^{-5}$ s^{-1} and the y-intercept is $(-6.2 \pm 0.5) \times 10^{-4}$. Error bars are 1 standard deviation, accounting for both variance in the values over the 120 s of each bin and known errors of the instruments.

ratio to the inert plume tracer, the rate of chemical O_3 destruction is constant within the first few minutes of plume evolution. In the expected chemical cycles the rate of O_3 destruction is dependant on the concentration of halogens in highly reactive (non-hydrogen halide) forms. Therefore a constant rate of reaction indicates that the ratio of these species to SO_2 is approximately constant during the first few minutes of plume evolution.

The spread of $\Delta[O_3]$ / $[SO_2]$ values increases with transport time, illustrating that the processes involved are not necessarily strictly linear, and that the simplistic calculation of transport time used (for instance assuming straight-line transport) has errors not captured in the determination of the uncertainties.

Depletion of ozone occurred on 30 July even when the relative humidity was <10 %. This is below the crystallisation point of any major aerosol component that would be expected to be present in the plume. It would therefore be expected that at such low humidities aqueous phase reactions would occur at a much slower rate, preventing the bromine explosion from converting HBr to very reactive forms of bromine. On inspection of the humidity measurements (Table 3.2), no significant increase in humidity due to volcanic H_2O was observed at the downwind sites (the humidity variation between

up-24 and d1-24 could be volcanic in origin, however it is also in the range of normal meteorological variability). The possible impacts of a short-lived elevated humidity within the crater due to volcanogenic H_2O are considered with the "dry" model runs in Section 3.4 of this Chapter.

Data points from all measurement sites appear to approximately fit the same line-of-best fit on Figure 3.5. This is despite the measurements spanning two separate days and these two days having very different circumstances. On 27 July the measurements were made in the plume of the North-East crater, and on 30 July the measurements were made in the plume of the central craters. The different craters are known to exhibit differing emission compositions (Aiuppa et al., 2005a). In addition, the relatively humidity on these two days was markedly different. It is unknown whether the cause of these two data sets' approximate alignment in Figure 3.5 is due to mechanistic reasons relating to the "effective source region" (see below) or coincidence.

A linear line of best fit was calculated using a Williamson–York iterative bivariate analysis (Cantrell, 2008), its gradient is $(-1.02 \pm 0.07) \times 10^{-4}$ s^{-1}. The r^2 value of this fit is 0.76. This linear trend can be interpreted as there being a rate of destruction of O_3 within the plume of approximately 10^{-4} molecules per molecule of SO_2 (the inert plume tracer) per second in the first few minutes of plume evolution. SO_2 is only used as a measure of plume intensity, SO_2 does not play a role in O_3 destruction.

Extrapolating the line of best fit on Figure 3.5 results in an intercept of the x axis of approximately -60 s. Assuming chemical O_3 destruction is not instantaneous in the plume, it would be expected that the line of best fit would pass through the origin. We determine that this offset is most likely the result of inaccuracy in the calculation of processing time. Firstly, the calculation assumes that air travels in a straight line between vent and sampling point; however, the path length is likely to be greater than this due to turbulence, the topology of the mountaintop, and variation in wind direction. Second, the distances between vents and sampling points were calculated only from their lateral displacement and did not consider the time taken for vertical transport from the vent to the crater rim. From our visual observations of the plume, we estimate this vertical transport time is likely to have been of the order of a minute.

Table 3.3 lists the composition of volcanic volatiles. These figures are calculated from June 2012 values of SO_2, HF, HCl, and HBr measured using various alkaline traps (Wittmer et al., 2014) (Bocca Nuova crater), as well as

Table 3.3: Fractional composition (by volume) of pure volcanic volatiles of Mt. Etna in June 2012 ("low Br/S") using data from Wittmer et al. (2014) (see text), and in 2005 ("high Br/S"), as used in von Glasow (2010). These compositions were used to initialise the HSC calculations (for results see Table 3.4).

Species	low Br / S	high Br / S
H_2O	8.75×10^{-1}	8.57×10^{-1}
CO_2	9.76×10^{-2}	9.56×10^{-2}
SO_2	1.63×10^{-2}	2.86×10^{-2}
H_2S	8.14×10^{-4}	1.43×10^{-3}
H_2	2.11×10^{-4}	3.72×10^{-4}
HF	2.96×10^{-3}	2.20×10^{-3}
HCl	6.87×10^{-3}	1.43×10^{-2}
HBr	9.99×10^{-6}	7.04×10^{-5}

the MULTIGAS measurements of CO_2 and SO_2 made on the main campaign (using all available data). All measurements were of the plume at the same temperature as the background atmosphere. As complete characterisation of the volcanic volatiles could not be made from the June 2012 measurements alone, the ratio of the gases to CO_2 were used in these calculations with absolute values of H_2O and CO_2 calculated from the values reported in Aiuppa et al. (2005b). Additionally, H_2 / SO_2 was taken from (Aiuppa et al., 2011), and H_2S / SO_2 was calculated from the values reported in (Aiuppa et al., 2005b). These values were then normalised to ensure that the sum equals unity.

The remote sensing results are shown in Table 3.5, along with the correlation between the BrO and SO_2 columns and the estimated plume age (based upon distance from the crater and wind speed, see Sect. 3.2.3). The BrO / SO_2 column ratios are within the range typically measured both in the Etna plume (Bobrowski and Giuffrida, 2012) and volcanic plumes in general (Boichu et al., 2011; Hörmann et al., 2013), though they are at the lower end of these ranges.

3.4 MISTRA modelling study

We used a vertically resolved 1-D numerical model MISTRA to simulate the chemical evolution of the volcanic plume in the atmosphere and to test the model's performance against the data presented above.

The model is the same as used in von Glasow (2010) with minor modifications. This model is *not* the WRF-Chem model discussed in Chapter 2, although it also uses KPP to compute chemical reaction rates and the chemical

mechanism used is similar.

MISTRA is a kinetic model, chemically similar in scope to WRF-Chem. It is unable to compute the very high temperature chemistry of the very early plume, an environment in which many species are atomised and determining which species are formed when such a mixture cools requires a modelling of the thermodynamics of the system. A different model is required to determine this, the output of which is the starting conditions for MISTRA.

Therefore, based on previous work (Gerlach, 2004; Martin et al., 2006; von Glasow, 2010) we used the thermodynamic equilibrium model HSC (Roine, 2007) to calculate the composition of the mixture of volcanic volatiles and ambient air in the "effective source region" which is located in the crater where temperatures are high enough so that the assumption of immediate thermodynamic equilibrium is still largely valid but also enough ambient air has been entrained to oxidise the main volcanic reduced gases (mainly H_2S and H_2) which leads to a dramatic change in halogen speciation. Recent studies (e.g. Aiuppa et al., 2007; Martin et al., 2012) have shown that the assumption of thermodynamic equilibrium is incorrect for a number of compounds, especially for H_2S and NO_x which makes the use of an equilibrium model such as HSC problematic but it is still regarded to provide a better approximation of the composition of volcanic volatiles than not assuming any equilibration. See also related comments in Roberts et al. (2014b). Compared to von Glasow (2010) we used a higher ratio of volcanic volatiles : ambient air (95 : 5), which is very rich in volcanic volatiles but already oxidised. This ratio was chosen empirically, such that the composition of the output roughly matched the limited measurements we have regarding the early plume.

It has been found that, in order to adequately reproduce observations of tracer species (i.e. SO_2) it is necessary to include an empirically-determined "dilution factor" to the HSC output prior to beginning MISTRA calculations. This approach is discussed further in the Materials and Methods section of von Glasow (2010). As an example, the dilution factor used for the "Low Br/S" runs discussed here is 9×, meaning that the model begins with a mixture of 10% HSC output and 90% ambient air. Because of this, the absence of O_3 in output relating to the early plume is not due simply to O_3 being absent from the volcanic output, but is rather an indication of chemical destruction.

MISTRA is run in Lagrangian mode, following the evolution of a "puff" of plume downwind of the volcano and explicitly modelling the interaction of the

plume with background air (see von Glasow, 2010). The modelled wind speed is 10 m s^{-1}, and the plume dispersal is assumed to be Gaussian and follows Kärcher (1999) using the Pasquill–Gifford scheme to calculate the parameters of the Gaussian plume (see e.g. (Seinfeld and Pandis, 2006)).

The S and Br elemental ratios of the volcanic volatiles used in the HSC calculation are taken from the average values measured at the crater rim (Table 3.3, column "low Br / S") on 26 and 27 June 2012. We also did a second set of model runs initialised with a much higher Br / S ratio (Table 3.3, column "high Br / S") based on unpublished data from Alessandro Aiuppa. Table 3.4 gives the composition of the volcanic volatiles and the results of the HSC calculations used as input for the 1-D model. Flourine-containing species are absent from this list, as, being almost entirely present as HF and very unreactive, they were not included in the MISTRA modelling.

The relative humidity varied significantly during the campaign (see Table 3.2), which is important as the bromine explosion is efficient in the presence of aqueous aerosol.

Following Seinfeld and Pandis (2006) a crystallisation humidity of 40 % for sulphate-containing particles is assumed in the model, but other studies suggest sulphate-containing particles to be liquid for lower relative humidities (e.g. Martin et al., 2003).

Regardless of the exact composition and crystallisation humidity of the volcanic aerosol present on the days of this study when simultaneous SO_2 and O_3 measurements were made, we wanted to test the implications of crystallised aerosol in the model. We therefore ran the model at the following three different settings regarding the deliquescence of the aerosol:

1. "moist": relative humidity $\sim$ 57 % (above the sulphate crystallisation humidity assumed in the model); aerosol aqueous phase chemical reactions occur throughout the plume;

2. "dry": relative humidity $\sim$ 21 % (below the assumed sulphate crystallisation humidity); aerosol aqueous phase chemical reactions consequently disabled; exception in the first $\sim$ 1 min, where water from the volcano elevates the humidity within the plume;

3. "noHet": where all heterogeneous chemical reactions were deactivated.

Being remote from major sources of anthropogenic pollution and above

Table 3.4: Initial conditions (in mol/mol) from HSC calculations for the subset of species that have been used in the model runs presented in this paper.

Species	low Br/S[a]	high Br/S[a]
H_2O	8.33-01	8.17e-01
O_2	9.12e-03	1.05e-02
CO_2	9.28e-02	9.09e-02
N_2	3.90e-02	3.90e-02
NO	1.66e-05	2.00e-05
NO_2	4.31e-08	4.19e-08
NO_3	2.72e-15	2.80e-15
HNO_3	7.16e-13	6.02e-13
HONO	1.95e-09	2.00e-09
NH_3	8.36e-15	2.08e-14
SO_2	1.60e-02	2.82e-02
H_2SO_4	2.95e-07	2.96e-07
SO_3	2.32e-04	2.99e-05
H_2S	0.00e+00	0.00e+00
SO	7.40e-10	3.10e-09
H_2S	0[b]	0[b]
O_3	3.43e-13	4.24e-13
CH_4	1.03e-30	1.05e-29
CO	8.23e-08	1.82e-07
HCOOH	4.47e-14	9.17e-14
OH	9.81e-06	1.46e-05
HO_2	2.10e-08	2.65e-08
H_2O_2	3.51e-09	4.34e-09
HCl	6.52e-03	1.36e-02
HOCl	1.56e-07	3.21e-07
Cl_2	3.62e-07	1.29e-06
Cl	5.74e-06	1.51e-05
ClO	1.73e-08	4.05e-08
HBr	7.32e-06	5.08e-05
HOBr	1.75e-10[c]	1.20e-09[c]
Br_2	8.97e-10	2.85e-08
BrCl	3.85e-08	4.08e-07
Br	2.14e-06	1.57e-05
BrO	2.80e-10	2.02e-09

[a] "Low Br/S" refers to volcanic volatile measurements taken in June 2012, "high Br/S" refers to the composition used in von Glasow, 2010. For more details see text.

[b] H_2S has been set to 0., as there are strong indications from field measurements (Aiuppa et al., 2007) that equilibrium models and kinetic models do not capture the chemistry of H_2S. On the times scales considered here, H_2S is considered inert.

[c] Note that HOBr is not included in HSC. It has been calculated from HBr using the HOCl/HCl ratio as determined by HSC.

Table 3.5: Spectroscopic measurements of the Mount Etna plume. These data are also plotted in Figure 3.12. R^2 refers to the correlation of BrO and SO_2 within the measurements.

Date	BrO / SO_2	R^2	Distance (km)	Wind speed (m s^{-1})	Plume age (min)
2012-07-24	0.9 $\times 10^{-4}$	0.94	11	8.7	21
2012-07-24	0.7 $\times 10^{-4}$	0.80	6.3	8.7	12
2012-07-25	1.2 $\times 10^{-4}$	0.66	10.4	6.2	28
2012-07-25	1.3 $\times 10^{-4}$	0.52	6.8	6.2	18
2012-07-26	1.1 $\times 10^{-4}$	0.64	17	9.3	30
2012-07-26	1.0 $\times 10^{-4}$	0.90	8.8	9.3	16
2012-07-27	1.2 $\times 10^{-4}$	0.48	16	22	12
2012-07-28	0.8 $\times 10^{-4}$	0.47	12	13	15
2012-07-28	0.9 $\times 10^{-4}$	0.50	9.0	13	11
2012-07-31	0.6 $\times 10^{-4}$	0.72	5.9	5.7	17
2012-08-02	1.0 $\times 10^{-4}$	0.48	6.0	12	8.1

the planetary boundary layer, the ambient NO_x levels at Etna are expected to be negligible compared to the amount of nitrogen oxides (NO_x) that thermodynamic models such as HSC predict would be formed in the effective source regions of volcanic vents. However Kaschka (2007) and Martin et al. (2012) discussed the problems associated with this, mainly that the time required to reach equilibrium for NO_x under the given temperatures in the effective source region is, by far, too long. The generation of NO_x could significantly perturb bromine chemistry due to the formation of $BrNO_2$ (see e.g. figure 2 in von Glasow, 2010). A detailed discussion of volcanic plume Br–NO_x chemistry, including a modelling study that includes additional $BrNO_2$ reactions, can be found in Roberts et al. (2014b). Use of their scheme would likely result in less bromine being present as $BrNO_2$ and might lead to somewhat different O_3 development. For each of the three aerosol settings described above, two model runs were done – one with volcanic NO_x in the quantities predicted in the thermodynamic model and one with no volcanic NO_x. These six runs were performed for both of the plume initialisations shown in Table 3.3.

3.4.1 "Low Br / S" modelled plume

Model results are shown for the core of the plume which is most appropriate for the grounded plume measured in our campaign. Comparison of modelled and measured plume SO_2 mixing ratios, shown in Figures 3.6 and 3.3, respectively,

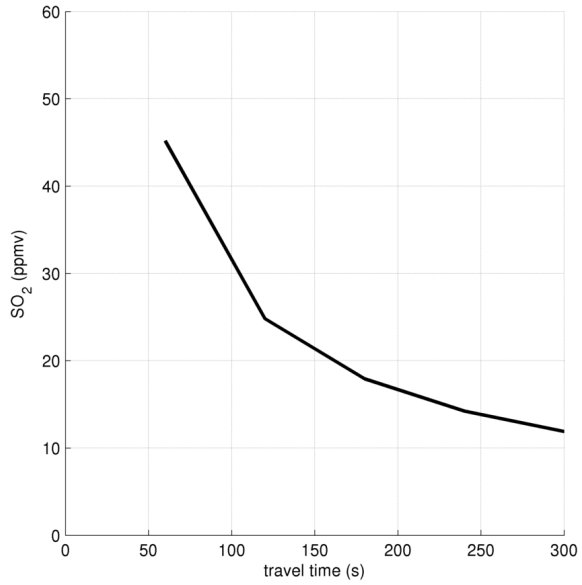

Figure 3.6: Modelled SO_2 mixing ratio in the plume core ("low Br / S" initialisation).

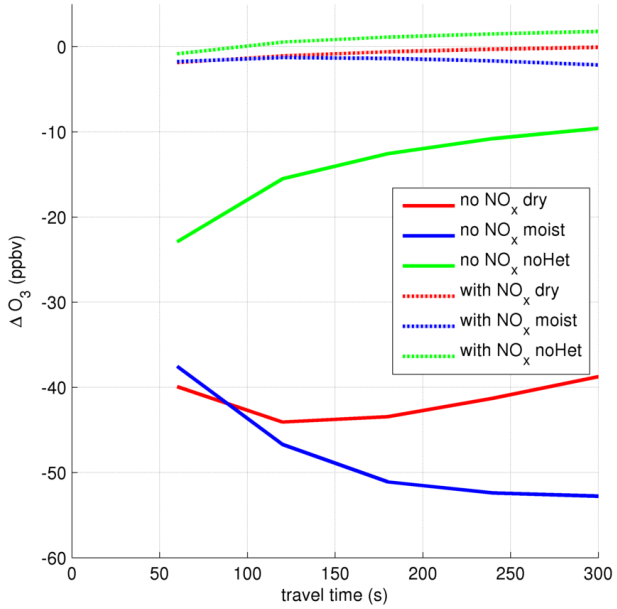

Figure 3.7: Evolution of ΔO_3 in the core of the plume for the six model scenarios discussed in the text ("low Br / S" initialisation).

show the plumes to be of similar intensity. Differences in SO_2 mixing ratio between the six model runs are negligible. In order to approximately reproduce the measured SO_2 mixing ratios at the crater rim, the "initial dilution" ratio of the HSC output with ambient air (see Materials and Methods in von Glasow, 2010) was set to a factor of $9\times$.

The 0–60 s section of the following figures are not plotted as the first data output from the model occurs at 60 s after plume release.

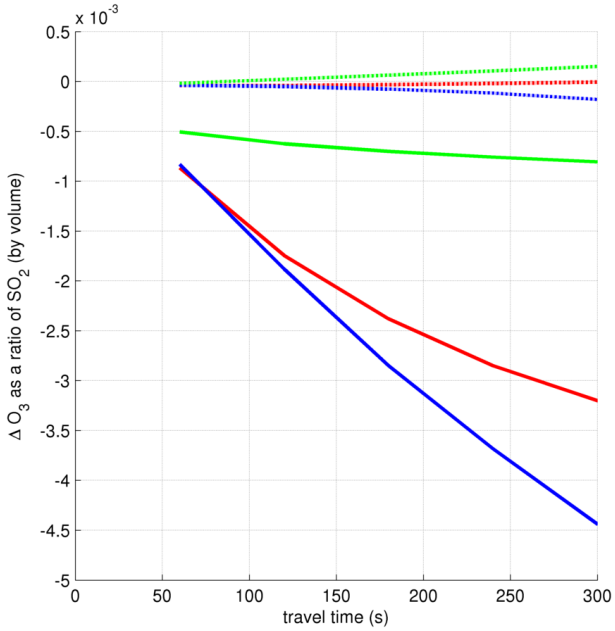

Figure 3.8: Evolution of ΔO_3 / SO_2 in the core of the plume for the six model scenarios discussed in the text ("low Br / S" initialisation). The colour code is the same as in Figure 3.7.

Figure 3.7 shows the modelled ozone depletion in the six runs. Figure 3.8 shows this as a ratio to SO_2 mixing ratio (c.f. Figures 3.4 and 3.5, respectively).

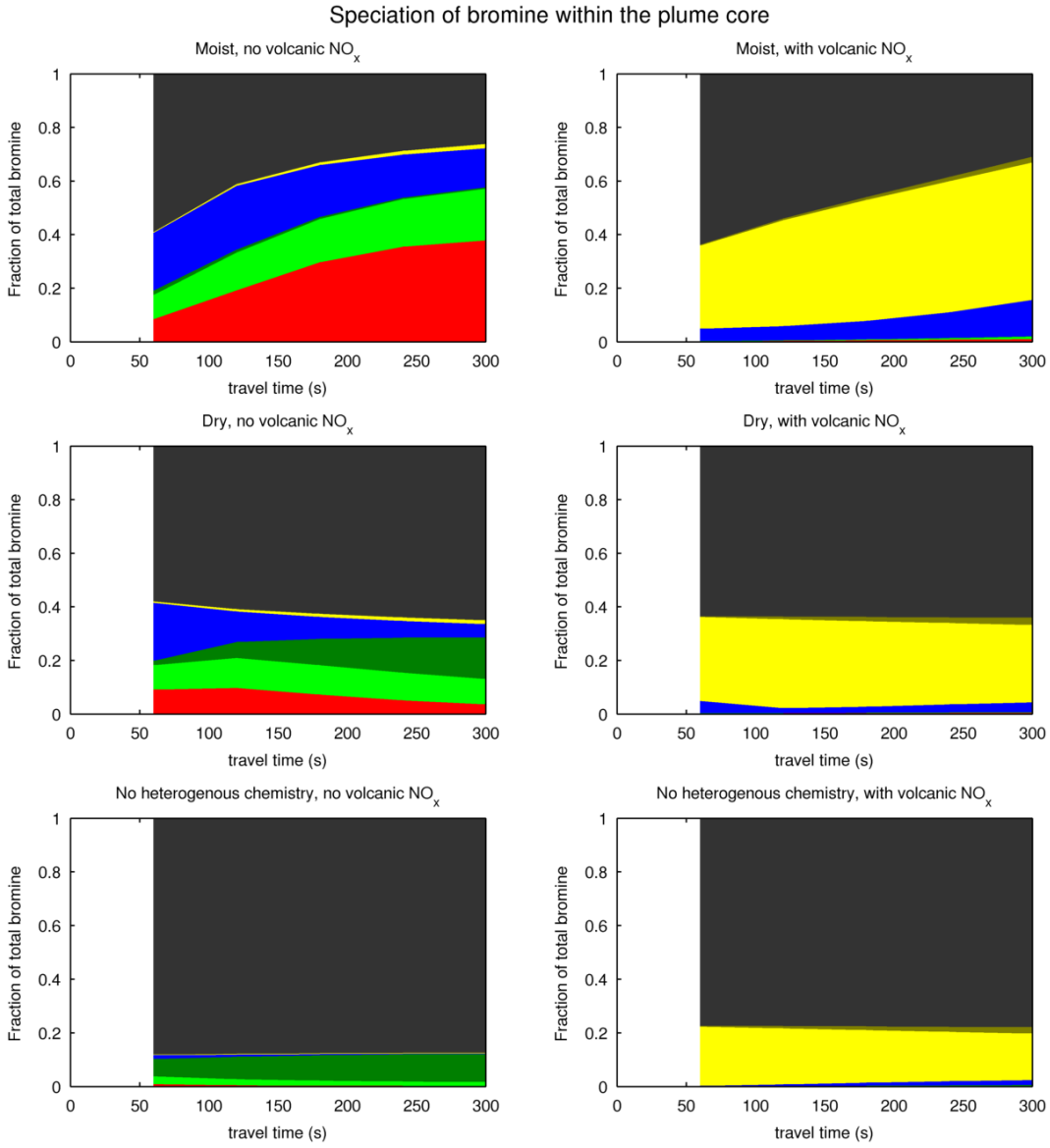

Figure 3.9: Speciation of bromine for the six model scenarios discussed in the text ("low Br / S" initialisation). Red – Br; light green – BrO; dark green - HOBr; blue – Br_2; yellow – $BrNO_2$; brown – $BrNO_3$; black – HBr.

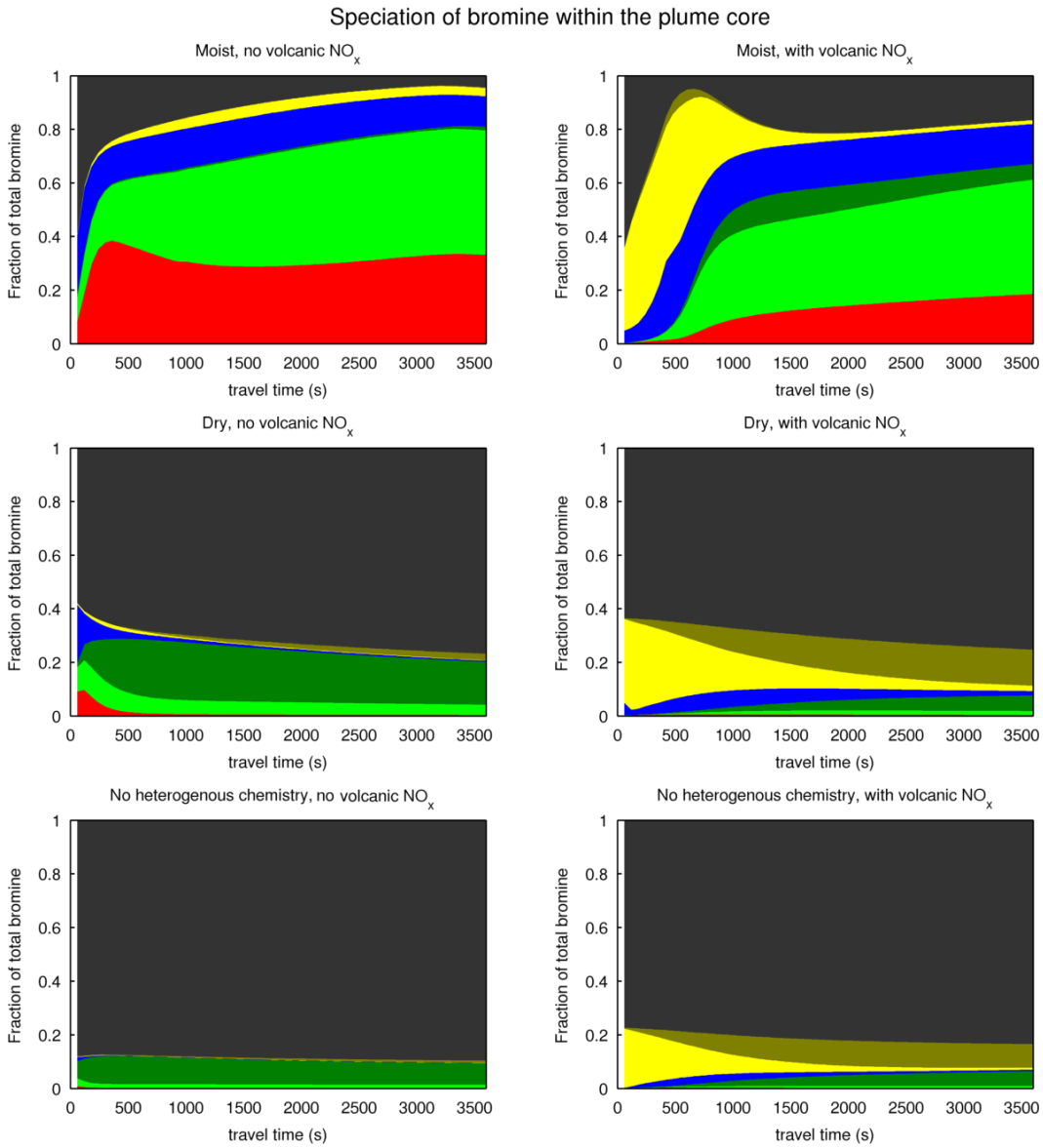

Figure 3.10: As Figure 3.9, extended to 3600 s from plume emission.

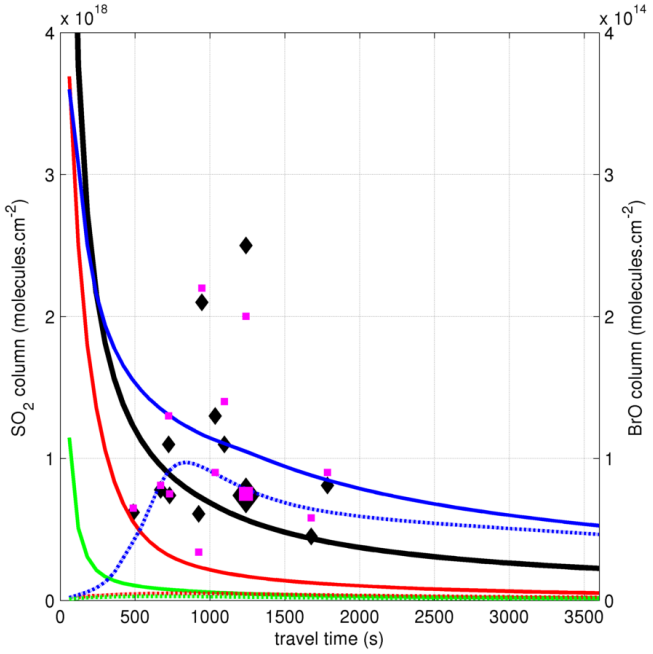

Figure 3.11: Evolution of vertical column SO_2 and BrO for the six model scenarios discussed in the text ("low Br / S" initialisation). SO_2 is plotted against the left axis scale in black (variation between the scenarios is minimal). The BrO columns are plotted against the right axis scale using the same colour code as in Figure 3.7. The black diamonds represent the spectroscopic measurements of SO_2, the magenta squares represent the spectroscopic measurements of BrO. The larger markers represent the 2012-07-27 measurement contemporaneous with near-crater measurements of both O_3 and SO_2.

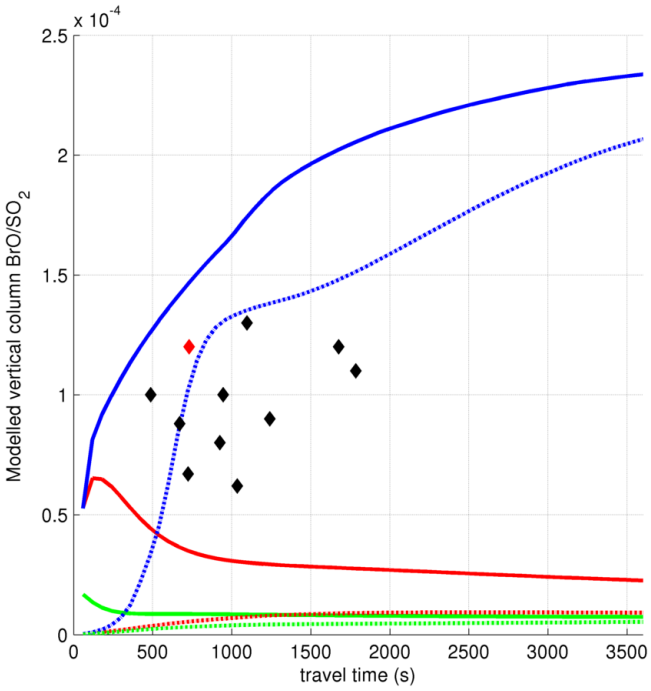

Figure 3.12: Evolution of vertical column BrO / SO_2 ratios for the six model scenarios discussed in the text ("low Br / S" initialisation). The colour code is the same as in Figure 3.7. The black diamonds represent the spectroscopic measurements listed in Table 3.5, the red diamond represents the 2012-07-27 measurement contemporaneous with near-crater measurements of both O_3 and SO_2.

In comparison to the measured data where bromine chemistry at the craters can only be inferred from O_3 and SO_2 data, the modelled bromine chemistry can be investigated directly; Figures 3.9 and 3.10 show the speciation of bromine in the six different runs for the first 300 and 3600 seconds respectively.

In all three runs with volcanic NO_x, the non-HBr bromine almost entirely initially partitions to $BrNO_2$. $BrNO_2$ does not contribute to O_3 depletion. As shown in Figure 3.7, in these runs the net O_3 change is almost zero for all runs and is actually positive in the "noHet" and "dry" cases as a consequence of O_3-generating NO_x chemistry.

The bromine explosion, as evidenced by conversion of HBr to other forms of bromine, can be seen in the "moist" runs and has also occurred between 0 and 60 s of the "dry" run (where volcanic H_2O is modelled to increase the plume's humidity). In the "noHet" runs and in the "dry" runs after the volcanic humidity increase has ended, the processes that convert HBr to other forms are effectively halted.

In all three NO_x-free runs, O_3 is depleted. Reactive bromine is generated by the high-temperature processes of the effective source region in all three runs. In the "moist" case, and to a slightly reduced extent in the "dry" case, this is supplemented by the generation of reactive bromine species via the bromine explosion, to the extent that in the "moist" case the O_3 depletion is near 100 %. The consequences of these three runs' differences in bromine chemistry can be seen on Figure 3.8, where the $\Delta[O_3]$ / $[SO_2]$ ratios diverge over the first few minutes.

A comparison of the O_3 depletion (Figures 3.7 and 3.8) after 60 s for the "noHet" run with that for the "dry" and "moist" runs shows the comparative influence of different processes within the crater. The ozone depletion in the "noHet" case must be due to reactive halogen generated in high temperature processes as heterogeneous reactions are required for low-temperature reactive bromine generation (the bromine explosion). The additional ozone depletion at 60 s in the "dry" and "moist" cases can therefore be attributed to the bromine released via the bromine explosion within the crater. As the plume moves away from the crater, the heterogeneous bromine explosion can only occur in the "moist" run so the increasing differences between the "moist" and "dry" runs are due to the continued bromine explosion in the "moist" run.

The model results can also be used to calculate vertical columns of BrO and SO_2 (Figure 3.11) and the corresponding ratios (Figure 3.12). These figures show

these data over the first 60 min of plume evolution and are also overlayed with the spectroscopic observations listed in Table 3.5. Due to logistical constraints, we have concurrent near-crater and downwind data only for 27 July; this datapoint is highlighted on Figure 3.12. As can also be seen in Figure 3.9, only the "moist" runs maintain significant amounts of volcanic bromine as BrO in the early plume and show column BrO / SO_2 ratios (Figure 3.11) comparable with measurements.

Also notable is the rise in the column ratio in the "moist-withNO_x" run after a few minutes. After significant dilution of the plume has occurred, the dominance of the $BrNO_2$ reservoir diminishes. This is evident on the "moist-withNO_x" plot of Figure 3.10, the speciation eventually tends to a similar state to the equivalent "no-NO_x" plot. Volcanic NO_x, if present, delays but does not prevent in-plume reactive bromine chemistry.

In the "moist no-NO_x" case, the 'far field' behaviour (after a few minutes, as seen on Figure 3.10) is mostly a continuation of that of the first 300 seconds, HBr continues to be converted to more reactive forms (though this rate slows as HBr becomes exhausted). In this case there is a change in behaviour at about 300 s, where Br begins to decline as the BrO:Br ratio shifts. In both the "moist" modelled cases, a substantial proportion of bromine exists as BrO an hour after emission.

The "dry" and "nohet" Figure 3.10 shows that without heterogeneous chemistry, no significant bromine cycling occurs and HBr remains stable. Without volcanic NO_x the rest of the bromine accumulates as HOBr, whereas with volcanic NO_x it exists as $BrNO_2$ which slowly transitions to $BrNO_3$. As the plume dilutes, there is a slow transition to the non-N-containing species seen in the equivalent "no-NO_x" output, though this transition is only partial after an hour.

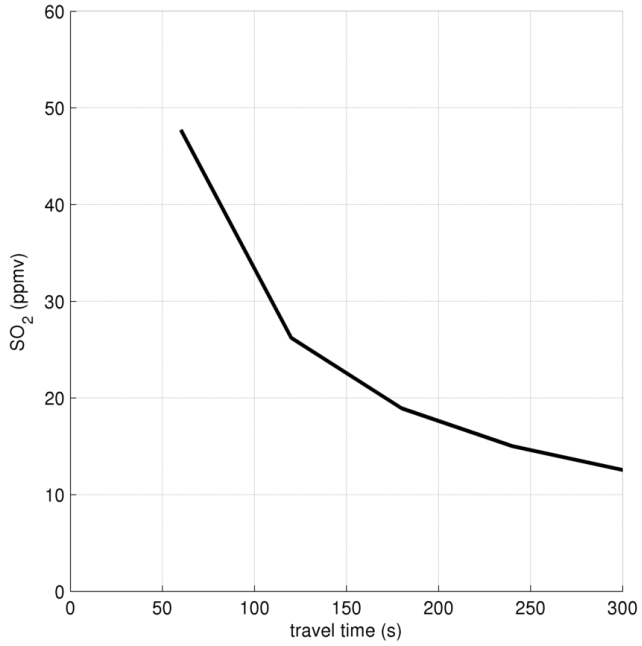

Figure 3.13: Modelled SO_2 mixing ratio in the plume core ("high Br/S" initialisation).

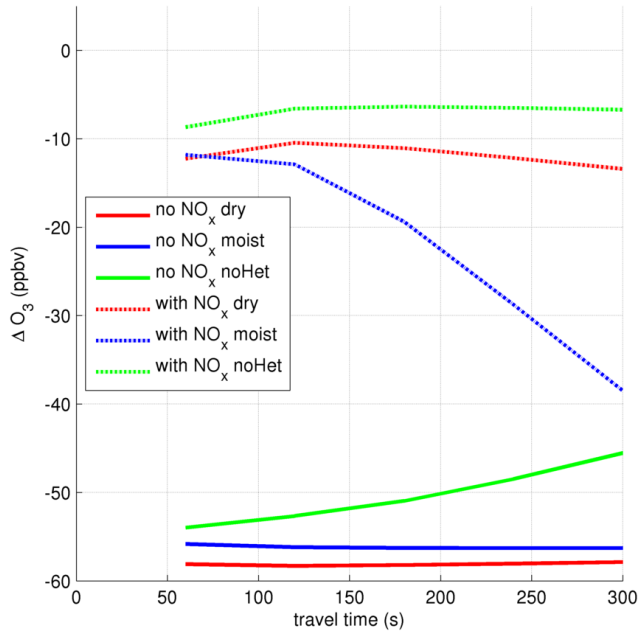

Figure 3.14: Evolution of ΔO_3 in the core of the plume for the six model scenarios discussed in the text using the "high Br / S" initialisation. The colour code is the same as in Figure 3.7.

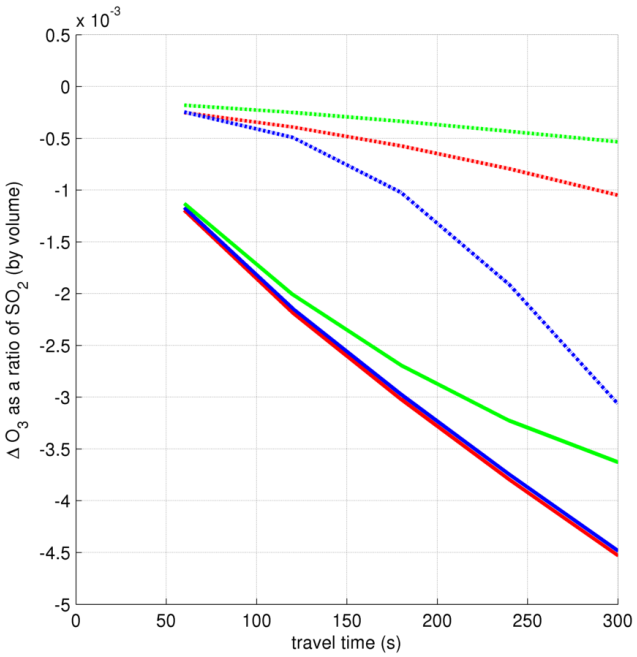

Figure 3.15: Evolution of $\Delta O_3/SO_2$ in the core of the plume for the six model scenarios discussed in the text ("high Br/S" initialisation). The colour code is the same as in Figure 3.7.

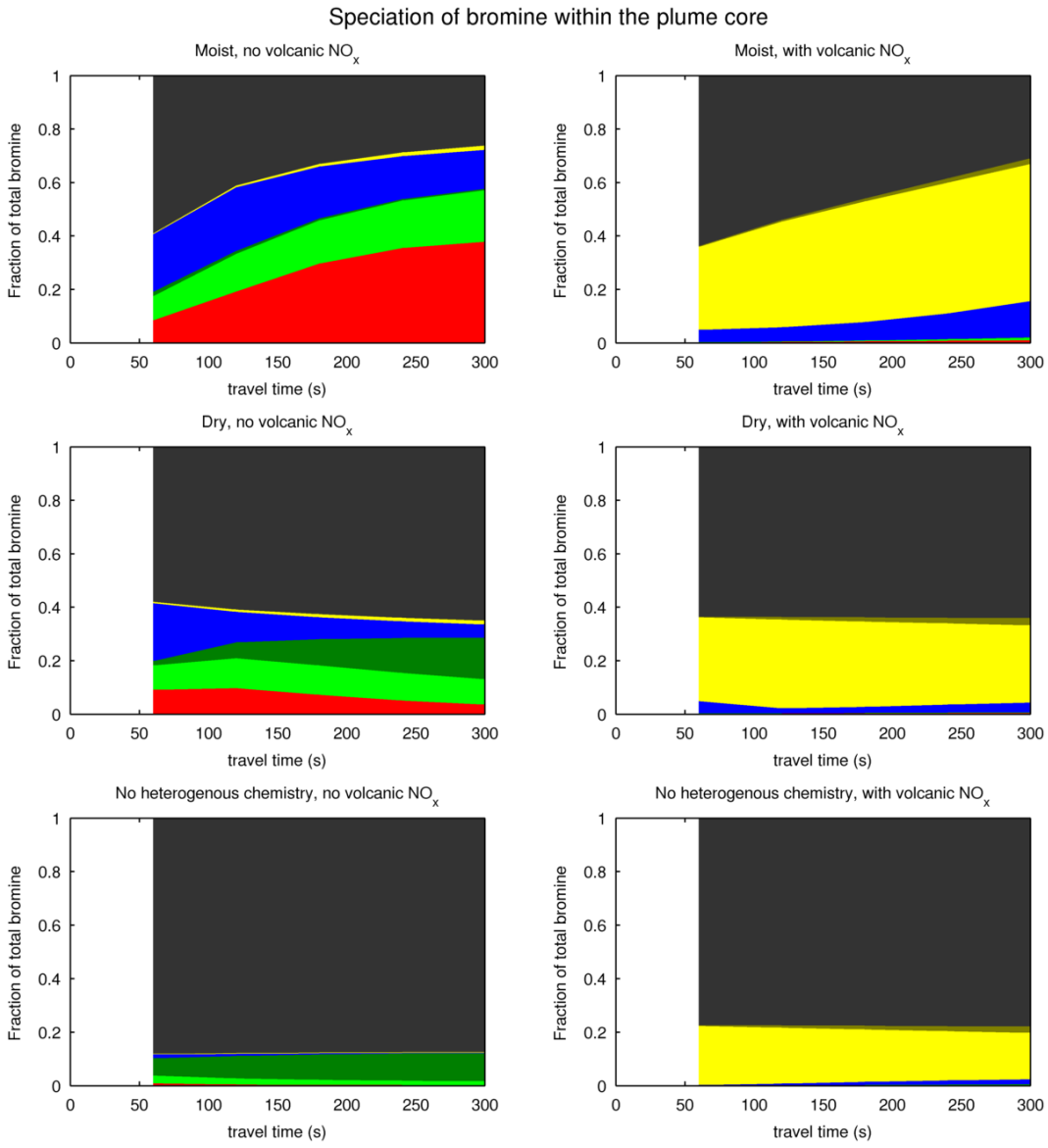

Figure 3.16: Speciation of bromine for the six model scenarios discussed in the text ("high Br/S" initialisation). The colour coding is the same as for 3.9.

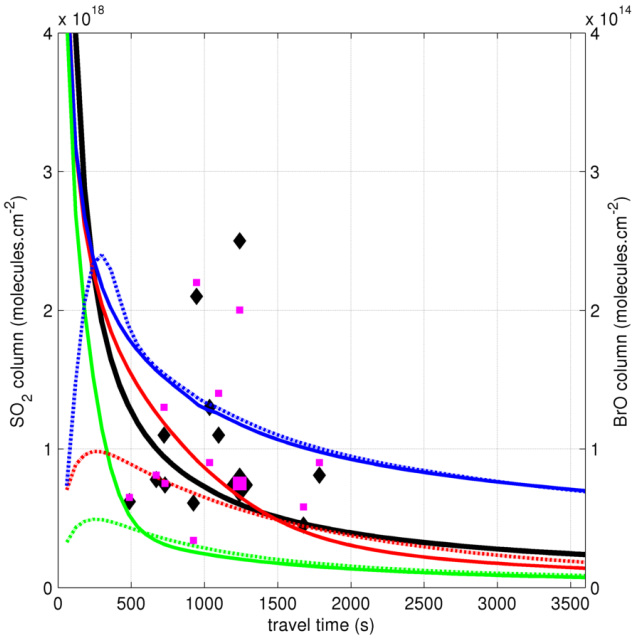

Figure 3.17: Evolution of vertical column SO_2 and BrO for the six model scenarios discussed in the text ("high Br/S" initialisation). SO_2 is plotted against the left axis scale in black (variation between the scenarios is minimal). The BrO columns are plotted against the right axis scale using the same colour code is the same as in Figure 3.7. The black diamonds represent the spectroscopic measurements of SO_2, the magenta squares represent the spectroscopic measurements of BrO. The larger markers represent the 2012-07-27 measurement contemporaneous with near-crater measurements of both O_3 and SO_2.

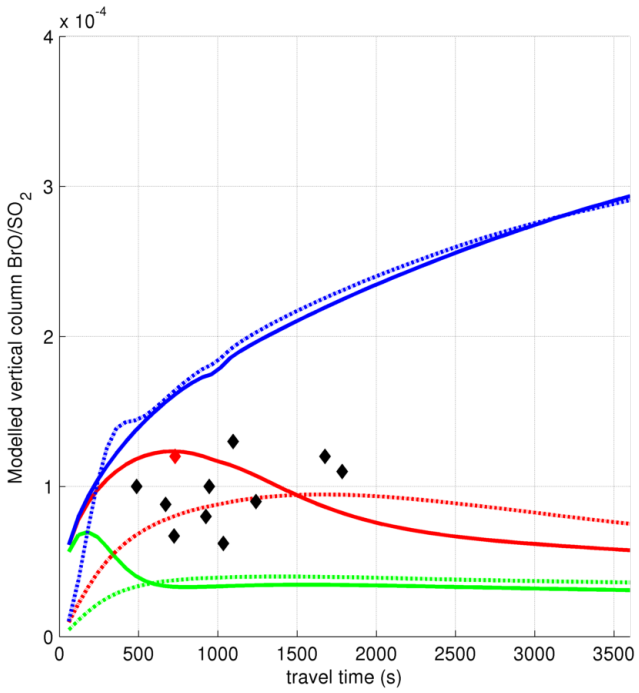

Figure 3.18: Evolution of vertical column BrO/SO_2 ratio for the six model scenarios discussed in the text ("high Br/S" initialisation). The colour code is the same as in Figure 3.7. The diamonds represent the spectroscopic measurements, the red diamond represents a measurement contemporaneous with near-crater measurements of both O_3 and SO_2.

The elemental emissions ratio of Etna is known to vary between craters and over time (Aiuppa et al., 2005a). Figures 3.14–3.18 show the evolution of the plume chemistry for the six runs where they have been initialised using the "high Br / S" ratios (see Table 3.3). As for the runs described previously, in order to approximately reproduce the measured SO_2 mixing ratios at the crater rim (and those from the prior runs) an "initial dilution" ratio was again used, in these runs it was set to a factor of 15× dilution.

The increase in the amount of volcanic bromine has a significant impact on the chemistry. In the NO_x-free runs the reactive bromine generated by the effective source region is sufficient to destroy almost all of the O_3 within the plume and the plume chemistry is O_3-limited. As can be seen in Table 3.4, the NO_x / S ratio is very similar for the "low Br / S" and "high Br / S" cases. As a consequence the Br/NO_x is very different, being 0.0875 in the "low Br / S" runs and 3.35 in the "high Br / S" runs. Whereas in the "low Br / S" runs with volcanic NO_x almost all reactive Br had partitioned to $BrNO_2$, in the corresponding "high Br / S" the partitioning of the reactive bromine to $BrNO_2$ is more moderate and a significant amount of reactive bromine in other forms remains. This results in moderate O_3 depletion in the early plume, with similar variation between the humidity cases as discussed above.

3.4.2 Comparison with measured data

This modelling study shows that the plume chemistry is highly sensitive to several factors: the presence of volcanic NO_x, the magnitude and composition of the primary volcanic emissions, and heterogeneous processes which are dependant on aerosol and humidity. Any comparison between the model results and the measurements must be made with caution. The following points should be stressed:

- Volcanic volatile Br / S ratios are known to vary considerably both over time and between Etna's different craters (Aiuppa et al., 2005a). The composition of the volcanic volatiles used in the "low Br / S" modelling study was based on measurements which were taken a month prior to the O_3 and SO_2 measurements. It is unknown how the emissions may have changed in the intervening period, and comparing the results with the two different initialisations shows that variations in volatile composition can be very significant.

- As measured by Salerno et al. (2009), the magnitude of emissions from Etna can change significantly on a timescale of days. Though less detectable, subterranean changes in the type of material comprising the magma and fluids coming to the surface over these timescales cannot be discounted. Therefore over the time that measurements were taken, the magnitude and composition of the volcanic emissions may have varied significantly. This cannot be reproduced in the model.
- We focussed on model output from the plume core. However, the varying wind velocity at the measurement sites mean that sampling will have been from varying parts of the plume.

As such it is not possible to conclude definitively from the comparison of the measurement and modelling studies the exact chemical processes that were occurring within the plume at the time of the measurement campaign. Nevertheless, the modelling study shows that the reactive bromine generated in the effective-source region is sufficient to cause appreciable ozone depletion within the early plume, however the effect is stronger and more sustained when further reactive bromine can be generated by the bromine explosion.

The model runs which are the best fit for the near-crater O_3 and SO_2 measurements are not the same runs which best match the BrO / SO_2 columns measured further downwind. This is a discrepancy which highlights the need for further investigation into plume chemistry and the relationship between in-plume bromine, NO_x and humidity.

3.5 Conclusions

In this study of chemical evolution in the plumes of Mount Etna during a passively degassing phase we have confirmed O_3 depletion to occur less than a few minutes after emission. This extends the limited data set regarding volcanic O_3 depletion and is the first data set to date based on ground-based data to include simultaneous measurements of O_3 and a plume tracer. The depletion process is ongoing over this time period, and the data suggests it occurred at an approximately constant rate. For the Etna craters measured in late July 2012, this rate was found to be a depletion of approximately 10^{-4} molecules of O_3 per molecule of SO_2 (the inert plume tracer) per second.

Substantial depletion of O_3 was observed within minutes after emission,

and occurred at very low humidities at which the heterogeneous processes of the bromine explosion would be significantly slowed. On the basis of this, an approximately constant rate of ozone depletion (as a ratio of the inert tracer), and analysis of our modelling study we conclude that most of the very reactive halogens that caused the observed O_3 depletion within the 1–4 min old plume were not a product of chemical cycling in the plume once it had emerged from the crater but rather generated in *effective source regions* near the vents in high-temperature processes that ceased shortly after emission, and/or very fast low-temperature chemical processes within the crater. This is in agreement with the thermodynamic modelling studies of Gerlach (2004), Martin et al. (2009), and von Glasow (2010) which predict oxidised halogens being produced by high-temperature effective source regions in volcanoes. The in situ measurements in this study were taken at distances less than 500 m from the vents. Measurements of BrO / SO_2 at such distances tend to be low compared to those measured further downwind (Bobrowski et al., 2007; Boichu et al., 2011). That substantial O_3 depletion can occur in such regions suggests these low levels of reactive bromine (and possibly chlorine) species that are generated within the crater are sufficient to cause the O_3 depletion observed in this study.

We have also shown that further downwind, contemporaneous spectroscopic observation of the plume shows BrO /SO_2 columns are within the typical range that has been observed within volcanic plumes. Our near-crater measurements are therefore likely to be typical for Mount Etna in its passively degassing phase.

Results from our modelling study suggest that a significant factor influencing the bromine-ozone chemistry in the very early plume is the presence or absence of volcanic NO_x and, if it is present, its source strength relative to that of Br. The modelling study shows that volcanic NO_x would be expected to significantly retard early O_3 depletion and therefore plume O_3 and Br data could be compared to model output to yield information on NO_x within a plume. Notably, the modelling showed that this NO_x delays but does not prevent the reactive bromine chemistry discussed, so measurements addressing this issue would need to be in the early plume. The measured data from this campaign are insufficient to definitively ascertain whether or not volcanic NO_x generation is occurring but it appears unlikely to be the case as near-crater O_3 depletion was observed whilst volcanic NO_x emissions suppressed such O_3 depletion in the modelling study.

The modelling study also shows how variations in humidity, and the

consequent variations in heterogeneous chemistry, may impact the plume chemistry in detectable ways. A comparison of the results from our three different humidity/heterogeneous chemistry cases gives an indication as to the extents that O_3 depletion can be ascribed to reactive halogens generated in high-temperature processes within the crater, low-temperature processes within the crater, and low temperature processes further downwind. When heterogeneous chemistry occurs, the modelling study shows a substantial proportion of bromine exists as BrO for an extended period of time, at least up till an hour after emission, which would be several km from the vent.

Other uses of field campaign data in this document

Some data collected as part of this field campaign, including some data not used in this Chapter's analysis, has been used elsewhere in this document:

1. Section 4.3.3 uses meterological observations made on 30 July and 1 August.
2. Section 4.4.2.1 uses O_3 observations made upwind from the volcano on 30 July and 1 August.
3. Section 4.4.2.2 uses aerosol observations made upwind from the volcano on 30 July and 1 August.
4. Appendix B uses aerosol observations made within the volcanic plume on 28 July.

Chapter 4

Model assessment

4.1 Introduction

Having described the WRF-Chem model and modifications made to it in detail (Chapter 2), I now proceed with its implementation as a research tool. In this and the following chapters I report results generated from a simulation using WRF-Chem to model a plume from Mount Etna. These results are analysed and I consider what can be concluded about the chemistry of volcanic plumes from these.

Before discussing the results of the model that pertain to the research questions (subsequent chapters), I assess in this chapter to what extent I can be confident that model is a reasonable simulation of the physical world. A model is said to have "skill" if it is adequate to the task of simulating the processes and phenomena of reality. This is generally assessed by comparing model output to corresponding measured data. It is also useful to check that model output does not show phenomena that are patently non-physical, or otherwise differing greatly from theoretical expectations.

I have in all cases below focussed on data and theory that relates to altitudes of approximately 1.5–5 km. This is the part of the lower free troposphere were the Mount Etna plume is predominantly located.

The skill of the model in regard to meteorology is discussed in Section 4.3, in Section 4.4 it is discussed in regards to the background atmospheric chemistry and aerosol, and in Section 4.5 it is discussed in regards to volcanic phenomena.

Although this model is intended to be a reasonable simulation of reality, it is inevitable that this model falls short of perfection in this regard. There are

several reasons for this, including a lack of data required to precisely constrain the model inputs, computational limitations, limitations in the theory the model employs (both qualitatively and quantitatively), as well as the general limitations of any model of physical reality.

These limitations are acceptable as a high-fidelity model of Mount Etna at a specific time is not required for this investigation; I am seeking to understand in a broader capacity the chemical mechanics of volcanic plumes. The intention is that the conclusions of this document are applicable to volcanic plumes of similar character worldwide, and not just the specific eruption of Mount Etna modelled. Additionally, most of my conclusions are based on differences between model runs with and without the plume, which would negate minor errors in background chemistry and physics.

Qualitative and order-of-magnitude comparisons to modelled data are made in this Chapter for purposes of validation. By showing that the model reproduces the major features of volcanic plume chemistry that are known from measurements, I demonstrate the model's skill, hopefully giving the reader confidence that the conclusions which are outside the domain of measured results have reasonable validity.

4.2 Output interpretation techniques

The following subsections of this introduction are general notes about the methodology used to interpret the model output. Several of these techniques are used to produce the figures in this chapter and also in the subsequent chapters of this document.

4.2.1 Computing differences between runs

Because the purpose of this investigation has been to assess the impact of the plume on the environment, it has often been instructive to run the model twice for a given scenario, once with the volcano emitting normally, and a second with no volcanic output. By comparing the difference in species' concentrations between the two cases, the impact of the plume can be isolated. This is calculated either as an absolute difference (Equation 4.1), or a computation of the relative concentration (expressed as a percentage) of one run compared to

another (Equation 4.2).

$$\Delta[A] = [A]_1 - [A]_0 \tag{4.1}$$

$$r = \frac{[A]_1}{[A]_0} \times 100\% \tag{4.2}$$

When computing the absolute difference between the ratios of two species [A]:[B] in two cases, it has been found to be more informative to report the ratio of the absolute differences of the two species rather than the difference between the ratios in the two cases (Equation 4.3).

$$\frac{\Delta[A]}{\Delta[B]} = \frac{[A]_1 - [A]_0}{[A]_1 - [A]_0} \tag{4.3}$$

4.2.2 Tracer1 - a measure of plume intensity

It is common in volcanology for SO_2 to be used as an 'inert' tracer for volcanic intensity. Observations suggest it performs well as a plume tracer, at least for the first few hours after emission (McGonigle et al., 2004). However SO_2 is not a wholly inert gas, it is removed from the atmosphere by deposition processes (Wesely, 1989) and is oxidised by OH radicals (Seinfeld and Pandis, 2006). In addition, because SO_2 is emitted from anthropogenic sources, and is present at low-levels in the atmospheric background, it is not an absolutely ideal plume tracer. SO_2 is sufficiently inert to be an adequate tracer for the investigations in Chapter 3 where the timescales involved are of the order of minutes, however in this part of the investigation the timescales involved are longer, and adding an artificial fully inert tracer is straightforward, of minimal computation expense, and useful.

In the model a truly inert tracer is used, this is referred to as "tracer1", which is given the characteristics of an ideal volcanic plume tracer. This modelled tracer does not correspond to any real-world species. The initial and boundary concentrations of the tracer are set to zero, and the only source is the volcano. It is also absolutely inert, with no chemical or physical sinks. The tracer is treated by the WRF-Chem system as a gas-phase species and is transported accordingly, however as it is absolutely inert it has no impact on any other species.

Tracer1 can therefore be used to indicate the location of volcano-influenced air (the plume) and distinguish between where the plume is weak and strong. By the same logic as was used to justify the meaning of the O_3/SO_2 ratio in Chapter 3, values of the volcano-induced change in a species' ratio to tracer1

can be used to isolate chemical perturbations from transport effects.

The volcanic flux of tracer1 is set in the input file. For simplicity I have chosen to set it to be the same as the flux of SO_2, however this setting is essentially arbitrary.

4.2.3 Tracer2 - a track of plume age

A second tracer used in the model, tracer2, is identical to tracer1 in almost all respects: it also reacts with no "real" species, has zero background concentration, has no physical sinks, and is emitted only by the volcano. Its flux is set to be the same as that of tracer1.

The difference between the two tracers is that tracer2 has a small first order decay rate, k, which can be exploited as outlined below. The value of k chosen is arbitrary.

Because tracer1 and tracer2 are emitted at the same rate in the same location, and therefore have identical downwind transport, the ratio of the two species would be 1:1 if it were not for the decay of tracer2. The ratio of [tracer2] to [tracer1][1] in any grid box in the plume is a simple function of the time elapsed since the tracers were emitted (t), and thus a simple function of the ratio yields this time:

$$[tracer2] = [tracer1]e^{-kt} \tag{4.4}$$

$$\frac{[tracer2]}{[tracer1]} = e^{-kt} \tag{4.5}$$

$$\ln \frac{[tracer2]}{[tracer1]} = -kt \tag{4.6}$$

$$\frac{1}{k} \ln \frac{[tracer1]}{[tracer2]} = t \tag{4.7}$$

Therefore, as k is known, and [tracer1] and [tracer2] are output by the model, it is possible to use Equation 4.7 to compute t, the age of the plume, for every plume-containing grid cell. This is an extremely useful piece of information and has been used throughout this document. Henceforth, wherever "plume age" is used in a plot or discussion regarding model data it has been calculated by the above method.

[1] Here *[X]* is used to mean *the concentration of X*.

4.2.4 Plume weighted averages

Using tracer1, one can determine from the model output for a particular time where the plume is located and the relative intensity of the plume in different grid boxes. By taking an average of a parameter weighted by the modelled concentration of tracer1 in each grid box (normalised such that the sum weighting of the entire plume is 1), a weighted average value of the parameter can be computed.

This can be combined with the plume age calculation from Section 4.2.3. Grid boxes are binned into age bins 0–1 hours, 1–2 hours, etc., and then a weighted average is taken for each bin. Plotting these produces figures where for a specific time of day the difference between plumes of different ages is shown.

4.2.5 Pseudo-Lagrangian tracks

WRF-Chem is a Eularian model, and doing a truly Lagrangian track of an air parcel is not possible. However it is possible to exploit the calculation of plume age in successive output to track a plume air mass.

An air mass which falls in the age bin α–$(\alpha + 1)$ hours at time t can be expected to fall into the age bin $(\alpha + 1)$–$(\alpha + 2)$ hours at time $(t + 1)$. Doing weighted averages as in Section 4.2.4 and extending this over several successive model outputs, it is possible to compute a series of values representing the same part of the plume as it ages, advects downwind, evolves chemically, and entrains background air.

4.3 Meteorology

There is a limited amount of data which the modelled meteorology in the zone of interest can be compared against. The majority of meteorological data is collected at ground level, which predominantly corresponds to the boundary layer. In this section I compare the model output to the few data which are available. In each of the following subsections there is a discussion of the data products and plots showing relevant comparisons of these data to model output. The assessment of the model's meteorological skill is made in section 4.3.5.

In this section I consider four different sources of data with which WRF's output can be compared:

- Reanalysis products
- Balloon soundings
- Data collected as part of the field campaign of Chapter 3
- Data from a flight campaign

4.3.1 Reanalysis products

The most comprehensive data products which model output could be quantitatively compared against are reanalysis products. These assimilate large amounts of observational data and the output of highly-skill Numerical Weather Prediction models in order to produce global fields with values for various parameters. The FNL Final analysis product (NCEP, 2000), which is used in this investigation for the WRF model's initial and boundary conditions is one such product.

In this subsection I compare WRF model output with output from the NCEP/NCAR Reanalysis 1 project.[2].

By operational necessity, reanalysis datasets are of low resolution, this dataset has a $1° \times 1°$ spatial resolution. One of the primary functions of regional models such as WRF is to focus on a region of interest, and produce a more detailed and more accurate forecast or hindcast than a global model is capable of. Assessing WRF by comparing its output to an global analysis product is therefore of limited utility, as it would be difficult to assess whether any differences that occur are due to errors in WRF, or WRF outperforming the lower-resolution model. Because the initial and boundary meteorological conditions of the model are set to values from a similar product, agreement does not necessarily indicate a high degree of model skill. This exercise is one of *validation* (checking the model has sufficient skill required for this investigation) rather than *verification* (checking the model results are "true"). In this exercise I am checking for anomalies in the model output.

Figures 4.1–4.5 plots side-by-side meteorological output from both the WRF model and this reanalysis product. For temperature and humidity I have selected 700hPa, as this is approximately the pressure at the top of Mount Etna. Also shown are 500hPa geopotential height and sea-level pressure, common

[2]NCEP Reanalysis Derived data provided by the NOAA/OAR/ESRL PSD, Boulder, Colorado, USA, from their Web site at http://www.esrl.noaa.gov/psd/

parameters used in assessing synoptic scale meteorology. Each plot is an average of all output relating to 2012-07-30 – 2012-08-01.

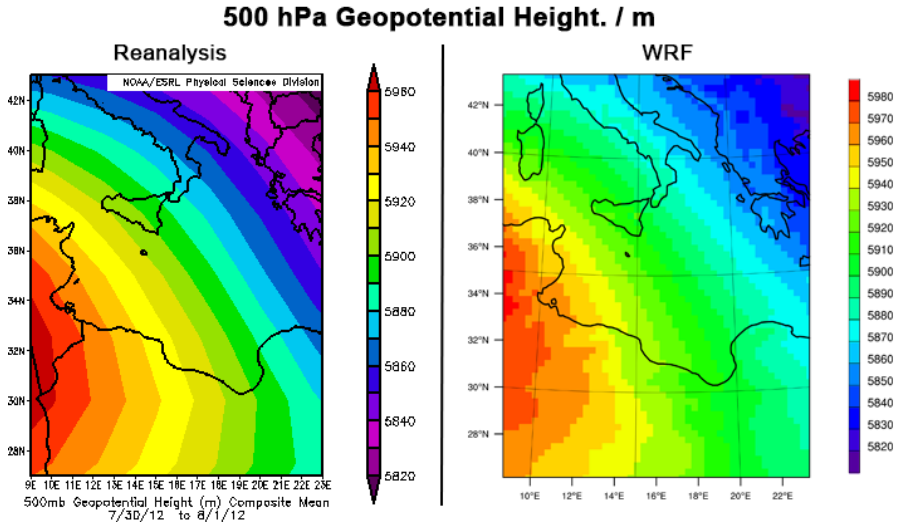

Figure 4.1: Comparison of the reanalysis product and WRF's values for 500 hPa geopotential height (average over 2012-07-30 – 2012-08-01 period)

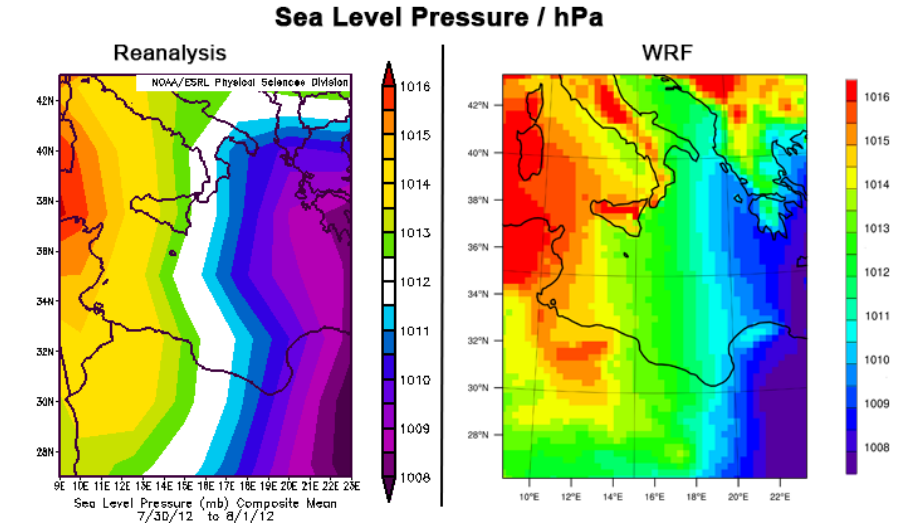

Figure 4.2: Comparison of the reanalysis product and WRF's values for sea-level pressure (average over 2012-07-30 – 2012-08-01 period)

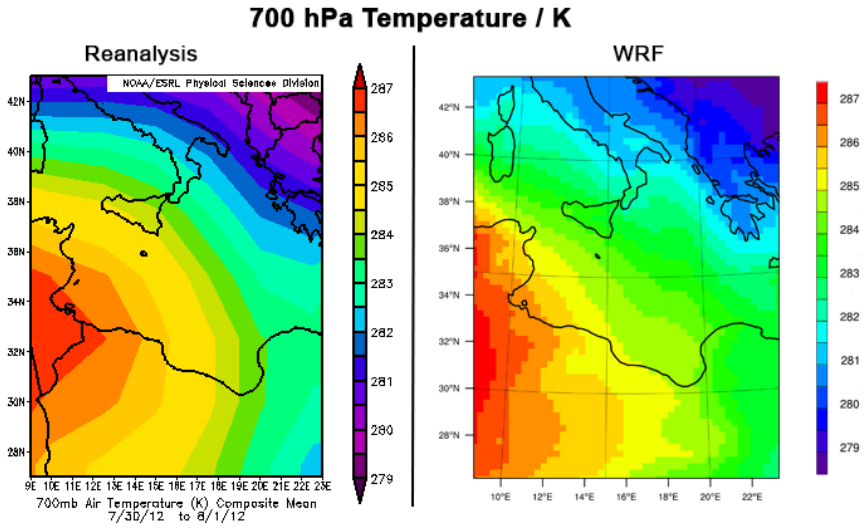

Figure 4.3: Comparison of the reanalysis product and WRF's values for air temperature at 700 hPa (average over 2012-07-30 – 2012-08-01 period)

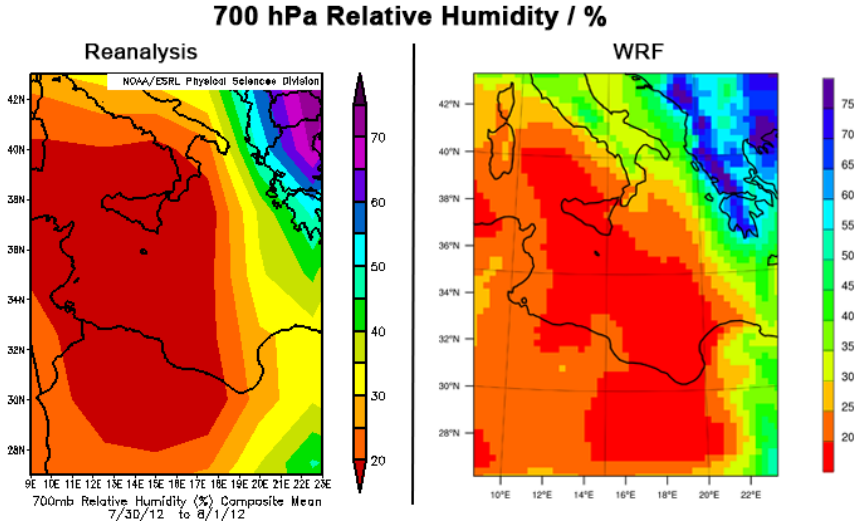

Figure 4.4: Comparison of the reanalysis product and WRF's values for humidity at 700 hPa (average over 2012-07-30 – 2012-08-01 period)

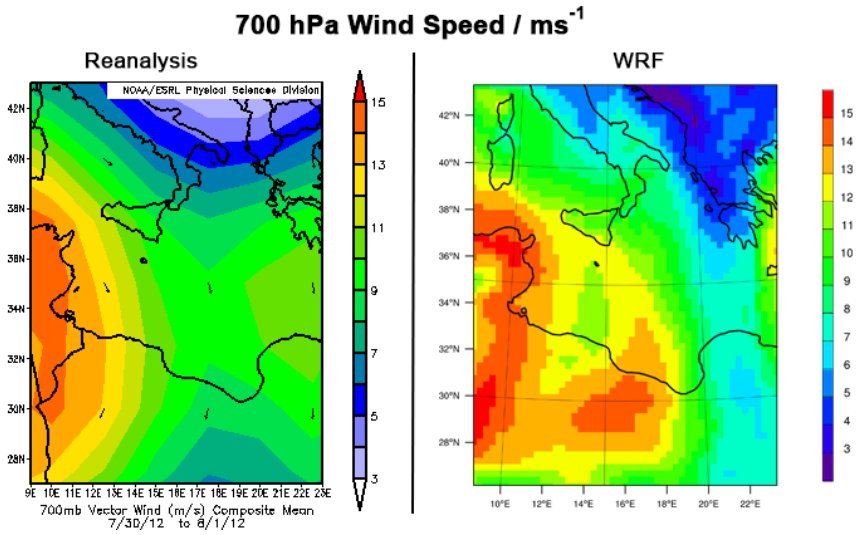

Figure 4.5: Comparison of the reanalysis product and WRF's values for wind speed at 700 hPa (average over 2012-07-30 – 2012-08-01 period)

Figures 4.1–4.5 show a high degree of agreement between the reanalysis product and the WRF output. Both output show a high pressure system to the west and low pressure to the east, resulting in moderate (approximately 10 m s^{-1}) northerly/north-easterly winds around Sicily. Both outputs agree that the area of interest is very dry, with average 700 hPa relative humidities of below 30%. Regarding temperature, the two outputs show similar values, and both show the same phenomenon of a warm south-east and and cooler north-west.

Both WRF and the reanalysis product show no precipitation south of Sicily for this period (not plotted).

Although there are some differences, there is a fair degree of agreement between these two outputs. I therefore conclude that the WRF output passes this verification test.

4.3.2 Balloon sounding from Trapani

The most widely available data for the altitudes of interest to this investigation come from balloon soundings. Such balloons are released at ground level, and are able to reach the mid-stratosphere, collecting data as they rise. The soundings discussed in this chapter report pressure, temperature, humidity, wind speed, and wind direction for multiple different altitudes.

The closest balloon sounding site to the volcano is Trapani (37.91°N, 12.50°E; the opposite site of the island (approx. 200 km) of Sicily from Etna). Soundings are made at midnight and noon (UTC) each day.
The data that is used in this section is taken from the University of Wyoming database (http://weather.uwyo.edu/upperair/sounding.html). This data can be compared with the equivalent model output. In this section, it will be assumed that all data from a particular sounding can be compared to model output relating to the latitude, longitude and time of launch. Although the balloons are likely to have drifted laterally slightly, and will have taken some minutes to reach the heights of interest, this exercise is focussed on atmospheric phenomena which are unlikely to be highly localised or subject to rapid change, and therefore these discrepancies should not be significant.

I compare in Figure 4.6 the observations and model output relating to altitudes of 1.5–5 km, as this is the range at which the plume is predominantly located.

These results show good agreement between the model and the observations

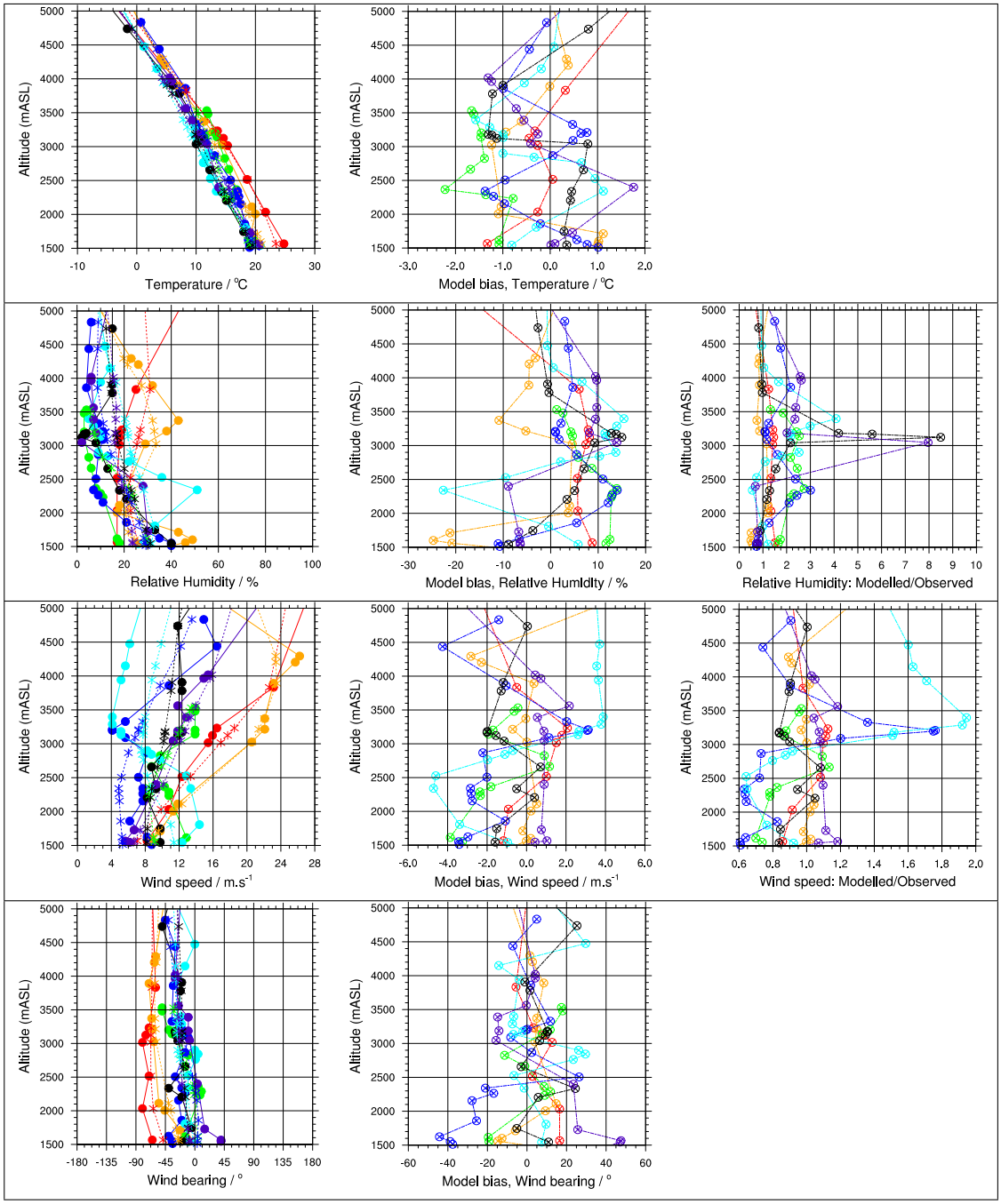

Figure 4.6: Meteorological parameters from Trapani balloon soundings, and corresponding model output. Both sets are plotted separately in the plots of the left column, the model bias is displayed on the plots of the central column, and computed as a fraction of the observations (where mathematically meaningful) on the plots of the right column.
In all plots the following colour coding distinguishes between different times: red – 2012-07-30 00:00:00; orange – 2012-07-30 12:00:00; green – 2012-07-31 00:00:00; blue – 2012-07-31 12:00:00; cyan – 2012-08-01 00:00:00; black – 2012-08-01 12:00:00; magenta – 2012-08-02 00:00:00.
In the left column plots: solid lines and circular markers — observational data; dashed lines and cross markers — model output.

in regard to temperature. The lapse rate (decrease in temperature with altitude) is similar in both and the calculated model bias (for all observations less than 2.5 K) is too small to cause significant errors in the model chemistry calculations.

The model mostly predicts greater relative humidities than are observed, with a typical bias at 3 km altitude of approximately +10 %. Despite this, both agree that the environment is dry, with relative humidities mostly less than 30 %. The model profiles of humidity show less variation with altitude than the observations, failing to reproduce measurements of extremely dry air masses.

The measured wind speed profiles is generally within 3 $m.s^{-1}$ of the modelled values. In the lower half of the altitudes of interest the model appears to have low bias, with no clear bias in the upper half.

In terms of direction, both data sets report north to north-easterly winds. There is moderate disagreement between the datasets, but no overall bias either clockwise or anticlockwise. At 3 km altitude, the model and observations agree to within approximately 20°.

4.3.3 Data from 2012 field campaign

The field campaign discussed in Chapter 3 collected basic meteorological data. This data is limited geographically to the peak of Mount Etna, and covers only the few hours of each morning when data was collected. However this data is particularly pertinent to this investigation, both because it was collected at the plume source, and because observational data at this altitude is extremely sparse.

Table 4.1 below compares the average values of the meteorological parameters measured at the different sites in the field campaign (which overlap with the time of the modelling). All these meteorological datasets are taken from the measurements of the tripod-mounted small weather station (the Kestrel instrument). The corresponding model output relating to the peak of Mount Etna (37.755°N, 14.995°E). As WRF outputs are instantaneous values on each hour, the most appropriate output is tabulated.

Table 4.1 includes three measurement sites which were chosen to intercept the volcanic plume. Although the volcano is a source of water vapour, as discussed in Chapter 3, this is not expected to have significantly perturbed the humidity at sites d1-30 and d2-30, there is no clear sign perturbation in the field campaign humidity data.

Table 4.1: Observed and modelled meteorological parameters at the peak of Mount Etna

Site	Date	Time (UTC)	Model timestep	WS / $m.s^{-1}$		WD / °		T / °C		RH /%	
				Obs.	Mod.	Obs	Mod.	Obs	Mod.	Obs.	Mod.
up-30	2012-07-30	09:12–09:34	2012-07-30 09:00:00	9.7	15	304	323	12	11	<5	28
d1-30	2012-07-30	10:05–10:43	2012-07-30 10:00:00	2.2	14	298	321	16	11	6	27
d2-30	2012-07-30	11:07–11:41	2012-07-30 11:00:00	4.4	13	307	309	15	12	5	25
up-01	2012-08-01	08:42–09:10	2012-08-01 09:00:00	2.2	4	299	298	9	10	10	42

WS: wind speed; WD: wind direction; T: temperature; RH: relative humidity

As in the previous comparisons, the model appears to perform well with regard to temperature and wind direction.

Compared to these observations, the model appears to perform poorly with regard to wind speed. However the observational data here was collected at ground level, in irregular terrain with high relief which is likely have had a frictional effect upon the wind, whereas the model output represents a larger, $1 \times 1°$, area. For the purposes of this investigation it is neither feasible nor necessary for WRF to resolve ground-level wind phenomena on such scales.

The model does appear to model the relative humidity poorly, failing to reproduce the extreme dryness observed.

4.3.4 Flight data

Contemporaneous with the field campaign, in the mornings 2012-07-30, 2012-07-31, and 2012-08-01 a research aircraft was flown in the vicinity of Mount Etna, with the purpose of intercepting the plume and gathering data from within it. These data were measured as part of the the Global Mercury Observation System project (GMOS, www.gmos.eu) by the Helmholtz-Zentum Geesthacht (HZG, www.hzg.de) and the Consiglio Nazionale delle Ricerche (CNR, www.cnr.it).

The flight paths are shown in Figure 4.7. As well as data for plume intersections, I also have data for the rest of the flights, including transport to and from the volcano area.

Chemical and meteorological data were collected during the flights. "Temperature" refers to the temperature of the inlet. The chemical data is used in section 4.4 for validation of the modelled chemistry.

Each point of data collected has an associated latitude and longitude,

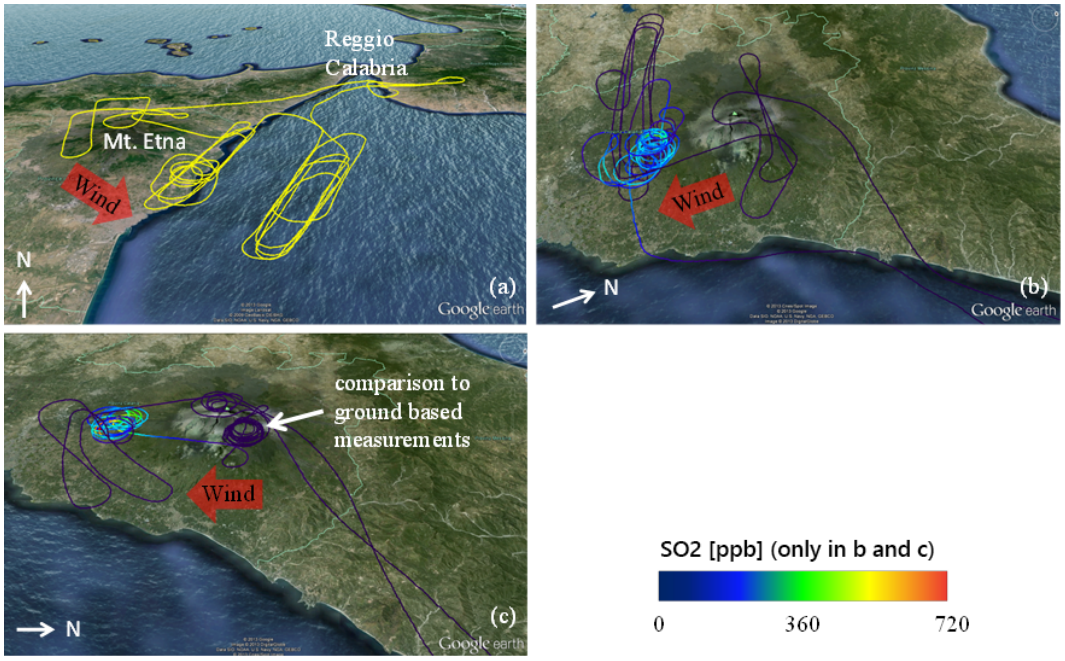

Figure 4.7: Flight track of the aircraft on July 30 (a), July 31 (b) and August 01, 2012 (c). While Fig. (a) shows only the flight track, the colour of the flight track in (b) and (c) indicate the measured SO_2 concentration. This image has been provided by Andreas Weigelt of the Global Mercury Observation System project and has been taken from an unpublished manuscript. The "comparison to ground-based measurements" label refers to mercury-related observations that are not part of this document.

altitude, and time. This allows the corresponding model output to be looked up. Data is associated with nearest model output time (model output is hourly), and the lateral grid cell which contains its latitude and longitude. Vertical interpolation between the two nearest grid points in that column is used to determine a value for each parameter. All data plotted below corresponds to altitudes between 1.5 km and 5.0 km.

In Figures 4.8 and 4.9 below, the model's predictions for temperature and humidity are plotted against the observed values of those parameters.

The flight did not collect wind speed or direction data. It is however possible to indirectly assess the wind direction by using SO_2 measurements to determine where the aircraft intersected the plume. It can be reasonably assumed that the vast majority of SO_2 detected by these flights are volcanic in origin. For each observation, the bearing of a line connecting the peak of Mount Etna to that point of observation can be calculated (Figure 4.10). The bearing with the highest SO_2 concentration is taken as an estimate of the wind direction. In Figure 4.11, the SO_2 concentration is plotted against the bearings for each of the

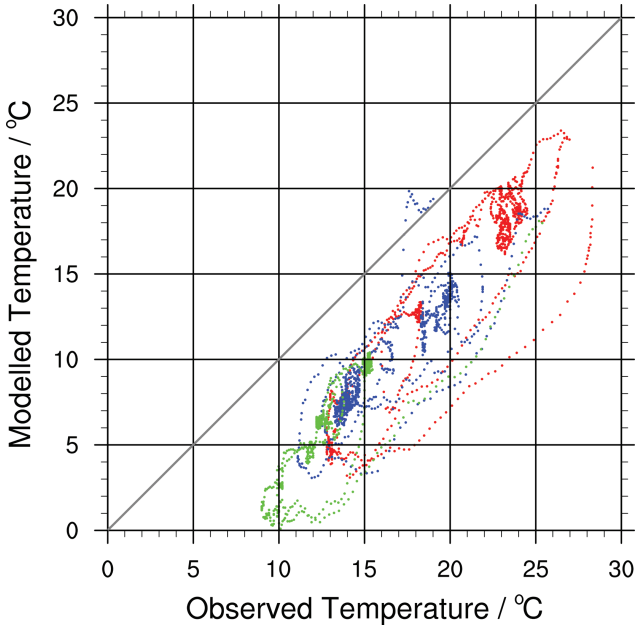

Figure 4.8: Modelled vs. observed temperature corresponding to the research aircraft flights. Red – 2012-07-30; blue – 2012-07-31; green – 2012-08-01.

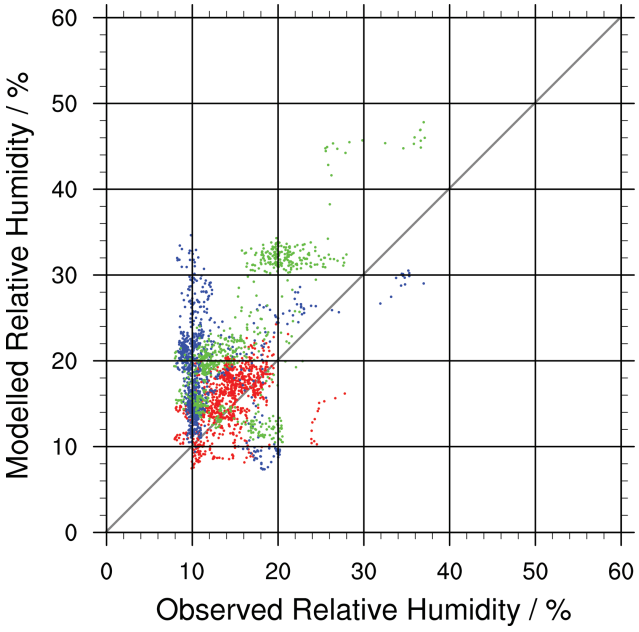

Figure 4.9: Modelled vs. observed relative humidity corresponding to the research aircraft flights. Colour-coding is the same as Figure 4.8

flight datasets. The modelled data is processed in a similar manner to generate Figure 4.12. The modelled SO_2 is plotted against the bearing (calculated in the same manner as above) for all model grid boxes which have a lateral distance from Mount Etna's peak of between 10 and 45 km (this is the approximate range of distances for which the aircraft intercepted the plume) and correspond

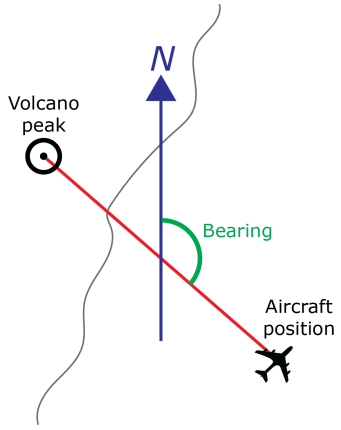

Figure 4.10: Methodology for calculation of bearing of volcano.

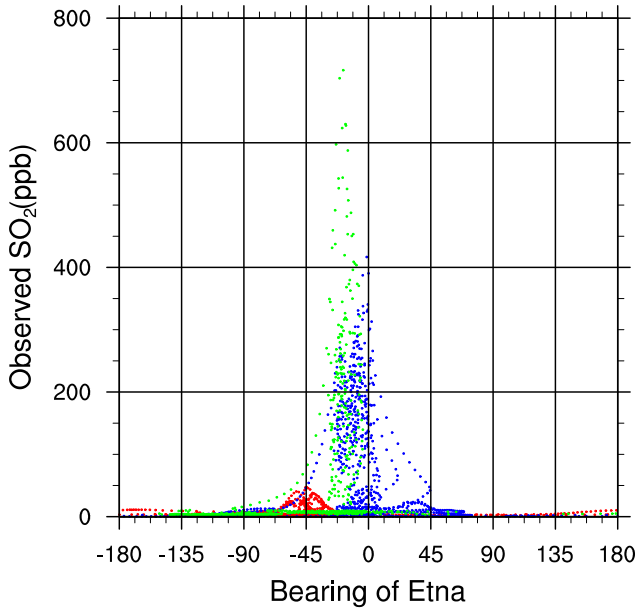

Figure 4.11: Observed SO_2 from the research aircraft flights vs. bearing of peak of Mt. Etna. Colour-coding is the same as Figure 4.8.

to altitudes between 1.5 and 5 km. Model output relating to 2012-07-30 08:00:00, 2012-07-31 08:00:00, and 2012-08-30 07:00:00 is used — these corresponding to the approximate mid-points of the time of the three flights.

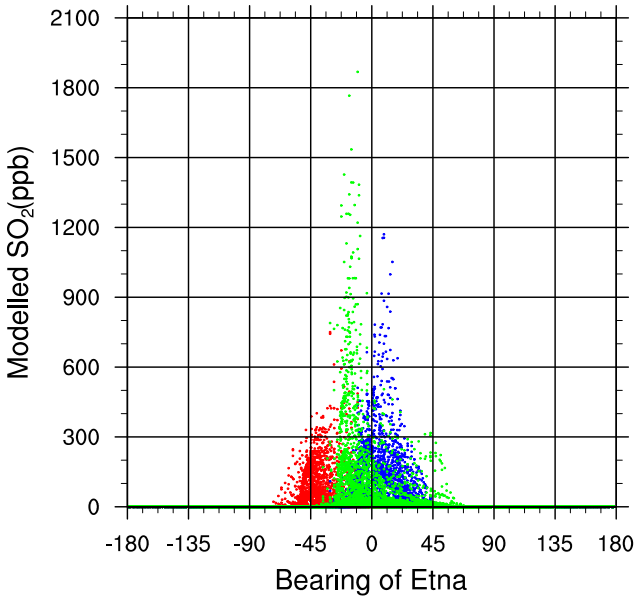

Figure 4.12: Modelled SO_2 vs. bearing from peak of Mt. Etna. Red – 2012-07-30 08:00:00; blue – 2012-07-31 08:00:00; green – 2012-08-01 07:00:00. These colours correspond to the equivalent observational data plotted on Figure 4.11.

The observations of temperature in Figure 4.8 but are typically 5K warmer than the corresponding model output (although the overall correlation is strong). Because the other verifications in this section suggest that the model performs well with regard to temperature, I determine here that this offset is likely due to an error in the observational dataset.

There is less correlation between the two datasets regarding humidity. The model mostly reports more moist values than the flight observations. Although the level of agreement is generally poor, both datasets agree that the environment is quite dry, with almost all datapoints in both datasets below 35% relative humidity.

For all three days the model and the observations agree to within a few degrees as to the direction in which the plume is blown.

4.3.5 Assessment

Overall, these comparisons have shown reasonable levels of agreement between the model and verification datasets regarding the meteorology.

The model appears to perform well regarding the overall synoptic situation in the area and time of interest, reproducing a system which generates a moderate north to north-easterly wind over Sicily. The meteorological situation

during the modelled time period is quite "simple", with minimal cloud or precipitation, and no weather fronts in the region of interest.

The representation of temperature and wind appears to show reasonable qualitative agreement. The discrepancies between the model output and these validation datasets are small enough that, if these do indeed represent errors, the effect upon the chemistry is likely to be small— differences of a few degrees will not significantly change the rates of most reactions.

There are greater discrepancies with regard to humidity. The model and these datasets may be considered to have qualitative agreement, both agreeing that the area of interest is dry during the modelled time period. Quantitatively however there are significant discrepancies. The model appears to have a high bias with regard to humidity, failing to reproduce very low humidity observations. Atmospheric humidity regulates aerosol growth and the production of OH radicals in the $O^1D + H_2O \longrightarrow 2\,OH$ reaction, thus this apparent error in the model's meteorology may cause errors in the chemical systems studied in this investigation.

4.4 Background chemistry and aerosol

This section will assess the quality of the modelling of the 'background' chemistry, i.e. that which is not perturbed by the plume. It is important for this to be reasonably accurate, as the composition of the air entrained by the plume will impact its evolution. To avoid complication by plume effects, all of the model output in this section is taken from a model run where the volcanic flux has been set to 0 for all species.

In comparison to the meteorological assessment above, there is even less data to compare against the modelled chemistry. Measurements of a small number of species were collected as part of the field and aircraft campaigns, and those measurements which are outside of the plume can be compared against the emission-free model run to assess its skill. As well as these direct comparisons with observations, I compare some model output with an atmospheric chemistry reanalysis product—a similar validity check to that I perform for meteorology in Section 4.3.1

Table 4.2: Average mixing ratio at 700hPa of various trace gases in the modelled area. Values from MACC reanalysis and WRF-Chem model.

Time	SO_2 / ppt		CO / ppt		HCHO / ppt		NO_x / ppt		O_3 / ppb		CH_4 / ppm	
	MACC	WRF	MACC	WRF	MACC	WRF	MACC[1]	WRF	MACC	WRF	MACC	WRF
2012-07-30 00:00:00	52.6	68.1	115	96	380	335	51.8	116	54.7	63.7	1.79	1.77
2012-07-30 06:00:00	40.5	52.6	117	94	372	371	53.7	87.7	53.7	61.9	1.79	1.77
2012-07-30 12:00:00	49.8	62.7	117	93	393	495	59.5	58.3	52.6	59.8	1.79	1.77
2012-07-30 18:00:00	56.6	96.4	117	93	406	440	65.3	70.0	53.6	59.5	1.79	1.77
2012-07-31 00:00:00	41.1	94.8	117	92	383	422	57.3	50.5	56.4	61.6	1.79	1.77
2012-07-31 06:00:00	33.8	89.4	117	92	372	408	63.0	71.6	59.8	64.0	1.79	1.76
2012-07-31 12:00:00	30.5	67.4	116	91	331	377	59.3	73.8	60.6	66.3	1.79	1.76
2012-07-31 18:00:00	29.4	63.4	114	90	336	367	66.6	84.0	62.4	67.0	1.79	1.76
2012-08-01 00:00:00	32.1	53.8	112	89	323	348	47.4	55.6	63.2	67.9	1.79	1.76
2012-08-01 06:00:00	25.9	52.2	111	88	302	328	45.4	70.7	63.0	67.7	1.79	1.76
2012-08-01 12:00:00	18.1	49.7	112	87	265	340	52.6	69.1	61.8	66.5	1.79	1.76
2012-08-01 18:00:00	28.7	59.7	111	87	312	340	58.9	71.3	60.9	65.1	1.79	1.76

[1] The MACC dataset reports mass ratios (kg species/kg dry air), which have been converted to volume mixing ratios for this table using the species' molecular masses. For MACC's NO_x values a molecular mass of 46 (the RMM of NO_2) has been assumed. As some daytime NO_x exists as NO, some of the volume mixing ratios in this column will be slightly too low.

4.4.1 Reanalysis product

The MACC reanalysis of global atmospheric composition (Inness et al., 2013), referred to herein as MACC, is a reanalysis product from ECMWF. It is similar to the reanalysis product discussed in Section 4.3.1, however it has outputs for the mixing ratios of some trace gas species. Output is available on a $1.125° \times 1.125°$ grid with a temporal resolution of 6 hours.

In this section I compare MACC output of SO_2, CO, HCHO, NO_x, O_3, and CH_4 with the equivalent output from the WRF model. This comparison has the same issues as were discussed for the similar exercise performed for meteorological fields in Section 4.3.1, and again this exercise is one of validation rather than verification.

The comparison of mixing ratios of these species is shown in Table 4.2. This table shows average mixing ratios at 700hPa (the approximate pressure level of Etna) across the modelled area from both MACC and WRF. Overall, the level of agreement between MACC and WRF-Chem is high. There are no obvious anomalies in these data. The WRF-Chem values are generally indicative of moderately more polluted air than that implied by the MACC values, however the differences are not sufficient to suggest there is an error with the chemistry of the WRF-Chem that would seriously impact this investigation.

The largest relative differences are seen in the SO_2 data, where for some timesteps the WRF-Chem mixing ratio is over twice that of MACC. However the main part of this investigation concerns volcanic plumes, wherein background SO_2 is dwarfed by volcanic SO_2 rendering such differences insignificant.

4.4.2 Data from field campaign

During the field campaign, aerosol and O_3 were measured. The observations on 2012-07-30 and 2012-08-01 coincide with the time of modelling and therefore can be used for this exercise. The observations made upwind of the volcano can be compared with the background chemistry model predictions for these parameters at that time. This section uses a similar approach to the atmospheric chemistry as is performed for meteorology in Section 4.3.3.

Field observations were also made of SO_2, however the MULTIGAS was set up for measuring very high SO_2 mixing ratios (in the plume). Observations at the background sites were below the limit of detection and are therefore not useful for this exercise.

4.4.2.1 Ozone (O_3)

Table 4.3 compares the observed O_3 at the background sites with the corresponding model output for the mountain peak from the highest resolution nested domain. Due to the "mountain flattening effect"(see Section 2.3.2), the modelled mountain is approximately 3.0 km in altitude, whereas in reality the Etna is approximately 0.3 km taller than this. Because O_3 mixing ratios can have strong variances with altitude, model output is therefore reported for both ground level (model level 0) and for model level 4, which at this location corresponds to a modelled altitude of approximately 3.3 km.

Table 4.3: Observed and modelled O_3 at the peak of Mount Etna

Site	Date	Time (UTC)	Model timestep	Obs. O_3 / ppb	Modelled O_3 / ppb	
					level 0 (3.0 km)	level 4 (3.3 km)
up-30	2012-07-30	09:12–09:34	2012-07-30 09:00:00	73 ± 1	62	72
up-01	2012-08-01	08:42–09:10	2012-08-01 09:00:00	61 ± 2	55	60

Comparison of the observational data to the level 4 model output in Table 4.3 suggests that the model has extremely good skill in regards to modelling O_3 at this altitude. As O_3 is involved in many reaction cycles, this is a positive sign regarding the overall chemical skill.

In the main model runs the volcanic emissions are injected into level 0 and not level 4, and therefore the O_3 mixing ratio of the air which the plume entrains would be underestimated by a moderate amount, the data here suggests this underestimation is likely to be approximately 10–15%.

4.4.2.2 Aerosol

In the field, aerosol was measured using an optical particle counter (TSI Trak-Pro).This measured aerosol in 6 size bins, each covering a range of aerosol diameters: 0.3–0.5, 0.5–1, 1–3, 3–5, 5–10, and >10µm. As the model only considers aerosol up to a diameter of 10µm, the data corresponding to the largest size bin is not used in this exercise.

In Figure 4.13, the modelled and observed number distribution for the observation sites are plotted.

Model output are plotted for both levels 0 and 4 (see discussion in Section 4.4.2.1). The difference between these two levels is relatively small (in comparison to the difference with the observations). It should be noted that for the 2012-08-01 case, the level 0 aerosol number density is consistently larger than the level 4 value, differing by up to a factor of 2.

For 2012-07-30 there is a substantial difference between the observations and the measurements, with the observations being approximately 1.5 orders of magnitude smaller than the model values across the entire range. For 2012-08-01, the difference is much reduced, and for the largest particles the observations exceed the model output.

These results suggest that the model may be substantially inaccurate with regards to aerosol, especially on 2012-07-30. The observations cover only a part of the aerosol size range that contributes substantial surface area for reactions, and is very limited in geographical and temporal scope. However they are the only direct observations of aerosol in the area of interest that are available.

In Section 4.4.3 below, I inspect the model output, and identify a likely cause of this phenomenon.

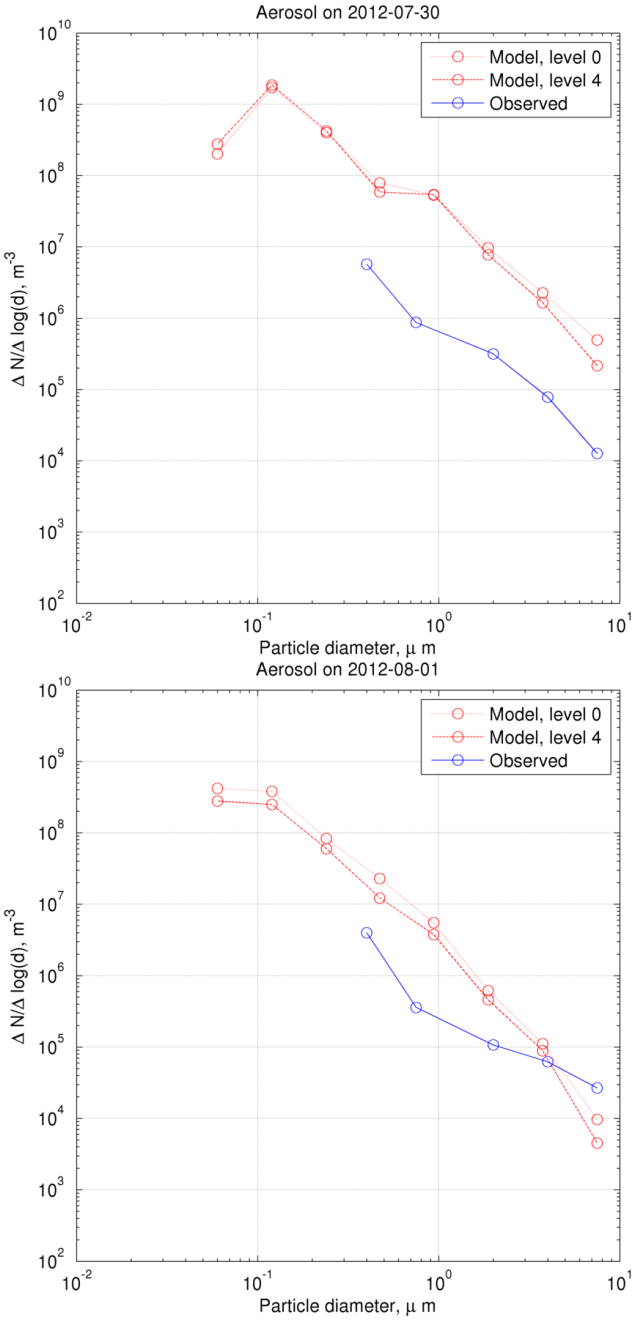

Figure 4.13: Modelled and observed aerosol number distributions at the upwind field campaign sites.

4.4.3 Inspection of aerosol

The observations reported in of section 4.4.2.2 indicated that the model may be substantially over-predicting background aerosol in the region of Etna, especially on 2012-07-30. This is of significance to this investigation, as heterogeneous reactions upon aerosol are part of the chemical cycles being investigated.

In the absence of further observational data, in this section I inspect the model output relating to aerosol. I identify a potentially anomalous phenomenon which may be the cause of this discrepancy.

To produce the values for Figure 4.14, I have taken an average of the modelled aerosol surface area (calculated from the model output as discussed in Section 2.2.1.7), at 3 km altitude over Sicily and the surrounding sea (specifically, this area is domain 3 of the model, see Figure 2.3).

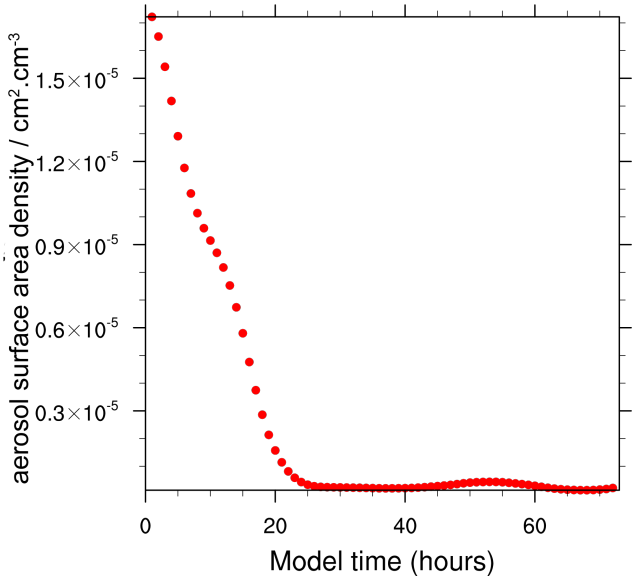

Figure 4.14: Modelled average aerosol surface area density at 3 kmASL in domain 3 of the model vs. time

Figure 4.14 shows that the model's initial aerosol surface area densities in this region are of the order of 10^{-5} cm^2 cm^{-3}. This is about two orders of magnitude greater than the level to which they fall after a day.

Inspection of the model output (e.g. Figure 4.15) shows that WRF-Chem initiates with a 'cloud' of high aerosol loading over part of the modelled area. Given its location, this may be RAQMS' representation of mineral dust blown in from Africa. This cloud is transported away from Sicily by the start of the second day of the model run.

Whether or not this high aerosol cloud is an error in the model, it is certainly anomalous. The modelled aerosol conditions that exist over Sicily after this cloud has passed (aerosol loadings of the order of 10 μg m^{-3}) are much closer to the typical free troposphere value of 4.8 μg m^{-3} from Seinfeld and Pandis (2006). Because the purpose of this investigation is to investigate typical plume behaviour, in the rest of this document I avoid using output relating to plume

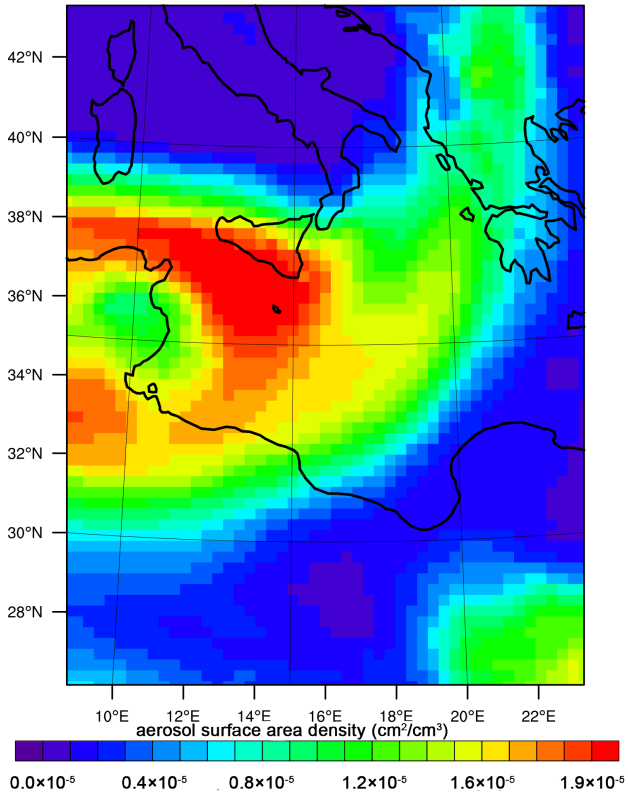

Figure 4.15: Modelled aerosol surface area density at 3 km altitude after 1 hour of model simulation.

emitted in the first 24 hours of the model.

The first 24 hours of the modelling are therefore considered "spin-up time". This avoids the specific aerosol issue I have identified above. Additionally it is general good practice to have a spin-up time in modelling investigations (Warner, 2011).

4.4.4 Inspection of bromine

There are no measurements against which the model's background mixing ratios of inorganic bromine, Br_{inorg}, can be checked. However the modelled background Br_{inorg} mixing ratio is generally less than 1.0 ppt, meaning that the bromine in the modelled plume will dwarf that of the background, rendering the accuracy of the background bromine representation unimportant.

4.4.5 Flight data

During the aircraft campaign, which is discussed in Section 4.3.4 regarding meteorological data, measurements of SO_2, O_3, NO, NO_2 and CO concentrations were also taken. The instruments used are listed in Table 4.4. Although the primary goal of the campaign was to collect data from within the plume, the aircraft spent considerable time outside of the plume and these data can used as a check for the background chemistry. Each of these species has the potential

Table 4.4: Instruments used on the aircraft to measure various trace gases.

Species	Instrument
CO	Aero Laser: AL5002
O_3	Teledyne API: 400A
SO_2	Teledyne API: 100E
NO and NO_2	Teledyne API: M200EU

to be perturbed by the volcanic emissions, it is therefore necessary to filter out measurements which are influenced by the plume. I have done this by setting a threshold value of 10 ppb to the SO_2 signal, with data points considered "background" when the mixing ratio is below this threshold. The choice of this threshold has been made upon inspection of the data.

Figures 4.16, 4.17, and 4.18 show timeseries of the observations of NO_x, CO, and O_3 respectively on each of the three flights. So as to indicate background chemistry only, observations flagged as being "in plume" by the measurement team have been excluded from these plots. The aircraft altitude is plotted on the secondary vertical axis of each plot.

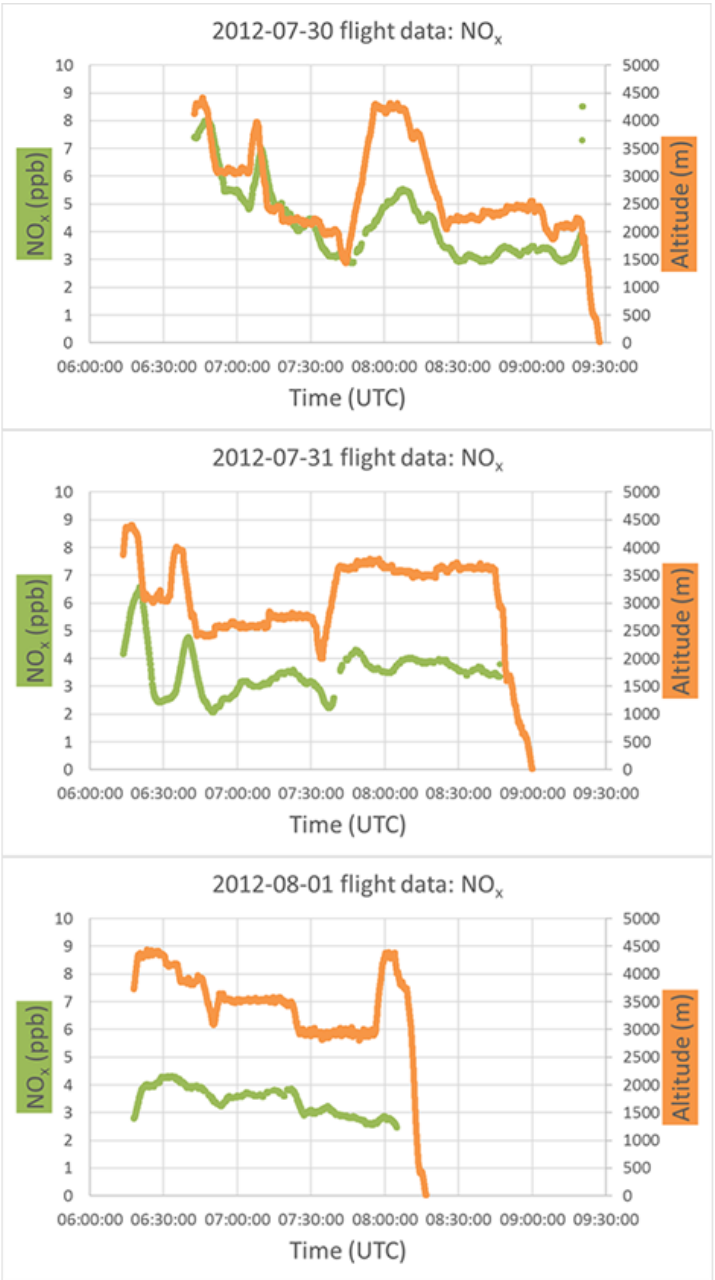

Figure 4.16: Time series of observed background mixing ratios of NO_x, and the aircraft altitude, from the three flights.

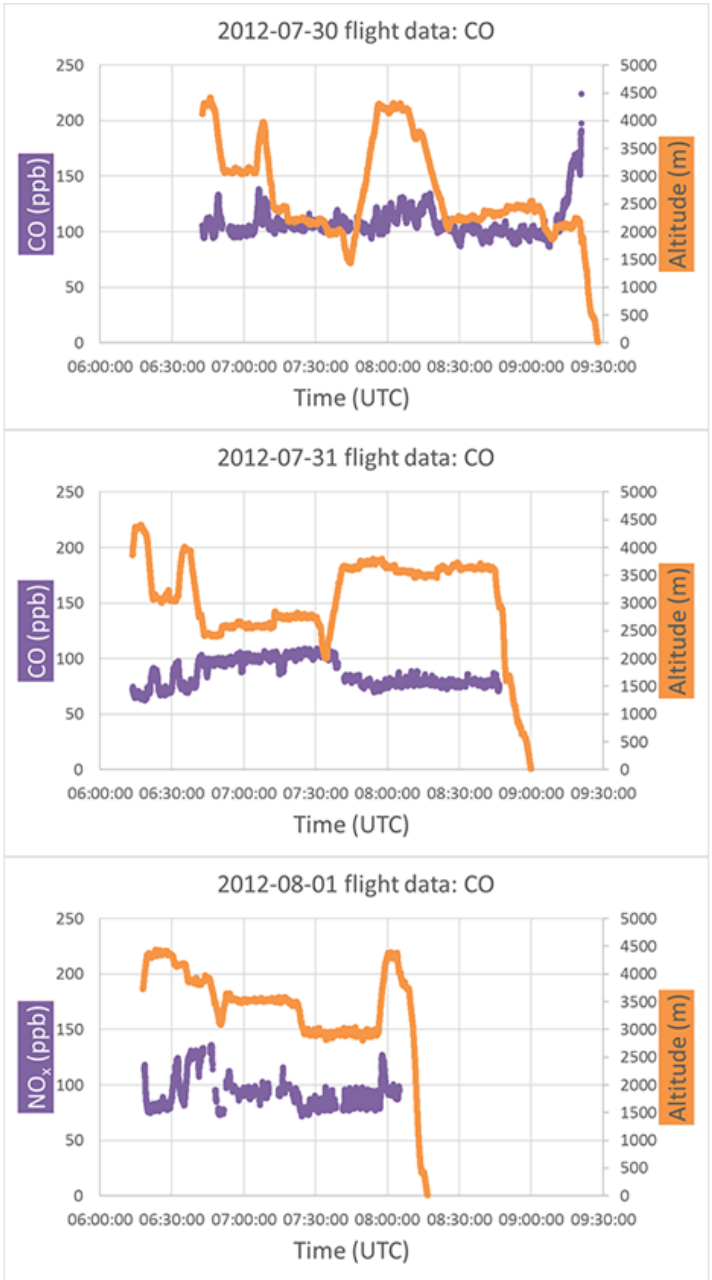

Figure 4.17: Time series of observed background mixing ratios of CO, and the aircraft altitude, from the three flights.

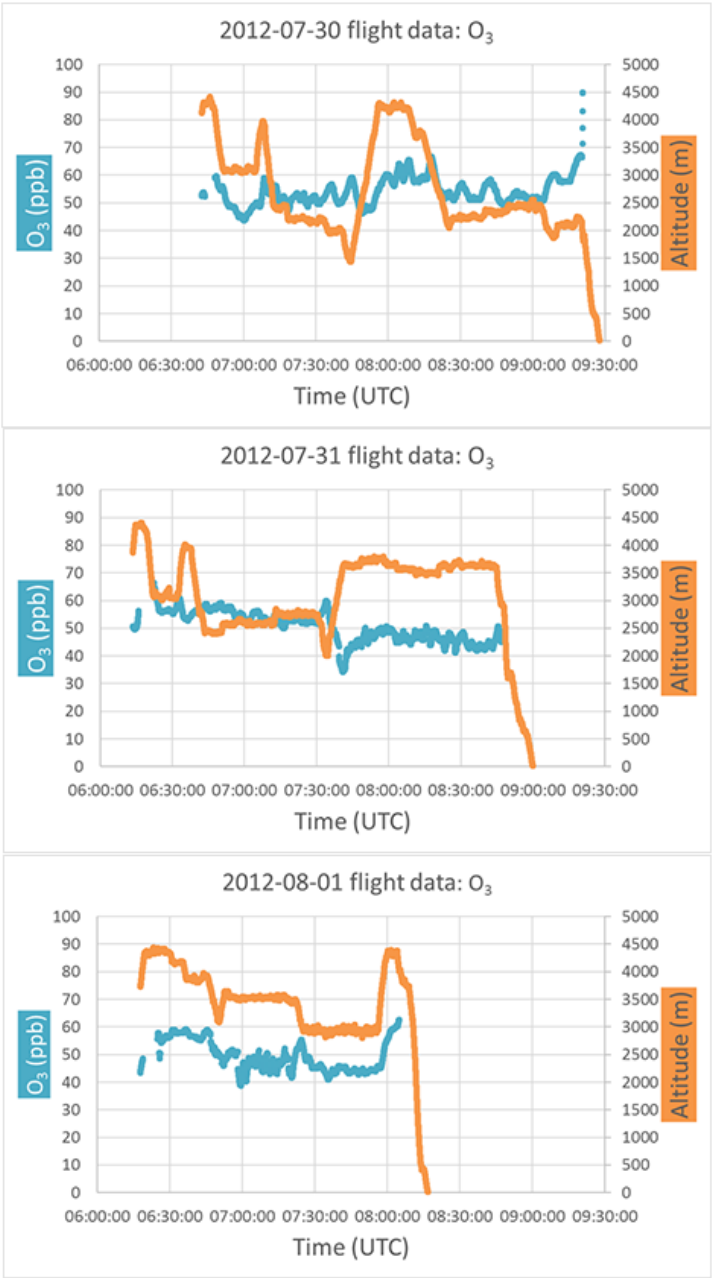

Figure 4.18: Time series of observed background mixing ratios of O_3, and the aircraft altitude, from the three flights.

All of the data plotted in Figures 4.19 and 4.20 are limited to the measurements taken at the altitudes of interest — between 1.5 and 5.0 kmASL. This is the same approach taken in Section 4.3.4. This approach excludes those observations taken within the boundary layer which are not of interest to this investigation.

Each observation has an associated time and geographical coordinate — as was performed in Section 4.3.4, the equivalent model output can be looked up and compared with each observation.

Although the SO_2 data can be used to identify the presence of plumes, it is not valid for assessing the background SO_2 mixing ratios. The values reported outside of the plume (not plotted) are clearly erroneous, frequently being of order of 1–10 ppb, whereas free tropospheric air is known to have a substantially smaller SO_2 content — of the order of tens of ppt (Seinfeld and Pandis, 2006).

Similarly the observations of NO and NO_2 appear to also be erroneous. As shown in figure 4.16, throughout all three flights, the observed NO_x mixing ratios are of the order of a few ppb, orders of magnitude above both the WRF-Chem model values and the reanalysis values (Section 4.4.1), as well as general expectations for free tropospheric NO_x (Seinfeld and Pandis, 2006). Though the reported detection limit is 0.05 ppb, and isolated observations of such mixing ratios could indicate a polluted airmass, these values are consistent throughout the observation dataset. The spread of times (Figure 4.16) and locations (see Figure 4.7) which the aircraft covers are too extensive for all these measurements to be an anomalous pollution episode. I therefore conclude that it is more likely that these values are erroneous.

Figures 4.19 and 4.20 compare the observation data versus the corresponding model output for CO and O_3.

Unlike for NO_x and SO_2, there is nothing clearly erroneous about either the observation CO and O_3 datasets, and the differences between these and the equivalent model output may be indications of inaccuracies in the modelling. Though there are clear differences, the observations and model output are of the same order of magnitude.

CO is a very long-lived species (of the order of months), however the WRF-Chem model is only run for three days. Thus the modelled mixing ratios of CO used in this section are predominantly controlled by the initial and boundary conditions of the model, rather than the tropospheric chemical processes modelled within it. It is likely that these initial and boundary

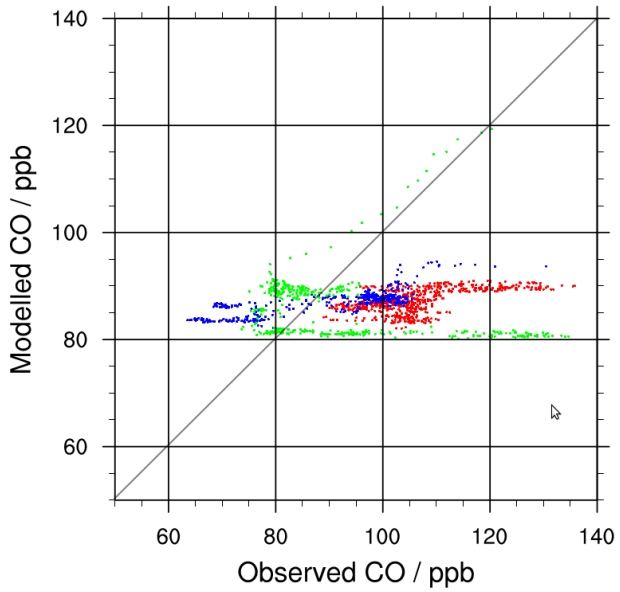

Figure 4.19: Modelled mixing ratios vs. observed mixing ratios of CO measured in the aircraft campaign. Colour-coding is the same as Figure 4.8.

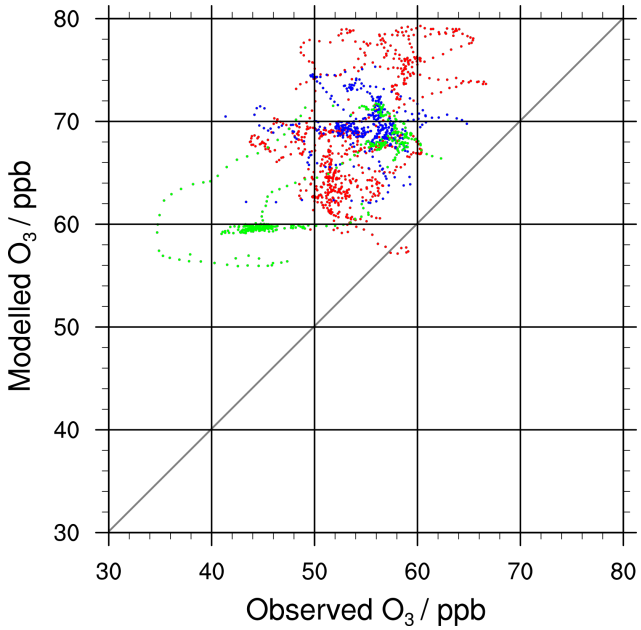

Figure 4.20: Modelled mixing ratios vs. observed mixing ratios of O_3 measured in the aircraft campaign. Colour-coding is the same as Figure 4.8.

conditions (see Section 2.1.2) do not capture the spatial variability of CO, resulting in fairly uniform modelled mixing ratios seen. Figure 4.21 is a 3 km cross section of modelled CO at the time of the second aircraft flight, the low modelled spatial variability of CO can be seen.

This discrepancy does not necessarily indicate inaccuracy in the

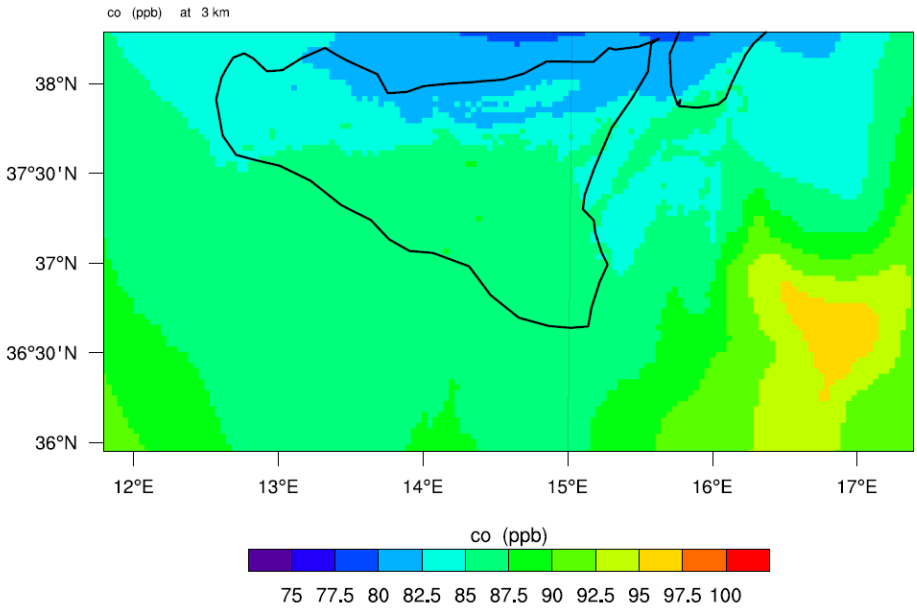

Figure 4.21: Modelled mixing ratios of CO at 2012-07-31 07:00:00 at an altitude of 3 km.

representation of the chemical reactions of CO within the WRF-Chem modelling.

CO is not directly involved in the chemical processes of primary interest to this investigation, and, if these measurements are indications of true inaccuracies in the modelled mixing ratios of CO, the resulting inaccuracies in the modelling of rates of reactions with CO as a reactant are not too large here as to render the model inadequate for this investigation.

If these aircraft observations are accurate, it would indicate that the model has inaccuracies in its representation of O_3. The chemistry of O_3 is extremely complicated and it would not be possible to determine from these data what the cause or causes of these discrepancies are likely to be. However, even if this is the case, the differences shown are not too large to render the model inadequate for this investigation. It should be noted that the only other local measurement of background O_3 (see Section 4.4.2.1) agrees more closely with the model output.

4.4.6 Overall assessment

Overall, this exercise suggests that the model's reproduction of the chemistry of the Mediterranean region at the time of interest should be adequate for the purposes of this investigation. This exercise has found no major anomalies in the

model output with the exception of the high aerosol event discussed in Section 4.4.3. Differences between modelled and aircraft observations of CO and O_3 may indicate some inaccuracy in the modelling of these species, though these inaccuracies are tolerable. There is no evidence of major discrepancies in the model's representation of tropospheric chemical processes.

I have decided to consider the first 24 hours of the model as spin-up. I do not use output relating to model plume emitted during the spin-up period in the remainder of this investigation.

There are not sufficient data to determine whether or not the model is highly skilled with regards to the background chemistry. However such skill is not required for this investigation, as I am investigating general aspects of plume chemistry, rather than trying to precisely reproduce a specific eruption and its setting. With the spin-up time discussed, the background chemistry of this model is adequate for this investigation.

4.5 Volcanic plume dispersion and chemistry

In this subsection I assess the treatment of the plume in the model, and compare the model output to available measurements. There are three phenomena which I discuss:

- The physical dispersion of the plume, both horizontally and vertically, as it travels downwind. The model run can be directly compared to observations from the aircraft campaign.
- The formation of BrO within the plume. The model output is compared to the ground-based spectroscopic observations discussed in Chapter 3.
- The depletion of O_3 within the plume. The model run can be can be directly compared to observations from the aircraft campaign.

As well as these directly applicable measurements, there also exist measurements from other eruptions and subsequently derived theory regarding these phenomena which are also useful for this exercise.

4.5.1 Physical dispersion of the plume

As plumes are transported downwind they disperse, entraining background air. Turbulent diffusion can cause plumes to expand and/or distort in shape as they travel downwind (Seinfeld and Pandis, 2006). A dispersion scheme is included within WRF (UCAR) and is implemented in the runs used for this investigation.

In this section I evaluate the physical dispersion of the model plume by comparing the model output with observations from the aircraft campaign. For this exercise I use the same comparison of observations of SO_2 and the equivalent model output as was used in Section 4.3.4.

The dispersion of the plume within 10s of km of the source can be seen in Figures 4.11 and 4.12 for the observational and modelled datasets respectively. As well as showing that the model output approximately agrees with the observation in terms of the direction of travel of the plume from the volcano, these data also show agreement in terms of the nature and magnitude of the dispersion.

In all cases, modelled and observed, the plume shows a concentrated core and more disperse edges—the profiles appear to be Gaussian. Previous studies have found volcanic plumes to have Gaussian profiles (e.g. Tiesi et al., 2006, and references therein).

The widths of these dispersions are also similar. These data suggest that, qualitatively and quantitatively, the model reproduces well the dispersion of the Etnean plume, at least for the first few 10s of km.

There is a substantial difference between the magnitude of the SO_2 concentrations observed and those modelled, with the model values being greater. However no conclusions can be drawn from this comparison, as it is unknown whether the aircraft intercepted the most concentrated regions of the plume. The model output necessarily includes the entirety of the plume, including the most concentrated values in its core.

Diffusion of the plume was also observed on very short timescales in the field measurements (see SO_2 observations in Chapter 3). These measurements cannot be compared with the model output, as the spatial scales involved are less than the highest resolution of the model.

4.5.2 BrO and spectroscopic observations

In this subsection I consider the extent to which the model output reproduces spectroscopic observations of BrO. Since the publication of Bobrowski et al. (2003) there have been multiple published measurements of such observations, and I compare the model output to these. Additionally, a spectroscopic observation was made near the volcano during the modelled time period, and I make direct comparisons to this. A discussion of the details of the plume bromine chemistry which cause such phenomena can be found in Section 1.1.5.5.

All of the observations and model output discussed in this subsection relate to the daytime, when the photochemistry necessary to form BrO in substantial quantities is expected to be active.

These measurements are typically reported in the form of BrO/SO_2 ratios with SO_2 being used as a plume tracer. Use of this ratio allows observations of differing magnitudes of plume intensity to be compared. I also discuss below the SO_2 columns independently of BrO.

4.5.2.1 Etna's measurement history

Bobrowski et al. (2003) made the first identification of reactive halogen chemistry in volcanic plumes by means of spectroscopic detection of elevated levels of BrO in atmospheric columns containing a the Soufrière Hills volcanic plume. Since then such BrO columns have been observed in many volcanic plumes, detected by observations from the ground based observations (see table 1 in Donovan et al., 2014, for a global overview) and from satellites (Hörmann et al., 2013).

Table 4.5: Reported BrO/SO_2 ratios for Mount Etna plumes in the literature. Satellite values are the fitted ratios from Hörmann et al. (2013) table 4.

Method of detection	Date	BrO/SO_2	Reference
Ground-based DOAS	August 2004	1.9×10^{-4}	Oppenheimer et al. (2006)
	May 2005	2.6×10^{-4}	Louban et al. (2009)
	Sept 2003	4.7×10^{-4}	Bobrowski and Platt (2007)
	Aug 2008	2.1×10^{-4}	Bobrowski and Platt (2007)
	Aug 2004	2.1×10^{-4}	Bobrowski et al. (2007)
	2004–2008	$1.1–2.4 \times 10^{-4}$	Bobrowski and Giuffrida (2012)
Satellite-based DOAS	November 2011	3.7×10^{-4}	Hörmann et al. (2013)
	May 2008	0.9×10^{-4}	
	May 2008	2.7×10^{-4}	

Table 4.5 lists the reported observations of the BrO/SO_2 ratio in Etnean plumes. Globally, BrO/SO_2 ratios for all volcanoes tend to be of roughly similar magnitude (within a factor of 5–10). It should be noted that the

satellite observations are of strong eruptions from Etna; eruptions which are of substantially greater magnitude than which has been modelled in this exercise.

Bobrowski and Giuffrida (2012) analyses measurements from several field campaigns (at Etna, Nyiragongo, and Popocateptl), determining trends in the variation of the BrO/SO_2 ratio with respect to distance of the plume from the crater. This showed that the ratio is generally negligible very near the crater, increases between 0–5 km, and then stabilises. Analysis by Bobrowski et al. (2007) suggests the BrO/SO_2 ratio is greater at the plume edges than the plume core.

4.5.2.2 July/August 2012 measurements

The spectroscopic detections made during the field campaign by Dr. Bobrowski are discussed in Chapter 3 and in Surl et al. (2015). The BrO/SO_2 ratios observed ranged from 0.6–1.3 $\times 10^{-4}$. One spectrum was taken during the 2012-07-30 –2012-08-01 period, which was an observation of a ratio of 0.6 $\times 10^{-4}$ on 2012-07-31. Details of this observation are given in Table 4.6.

Table 4.6: Details of the 2012-07-31 spectroscopic observation of the plume.
SCD: Slant Column Density.
The BrO/SO_2 is calculated from the correlation of multiple spectra and can differ slightly from the absolute ratio of the reported SCDs.

Date	2012-07-31
Time (nearest hour)	10 UTC
Latitude	37.698 N
Longitude	14.998 E
Lateral distance from peak	5.9 km
SO_2 SCD	1.3×10^{18} molec cm^{-2}
BrO SCD	9.0×10^{13} molec cm^{-2}
BrO/SO_2 ratio	6.2×10^{-5}

4.5.2.3 Model output

In Figure 4.22 I plot model output from the base run (with volcanic emissions) for 2012-07-31 10:00:00. These plots are vertical column densities of SO_2 and BrO, and the ratio of these. Model output from domain 2 and domain 4 are plotted for each. In order to focus on the plume, only cells with an inert tracer column above an arbitrarily defined threshold are plotted. This threshold is chosen such that 80% of the inert tracer within the domain is present in plotted

columns. Note that, for a given snapshot, this will exclude more of the aged, dispersed plume than the younger more concentrated plume, giving the illusion that the plume narrows with age. A circle has been drawn on the domain 4 plots centred on Etna and with radius 5.9 km (the lateral distance of the observation from the mountain peak).

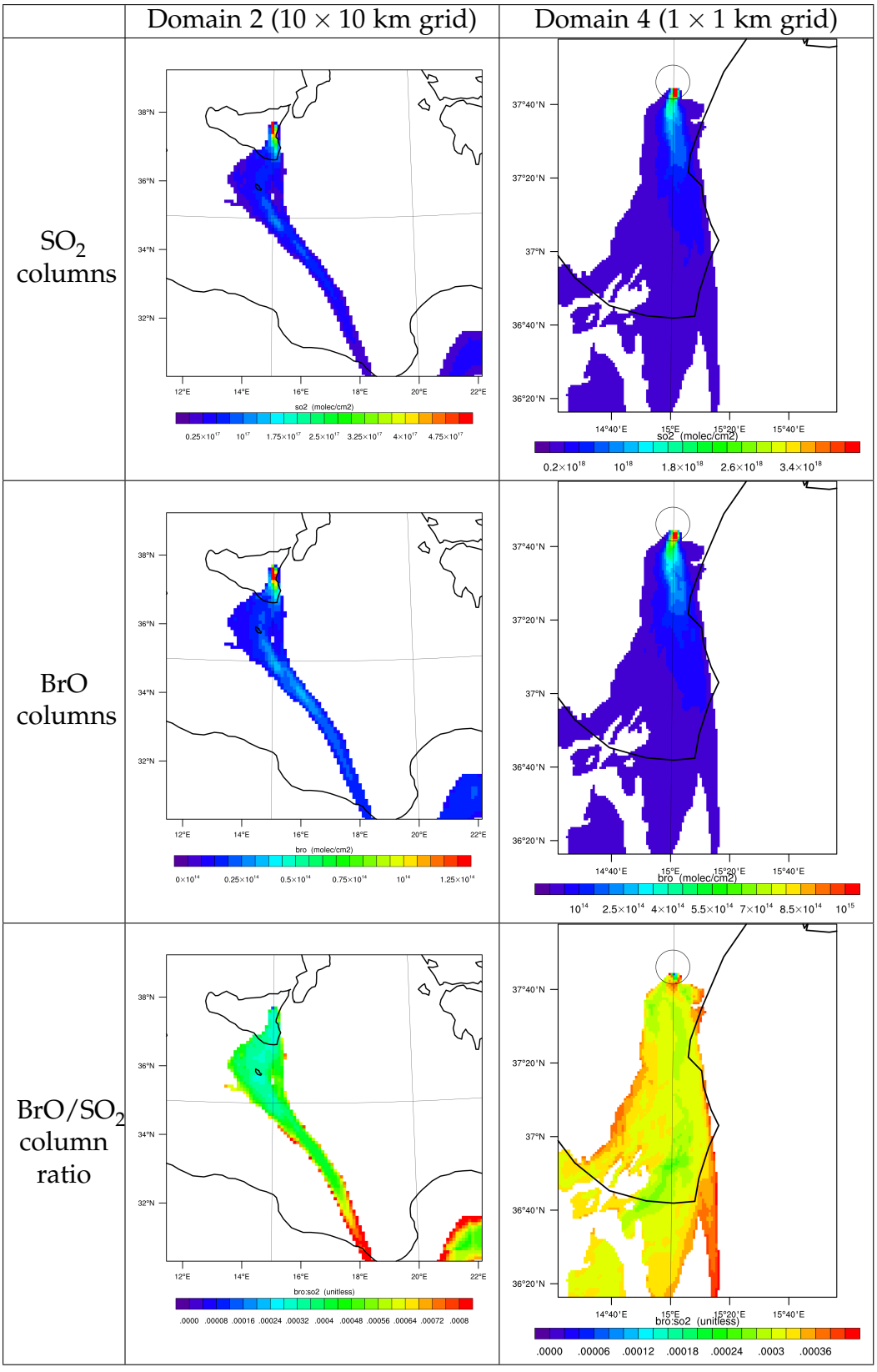

Figure 4.22: Modelled vertical columns of BrO, SO_2 at 2012-07-31 10:00:00, and the ratio of these. Note that the colour scale is different in each plot.

As the columns of SO_2 and BrO in Table 4.6 are slant column densities and those in Figure 4.22 are vertical column densities, these cannot be directly compared. However, as direction of the scan was set to be perpendicular to the plume's direction of travel, the discrepancy between the slant columns and the corresponding vertical columns from the model should be a small factor.

4.5.2.4 Assessment

In the model output, the peak vertical column of SO_2 at 5.9 km from the peak is approximately 2.5×10^{18} molec cm^{-2}. This model output exceeds the SCD of the observation by a moderate factor (2–3).

The model output shows appreciable BrO, showing columns of intensities which would be detectable by ground-based instruments. This is an indication that the bromine chemistry in the model is functional—-negligible BrO is directly emitted by the modelled volcano. The peak BrO column at 5.9 km from the peak is approximately 8.5×10^{14} molec cm^{-2}, which is an order of magnitude above the corresponding observed SCD.

The modelled BrO/SO_2 ratios are generally of the order of a few 10^{-4}, within the ranges of ratios listed in Table 4.5.

The ratio at the point of maximum plume intensity 5.9 km from the peak is approximately 3.5×10^{-4}. This is roughly 5 times greater than the observed ratio.

The comparison of the model output and the field observation suggest that, either for reasons of a discrepancy between the modelled and actual volcanic flux of bromine or SO_2, or an error in the model's chemistry, the model over predicts BrO for the morning of 2012-07-31. However the modelled BrO/SO_2 column ratios, both near to and far from the volcano, are within the ranges of the observations in Table 4.5. The 2012-07-31 observed BrO/SO_2 ratio is lower than all the values in Table 4.5, and is indeed the lowest ratio observed over the entire field campaign (see Table 3.5 in Chapter 3). This is possibly a consequence of natural variability in the volcanic flux—the ratio of the volcanic flux of Br to that of S was likely low during the time of the field campaign (the modelled ratio of the volcanic fluxes is based on June 2012 data from Wittmer et al. (2014)), and this ratio may have been at particularly low on 2012-07-31. The purpose of this investigation is to provide insight into the general behaviour of volcanic plumes. Therefore I have not "corrected" the model to more closely reproduce

the 2012-07-31 observation, as this may be a somewhat anomalous case.

That the BrO/SO_2 ratio is maintained at a level of a few 10^{-4} hundreds of km downwind of the volcano is in agreement with the results from satellites, which detect BrO columns at such distances. No direct comparison is possible in this case however, as Etna's activity during late July/early August 2012 was too weak to be detected by satellite.

The spatial structure of the modelled BrO/SO_2 ratio shows evidence of the structural features discussed above, with both an increase in BrO/SO_2 over the first ~5 km of plume transport, and slightly smaller BrO/SO_2 ratios at the core of the plume than at its edges. This phenomena is examined in more detail in Chapter 5.

Overall, when considered qualitatively the model shows very good skill in reproducing the BrO-related phenomena. Quantitatively the model shows reasonable skill. It is impossible to tell whether the discrepancy between the observed and modelled BrO column and BrO/SO_2 column ratio is due to errors in the model's volcanic flux or its chemistry (indeed even a perfect reproduction could be the result of two compensatory errors). However the modelled BrO/SO_2 column ratio agrees with the long-term observational record. For the purposes of this investigation, reproducing these "general" results is a sign of adequate skill (sufficient for the purposes of this investigation).

Similarly, the discrepancy in the SO_2 column could be due to errors in modelled wind speed or in volcanic SO_2 flux. The model's skill in regards to wind speed is discussed in 4.3. The flux of SO_2 is known to be highly variable (Salerno et al., 2009). Precisely reproducing the flux in relation to a specific observation is unnecessary for this investigation.

4.5.3 O_3 destruction

In this section I evaluate how the modelled destruction of ozone within the volcanic plume compares with observational data of the same phenomenon.

Destruction of O_3 has been observed in a small number of volcanic plumes; (see Section 1.3 and Table 1.1).

In this section I do not compare the model directly with the downwind field observations of O_3 and SO_2. The distances from the vents to the measurement sites are less than the grid size dimension of the model, and so it would not be

expected that the model would well reproduce these results. Additionally each of these measurements was made downwind of a single volcanic vent, whereas the model has only a single volcanic source, representative of the combined emissions of all active vents.

The aircraft measurements of O_3 and SO_2 are useful for this exercise. Although in section 4.4.5 the SO_2 data was discarded for the purposes of checking the model's background chemistry, it is assumed the instrument is reasonably accurate for measurements within the plume where SO_2 is much greater, reducing the significance of small biases or inaccuracies.

The O_3 measurements also showed a consistent discrepancy with the model which may be bias, however in this exercise I will be considering variations within this signal with plume intensity, rather than absolute values. As such, any offset would be unimportant. The aircraft O_3 data used to plot Figure 4.20 shows plausible variation in O_3 with altitude, suggesting that the instrument is sensitive to changes in O_3.

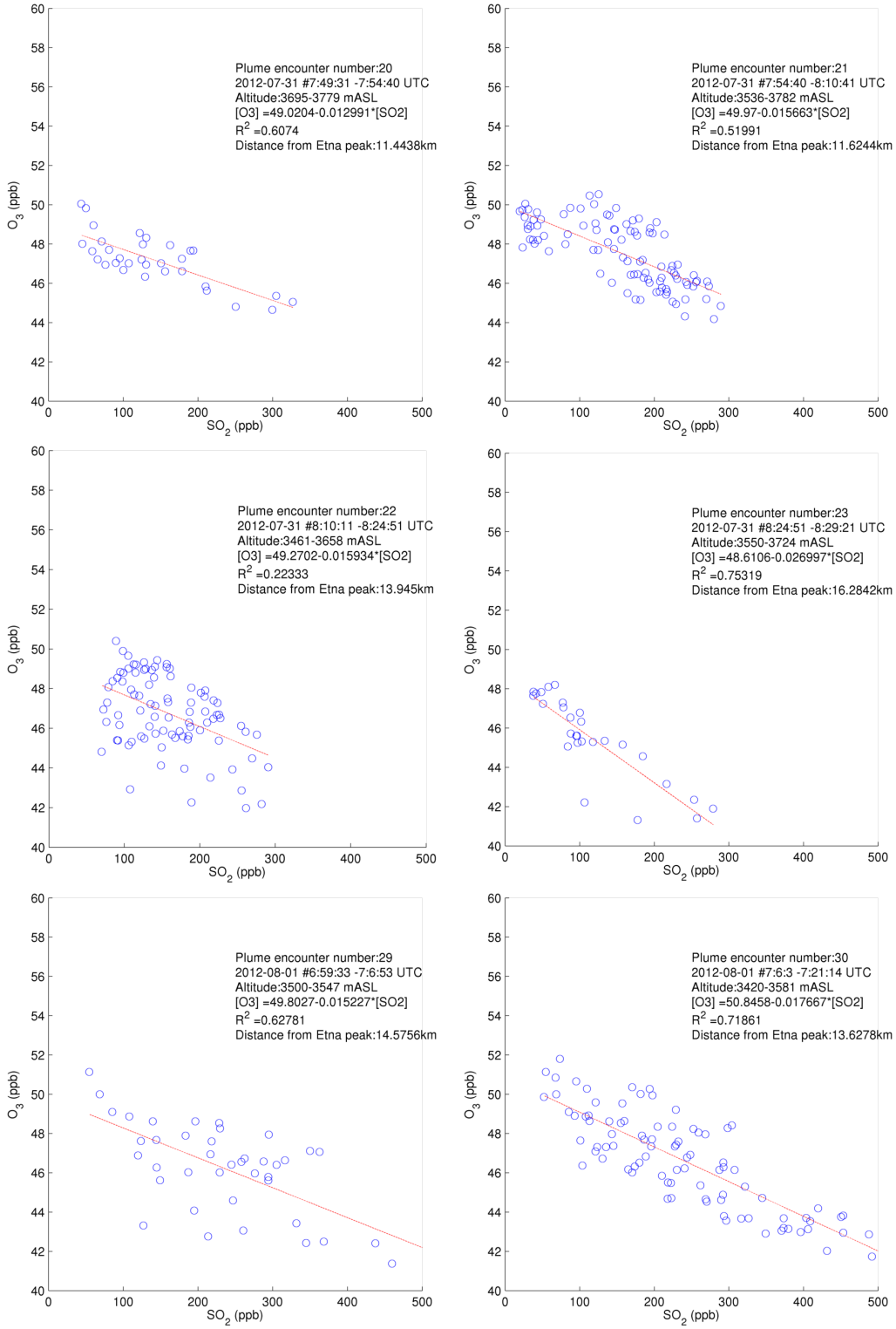

Figure 4.23: Aircraft observations of O_3 vs. SO_2 in six plume intersections. Details of each intersection and the fitted line-of-best-fit to the data are written on each plot.

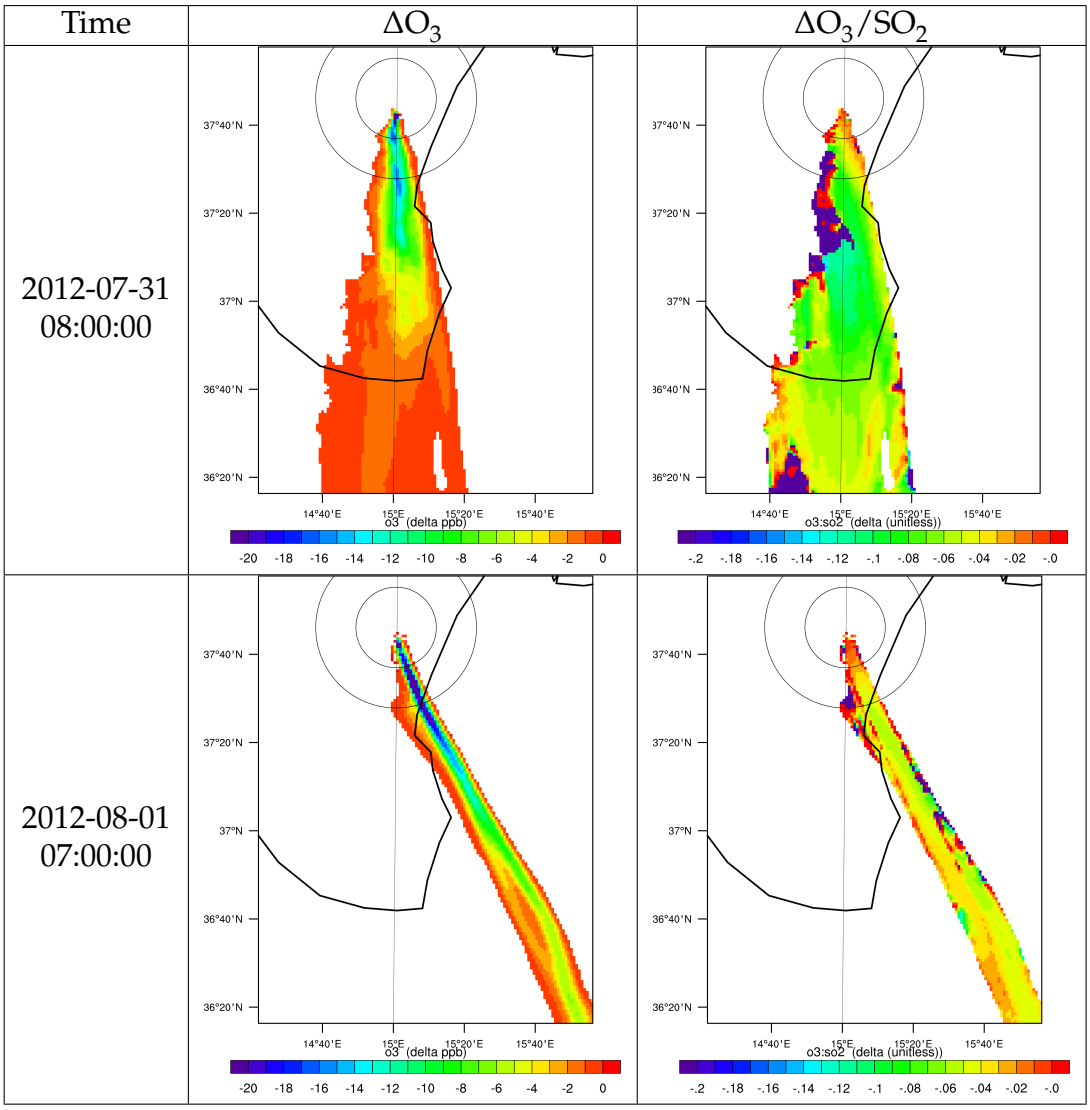

Figure 4.24: Cross sections of model output at 3200 m altitude, corresponding to the times shown in the leftmost column. For visual reference circles centred upon Mount Etna's peak with radii 10 and 20 km have been drawn.

Figure 4.23 shows data from six intersections of the plume. The measured O_3 mixing ratio is plotted against the SO_2 mixing ratio. I have chosen to use these intersections for this exercise as they show a strong SO_2 signal and were each taken at a narrow range of altitudes, minimising the influence of altitude variations in the O_3 signal.

Figure 4.24 shows model output for a horizontal cross section of the plume in the highest resolution domain of the model. Model output for 2012-07-31 08:00:00 and 2012-08-01 07:00:00 are shown, as these outputs are the closest available outputs to the time of the intersections of Figure 4.23. Only grid cells with SO_2 concentrations above 5 ppb have been plotted. Because the

aircraft data of Figure 4.23 is from approximately 3500 m ASL, which is 200 m above the peak of Etna, the model cross sections have been taken at 3200 m ASL, as this is roughly 200 m above the height of Etna in the model (see 2.3.2). Plotted are O_3 losses and the associated $\Delta O_3/SO_2$ ratio.

The aircraft data and model output show a high level of agreement. In a qualitatively sense, the model and the observational data both show the depletion of ozone, and that the magnitude of this depletion correlates with plume intensity. Quantitatively there is also good agreement; the aircraft data shows depletions of up to approximately 10 ppb at distances approximately 15 km from the volcano, and the depletion in the model output is very similar.

The $\Delta O_3/SO_2$ ratio is calculated explicitly in the model output and can be inferred from the gradient of the plots in Figure 4.23. At approximately 15 km from the volcano this ratio is around -0.015 in the observational data and about double this in the model output, although both the model and the observations show large spatial variations in this ratio.

Overall this comparison shows that the model has skill in regards to the O_3-related chemistry. In-plume O_3 depletion is modelled, extending far from the volcanic vent. That the model also reproduces the observed O_3 destruction with reasonable quantitative skill suggest that the halogen chemistry system of the model is a reasonable representation of the O_3-destructive chemistry of the real-world plume.

4.6 Overall assessment of model skill

Having assessed the model's skill versus available data with regards to meteorology (Section 4.3), non-volcanic chemistry (Section 4.4), and volcanic phenomena (Section 4.5), I have found the model to be generally adequate for the purposes of this investigation. This model is not a precise reproduction of the Mediterranean environment during the Summer of 2012, however such precision is not required as this is an investigation into general features of volcanic plume chemistry.

The two most significant caveats to this are the model's failure to reproduce very low relative humidities and its representation of aerosol. The first 24 hours of the model is considered spin-up, which prevents a region of very high aerosol loading perturbing the results.

The levels of confidence in conclusions inferred from model data in the rest of this investigation are informed by the findings of this assessment. In particular, this assessment shows that systems which may be sensitive to humidity or aerosol loading may be impacted by errors in the model's representation of these.

Chapter 5

Base case modelled volcanic plume

Having presented an assessment of the model in Chapter 4, and having shown that the model has adequate skill for this investigation (with some caveats), this section considers the model output in the "base case" and what these say about the chemistry occurring within the plume. In this section I describe various modelled phenomena, and explain the causes of these phenomena, exploiting the "modeller's advantage" (see section 1.4.1).

This "base case" uses the settings described in Chapter 2, including the runtime options described in section 2.3. The volcanic behaviour modelled here is intended to roughly represent typical passive degassing activity of Etna, similar to that encountered in the field campaign of Chapter 3. The model output is here analysed in detail, using various techniques (including those outlined in Section 4.2) in order to identify and assess the phenomena occurring.

I have divided this Chapter into sections based upon phenomena in different chemical systems (including aerosol).These chemical systems are all, to varying extents, inter-related, adding to the complexity of the overall system.

5.1 Sulphur chemistry within the plume

SO_2 is generally used as a plume tracer in volcanology. Such use assumes that plume SO_2 is practically inert, with minimal loss via chemical or physical processes over the time period of the given study. The observational results of McGonigle et al. (2004) suggest that this is valid for near-vent studies such as those used to quantify a volcano's SO_2 flux. In this section I consider the plume SO_2 chemistry in the model output throughout the domain of the model and

consider the magnitudes and causes of the observed phenomena.

The sulphur chemistry in the model is very simple, consisting only of Reaction R39[1]

$$SO_2 + OH \longrightarrow H_2SO_4 + HO_2 \quad \text{(R39)}$$

The H_2SO_4 produced by the oxidation of SO_2 forms sulphate aerosol.

The main gas phase reaction of SO_2 is with OH, indeed this is the only gas-phase sulphur reaction implemented in the model. This reaction removes SO_2 from the atmosphere, converting it to H_2SO_4 (sulphuric acid). The lifetime of SO_2 with respect to this reaction will depend on the OH concentration; a benchmark figure for the atmospheric lifetime of SO_2 with respect to oxidation by OH is about one week (Seinfeld and Pandis, 2006). SO_2 can also be removed from the atmosphere by dry and wet deposition.

To determine the magnitude of SO_2 loss in the modelled plume I consider the volcanic SO_2/tracer1 ratio (see 4.2.2 for an overview of this tracer). "Volcanic" SO_2 here refers to the difference between SO_2 concentrations in the output of the base model run, minus the equivalent SO_2 concentrations in the plume-free model run.

This tracer and SO_2 are emitted from the model volcano with the same flux. In theory, at the point of emission this ratio would equal 1, and then decrease as the plume is transported downwind and SO_2 is lost via physical or chemical processes. The loss of SO_2 can therefore be traced by observing the relationship of this ratio to the plume age.

To distinguish between physical and chemical loss of SO_2 I have used another tracer, tracer5P. This tracer acts like tracer1 in that it is completely inert. However tracer5P is not emitted by the volcano, but is instead created as an additional "product" of Reaction R39. Thus, whenever an SO_2 molecule is destroyed chemically it is "replaced" by a tracer5P molecule, which will continue to transport identically to how the SO_2 molecule would have travelled had it not been destroyed.

Thus volcanic SO_2/tracer1 is the fraction of volcanic SO_2 that has not been removed, tracer5P/tracer1 is the fraction that has been removed by chemistry, and the fraction that has been removed by physical processes can be simply calculated from these. The processes are wet and dry deposition. The model

[1] SO_2 is converted to $HOSO_2$, which is then converted to SO_3, and in turn converted to H_2SO_4. These latter two reactions are rapid, and the reaction in the model is a valid simplification that saves computational resources.

does not consider include aerosol-phase chemical losses of SO_2, which are known to occur within clouds and fog (Seinfeld and Pandis, 2006).

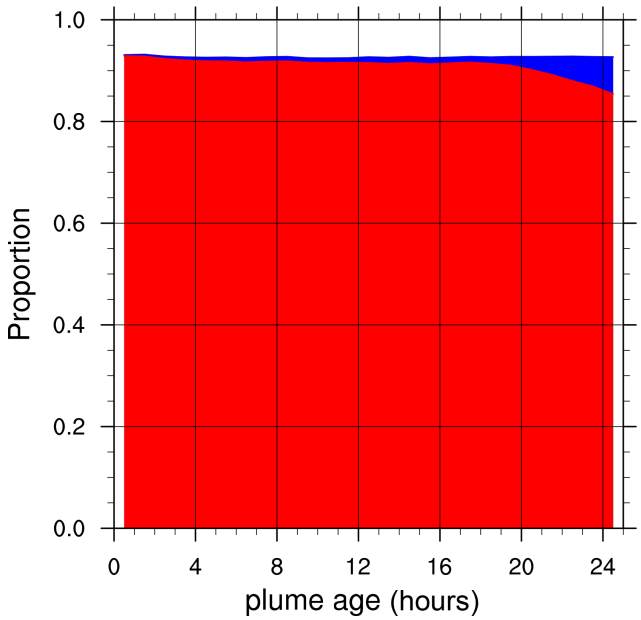

Figure 5.1: Proportions of volcanically emitted SO_2 remaining (red) and chemically destroyed (blue) vs. time since emission, for plume emitted between 2012-07-31 11:30:00 and 2012-07-31 12:30:00. The method of computation of these two values is described in the text.

In Figure 5.1 I show the model output of these ratios for pseudo-Lagrangian tracks of plume. The following phenomena are evident:

- Most SO_2 loss occurs within the first hour after emission, and amounts to roughtly 10% of the emissions.
- This loss is physical deposition rather than chemical destruction.
- Chemical destruction of volcanic SO_2 in the plume is generally negligible for the rest of the daylight on the day of emission.
- There is no chemical destruction of SO_2 at night. This is expected, as OH is a daytime-only species.
- There is an acceleration in the chemical loss of SO_2 towards the end of this 24 hour period (i.e. after sunrise).

The phenomenon of physical losses of SO_2 occurring only shortly after emission is logical, as Mount Etna's plume is only in close proximity to the ground

immediately after emission — downwind it is in the free troposphere, out of contact with the ground and no dry deposition occurs.

That chemical destruction of SO_2 is negligible for several hours after emission suggests that the near-vent related conclusions of McGonigle et al. (2004) can be extended for several hundred km downwind for volcanic emissions of the strength discussed here.

The model output shows that the chemical SO_2 lifetime is increased in the plume, compared to out-of-plume air. Figure 5.2 plots the instantaneous SO_2 chemical lifetime in a horizontal cross section of the model, and the plume is clearly visible as a region of elevated values. This effect clearly is lesser where

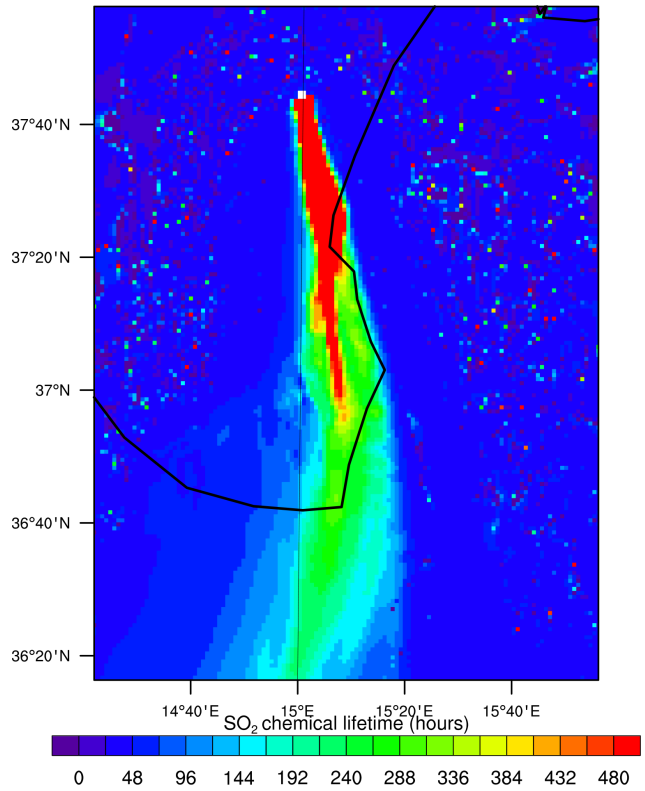

Figure 5.2: Instantaneous chemical lifetime of SO_2 at 2012-07-31 12:00:00 in a 3 km altitude horizontal cross section of the model.

the plume intensity is weaker. This is the cause of the acceleration seen after sunrise in 5.1, by this time the plume has dispersed considerably, and the SO_2 lifetime reverts towards normal values.

The chemical lifetime of SO_2 in the plume is given by Equation 5.1 where k is the rate coefficient of Reaction R39

$$\tau = \frac{1}{k[OH]} \tag{5.1}$$

This coefficient is not changed by the volcanic emissions, therefore the cause of the increased lifetime must be due to depreciated OH concentrations within the plume. This and related volcanic HO_x chemistry is discussed in the following section.

As discussed below and in Appendix C, the modelled in-plume OH depletion is over-estimated due to a bug in the code. However, even with slightly greater in-plume OH concentrations, the conclusions of this section would still hold.

5.2 HO_x chemistry within the plume

Quantitatively, the systems discussed in this section are significantly affected by the bug (Appendix C). This is addressed in the text. The Figures in this section should be considered qualitatively valid only.

The OH radical is the primary oxidant of the atmosphere, and OH reactions are part of most tropospheric chemical systems. OH is rapidly inter-converted with HO_2, a species which also interacts with other chemical systems. I use the term HO_x in this subsection to refer to the sum of OH and HO_2 — the term is sometimes used to refer to a larger family of radicals.

As was seen in Section 5.1, and is shown in later sections of this chapter, this volcanic influence on HO_x has knock-on effects in other chemical systems.

Figures 5.3–5.4 show horizontal cross-sections of the model output OH and HO_2 concentrations. These clearly show the influence of the plume. OH concentrations are reduced greatly, almost to zero. HO_2 concentrations are also significantly reduced, though, proportionately, not by as much as OH is.

By inspection of the rates of the various HO_x reactions within the plume, the cause of these phenomena are determined. The discussions below are based upon inspection of these rates in the model output. Because this chemical system is significantly influenced by the bug (Appendix C) I have chosen not to present quantitative results here; rather I present qualitative determinations that I derive from the model output after considering the bug's likely impact.

In the clean air outside of the plume, Reaction R39 is of negligible importance. However SO_2 is in very high concentration within the plume, and Reaction R39 causes OH to be substantially depleted. Reaction R40 also has a

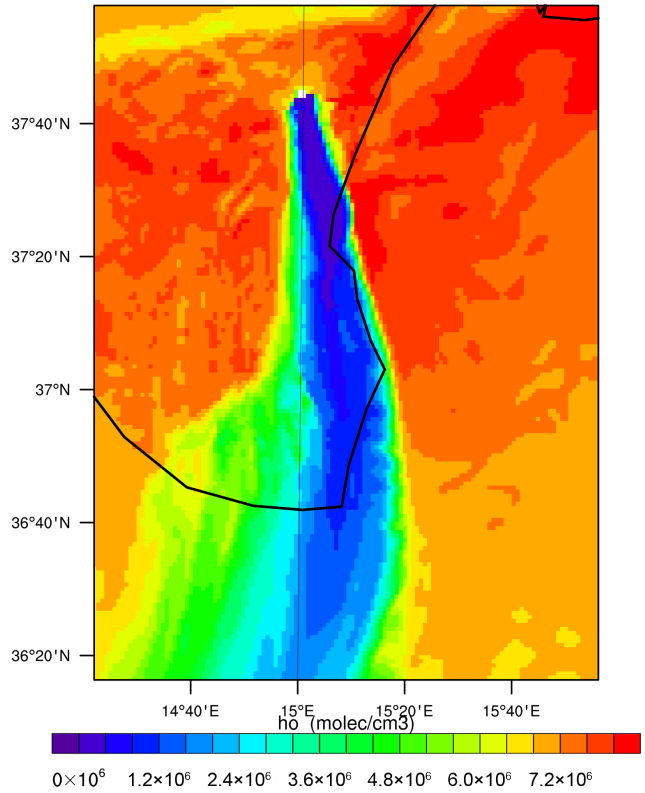

Figure 5.3: Modelled concentrations of OH at 2012-07-31 12:00:00 in a 3 km altitude horizontal cross section of the model.

significant impact.[2]

$$HCl + OH \longrightarrow Cl + H_2O \tag{R40}$$

HO_2 concentrations in the plume are also depleted. HO_2 is supplied by the aforementioned Reaction R39, however this is compensated for by decreases in various other $OH \longrightarrow HO_2$ conversion reactions which decline in rate due to the overall OH destruction (and, in the case of ozone destruction via reaction with OH, the in-plume destruction of both reactants).

However the most substantial in-plume influences on HO_2 are due to the bromine chemistry, a chemical system which is of negligible importance outside of the plume. The main bromine cycle is HO_2-destructive, due to Reaction R41.

$$BrO + HO_2 \longrightarrow HOBr \tag{R41}$$

Though a couple of bromine reactions can form HO_2, the overall effect of

[2]In the bug-affected output Reaction R40 causes a greater OH loss than Reaction R39, but after factoring in the bug the HCl-related flux is likely to be 2–3 times smaller.

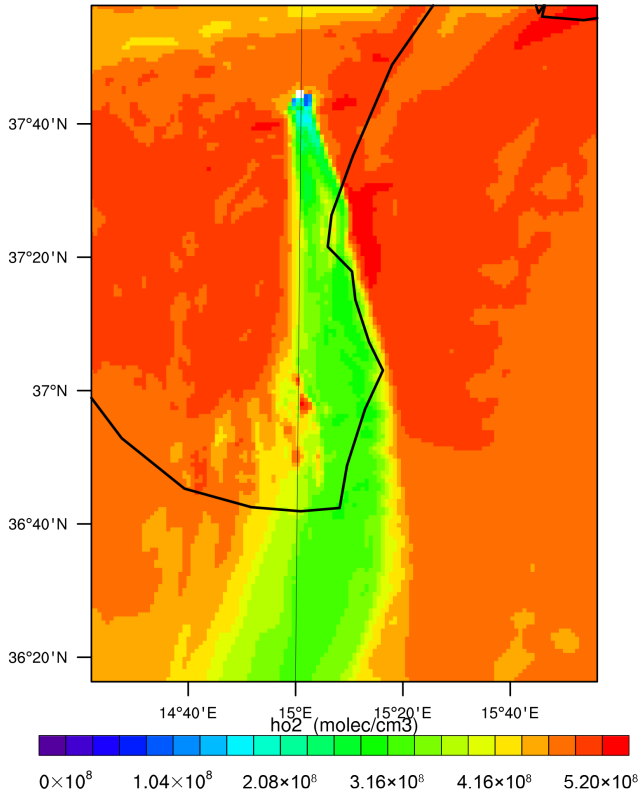

Figure 5.4: Modelled concentrations of HO_2 at 2012-07-31 12:00:00 in a 3 km altitude horizontal cross section of the model.

bromine chemistry is to cause a depletion in the concentrations of HO_2 within the plume.

5.3 Reactive nitrogen within the plume

In this subsection I discuss how the plume influences the balance of reactive nitrogen within the plume. In this subsection I use the term NO_x to refer to the sum of NO and NO_2, and NO_y to refer to the sum of NO_x and other forms of inorganic nitrogen which are less reactive –the principle additional species being HNO_3. N_2 and N_2O, which for the purposes of this investigation may be considered completely inert, are not included in NO_y.[3] As the free troposphere into which Mount Enta's plume is emitted is modelled to be a low-NO_x environment (see Section 4.4.1), this is a redistribution of a relatively small amount of nitrogen.

Figures 5.5–5.8 show the the modelled mixing ratios of NO, NO_2, HNO_3,

[3] N_2 and N_2O are sufficiently inert that they are not even modelled in the KPP.

and NO_y both in plume as it ages (blue), and the in corresponding model output for the model run without the plume (black). A plume track starting at 2012-08-01 12:00:00 is plotted.

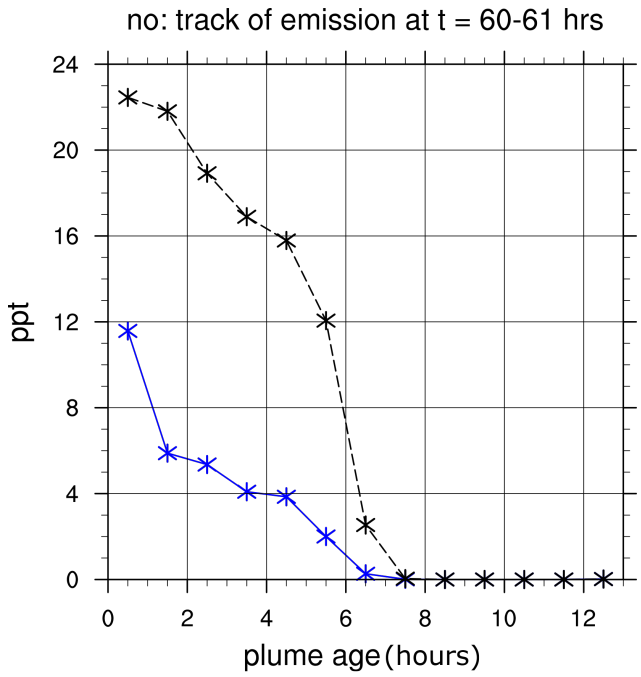

Figure 5.5: Average mixing ratios of NO within the plume as it ages, for plume emitted between 2012-08-01 11:00:00 and 2012-08-01 12:00:00 (blue) and the mixing ratio in the equivalent model output of the plume-free run (black).

There are two phenomena shown in Figures 5.5–5.8 which I discuss below:

1. The total amount of NO_y is substantially increased within the plume.
2. NO_x is substantially reduced in the plume.

The rise in modelled gas phase NO_y is due to revolatisation of ambient nitrate aerosol by volcanic acid gases, a phenomena which has been observed occurring at Masaya volcano (Allen et al., 2002). The corresponding decline in aerosol-phase nitrate can be seen in Figure 5.9. In this figure I have plotted the total amount of nitrate aerosol in units of "ppt equivalent", which is the mixing ratio which a gas formed from the complete volatilisation of the aerosol nitrate would have (assuming one nitrate group per gas molecule). This "mixing ratio" is substantially reduced in the with-plume model output and correlates with the associated rise in HNO_3. It should be noted that my choice of which time to track the plume for was made to highlight this effect — generally ambient nitrate aerosol is lower in the model output and this effect is smaller in magnitude.

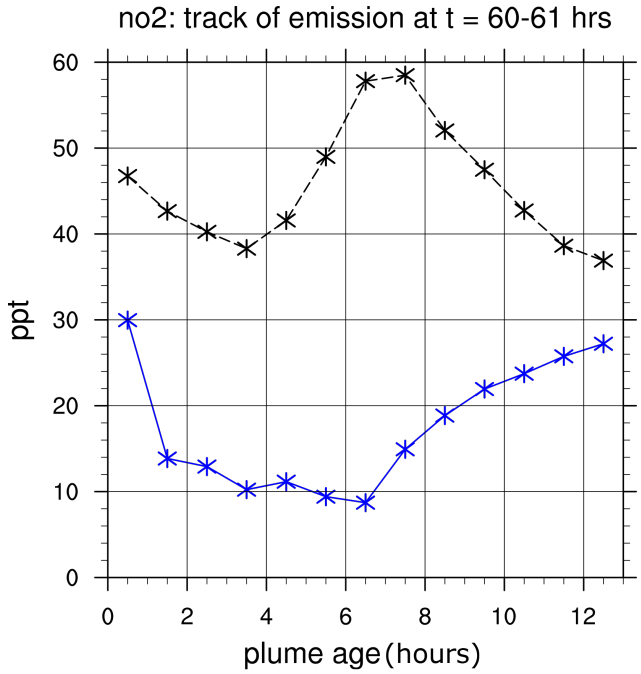

Figure 5.6: Average mixing ratios of NO_2 within the plume as it ages, for plume emitted between 2012-08-01 11:30:00 and 2012-08-01 12:00:00 (blue) and the mixing ratio in the equivalent model output of the plume-free run (black).

This phenomenon probably does not explain the observations of Mather et al. (2004b) and others (see table 1 in Martin et al., 2012, for a list of such observations) which observe substantially elevated NO_y in volcanic plumes. Revolatisation of aerosol nitrate is specifically discussed and dismissed as a possible explanation of these observations by Mather et al. (2004b).

The second phenomenon listed above is somewhat surprising, as OH concentrations are suppressed in the plume and the main destruction pathway of NO_x in the normal troposphere is oxidation via OH. However this is compensated for by the reaction of NO_2 with BrO to form $BrNO_3$, which then undergoes heterogeneous chemical reactions which release gas-phase HNO_3 (BrO concentrations outside of the plume are negligible, making this reaction unimportant). NO_2 and NO are sufficiently coupled that the loss of NO_2 results in a similar proportional reduction in the NO concentration. In terms of the bromine explosion this is a minor side-branch, however it is of sufficient magnitude to cause the effect shown. This chemistry also increases HNO_3, however as ambient HNO_3 concentrations are much larger than that of NO_x anyway, the proportionate increase in HNO_3 from this effect is small.

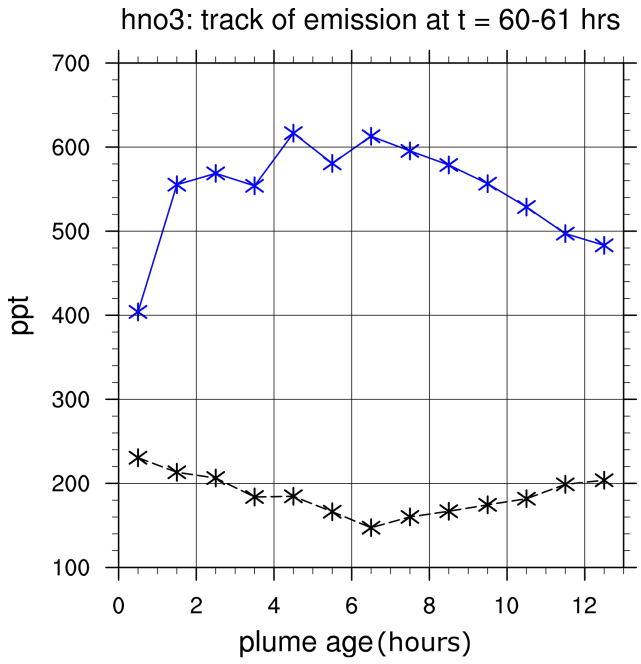

Figure 5.7: Average mixing ratios of HNO_3 within the plume as it ages, for plume emitted between 2012-08-01 11:00:00 and 2012-08-01 12:00:00 (blue) and the mixing ratio in the equivalent model output of the plume-free run (black).

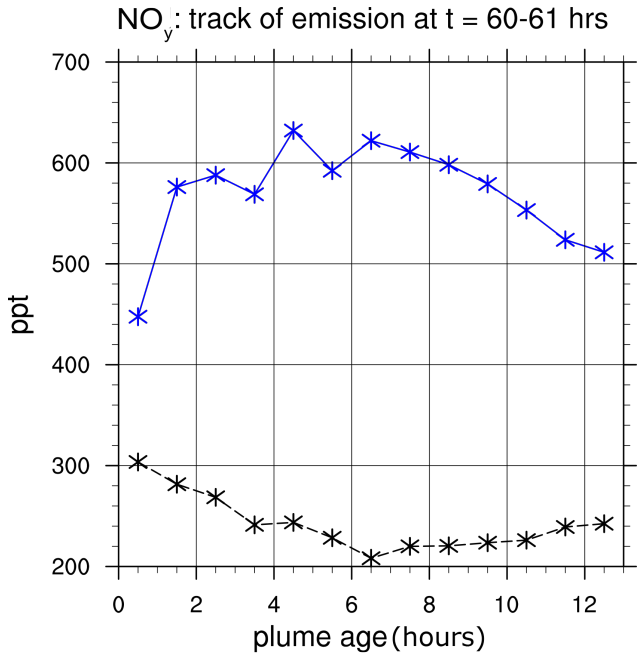

Figure 5.8: Average mixing ratios of NO_y within the plume as it ages, for plume emitted between 2012-08-01 11:00:00 and 2012-08-01 12:00:00 (blue) and the mixing ratio in the equivalent model output of the plume-free run (black).

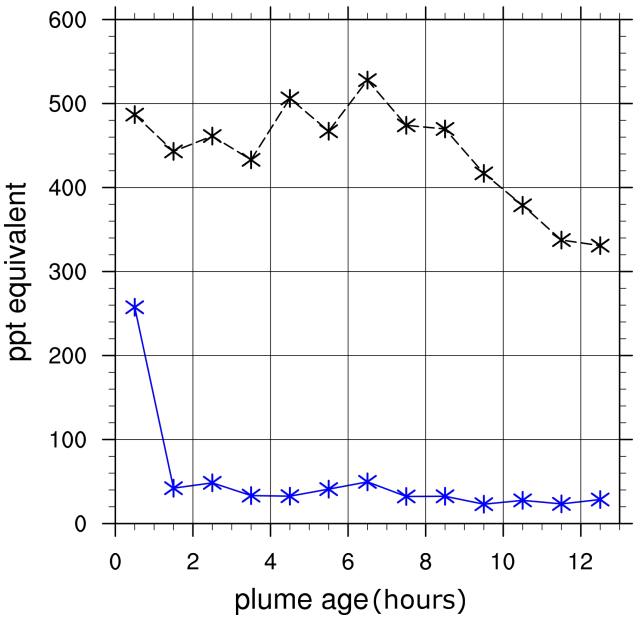

Figure 5.9: Average "mixing ratio" of nitrate contained within aerosol within the plume as it ages, for plume emitted between 2012-08-01 11:00:00 and 2012-08-01 12:00:00 (blue) and the "mixing ratio" in the equivalent model output of the plume-free run (black). The units of this plot, "ppt equivalent" are explained in the text.

5.4 Chlorine—organic chemistry

The systems discussed in this section are significantly affected by the bug (see Appendix C). This is addressed in the text. As a consequence of the bug, as in Section 5.2, the conclusions derived from the modelling in this Section are qualitative rather than quantitative.

During the daytime, Cl radicals are produced within the modelled plume by both the photolysis of BrCl — a part of the bromine explosion — and by Reaction R40. The rate of Reaction R40 is over-predicted by the model due to the bug (see Appendix C). Accounting for this suggests that BrCl photolysis is the dominant source of Cl radicals throughout the plume. Inspection of the modelled rates shows that the average production rate of Cl radicals from BrCl photolysis is of the order of 5×10^6 molec cm^{-3} s^{-1} in the first few hours of the plume at around midday. This declines as the plume disperses and sunlight intensity declines.

As discussed in Appendix C, the model erroneously considers the Cl radicals to react immediately, rather than some contribute to a chlorine oxide reservoir. The build-up of this reservoir would take an unknown length of time — without the bug the organic phenomena discussed in this Section may build up gradually while the reservoir accumulates.

Cl radicals react with alkanes, particularly CH_4. Despite the in-plume depletion of OH (suppressing the reaction of Ch_4 with OH), these Cl radicals mean that the total oxidation of CH_4 is substantially increased due to the plume.This does not substantially change CH_4 mixing ratios. CH_4 has a relatively invariant mixing ratio of roughly 1.8 ppm throughout the troposphere, and trace gas reactions are not of sufficient magnitude to substantially alter this on the time scales considered in this investigation. However the oxidation of CH_4 creates non-methane volatile organic compounds (NMVOCs), and mixing ratios of these in the modelled plume are substantially above background levels.

Organic radicals produced by alkane oxidation rapidly react with O_2 to produce alkyl peroxy radicals. Atmospheric organic chemistry is complex and involves many branching reaction pathways (Seinfeld and Pandis, 2006). For simplicity, in this section I will only discuss further the fate of the main peroxy radical produced by Cl radical reactions, CH_3O_2.

Figure 5.10 shows the major organic reaction pathways for single-carbon organics. As an illustration of the relative magnitude of the reactions within the

plume the figures is annotated with the average modelled rate of each reaction relating to plume aged 4.5–5.5 hours at 2012-07-31 12:00:00. The bug means that the magnitude of the fluxes through this system are moderately overestimated, but the overall system remains correct.

The organic chemistry within the plume differs from typical organic chemistry in two major ways:

- OH, HO_2, and NO are, to varying extents, suppressed in the plume (see previous sections). The rates of reactions where these are reactants are therefore reduced.
- There is an abundance of reactive bromine within the plume, and consequently bromine reactions which in the normal troposphere are of negligible importance are significant organic reaction pathways within the plume.

Inspection of Figure 5.10 shows that while the formation and destruction fluxes of CH_3O_2 are roughly equal, formation of both CH_3OOH and HCHO occur at a greater rates than their destruction via oxidation, meaning that these species are accumulating within the plume. This accumulation occurs both because of the Cl-induced increased formation of peroxy radicals, and because the rates of destruction of these species is substantially reduced due to the depletion of OH.

Overall, the concentrations of all three species are substantially increased within the plume. Figure 5.11 shows the concentrations of these organic species over a horizontal cross-section containing the plume. The effect of the plume is clearly visible.

In Figure 5.11 it can be seen that the spatial distribution of these three species differ slightly. This is a further characteristic of a reaction system that is not in a steady state — the elevated levels of CH_3O_2 in particular form faster and therefore nearer to the volcanic source than those of the "downstream" chemical products.

In conclusion of this subsection, the Cl generated within the plume increases the rate of formation of peroxy radicals. This, coupled with the decreased loss rate caused by the suppression of OH within the plume, results in accumulation of substantially increased concentrations of reactive organic species being a prominent feature of the plume. This modelled chemical system is particularly affected by the bug in the setup, though, as discussed in Appendix C, it

is still valid to identify this phenomenon in the model results, though the phenomenon's magnitude is likely to have been over-predicted due to the bug.

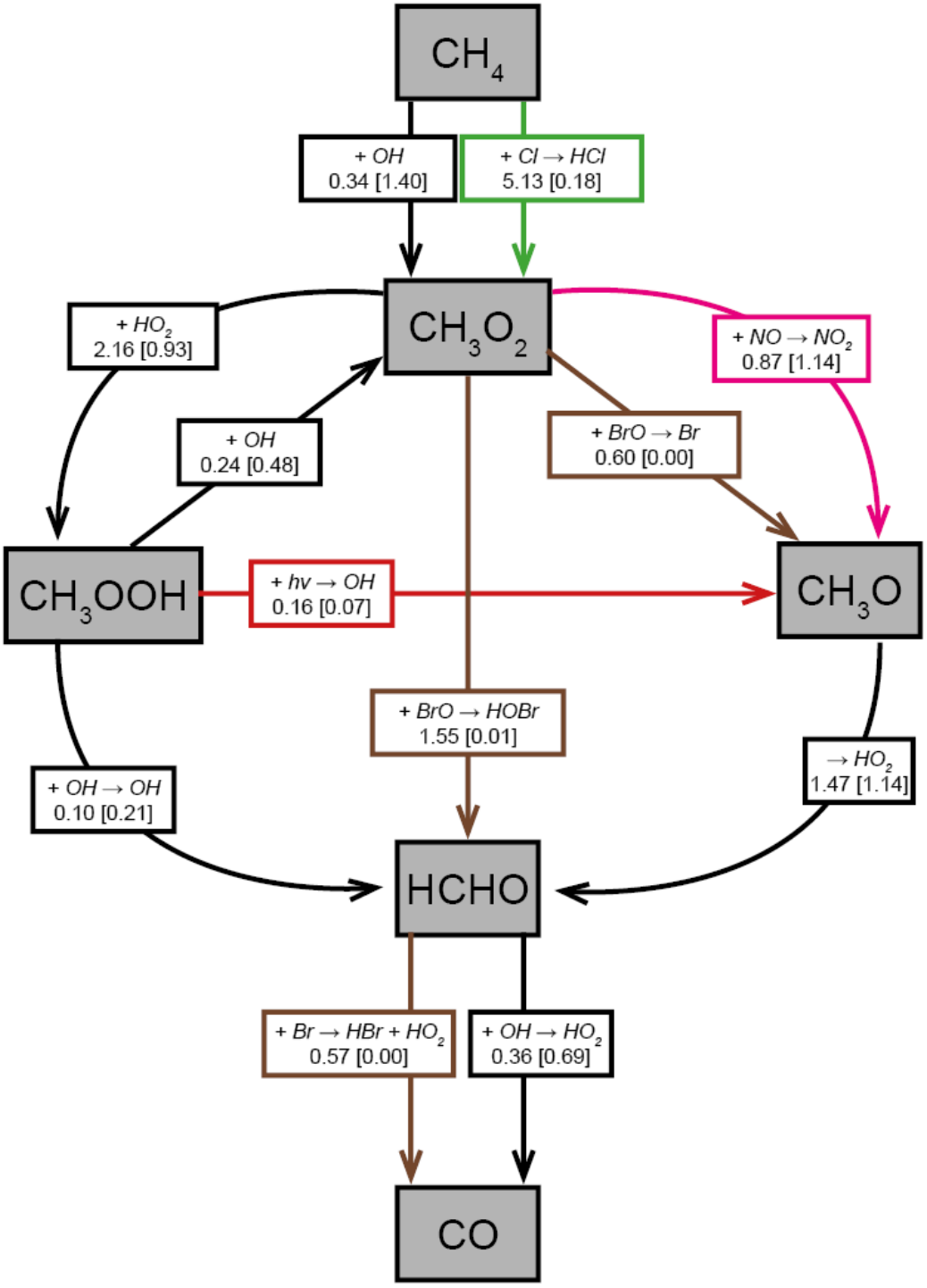

Figure 5.10: Major reaction pathways of single-carbon organics within the modelled plume during daylight. Boxes show non-organic reactants and products of each reaction. Values are the average rate of reaction within the modelled plume aged 4.5–5.5 hours at 2012-07-31 12:00:00, in units of 10^6 molec cm^{-3} s^{-1}, values in square brackets relate to rates in the equivalent space in the plume-free run.

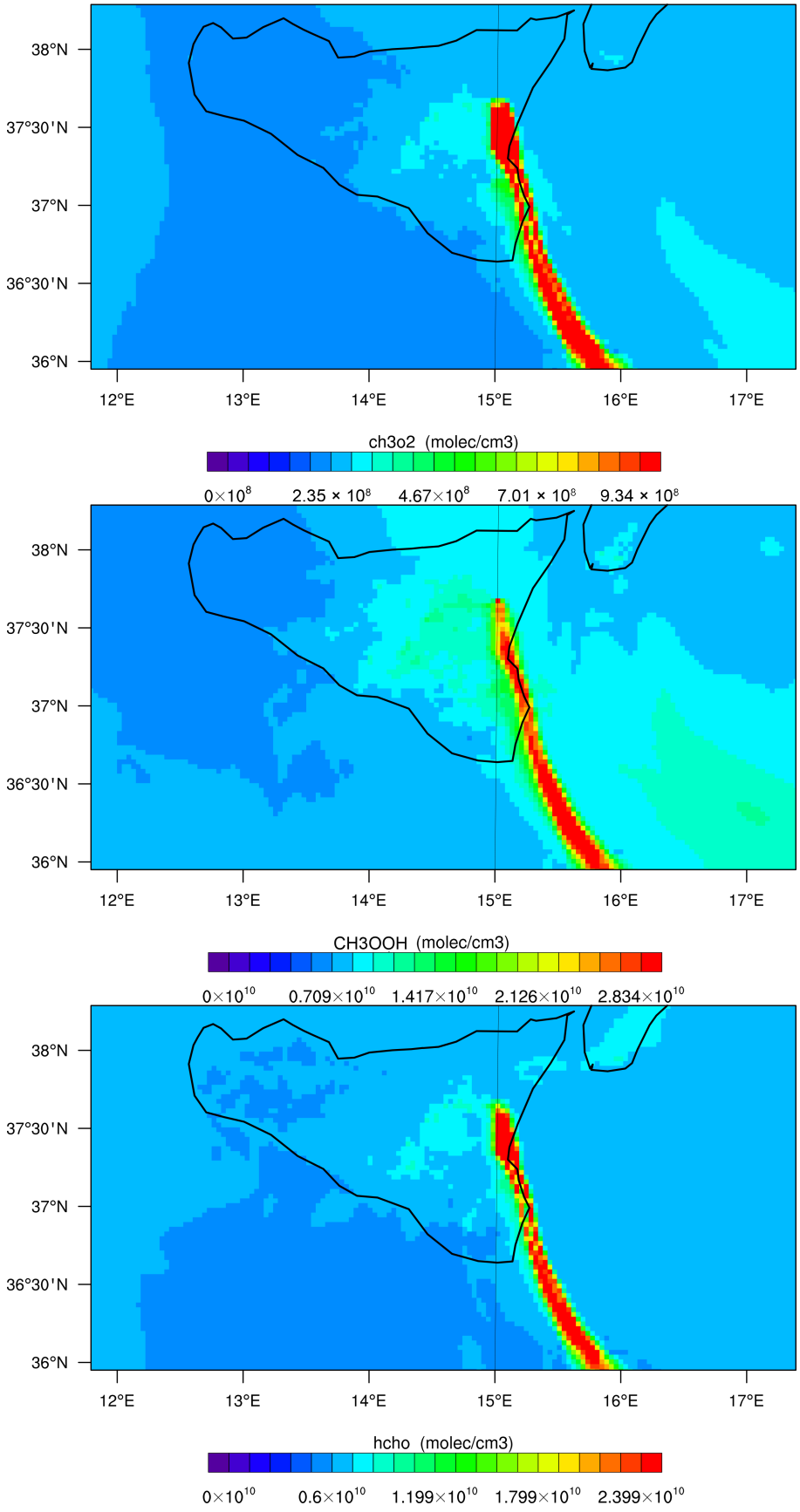

Figure 5.11: Modelled concentrations of CH_3O_2, CH_3OOH, and HCHO in a 3 km altitude cross-section over Sicily at 2012-08-01 12:00:00.

5.5 Aerosol within the plume

The bromine explosion relies upon heterogeneous reactions to recycle bromine. In the model the effective rate coefficients of these reactions are proportional to the available aerosol surface area. This subsection discusses the influence which the plume has on aerosol. Because of its importance to the bromine explosion, I use the aerosol surface area concentration (in units $cm^2\ cm^{-3}$) as my primary diagnostic variable.

The background aerosol provides some surface area for reaction. The modelled concentration (after the spin-up time) in the average surface area at 3 km over Sicily is of the order of a few $10^{-7}\ cm^2\ cm^{-3}$.

In the model setup I have set volcanic emissions of aerosol to be 2.4 kg s^{-1}, representing ash emissions and sulphate aerosol formed within the craters. I consider these to be *primary* aerosol from the volcano. This aerosol advects along with the gaseous volcanic emissions, and provides surface area for heterogeneous reactions to occur upon.

Additionally, *secondary* aerosol is formed within the volcanic plume. This is sulphate aerosol, formed from H_2SO_4 created by Reaction R39. Although in section 5.1 I show that this oxidation is of negligible importance in terms of the total SO_2 content of the plume, I show in this subsection that the amount of sulphate aerosol formed is sufficient to be significant in regards to the plume's aerosol content.

A cross section of the model output at 3 km altitude is shown in Figure 5.12. The plume is clearly visible as a region of greatly elevated aerosol surface area concentration. Also showing the same phenomenon, Figure 5.13 shows the modelled average aerosol surface area within an ageing plume as well as the equivalent model output from the plume-free run.

These figures show that the modelled plume acts to greatly increase the available aerosol surface area above that of the background and that this phenomenon persists for a long period downwind. In the young plume (few hours old) the available surface area actually slightly *increases* with plume age, despite plume dispersion; I discuss this phenomenon below. The relative contribution to the total in-plume aerosol from the background is therefore small in the young plume (~20%), with this percentage slowly increasing as the plume ages and disperses.

In Section 4.4 I note that there is a large degree of uncertainty regarding the

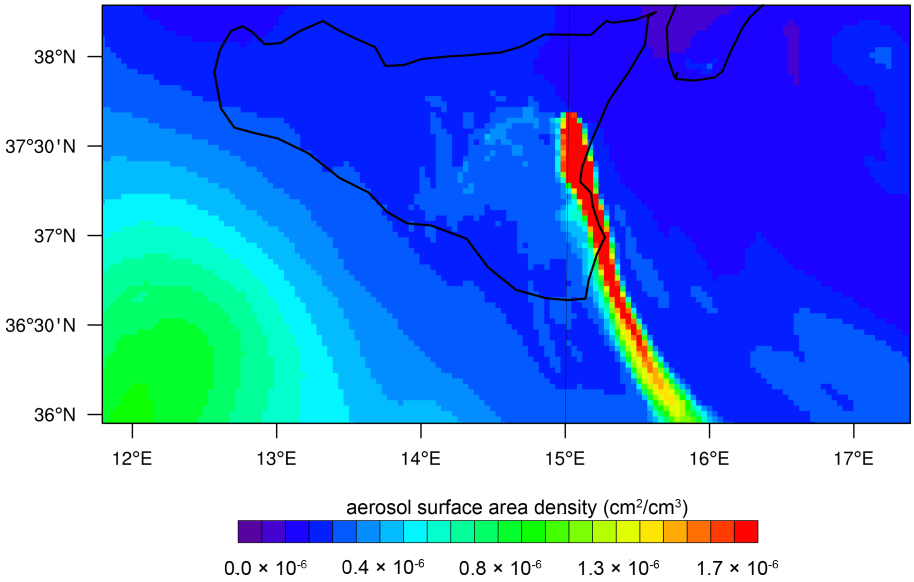

Figure 5.12: Modelled aerosol surface area concentrations in a 3 km altitude cross-section over Sicily at 2012-08-01 12:00:00.

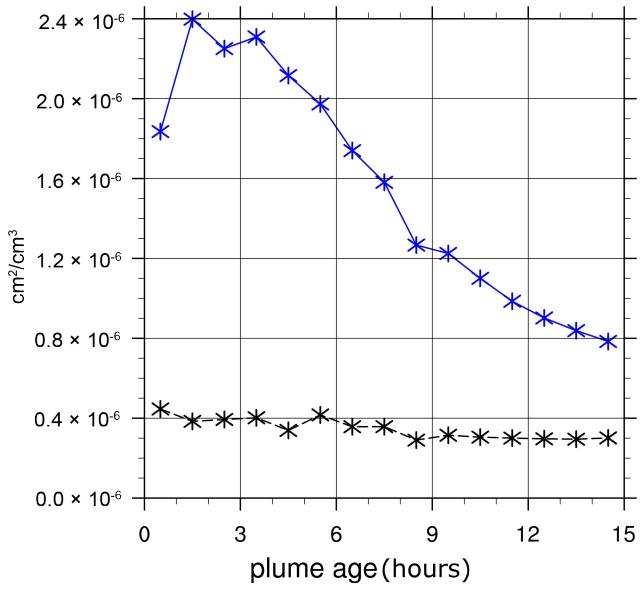

Figure 5.13: Modelled variation in average aerosol surface surface area for plume emitted between 2012-07-31 09:00:00 and 2012-07-31 10:00:00 as the plume ages (blue) and the values for the equivalent grid boxes in the plume-free run (black).

model's representation of background aerosol. However, this result suggests that the background aerosol is only a minor part of the aerosol in the young plume, and therefore uncertainty in the background aerosol is of reduced significance. For example, if the background aerosol was over-predicted by an order of magnitude by the model, this would change the average aerosol surface area concentration in the 0–5 hour plume tracked in 5.13 by only ~20%.

Figure 5.13 illustrates the relative contribution of the background aerosol and plume aerosol to the aerosol surface area concentration of the plume. It is also possible to elucidate the relative contributions of primary and secondary aerosol to this "plume aerosol" fraction.

The procedure used in the model for calculating the surface area concentration is described in chapter 2. Using the same method, the primary aerosol emissions can be calculated as a "surface area flux". An equivalent "volume flux" can be computed by calculating the volume of the representative spheres. These results are shown in Table 5.1. I have also computed the ratio of these emission rates of SO_2 flux (60 kg s^{-1}, which equals 5.6×10^{26} molec s^{-1}).

Table 5.1: Primary aerosol emissions from the volcano

	Emissions flux	As ratio of SO_2 emissions
Surface area	$9.8 \times 10^7 cm^2\ s^{-1}$	$1.7 \times 10^{-19} cm^2\ molec^{-1}$
Volume	$1.1 \times 10^3 cm^3\ s^{-1}$	$1.9 \times 10^{-24} cm^3.molec^{-1}$

SO_2 and tracer1 are emitted from the model volcano at the same rate, therefore the primary aerosol surface area/SO_2 flux ratio in Table 5.1 is identical to the model's primary aerosol surface area/tracer1 flux ratio.

By definition, primary aerosol cannot be created within the plume as it ages. Assuming that it is not significantly deposited either,[4] the primary aerosol volume/tracer1 ratio should remain constant (i.e. equal to the ratio of fluxes) as the plume ages — implying that any additional plume aerosol must be secondary. The same approach can be used for aerosol surface area/tracer1 ratios, though this requires the additional assumption that the ratio of the aerosol surface area to the amount of aerosol (a function of the aerosol size distribution) remains constant.

Figure 5.14 plots for the same model output as Figure 5.13 the evolving ratio of the average aerosol surface area and volume in the plume to that of the tracer. The values used in these plots are the differences between the with-plume and without-plume model runs; these plots show only "plume aerosol". The pink horizontal line on this plot indicates $1.7 \times 10^{-19} cm^2.molec^{-1}$, the ratio relating to the primary surface area flux.

Figure 5.14 shows that the secondary aerosol formation within the plume is substantial. The average plume aerosol surface area/tracer1 ratio within the

[4]Some primary aerosol is likely to be deposited in the early plume. This methodology produces an upper bound for the amount of primary aerosol within the plume.

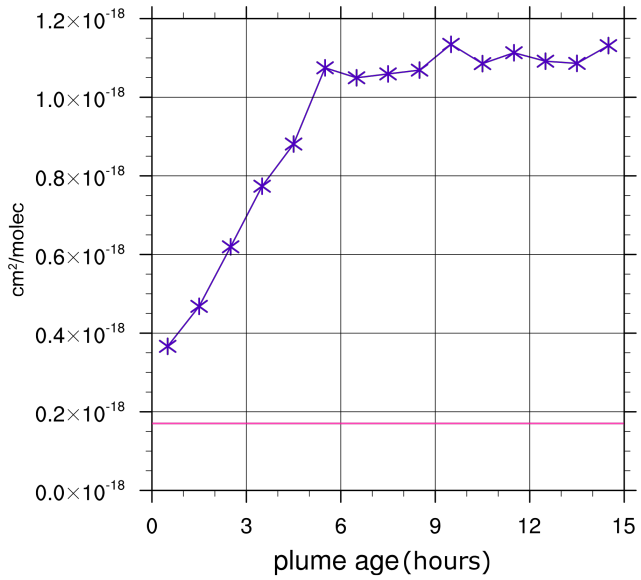

Figure 5.14: Modelled average ratio of "plume aerosol" surface area (calculated as the difference in aerosol surface area between with- and without-plume model runs) and the concentration of the inert tracer for plume emitted between 2012-07-31 09:00:00 and 2012-07-31 10:00:00 as the plume ages. The horizontal pink line indicates 1.7×10^{-19}cm^2.molec^{-1}, the ratio relating to the primary surface area flux.

0–1 hour-old plume is about 3.8×10^{-19}cm^2.molec^{-1}, which is roughly twice the ratio of the flux of primary aerosol to that of the tracer (indicated by the pink line). This shows that even in this very young (daytime) plume the split between primary and secondary aerosol, in terms of contribution to the aerosol surface area, is approximately 50:50. As the plume ages, the plume aerosol surface area/tracer1 ratio increases, as more secondary aerosol is formed via photochemistry. The implied secondary/primary ratio of contributions to the plume aerosol surface area increases substantially until nightfall causes the photochemical processes to cease.

In conclusion of this subsection, the plume substantially increases the aerosol surface area available for heterogeneous reactions above that of the non-volcanic background aerosol. This effect does dissipate as the plume disperses, but in the first few hours after emission this is mitigated by the formation of secondary aerosol. Overall secondary aerosol contributes substantially more than primary aerosol to the available surface area for reactions.

5.6 Bromine chemistry within the plume

In Section 4.5 in checking the model output, I show that the plume contains elevated levels of BrO (Subsection 4.5.2) and reduced mixing ratios of O_3 (Subsection 4.5.3). These are both indirect indications of the reactive cycle known as the bromine explosion. In this section I discuss this reaction cycle in detail.

There are many interconnected phenomena regarding the bromine chemistry of the plume, and as such this subsection is divided into several parts focussing on different aspects of the chemistry. The bromine cycle, which is central to all the discussions of this subsection, is illustrated in Figure 5.15.

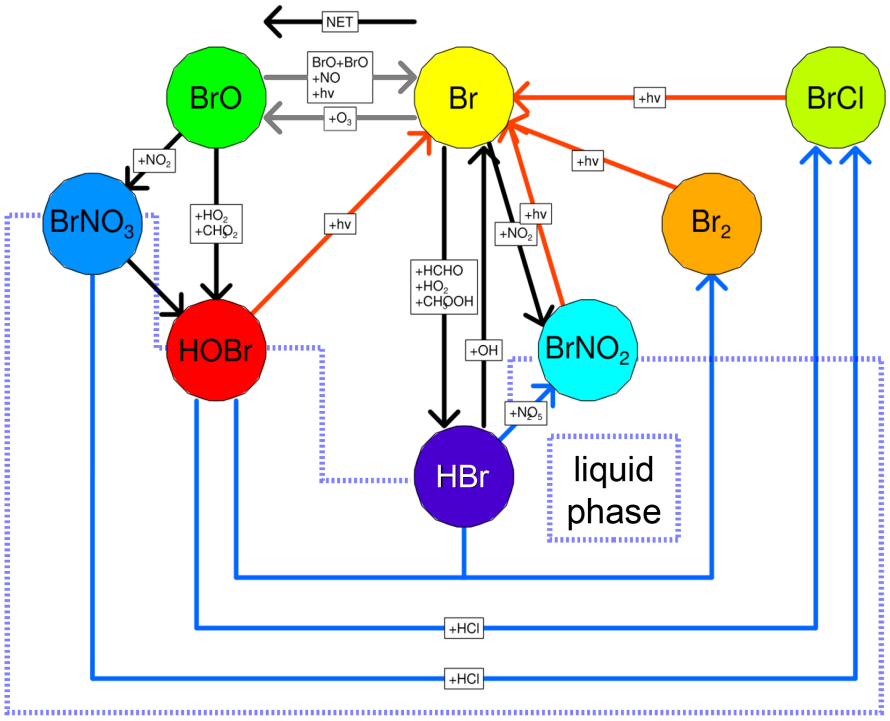

Figure 5.15: Diagram of the major reactive pathways of the bromine cycle within the plume.

5.6.1 Bromine partitioning in the first hour of the plume

The reactions are also listed below as they appear in the model mechanism. I refer to these labels throughout this discussion. These are most, but not all, of the bromine-related reactions in the mechanism — others turn out not to be important for understanding plume chemistry.

Photolysis reactions:

$$BrO + h\nu \longrightarrow Br + O_3 \quad \text{(R42)}$$
$$Br_2 + h\nu \longrightarrow 2\,Br \quad \text{(R43)}$$
$$HOBr + h\nu \longrightarrow Br + OH \quad \text{(R44)}$$
$$BrNO_2 + h\nu \longrightarrow Br + NO_2 \quad \text{(R45)}$$
$$BrCl + h\nu \longrightarrow Br + Cl \quad \text{(R46)}$$

Gas-phase reactions:

$$BrO + BrO \longrightarrow 0\cdot621\,Br + 0\cdot19\,Br_2 \quad \text{(R47)}$$
$$BrO + NO \longrightarrow Br + NO_2 \quad \text{(R48)}$$
$$BrO + NO_2 \longleftrightarrow BrNO_3{}^5 \quad \text{(R49)}$$
$$BrO + HO_2 \longrightarrow HOBr \quad \text{(R50)}$$
$$BrO + CH_3O_2 \longrightarrow 0\cdot72\,HOBr + 0\cdot28\,Br + 0\cdot28\,HO_2 + HCHO \quad \text{(R51)}$$
$$Br + O_3 \longrightarrow BrO \quad \text{(R52)}$$
$$Br + HO_2 \longrightarrow HBr \quad \text{(R53)}$$
$$Br + CH_3OOH \longrightarrow CH_3O_2 + HBr \quad \text{(R54)}$$
$$Br + HCHO \longrightarrow HBr + CO + HO_2 \quad \text{(R55)}$$
$$Br + NO_2 \longrightarrow BrNO_2 \quad \text{(R56)}$$
$$HBr + OH \longrightarrow Br + NO_2 \quad \text{(R57)}$$

Heterogeneous reactions:

$$BrNO_3 + HCl \longrightarrow BrCl + HNO_3 \quad \text{(R58)}$$
$$HOBr + HCl \longrightarrow BrCl \quad \text{(R59)}$$
$$HOBr + HBr \longrightarrow Br_2 \quad \text{(R60)}$$
$$BrNO_3 \longrightarrow HOBr \quad \text{(R61)}$$
$$HBr + N_2O_5 \longrightarrow BrNO_2 + HNO_3 \quad \text{(R62)}$$

In this section I show how bromine is distributed between the different species within the plume, and how this distribution changes with age.

In the default model run setup (see section 2.3.2), the bromine emissions

were set to 0.06% of the SO_2 emissions (by volume), with 23% of this emitted as Br radicals and 77% emitted as HBr (emissions of other bromine species are negligible). However the proportion of bromine in both of these forms fall rapidly after emission. Figure 5.16 shows the changing proportion of bromine in each of the major forms of bromine. Unlike previous pseudo-Lagrangian plots in this chapter, these plots represent a *snapshot* of the model output at a single time, with information about the plume aged 0–1 hours plotted. However, due to the short time-scale involved, these plots can be considered representative of how plume evolves as it ages.

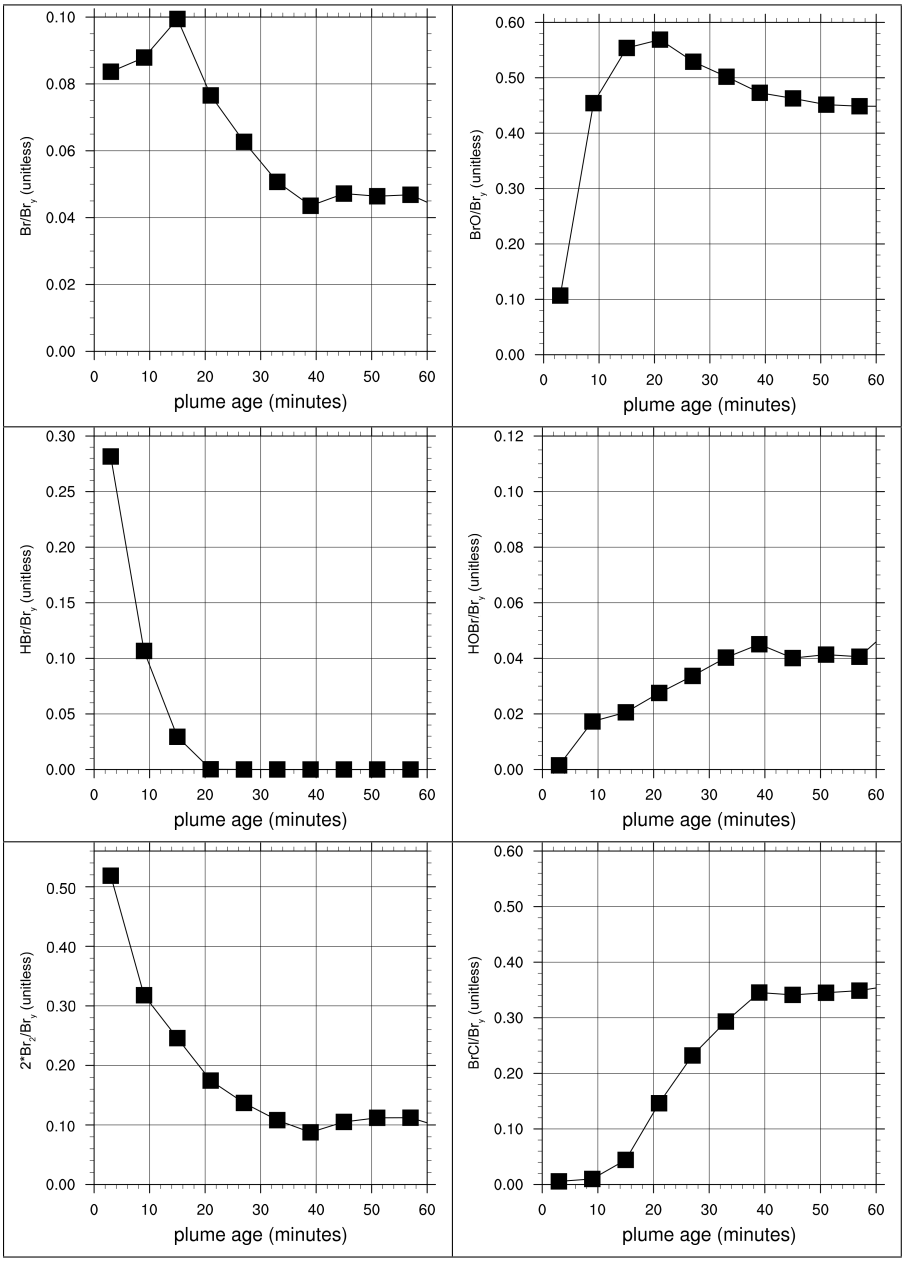

Figure 5.16: Fraction of modelled bromine in the different forms within the 0–1 hour-old plume at 2012-07-31 12:00:00.

$BrNO_2$, $BrNO_3$, HgBr, and $HgBr_2$ are absent from both Figure 5.16 and the discussion below. Although modelled, these species are present only in insignificant quantities in the modelled plume.

Figure 5.16 shows that there is a rapid change in the bromine chemistry occurring within the first hour of the plume's existence. For the purposes of explaining the phenomena, I consider there to be three somewhat distinct chemical regimes occurring.

Regime 1, 0–15 minutes: Depletion of HBr

Although HBr constitutes 77% of modelled bromine emissions, it is rapidly depleted within the plume — even for the very first markers of Figure 5.16 (0–6 minute average) it is only ~28% of the total plume bromine. It takes about 15 minutes for HBr to be effectively eliminated from the plume.

In this very early plume, the proportion of bromine present as Br_2 is high. This is formed in the same reaction that depletes HBr, the heterogeneous Reaction R60. The high aerosol loading in this very early, highly concentrated, plume makes this reaction especially rapid. Although Br_2 is not directly emitted from the model volcano in any substantial amount, it is already the majority form of bromine for the 0–6 minute period. This Br_2 is produced in a "flurry" of rapid re-equilibration of the volcanic volatiles that occurs within seconds of emission.

During this period, this reaction consumes HOBr and therefore keeps HOBr levels low. Competing with its destruction is the formation of HOBr from BrO. This HOBr proportion rises within this period as BrO, and therefore the production, rises.

BrO and Br exist in equilibrium, mediated primarily by Reactions R52 and R42. Typically in the troposphere this equilibrium results in large BrO/Br ratios. However in the very early plume O_3 is substantially depleted, resulting in a greater proportion of Br radicals. Additionally Reaction R47 reaction occurs rapidly within the very concentrated early plume, which also shifts the equilibrium in the same manner.

The overall proportion of bromine in the Br $\longleftrightarrow$ BrO system rises over this period, due to the supply of Br from photolysis of the elevated levels of Br_2.

The entrainment of background air brings the concentration of O_3 closer to ambient levels, and the dispersion of the plume lowers the concentration of BrO

which reduces the rate of the BrO + BrO reaction. These effects bring the BrO/Br ratio closer to a "normal" value.

This regime can be considered to come to an end once HBr has been depleted to negligible levels within the plume, this occurs at about 15 minutes after emission.

Regime 2, 15–35 minutes: Transition to BrCl reservoir

During regime 1, Reaction R60 rather than Reaction R59 dominates the recycling of HOBr, the model considers that HBr is "preferred" as a reactant over HCl. However once HBr is depleted, and its reaction with HOBr becomes far less significant for bromine cycling, Reaction R59 "takes over" this function. HCl is abundant within the plume, its emission flux being approximately 650 times that of bromine, and, as discussed in Section 5.4, it is quickly reformed after reactions which destroy it.

The modelled photochemical lifetime of Br_2 at this time in the model is about 2 min^{-1}. With the Reaction R60 source of Br_2 diminished in this second regime, it would therefore be expected that Br_2 would decline rapidly in a few minutes. However, although the proportion of Br_2 declines, it does so at a slower rate than its photolysis lifetime would suggest.

This occurs because the early plume is very concentrated, and BrO constitutes a large part of volcanic bromine. This results in high concentrations of BrO which makes the self-reaction of BrO significant. Reaction R47 normally produces two Br radicals, but 19% of the yield of this reaction is considered to be Br_2. This Br_2 supply is sufficient to produce the trend shown. As the rate of this reaction is quadratically related to the concentration of BrO, this flux declines substantially as the plume disperses (which reduces the concentration of all bromine species).

The proportion of bromine as Br_2 does not decline to zero within the plume, instead it falls to a "baseline" of ~10%. This is sustained by the Reaction R55 the HBr generated is almost instantly consumed in Reaction R60, generating a low but sustained fraction of Br_2.

With the suppressing factor of the rapid Reaction R60 lifted, during this period the bromine fraction as HOBr rises slightly. However the heterogeneous reactions are fast enough to keep this level below 5%.

During this second regime, the proportion of bromine present as BrCl

Table 5.2: Fraction of bromine in each of the major species in 1 hour old plume at 2012-07-31 00:00:00

Species	Fraction of total bromine / %
Br	5
BrO	45
HOBr	4
BrCl	35
Br_2	11
HBr	0

steadily rises, being formed through Reaction R59. As an increasing amount of bromine is held in BrCl the amount within the Br $\longleftrightarrow$ BrO equilibrium system declines from its peak at the end of regime 1. Both BrO and Br proportions decrease during this regime, though as this decline occurs simultaneously with the continuing "re-normalising" of the BrO/Br ratio, the decline of Br is, proportionately, more pronounced than that of BrO. The (smaller) decline in BrO fraction causes there to be local maximum in the profile of the BrO fraction plotted against time.

This regime can be considered to come to an end once the proportions of plume bromine as Br_2 and BrCl stabilise at approximately 10 and 35% respectively. In this model output this occurs at about 35 minutes after emission.

Regime 3, post-35 minutes: Stability

In this third regime the distribution of bromine between the different forms is approximately stable. This does not mean that reactions are not occurring, but rather than for each species creation and destruction occur at approximately equal rates. Overall the speed of this chemistry does decline as plume dispersal lowers the concentrations of all species, and therefore lowers the rates of reactions. Additionally the predominant reservoir species in this regime is BrCl, which is the most stable of all the bromine species considered here (its photolysis rate is approximately one-third that of Br_2).

Table 5.2 shows these "stable" levels of bromine fractionation.

5.6.1.1 Assessment

This model output shows three stages of plume evolution. The first is characterised by the destruction of the emitted HBr, a process which is complete

within a few minutes, transferring this bromine to other forms. The second, transitional, stage is characterised by the indirect transfer of bromine from Br_2 to BrCl. This process takes around 20 minutes to reach a stable situation.

It is apparent that in the daytime, all of the emitted bromine can be considered to be part of the reactive inorganic bromine chemistry of the modelled plume. Heterogeneous chemistry consumes HOBr rapidly. When it is available, this HOBr reacts with HBr. However once this is consumed the heterogeneous cycling does not slow to the rate of HBr production, as Reaction R59 fulfils the role of the heterogeneous part of the bromine reaction cycle.

In terms of comparison with real-world observations, it is the BrO output which is the most useful. Section 4.5.2 shows that the model reproduces in a general sense the observed increase in BrO/SO_2 in the first few km of plume transport, however the results of this section permit a more precise assessment.

This rise can be attributed to two factors, the release of bromine from HBr which happens within regime 1, and the declining importance of the Br_2-creating BrO + BrO reaction. In terms of the BrO concentrations, the BrO/Br balance is of low importance after the first few minutes, as BrO significantly dominates this equilibrium.

Figure 5.17 shows the ratio of the concentrations of BrO and SO_2 for this model output. The form of this graph is near-identical to that of the BrO/total bromine ratio. This occurs because the non-volcanic sources and the sinks of both SO_2 and bromine are negligible over this timescale, and therefore the bromine/SO_2 ratio is effectively constant.

It is instructive to compare this plot with the results of section 3.1 of Bobrowski and Giuffrida (2012). Given a linear relationship between the time since emission and the distance from crater (i.e. assuming a steady wind speed. Bobrowski and Giuffrida (2012) use an estimate of 10 m s^{-1} (1 km $\approx$ 100 s)), these two datasets can be compared. The observational data show the BrO/SO_2 ratio in the plume rising quickly over the first few km, and then reaching an approximately stable level. The data are of insufficient quantity/quality to determine whether or not the local maximum of BrO modelled at approximately 20 minutes after emission occurs in the measured plumes, however a levelling-off of the BrO/SO_2 occurs in both datasets at roughly equivalent times.

If the modelled situation is accurate in terms of the bromine partitioning, this suggest that measurements of in-plume BrO in these types of plumes made after

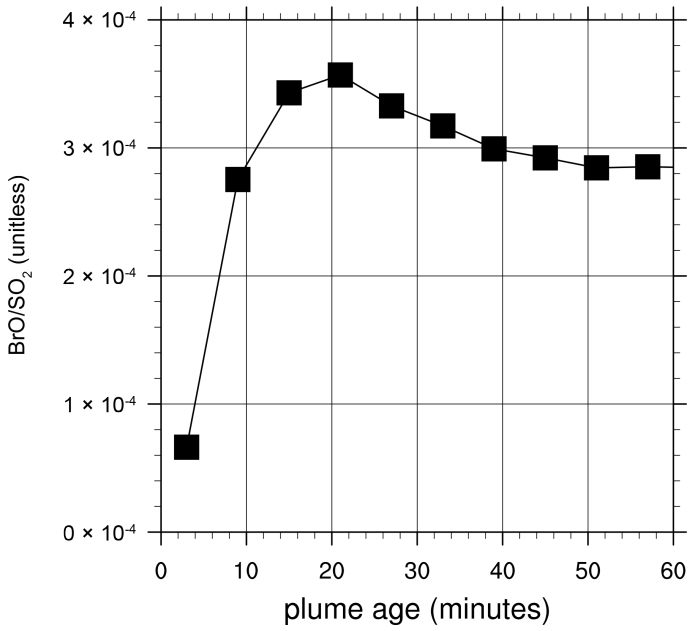

Figure 5.17: Modelled ratio of BrO to SO_2 within the 0–1 hour-old plume at 2012-07-31 12:00:00.

the "levelling off" has occurred can be converted to estimates of total in-plume inorganic bromine (Br_y) via multiplication by a linear factor, which henceforth I shall refer to as Ω. Mathematically, this can be written as:

$$Br_y = \Omega BrO \tag{5.2}$$

I will refer to the fraction of Br_y as BrO, i.e. $\frac{1}{\Omega}$, as Z.

In the case modelled in this section Ω is approximately 2 (Z = 0.5). This model output shows that the variation of the BrO/total bromine ratio is small after regime 1 has ended, meaning that were this factor is calculated assuming the plume was in the "stable" regime 3, but actually a measurement was made of plume in regime 2, the resulting error would be small. For the purposes of using BrO measurements to monitor bromine emissions from volcanoes this is a fortuitous phenomenon. If one can be confident that a measurement was taken after regime 1 had ended, and have confidence in a value of Ω, then $Br_y = \Omega BrO$ can be used to estimate the total Br_y in the plume.

The utility of this equation for interpreting observations would depend upon the ease of estimating Ω for a plume, regime 1 being short-lived, and the local maximum in the BrO faction being of relatively small magnitude. To address these questions, in the following section I consider similar model output from different times in the model.

5.6.2 BrO fraction variability with time of emission

In this subsection I show model output regarding the BrO content of young plumes emitted at different times within the model, in order to assess how consistent the phenomena identified in Section 5.6.1 are.

This exercise only directly considers one parameter which could potentially impact the evolution of the plume: the actinic flux. Looking at model output for different times within the model indirectly varies the meteorology considered, however in this case the local weather is generally consistent.

Figure 5.18 shows plots of BrO fraction of total bromine for plume (Z) aged 0–1 hours for 8, 9, 12, 15 and 16 UTC on both 2012-07-31 and 2012-08-01. This represents the likely range of times that a spectroscopic measurement would be taken.

Figure 5.18 shows that the behaviour observed at noon (i.e. those studied in Section 5.6.1) is replicated at other modelled times, however the development through the regimes is slower — the greater the time difference from noon the slower the progression.

This occurs because photolysis is the main driver of almost all of the chemistry of the bromine explosion, either directly (i.e. the photolysis of Br_2 and BrCl) or indirectly (radical reactants being produced by photolysis-dependant processes).

Despite this shift, the "stable" BrO/Br_y fraction attained is approximately consistent across all of these cases, being between 45 and 60%. This value fraction is greatest in the early morning and late afternoon cases, i.e. when the actinic flux is lowest. This variation is sufficiently small that, to one significant figure, an Ω value of 2 is appropriate for each case.

The stability of this system occurs because both the main source and the main sink of the BrO are dependant on photolysis. For the purpose of this discussion, I will consider reactions which create and destroy Br to be sources and sinks of BrO as Br and BrO exist in a rapid BrO-dominated equilibrium. Similarly, I do not consider interconversion reactions of BrO and Br to be either sources or sinks of BrO.

In the "regime 3" state, the main sources of BrO are the photolyses of BrCl and Br_2 (Reactions R46 and R43, which produce Br which in turn forms BrO through Reaction R52). The main sink of BrO is Reaction R41 reaction. The concentrations of HO_x, of which HO_2 is the dominant component, vary diurnally as HO_x is produced from a chain of reactions starting with the photolysis of O_3 to produce $O(^1D)$.

Although HO_x concentrations are perturbed by plume chemistry (Section 5.2), the diurnal variation of HO_x holds within the plume as well as without. Additionally, the depletion of HO_2 within the plume is compensated for by the formation of CH_3O_2 (see Section 5.4), which is also able to react with BrO. The Cl which forms this CH_3O_2 is also formed by photolysis; either directly from Reaction R46, or indirectly through Reaction R40 reaction.

The rate coefficient of Reaction R50 is, at a temperature of 300K, 1.6×10^{-12} molec^{-1} cm^3 s, whereas the rate coefficient for Reaction R51 is 6.9×10^{-12} molec^{-1} cm^3 s. This means that, in terms of BrO destruction potential, a plume chemistry-caused HO_2 depletion of 2×10^8 molec cm^{-3} (such as shown in the model output in Figure 5.4) is more than compensated for by a CH_3O_2

concentration increase of 10×10^8 molec cm^{-3} (see Figure 5.11). The effective rate constant of the destruction of BrO is therefore relatively unchanged by plume chemistry.

The variations of the photolysis rate coefficients of Br_2 and BrCl over a diurnal cycle are near-identical in form, with only a linear factor differentiating them. The profile of the photolysis coefficient of O_3 (which is, indirectly, the source of HO_x) is different, falling away more sharply from its noontime peak in the morning and afternoon. Compared to noon, the afternoon regime 3 ratio of BrO's production from $BrCl/Br_2$ photolysis to that of its removal via HO_x is increased. The effect of this can be seen in the model output, Z is at its smallest at noon, and is moderately larger in the afternoon and morning.

In general, with both the rates of destruction and creation of BrO varying with the intensity of sunlight, the overall effect of variations of sunlight intensity on Ω and Z are consequently small. This effect has been investigated in this subsection by looking at model output for different times of day. This effect should be consistent with other causes of variation in photolysis, such as variations in the season or latitude of emission (if considering non-Etna volcanoes).

A second consequence of BrO creation and destruction being dependent on actinic flux is that, assuming the HOBr destruction by heterogeneous chemistry is very fast, the speed of the cycling, and therefore the O_3 loss, is dependent on the actinic flux.

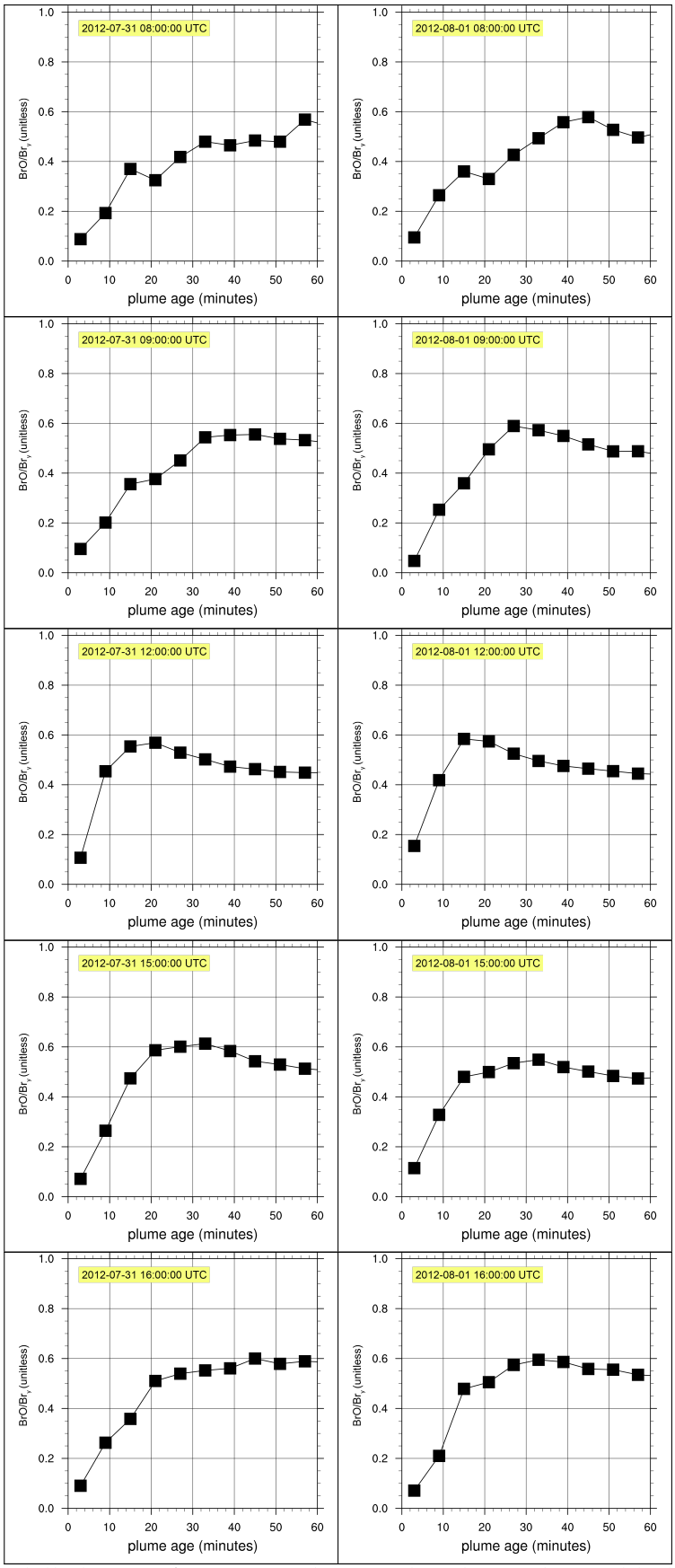

Figure 5.18: Modelled ratio of BrO to total Br_y within the 0–1 hour-old plume at various times.

5.6.3 Long-term (>1 hour) bromine chemistry

In the previous subsection I examined the bromine chemistry occurring within the first hour of plume evolution, and found that an approximate photochemical steady-state seems to emerge within this time frame. In this subsection I consider the evolution of the plume on a longer time-scale.

There are two major physical changes that impact the development of the plume as it ages (going from left to right in Figure 5.19):

- **Variations in the actinic flux**. When considering plume evolution over a timespan of hours, it is necessary to consider the diurnal cycle. Figure 5.19 plots a modelled volcanic plume emitted at approximately solar noon (hour 36), thus the actinic flux declines over the next few hours, with the sun setting about 6–7 hours after noon. Sunrise occurs 4–5 hours after midnight.[6] As discussed in Section 5.6.2, the variations in actinic flux, and therefore the variations in rate of photolysis reactions, can influence the plume chemistry.

- **Dispersion of the plume.** As shown in Section 4.5.1, the plume disperses as it travels downwind. This will decrease the rate (as measured in the units reactions cm^{-3} s^{-1}) of all reactions involving volcanic volatiles and their products. When considering the fluxes within the plume as a whole, this will not influence first-order reactions or photolysis reactions as the decrease in rate in terms of molecules cm^{-3} s^{-1} will be directly compensated for by an increase in the volume over which these reactions occur. This will also be the case for reactions of plume components with background species, assuming the concentrations of these background species are not significantly changed by plume chemistry; if this assumption does not hold, then the relation of chemical flux to plume dispersion will be complex. For reactions between plume species, including the heterogeneous reactions (which are effectively reactions of a plume species with aerosol surface area), the relationship between plume intensity and the rate of these reactions will be quadratic — therefore these reactions would be expected to become less significant in terms of the overall flux as the plume disperses.

[6] It is not possible to define a precise solar time for a given portion of the plume nor to define for such a portion precisely when sunrise and sunset occur. Plume dispersion means that plume of the same or similar ages will can be at different locations, and local solar time will vary slightly across over these distances

In addition to these physical effects upon plume chemistry evolution discussed above, there are also purely chemical ways in which the plume can evolved over time:

- **Perturbation of background chemistry.** As discussed in this chapter, there are several ways in which the plume impacts the concentrations of various chemical species which are not volcanic volatiles or their immediate products, for example the depletion of OH and HO_2 (Section 5.2). These can then have feedbacks to the chemistry of the volcanic volatiles. This effect is mitigated by the dispersion, which brings in previously unperturbed air into the plume.
- **Resolution of disequilibrium.** A steady state assumption considers that the chemical system reacts rapidly to forces perturbing the balance of different species, maintaining a thermodynamic equilibrium. However if such transitions take significant length of time, there would exist a period whereby the net formation and destruction of plume species could be considered kinetically, rather than thermodynamically controlled.

Figure 5.19 tracks (using the pseudo-Lagrangian method described in Section 4.2.5) plume emitted between between 2012-07-31 11:00:00 and 2012-07-31 12:00:00, and plots the distribution of the bromine within this plume hourly from 2012-07-31 12:00:00 onwards.

As well as the concentrations of the bromine species, I have amended the model such that all of the additional information needed to calculate the rates of the major bromine chemistry reactions is in the model output. This allows for the creation of the cycle figures in this Chapter (Figures 5.20, 5.23, 5.22, and 5.21).

Each figure corresponds to a particular time of model output (i.e. one of the columns of 5.19). The relative proportions of bromine as each species corresponds to the size of the coloured circles. The main reactions are depicted as arrows, with the weighted average rate of the reactions corresponding to the width of the lines. Some lines correspond to the sum of multiple reactions. Because BrO and Br are rapidly inter-converted, this dynamic line width is applied to the net Br $\longleftrightarrow$ BrO conversion instead. Blue lines are heterogeneous reactions, red lines are photolysis reactions, and black lines are other gas-phase reactions.

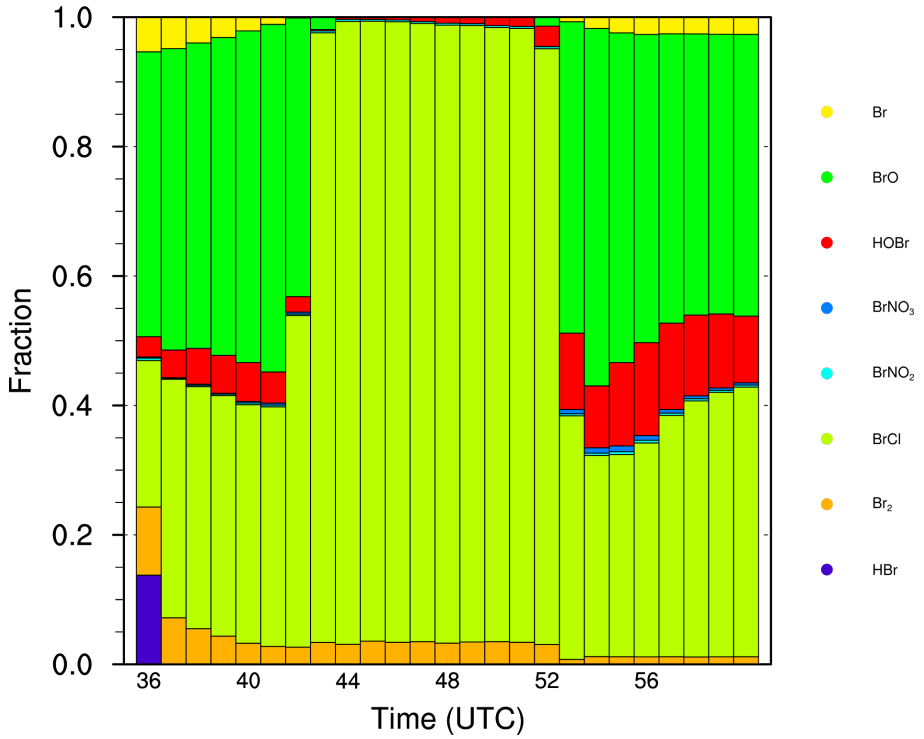

Figure 5.19: Average in-plume modelled distribution of bromine between the different forms plotted versus time, for plume emitted between 2012-07-31 11:00:00 and 2012-07-31 12:00:00.

As can be seen in Figure 5.19, the daytime and night-time bromine partitioning within the plume is very different, the plume evolution over this 24 hour period can be clearly divided into three time periods, the afternoon immediately after emissions, the night, and the morning.

5.6.3.1 First few hours of plume evolution (afternoon)

The first column of Figure 5.19 is an average of plume that is 0–1 hours old. As discussed in section 5.6.1 the modelled plume bromine chemistry changes significantly during this time. As such, an average taken over this period is not an informative measure of plume chemistry. The analysis of this subsection considers the plume from age 1 hour and older.

Inspection of Figure 5.19 shows that the "regime 3" steady state discussed in Section 5.6.1 is maintained until sunset with only moderate steady changes. Figure 5.20 illustrates the the reaction cycle of the steady state:

- Br is produced by the photolysis of Br_2 (Reaction R43) and BrCl (Reaction R46).

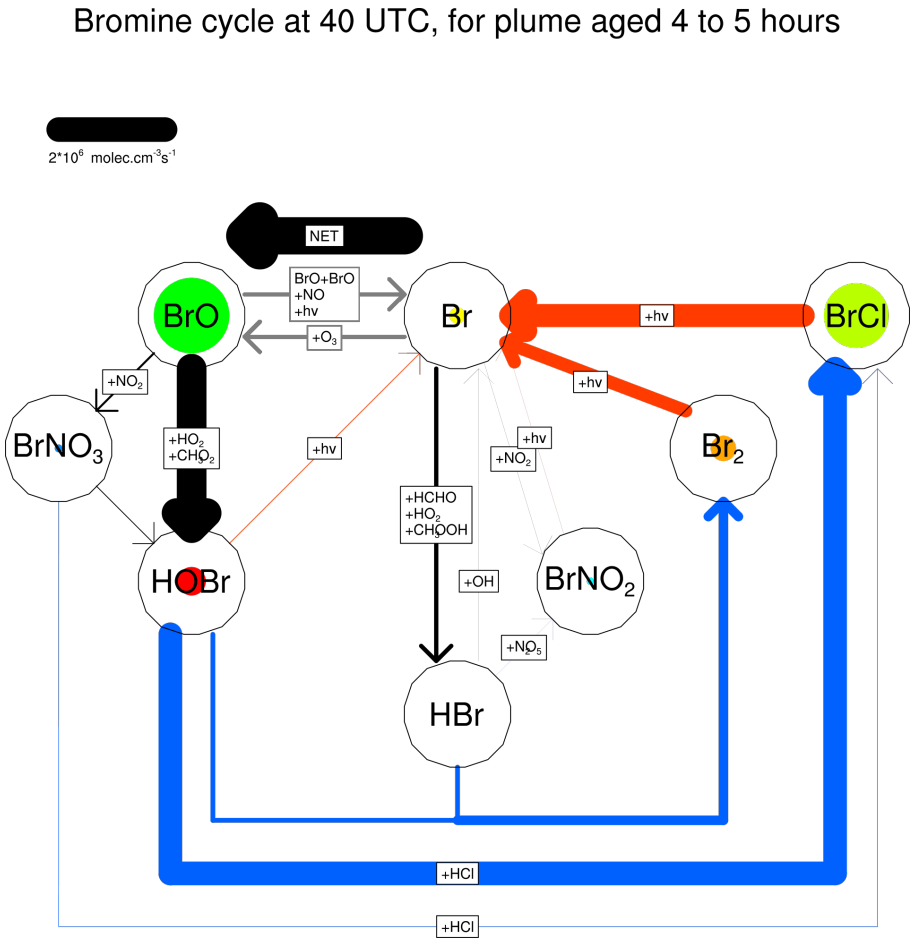

Figure 5.20: Modelled bromine cycle for plume aged 4–5 hours at 2012-07-31 16:00:00. Circle sizes relate to proportion of total bromine in each form. Arrow widths relate to average rate of each fluxes, see reference line top left.

- Br and BrO exist in a fast equilibrium. This equilibrium is dominated by BrO. Both BrO and Br can be converted to other forms, however the total rate of such reactions of BrO (predominately forming HOBr) exceed those of Br (predominately forming HBr). This results in a net Br $\longrightarrow$ BrO flux.

- HOBr undergoes heterogeneous reactions forming either Br_2 (Reaction R60) or BrCl (Reaction R59). There is sufficient aerosol surface area such that the heterogeneous recycling of bromine is quick, and only a small fraction of plume bromine exists as HOBr

  - Reaction R60 is rapid, but limited by the rate of formation of HBr; the reaction essentially occurs at the same rate as the formation of HBr resulting in the HBr proportion being negligible.

  - Because of the exhaustion of HBr within the plume, and the abundance of HCl, Reaction R59 becomes a significant loss of HOBr even

though it is the least "preferred" of the two reactions (see Section 2.2.2.4).

This regime is stable until sunset (when the lack of photolysis reactions breaks the chemical cycling). Notably there is not a substantial increase in the fraction of HOBr, which implies that for several hours after the plume emission, the rate of the HOBr-consuming heterogeneous reactions are fast. The rate of these reactions are proportional to both the concentration of HOBr and the aerosol surface area. As both significant levels of bromine and elevated aerosol are plume features, it might be expected that the importance of this reaction would diminish rapidly as the the plume disperses. However this does not occur.

As shown in Section 5.5, secondary aerosol formation means that the aerosol surface area remains high for the first few hours of plume evolution, even after the volcano's primary aerosol has dispersed. This, and the sustained abundance of HCl within the plume, means that the heterogeneous loss of HOBr remains quick within the plume.

The importance of both secondary aerosol formation to the evolution of the plume are investigated further in a perturbation study (Section 8.2).

There are some relatively small, continuous changes occurring to the modelled bromine partitioning during this period:

- The proportion of plume bromine as Br radicals decreases. This occurs because of a shift in the $Br \longleftrightarrow BrO$ equilibrium. The main reaction converting BrO to Br is the photolysis of BrO, whereas the rate of the reverse reaction (Reaction R52) is less strongly dependant upon sunlight. Therefore, as the intensity of sunlight drops over the course of the afternoon, the $Br \longleftrightarrow BrO$ equilibrium shifts further towards BrO.
- The proportion of plume bromine as Br_2 decreases. This occurs because the formation of HBr (which reacts rapidly with HOBr to form Br_2 in Reaction R60) is reduced due to the reducing Br concentrations.
- The modelled proportion of the plume bromine present as BrO increases, at the expense of BrCl. Both losses of BrCl (to photolysis) and BrO (to reaction with HO_2 or CH_3O_2) slow with decreased actinic flux, though the former declines more quickly causing this minor phenomenon.

Overall however these variations are moderate, and it can be considered that the "Regime 3" described prior is stable until sunset fundamentally changes the chemistry of the system.

5.6.3.2 Sunset and night-time

The most prominent feature of Figure 5.19 is the difference between the daytime and night-time distribution of plume bromine. During the night almost all of the bromine is present as BrCl (the reasons for the dominance of BrCl over Br_2 are discussed in Section 5.6.1).

This occurs because the only loss mechanism for BrCl within the model is photolysis (Reaction R46). During the night this photolysis does not occur, thus the bromine cycle has "dead ends" at Br_2 and BrCl until sunrise.

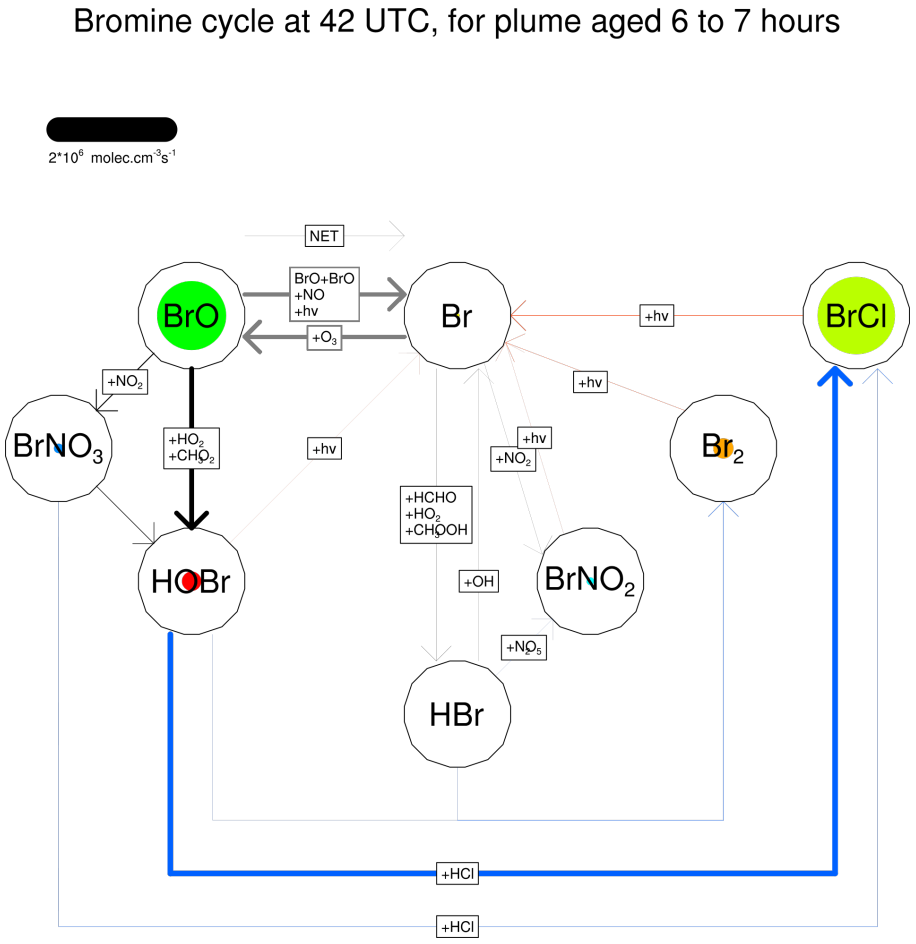

Figure 5.21: Modelled bromine cycle for plume aged 6–7 hours at 2012-07-31 18:00:00 (sunset). Circle sizes relate to proportion of total bromine in each form. Arrow widths relate to average rate of each fluxes, see reference line top left.

The breaking of this cycle can be most clearly seen in Figure 5.21 which corresponds to the modelled time at and just after sunset in the model. At this time the rates of the photolysis reactions are zero, which means that the concentration of Br radicals falls to negligible levels, as photolysis of BrO has ceased. Although the means of their production is also cut off at sunset, the

lifetime of HO_2 and CH_3O_2 is sufficient that this reservoir of BrO is emptied, producing HOBr. The other requirements for heterogeneous Reaction R59 (HCl and aerosol surface area) do not deplete at sunset, therefore the creation of BrCl remains efficient. There is no corresponding rise in Br_2, instead the levels of Br_2 present in the late evening remain stable, effectively being "frozen in" by the withdrawal of daylight.

At night there is essentially no bromine chemistry, as almost 100% of plume bromine is present as photolysible species which are completely stable at night time. This is illustrated in Figure 5.22.

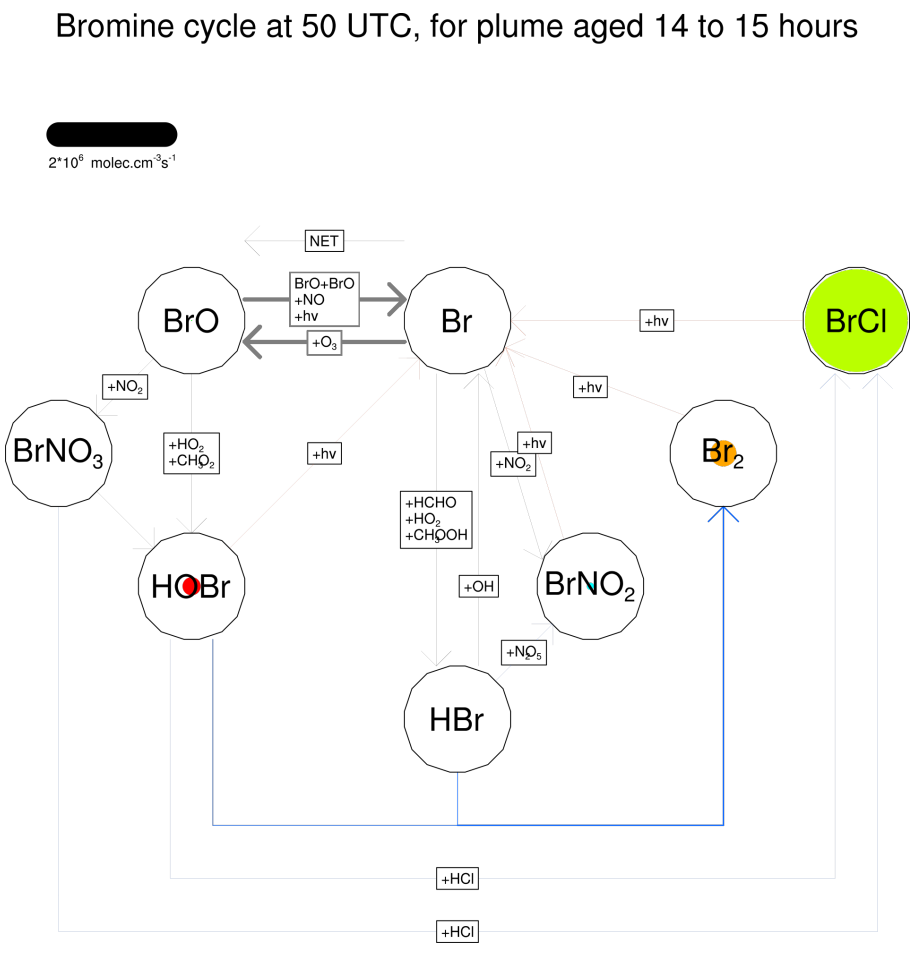

Figure 5.22: Modelled bromine cycle for plume aged 14–15 hours at 2012-08-01 02:00:00 (night). Circle sizes relate to proportion of total bromine in each form. There are essentially no reactive fluxes occurring in the system at night.

5.6.3.3 Sunrise and morning

Upon sunrise the large reservoir of photolysable species (principally BrCl) stops being stable, and active bromine chemistry returns. The bromine cycling that

returns after sunrise is very similar to that observed before sunset (c.f. Figures 5.23 and 5.20), and the proportions of BrO, Br and BrCl follow the same patterns that they did in the afternoon; this time with actinic flux rising over time as noon is approached.

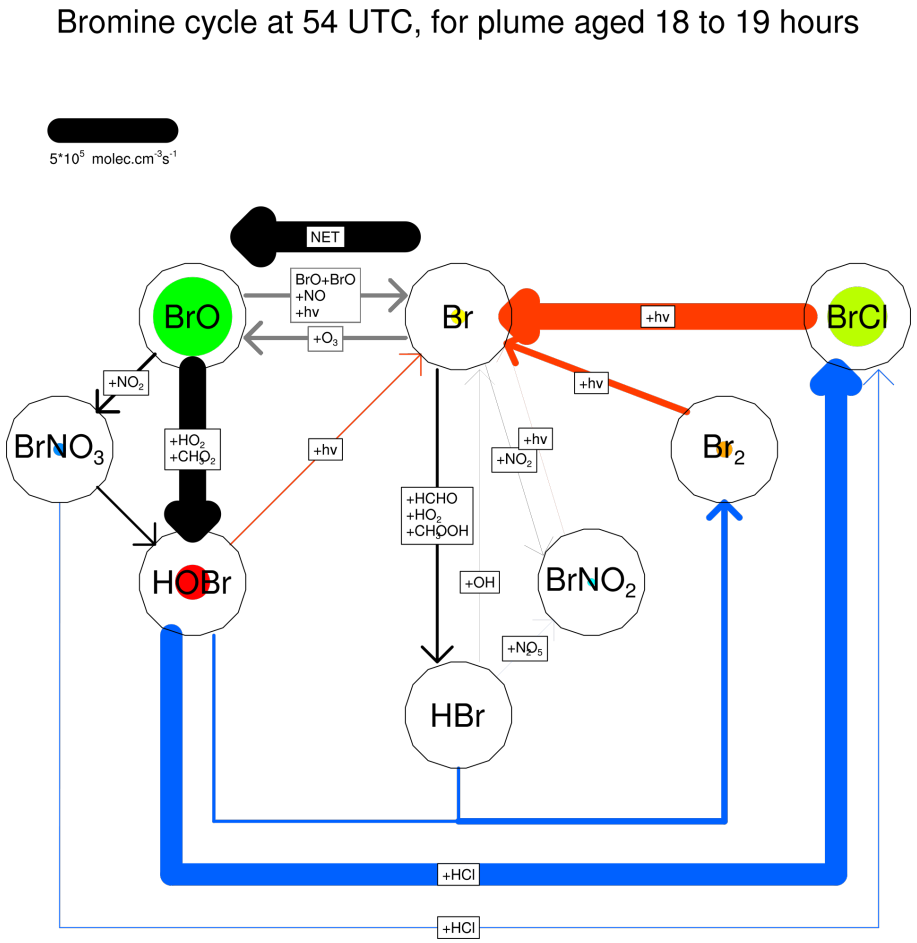

Figure 5.23: Modelled bromine cycle for plume aged 18–19 hours at 2012-08-01 06:00:00 (daytime). Circle sizes relate to proportion of total bromine in each form. Arrow widths relate to average rate of each fluxes, see reference line top left, note that this reference is different to the lines used in Figures 5.20–5.22

The only major change is the increase in the HOBr proportion, which is approximately double that of the pre-night situation. This occurs because the aerosol surface area concentration has decreased — the aerosol which existed at sunset has dispersed during the night, and secondary aerosol creation is a daytime-only process. Therefore in this morning period, the lifetime of HOBr is longer and its proportion increases. Despite this, the heterogeneous cycling is still sufficiently fast that HOBr is still only a minor constituent of the plume, and the bromine cycling still continues.

The endurance of the plume's reactive bromine cycling for 24+ hours after

emission is a notable phenomenon in these model results. At this time, the modelled available aerosol surface area for heterogeneous reactions within the plume is elevated, by a factor of 2–2.5. As, in the absence of a rain event, there is no significant sink of HCl from the plume, HCl remains abundant in the plume, far in excess of all forms of bromine.

5.6.3.4 Assessment

The "Regime 3" situation identified in 5.2 is sustained as the plume ages.

The active bromine cycling is fuelled by photolysis and sustained by the continued abundance of HCl and elevated aerosol surface area within the plume. Both of these components are modelled to endure for at least 24 hours, meaning that, although dispersed over a large area, the bromine cycling persists. Compared to Reaction R59, Reaction R60 is of only minor importance in the long-term bromine cycling.

As photolysis is necessary for the bromine cycling, it ceases at sunset. However on sunrise the cycling resumes.

This investigation has not found any point at which the dispersal of the plume, or any chemical negative feedbacks, causes the daytime bromine cycling to stop or become negligible. It may be the case that, were the modelled plume tracked for a longer period of time, the plume dispersal would eventually render the in-plume aerosol surface area boost negligible, and cause the heterogeneous bromine cycling to significantly slow. However the limited spatial and temporal extent of the model used in this investigation is not adequate to assess this.

It should also be noted that as the plume disperses, the model's accuracy in representing both heterogeneous reactions and the surface area of the background aerosol becomes more important.[7] These are aspects of the model with which there is the most uncertainty regarding the model's accuracy (see Chapter 4, particularly section 4.4.2.2). Therefore the confidence in the model output as a representative model of the chemistry of the plume decreases as the plume ages.

The case considered here has no rain or cloud events intersecting with the

[7] In the early plume the high concentration of volcanic aerosol (primary and secondary) means that heterogeneous cycling would be sufficiently fast, even if the effective rate of this equation were reduced by a small factor, and that the background aerosol is unimportant. In the aged plume the heterogeneous cycling is slower, and background aerosol makes up a greater fraction of the aerosol surface area.

plume, thus wet deposition (which would be expected to wash-out various components of the plume, including aerosol and HCl) is negligible.

5.7 Ozone chemistry within the plume

Active bromine chemistry destroys ozone (Wennberg, 1999). In Section 4.5.3 I show that this phenomena, which has been observed in real volcanic plumes, also occurs within the modelled plume.

The O_3 destruction caused by the plume can easily be assessed by comparison of equivalent grid boxes in model runs with and without the volcanic plume. The rate of O_3 destruction is a measure of the speed of the bromine cycling, and its most prominent impact upon the general chemistry of the atmosphere.

5.7.1 Understanding plume ozone-destructive reactions

The rate of the ozone destruction via bromine chemistry is equal to the the rate of the $Br + O_3 \longrightarrow BrO + O_2$ reaction (Reaction R52) minus the sum of the reverse reactions which re-form O_3 (principally the photolysis of BrO, Reaction R42). However, as shown in Section 5.6 an understanding of plume bromine chemistry requires consideration of the entire bromine cycle.

To a first approximation, the bromine cycle runs as $Br \longrightarrow BrO \longrightarrow HOBr \longrightarrow BrCl$ or $Br_2 \longrightarrow Br$ with one O_3 molecule destroyed per Br atom that passes through the cycle, and therefore the rate of destruction of O_3 would be identical to the rate of this cycling. However a more precise understanding of the chemistry requires consideration of three reactions that provide "short-cuts" to this chemical cycle:

- The $BrO + BrO$ reaction (Reaction R47) produces Br atoms and Br_2 (the yield in terms of moles of Br atoms in the model is 81% Br, 19% Br_2), effectively bypassing the steps of formation of HOBr, the heterogeneous cycling, and, for most of the bromine, photolysis. The rate of this reaction will decrease rapidly as the plume disperses.
- The $BrO + CH_3O_2$ reaction (Reaction R51) primarily produces HOBr as its bromine product, however a small amount (28% in the model mechanism)

of the yield is Br atoms (for a detailed discussion of this reaction, see Shallcross et al., 2015).

- The photolysis of HOBr produces Br atoms.

Also it should be noted that a bromine atom that takes the path $Br \longrightarrow HBr \longrightarrow Br_2$ does not itself destroy O_3.

The relative importance of these "bypass" reactions in the model can be assessed by comparing in the model output the sum rate of the heterogeneous reactions (paths taken by all bromine atoms in the full cycle) to the rates of these bypass reactions. For the portions of the plume considered in Section 5.6,[8] Figure 5.24 plots the weighted average rates of the HOBr-consuming heterogeneous reactions (sum of both) and the effective bromine recycling rate of each of the bypass reactions listed above.[9] Figure 5.25 plots the rate of the bypass reactions as a fraction of the rate of heterogeneous HOBr consumption.

Figures 5.24 and 5.25 show that in the very early plume the plume is sufficiently concentrated that Reaction R47 recycles more bromine than the heterogeneous reactions (and is therefore "responsible" for more O_3 destruction), however after about an hour of plume dispersal this situation reverses. From then on the bypass reactions supplement the heterogeneous recycling to a moderate extent. After sunrise, where the plume is very disperse, this supplement is very small.

Even when the rates of these bypass reactions exceed or approximately equal the heterogeneous cycling, this does not mean that the "main" bromine cycle is unimportant or unnecessary for the bromine–ozone chemistry of the plume. Were the heterogeneous cycling not to occur, the plume bromine would accumulate as HOBr, with the only recycling method available being photolysis of this species; as can be seen by Figure 5.24 this would be very slow. The non-reactive state of the modelled bromine chemistry at night is evidence to the importance of the photolysis-dependant steps of the cycling.

It is therefore more useful to think of these bypass reactions as a multiplier on the O_3-destruction caused by the main bromine cycle rather than as a substitute

[8]For the parts of these Figures relating to plume aged 0–1 hours the approach is that of Section 5.6.1; plotting values relating to different ages of the plume at 2012-07-31 12:00:00. For the rest of the data the approach used is the pseudo-Lagrangian method of Section 5.6.3; considering plume emitted between 2012-07-31 11:00:00 and 2012-07-31 12:00:00

[9]For Reaction R47 reaction $2\times$ the reaction rate is plotted as this reaction recycles two bromine atoms. For Reaction R51 $0.28\times$ the reaction rate is plotted as this is the modelled Br yield.

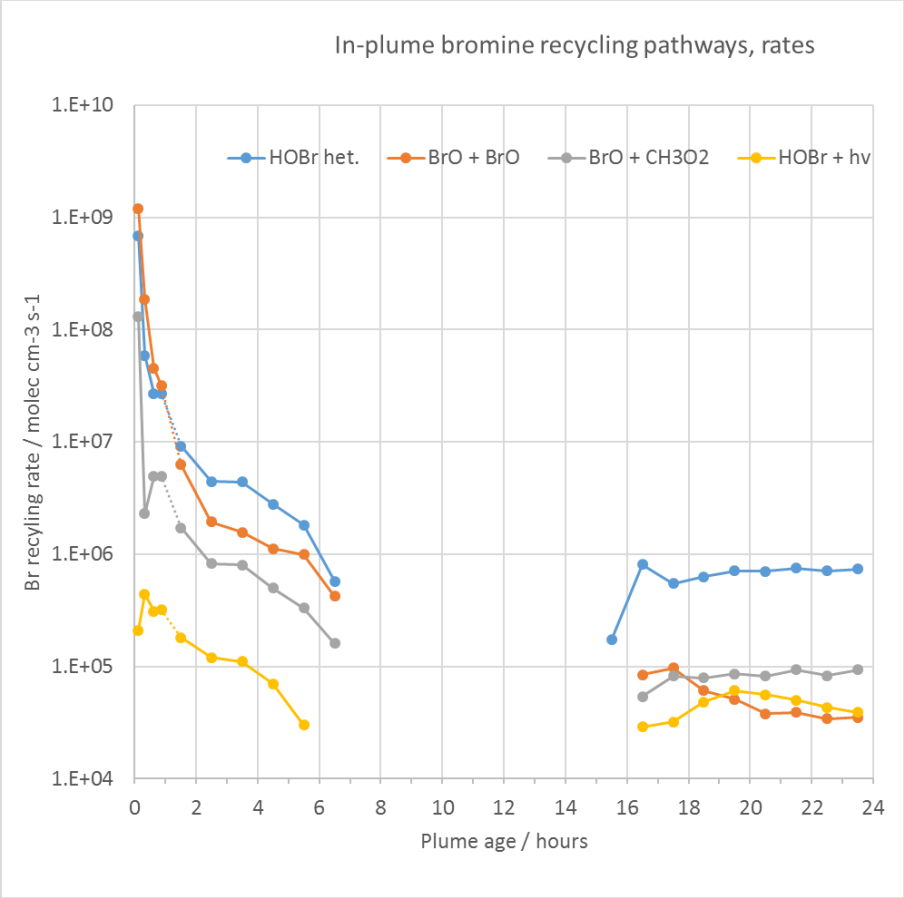

Figure 5.24: Variation in the average rates of the different bromine cycling pathways in the plume as it ages. Y-axis is logarithmic. Rates at night-time are negligible and are not plotted.

to these. This multiplier is high in the very early plume, and then of modest importance once the plume is a few hours old.

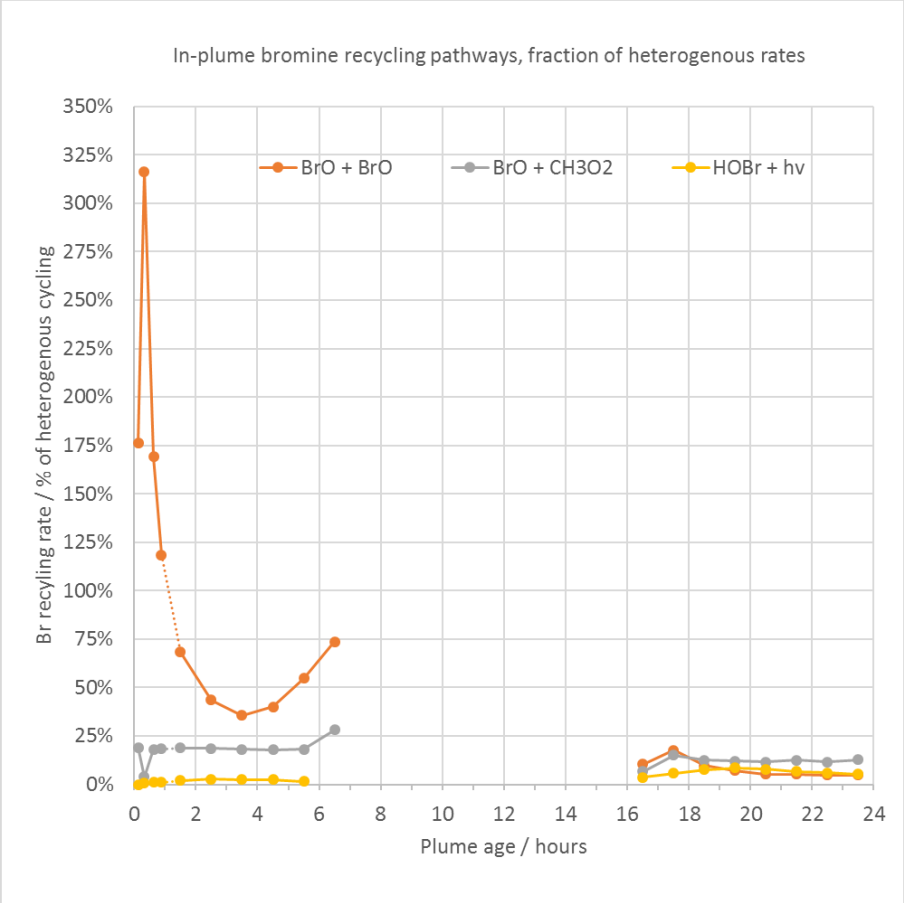

Figure 5.25: Variation in the average rates of the different bromine cycling pathways in the plume as it ages, as percentage of the rate via heterogeneous HOBr reactions. Y-axis is linear. Fractions relating to night-time are not plotted.

5.7.2 Quantifying ozone loss within the model plume

The bromine chemistry within the plume destroys O_3. This is partially compensated for by the entrainment of background air into the plume. This second effect can also be considered as dispersing the O_3 depletion over a larger volume.

Figures 5.26 and 5.27 show the modelled average in-plume depletion of O_3 (compared to the plume-free run, negative numbers indicate loss within the plume) for plume aged 0–1 hour at 2012-07-31 12:00:00 in both absolute (ppb) and relative (%) terms. Figures 5.28 and 5.29 plot the same for a pseudo-Lagrangian track of plume emitted between 2012-07-31 11:00:00 and 2012-07-31 12:00:00.

There are substantial O_3 losses within the very early plume amounting to 10s of %. The influence of the O_3 depletion on the Br $\longleftrightarrow$ BrO steady state

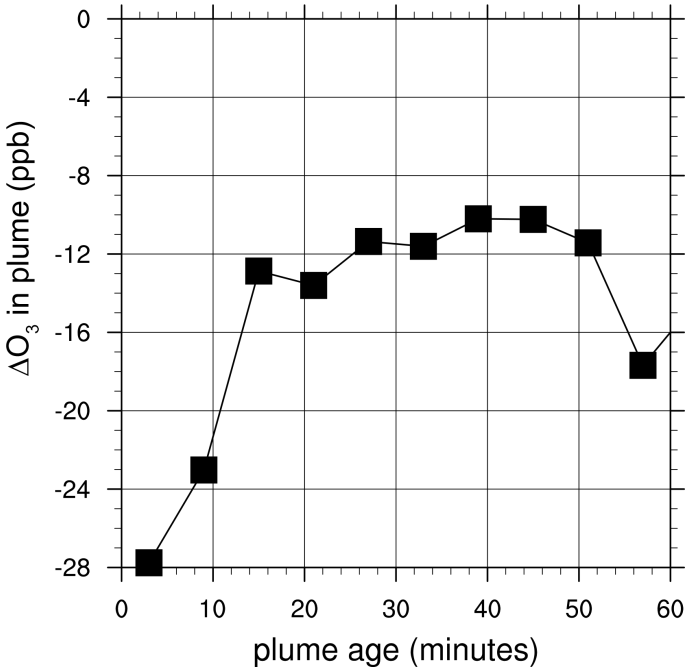

Figure 5.26: Modelled average absolute loss of O_3 in the plume (compared to the plume-free model run) for plume aged 0–1 hours at 2012-07-31 12:00:00.

is discussed in Section 5.6.1 — although large the depletion is not sufficient to interrupt the bromine cycling. Once the plume is evolved the modelled O_3 depletion is moderate, around a few ppb below background levels. As it is difficult to distinguish from Figures 5.26–5.29 between the competing chemical loss and from-background entrainment of O_3 (a physical phenomenon), in Figures 5.30 and 5.31 I plot the corresponding in-plume ratios of the O_3 depletion to the concentration of the inert tracer in order to show only the chemical effect. This is effectively the same technique used isolate the chemical O_3 loss from the field campaign data, see Appendix A for a justification of this method. In these plots tracer1 is used as the inert tracer rather than SO_2, however as both are emitted from the modelled volcano at the same rate these are effectively equivalent.

Figure 5.30 shows that, despite the complex bromine chemistry in the very early plume, the trend of the chemical O_3 loss in the first hour of plume evolution is remarkably linear. Fitting a linear line of best fit to the data of Figure 5.30 yields a gradient of approximately 8×10^{-6} molecules O_3 loss per molecule of inert tracer per second.

This value can be compared to that derived from the data plotted on Figure 3.5. Although Figure 3.5 considers observational data rather than model output and considers data only from plume a few minutes old, its gradient (1×10^{-5}

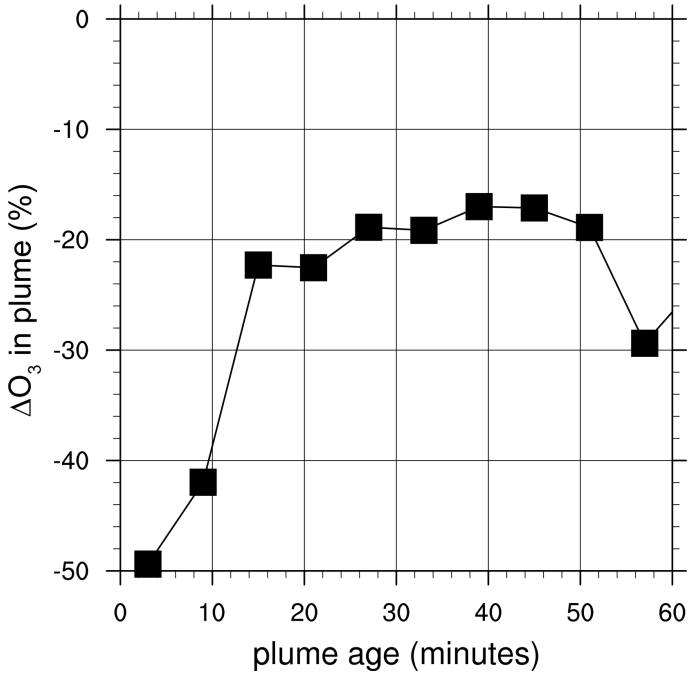

Figure 5.27: Modelled average relative loss of O_3 in the plume (compared to the plume-free model run) for plume aged 0–1 hours at 2012-07-31 12:00:00.

molecules O_3 loss per molecule inert tracer per second) is almost identical to that in the model output. This and the agreement of the model with the aircraft data (Section 4.5.3) suggest that the model has very good skill in terms of reproducing volcanic O_3 destruction in the early plume.

As the plume evolves further downwind (Figure 5.31) this linear trend approximately continues, however the gradient lessens as the actinic flux declines. Volcanic O_3 destruction ceases at sunset, which is expected as the bromine cycling ceases at this time.

During the night the net effect of the volcanic chemistry is positive regarding O_3, this is manifest as a positive slope in Figure 5.31. The in-plume NO_x depletion (see Section 5.3) means that there is less O_3 destruction via the $O_3 + NO_2 \longrightarrow NO_3$ reaction within the plume than without. Thus, although there is no volcanically-induced O_3-creative process, when model runs involving the volcanic plume are compared with model runs with no volcanic plume, the net effect of the volcano is positive in terms of O_3. However, compared to the daytime destruction of O_3 via bromine chemistry this phenomena is small; between sunset and sunrise this effect has only "undone" approximately a third of the O_3 destruction that occurred between noon and sunset the previous day.

On sunrise the bromine chemical cycling, and the associated O_3 destruction,

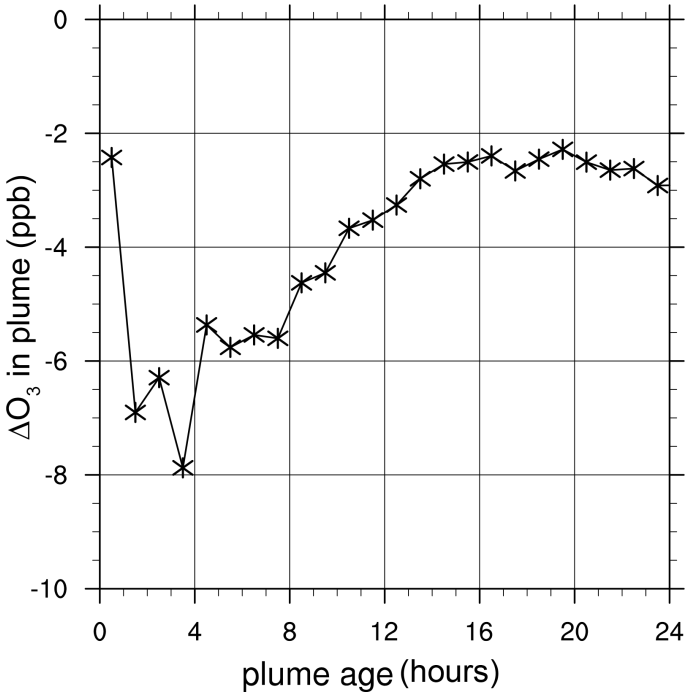

Figure 5.28: Track of the modelled average absolute loss of O_3 (compared to the plume-free model run) in a portion of the plume emitted between 2012-07-31 11:00:00 and 2012-07-31 12:00:00 as it ages.

resumes. The modelled destruction (per molecule of the intert tracer) accelerates as noon is approached and the actinic flux increases.

Overall the average net O_3 destruction within 24-hour old plume, which has experienced an entire diurnal cycle, is approximately 0.25 molecules per molecule inert tracer, which yields an average O_3 loss rate over the day of 3×10^{-6} molecules O_3 per molecule inert tracer per second. By volume, the emission ratio of bromine to that of the tracer is 6×10^{-4}, thus this ozone destruction rate can also be considered to be 5×10^{-3} molecules O_3 per atoms of bromine per second.

Assessment: Overall the modelled destruction of ozone in the early plume is substantial (10s of %), and agrees with observational results.

The dispersal of the plume means that, in absolute terms, the in-plume O_3 destruction by this modelled passively degassing volcano is small (a few ppb or %). However in the aged model plume this low-level O_3 depletion is occurring throughout a very disperse plume, meaning that in total the plume is modelled to be destroying a large amount of ozone.

By inspecting the ozone loss as a ratio of the inert tracer, we can see that the

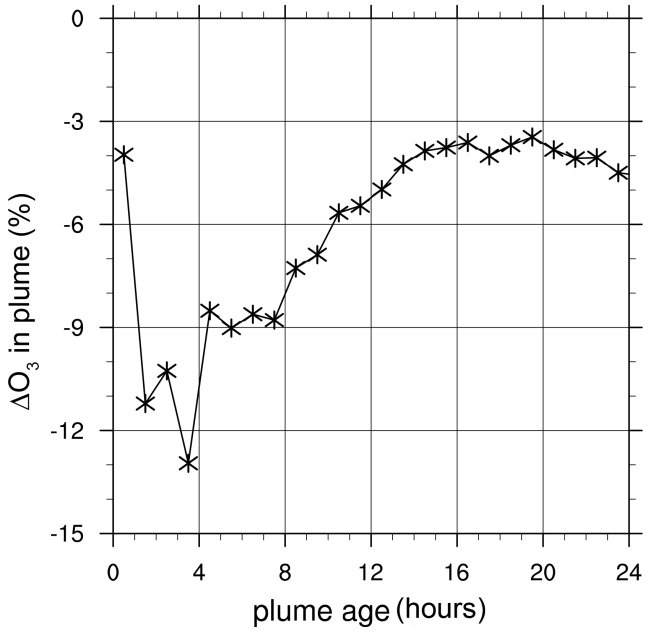

Figure 5.29: Track of the modelled average relative loss of O_3 (compared to the plume-free model run) in a portion of the plume emitted between 2012-07-31 11:00:00 and 2012-07-31 12:00:00 as it ages.

rate of ozone loss varies according to the actinic flux, being faster at noon than in the morning or evening. During the night the net O_3 change induced by the volcano is slightly positive, although is small compared to the daytime effects. Overall the modelled volcano destroys O_3 at a net rate of a few 10^{-6} molecules per molecule of the inert tracer per second.

This model investigation has not been able to find a plume age at which the bromine cycling ceases or becomes negligible (see Section 5.6.3.4) it is not possible to estimate for how long the plume bromine continues to destroy ozone at this rate. Therefore it is not possible to estimate the overall impact of the volcano on the regional/global ozone budget.

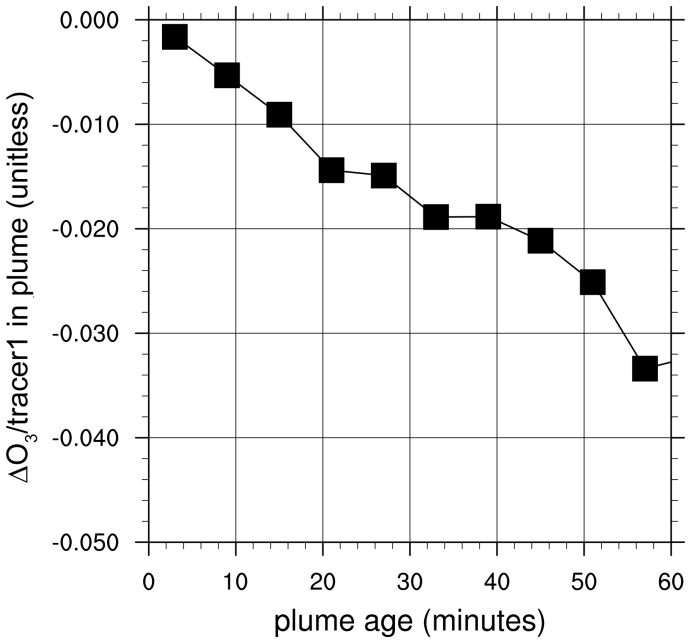

Figure 5.30: Modelled average absolute loss of O_3 in the plume (compared to the plume-free model run) as a ratio of the concentration of the inert tracer for plume aged 0–1 hours at 2012-07-31 12:00:00.

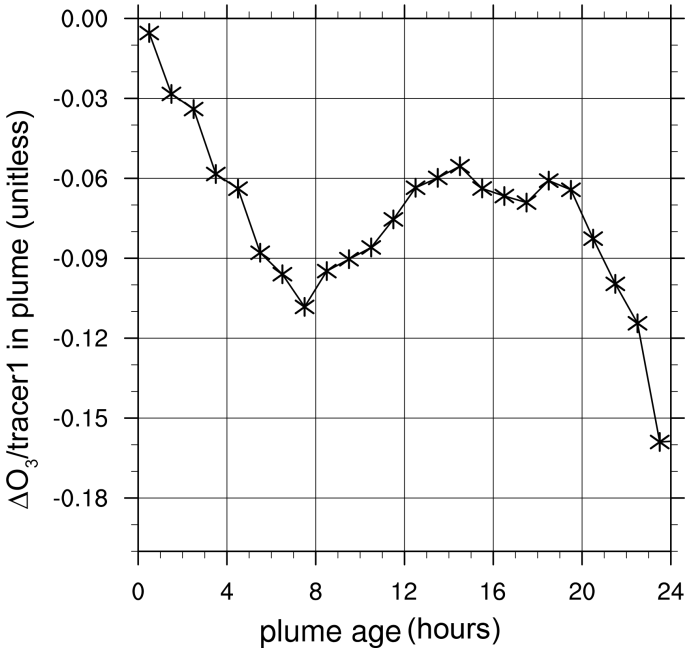

Figure 5.31: Track of the modelled average absolute loss of O_3 (compared to the plume-free model run) as a ratio of the concentration of the inert tracer in a portion of the plume emitted between 2012-07-31 11:00:00 and 2012-07-31 12:00:00 as it ages.

5.8 Comparison with plume models

In Section 1.3.2 I discuss the two models, *MISTRA* and *PlumeChem* which have been used to produce published modelling studies regarding the chemistry of volcanic plumes. In this section, I compare the results presented in this Chapter with those from *MISTRA* and *PlumeChem*. This discussion is predominately about bromine chemistry, as this is the focus of these publications.

The equivalent comparison with observational data can be found in Section 4.5.

The modelling studies of Surl et al. (2015) (*MISTRA*) and Roberts et al. (2014b) *PlumeChem*) report results from a variety of different modelled plume setups. The cases most directly similar to the modelling discussed in this Chapter are the runs with heterogeneous chemistry but without volcanic NO_x in Surl et al. (2015), and, in Roberts et al. (2014b), the low/medium Br/SO_2[10] with V_M:V_A = 95:5.

In Section 5.6.1 I show that in the WRF-Chem modelled plume, the initial BrO/SO_2 ratio is near-zero. It then rises over the first few minutes of plume evolution, peaks at a local maximum, then falls slightly to a "plateau" level of a few 10×10^{-4}. In Section 5.6.1 I describe this evolution in terms of three regimes — the third regime (the plateau) is reached within an hour of emission.

The modelled BrO/SO_2 ratio results from *PlumeChem* show a similar form (Roberts et al., 2014b) and magnitude. *MISTRA* also shows a gradual rise to ratios of a few 10×10^{-4} over the first few minutes of plume evolution, but do not show the "local maximum" phenomenon (Bobrowski et al., 2015; Surl et al., 2015).

The WRF-Chem model shows HBr to be very short-lived within the plume, being consumed within a few minutes of emission via heterogeneous reactions. The same phenomenon is seen in the low Br/SO_2 case (and, with slower consumption, the medium case) in *PlumeChem* Roberts et al. (2014b). Output *MISTRA* does not show this phenomenon — significant amounts of HBr are present within the plume for at least an hour after modelled emission (Bobrowski et al., 2015; Surl et al., 2015).

This is likely because O_3 in the early plume in *MISTRA* model runs is very low, making the bromine cycling O_3-limited in the plume core (Bobrowski et al.,

[10]The modelled Br/SO_2 emission ratio in this WRF-Chem study is less than that in the medium but more than the low cases in Roberts et al. (2014b).

2015; von Glasow, 2010). The O_3 loss in the *PlumeChem* base run discussed in Roberts et al. (2014b) is more moderate, similar to the modelled plume discussed in this Chapter. The large differences in bromine partitioning between the outputs of *PlumeChem* (base runs) and WRF-Chem on the one hand, and *MISTRA* on the other, is therefore likely to be because these models have been used to model very different plumes. *MISTRA*'s results are more similar to the results relating to more intense modelled plumes discussed in Roberts et al. (2014b) and Chapter 7.

Roberts et al. (2014b) also shows another "regime 1" phenomenon, the partitioning of a large fraction of the plume bromine to Br_2 very shortly after emission. In both WRF-Chem and *PlumeChem* the fraction of Br_2 falls as the plume evolves, however the models differ to where this bromine partitions. While both models return similarly-sized BrO fractions, in *PlumeChem* the main reservoir species is HOBr (Roberts et al., 2014b), while in WRF-Chem the Br_2 reservoir mostly transitions to BrCl. This shows the most fundamental difference between *PlumeChem* and WRF-Chem: in WRF-Chem the heterogeneous steps in the cycling is fast and the cycling is photolysis-limited, whereas in *PlumeChem* the heterogeneous step is rate-limiting. *PlumeChem* also shows a transition to HCl-mediated cycling (shown by the relative increase in BrCl compared to Br_2), however this transition is slower than in WRF-Chem and both BrCl and Br_2 are dwarfed by the size of the HOBr reservoir.

PlumeChem also models substantial reservoirs of nitrogen-containing bromine species — the absence of such reservoirs in WRF-Chem is because WRF-Chem does not model reactive nitrogen emissions from the volcano. However the conversion of reactive nitrogen to HNO_3 via plume chemistry is common to both models (Roberts et al. (2014b), Section 5.3).

Overall, the WRF-Chem model, despite being a fundamentally different model to *PlumeChem* (see discussion in Section 1.3.2), reproduces many of the same bromine chemistry phenomena seen in *PlumeChem*. The models differ in which step of the reaction cycle is rate-limiting, and therefore which species are the main reservoir.

5.9 Conclusions

The chemistry of the modelled volcanic plume results in various interrelated chemical phenomena:

- SO_2's lifetime is increased within the plume, supporting its use as a plume tracer.
- HO_x is depleted within the plume.
- NO_x is depleted within the plume, however concentrations of HNO_3 are increased by plume chemistry
- Chlorine radicals are produced within the plume, and kick-start chains of reactive organic chemistry, which substantially increases concentrations of oxidised organic compounds in the plume.
- The plume increases the amount of aerosol surface area available per unit volume. The main driver for this is the creation of secondary aerosol.
- A reactive bromine chemical cycle in a photochemical steady-state establishes itself within approximately 1 hour of volcanic emission. Volcanic HCl is a necessary component of this cycling and the elevated available aerosol surface area for reaction also sustains the cycling. This cycling is driven by sunlight. Although there is some variation, an approximation that 50% of plume bromine is present as BrO would seem to be roughly accurate for plume aged >1 hour for most of the daytime.
- Bromine chemistry destroys ozone during the day, resulting in moderate but widespread O_3 depletion in the evolved plume. The rate of this in-plume destruction varies with the actnic flux, and averages a few 10^{-6} molecules per molecule of the inert tracer per second over a 24-hour period.

Despite these varied results, the scope of this chapter can be considered to be narrow. I have considered only one set of values for the volcanic emissions, and I have only considered emissions which occur during the day. In the following chapters I expand this investigation, looking at plumes emitted at night (Chapter 6), variations in plume strength (Chapter 7) and the impact of various changes to the model inputs (Chapter 8). In each of these I refer back to the results of this chapter to show what the impacts of these variations are.

Chapter 6

Volcanic emissions at night

In Chapter 5 I considered a plume which is emitted during the daytime. For simplicity in most cases I plotted model output relating to a plume emitted around midday. In Chapter 5 it was noted that the chemistry of the plume changes at sunset, entering a mostly inactive state during the night. The cause of this is that most of the daytime chemistry relies, directly or indirectly, on sunlight in order for it to occur.

In this Chapter I evaluate the chemistry of a plume emitted at night. The scope of this chapter can be divided into two main questions:

1. Does any significant chemistry occur within a volcanic plume that has not been exposed to daylight?
2. For daytime chemistry, is there a significant difference between a plume which was emitted at night and one emitted during the day?

In this chapter I consider the fate of a plume emitted between 2012-07-31 11:00:00 and 2012-08-01 00:00:00. This plume evolves in darkness for approximately 6 hours before being exposed to sunlight. I compare the effects of the night-time-emitted plume to those of the daytime-emitted plume studied in Chapter 5. It is not possible to do a precise quantitative inter-comparison between these two cases because of variations in background chemistry and plume dispersion (a function of wind), so the comparisons are qualitative and semi-quantitative.

6.1 HO_x and sulphur chemistry

Both OH and HO_2 are daytime-only species, and therefore during the night there is effectively no HO_x system for the plume to perturb. The volcano is modelled to produce some OH directly, however this is very short-lived and insufficient to cause any long-term effects to the HO_x system.

In Figures 6.1 and 6.2 I plot the average volcanically-induced change of OH and HO_2 concentrations within plume emitted at night against plume age over the following 24-hour period. For comparison, I have plotted in Figures 6.3 and 6.4 the same for plume emitted in the middle of the day.

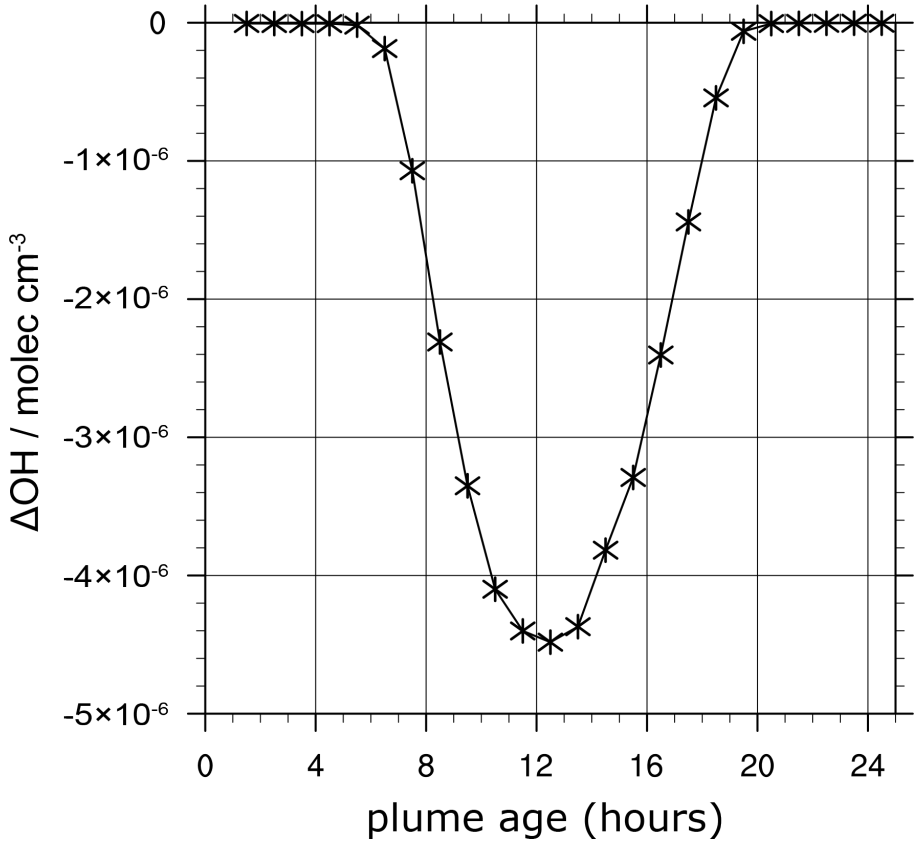

Figure 6.1: Modelled weighted average in-plume change in OH concentrations, a comparison with the equivalent model output from the plume-free run. Plot tracks for plume emitted between 2012-07-31 23:00:00 and 2012-08-01 00:00:00 as it ages. Negative values indicate depletions caused by the plume.

As can be seen from Figures 6.1–6.4 the influence of the plume on the daytime HO_x system is both qualitatively and quantitatively similar for daytime and night time emissions.

Therefore, regarding the HO_x system, the answers to both the questions

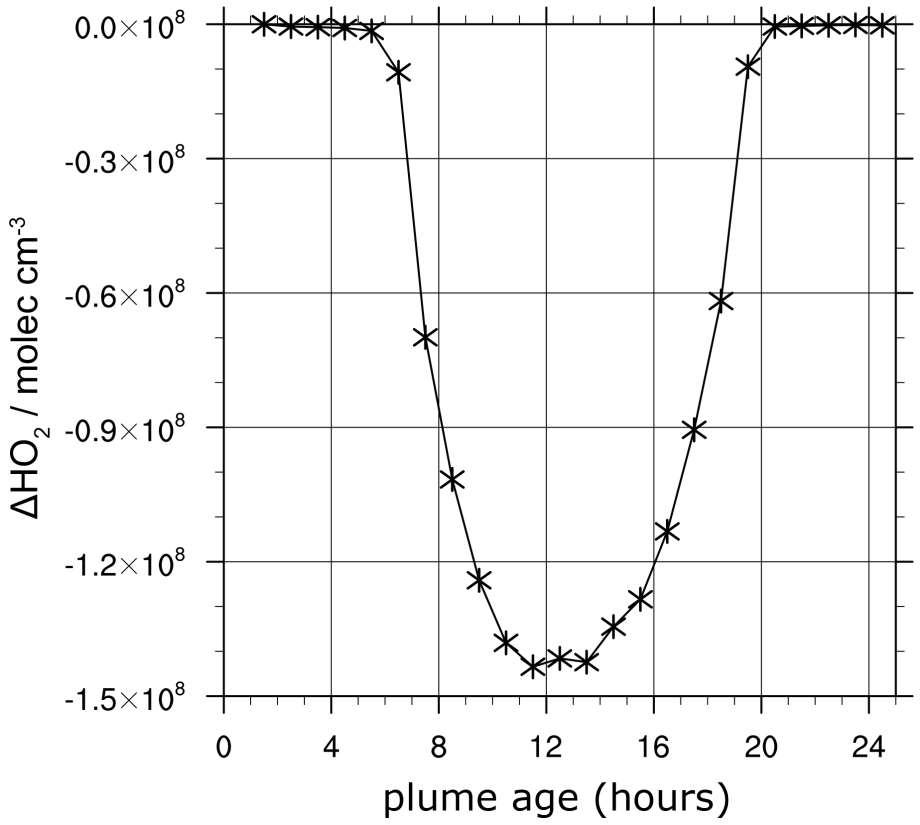

Figure 6.2: Modelled weighted average in-plume change in OH concentrations, a comparison with the equivalent model output from the plume-free run. Plot tracks for plume emitted between 2012-07-31 23:00:00 and 2012-08-01 00:00:00 as it ages. Negative values indicate depletions caused by the plume.

posed at the beginning of this chapter are no.

The sulphur chemistry of the plume is strongly dependent on the levels of OH. The chemical SO_2 lifetime at night (where OH concentrations are negligible) is essentially indefinite, and plume chemistry does not change this situation. As is seen by comparing Figures 6.1 and 6.3 the daytime depletion of OH does not substantially differ between the two cases. As such the overall chemical lifetime of volcanic SO_2 can be expected to be similar regardless of when it is emitted.

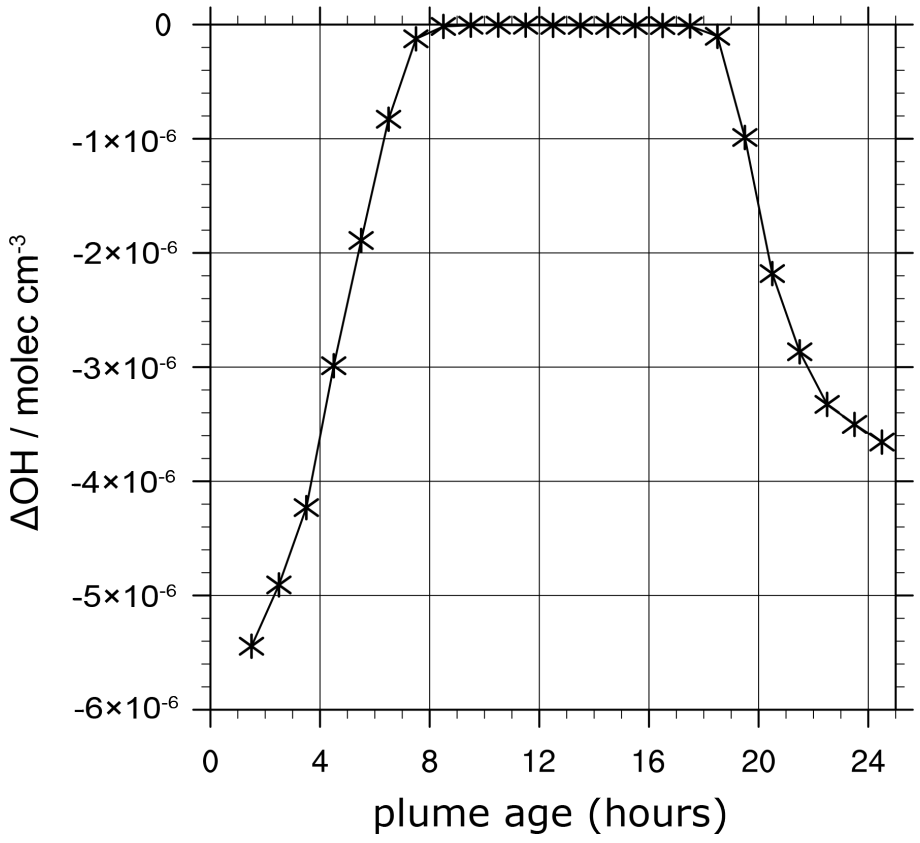

Figure 6.3: Modelled weighted average in-plume change in OH concentrations, a comparison with the equivalent model output from the plume-free run. Plot tracks for plume emitted between 2012-07-31 11:00:00 and 2012-07-31 12:00:00 as it ages. Negative values indicate depletions caused by the plume.

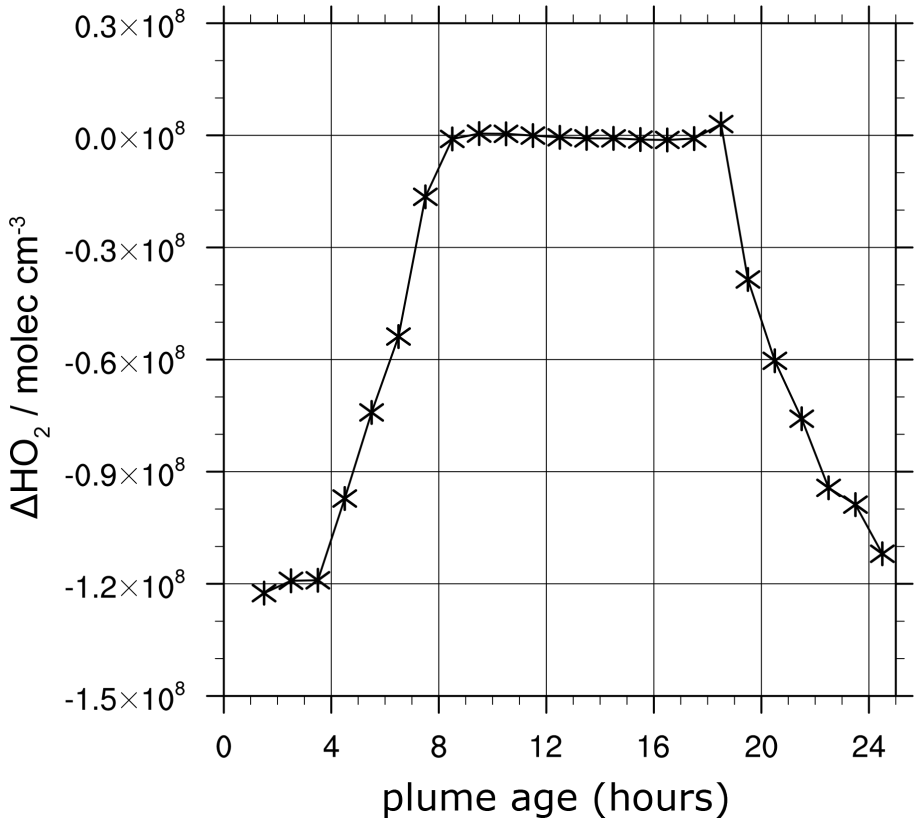

Figure 6.4: Modelled weighted average in-plume change in HO_2 concentrations, a comparison with the equivalent model output from the plume-free run. Plot tracks for plume emitted between 2012-07-31 11:00:00 and 2012-07-31 12:00:00 as it ages. Negative values indicate depletions caused by the plume.

6.2 Reactive nitrogen chemistry

In Section 5.3 I observed two phenomena occurring within the plume, a substantial in-plume increase in NO_x caused by bromine chemistry, and a substantial increase in in-plume HNO_3, a result of nitrate displacement from aerosol by sulphate.

Figures 6.5–6.8 show that the modelled evolution of a night time emitted plume displays the same phenomena as the daytime plume shown in Figures 5.5–5.9. As in the daytime plume figures, the model output corresponding to the plume (blue lines) are on the same plot as the corresponding model output from the plume-free model run (black lines).

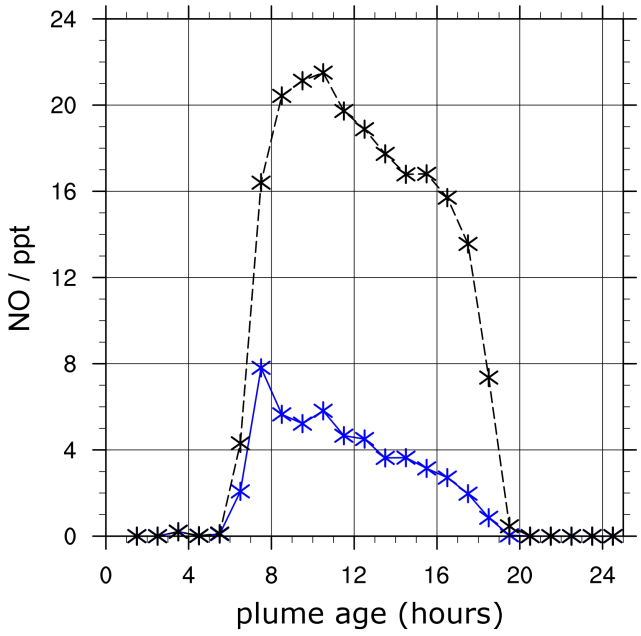

Figure 6.5: Average mixing ratios of NO within the plume as it ages, for a plume emitted between 2012-07-31 23:00:00 and 2012-08-01 00:00:00 (blue) and the mixing ratio in the equivalent model output of the plume-free run (black).

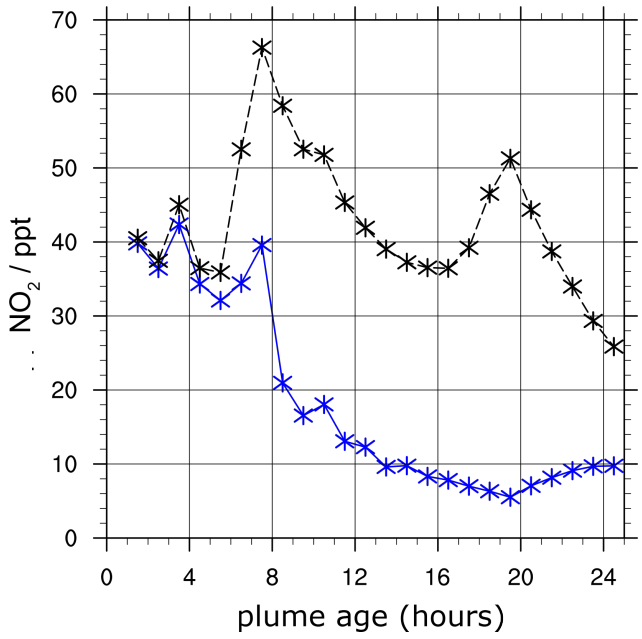

Figure 6.6: Average mixing ratios of NO_2 within the plume as it ages, for a plume emitted between 2012-07-31 23:00:00 and 2012-08-01 00:00:00 (blue) and the mixing ratio in the equivalent model output of the plume-free run (black).

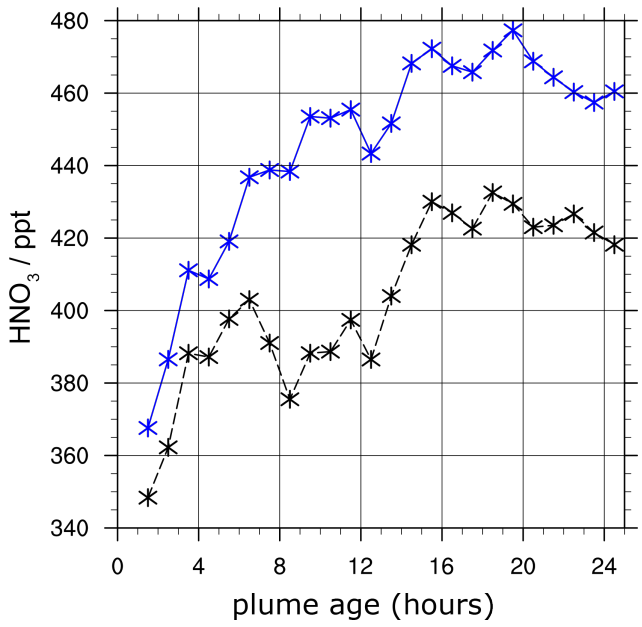

Figure 6.7: Average mixing ratios of HNO_3 within the plume as it ages, for a plume emitted between 2012-07-31 23:00:00 and 2012-08-01 00:00:00 (blue) and the mixing ratio in the equivalent model output of the plume-free run (black).

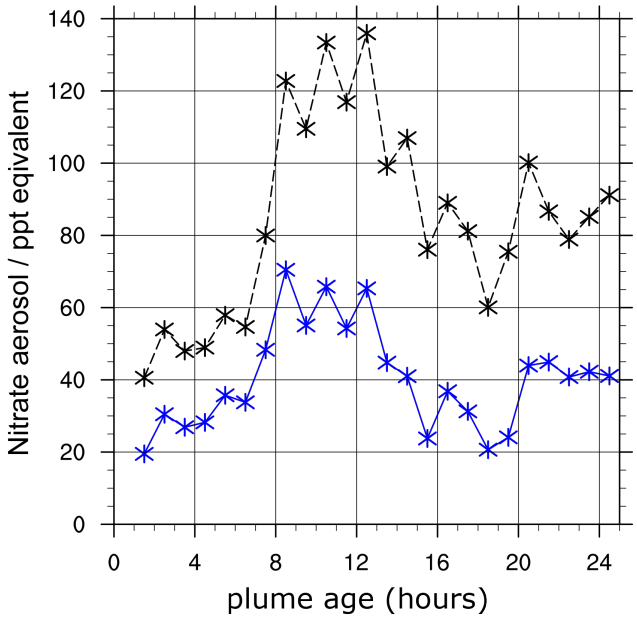

Figure 6.8: Average "mixing ratios" of nitrate aerosol within the plume as it ages, for a plume emitted between 2012-07-31 23:00:00 and 2012-08-01 00:00:00 (blue) and the mixing ratio in the equivalent model output of the plume-free run (black). The units of this plot, "ppt equivalent" are explained in Section 5.3.

Figures 6.5 and 6.6 show that the plume has a negligible effect on in-plume NO_x until sunrise. During the daytime the NO_x depletion within this plume is of a similar magnitude to that for the daytime-emitted plume.

In Figure 6.8 and 6.7 it can be seen that the re-volatilisation effect discussed in Section 5.3 occurs during the nighttime as well. In the case plotted in this section the background nitrate aerosol level is lower compared to those observed in Chapter 5, and therefore the HNO_3 increase is not as substantial — this is caused by the variation in the modelled background aerosol and is not connected to the questions considered in this Chapter.

Although one of the two plume reactive nitrogen effects occurs during the night and the other does not, upon sunrise the in-plume reactive nitrogen chemistry is qualitatively similar to that observed in plume which has evolved during sunlight. Therefore the time-of-emission is relatively unimportant in regards to the daytime in-plume chemistry.

6.3 Chlorine-induced organic chemistry

In Section 5.4 I present model output showing elevation of CH_3O_2, CH_3OOH, and HCHO within a volcanic plume emitted during the day. Bug-related qualifiers (see Appendix C) to the results in that Section also apply here.

Figures 6.9–6.11 plot the variation in the average mixing ratio of these species within a night time emitted plume as it ages (blue), with the equivalent model output from the plume-free model run on the same plots (black). For comparison, Figures 6.12–6.14 plot the same for the daytime-emitted plume.

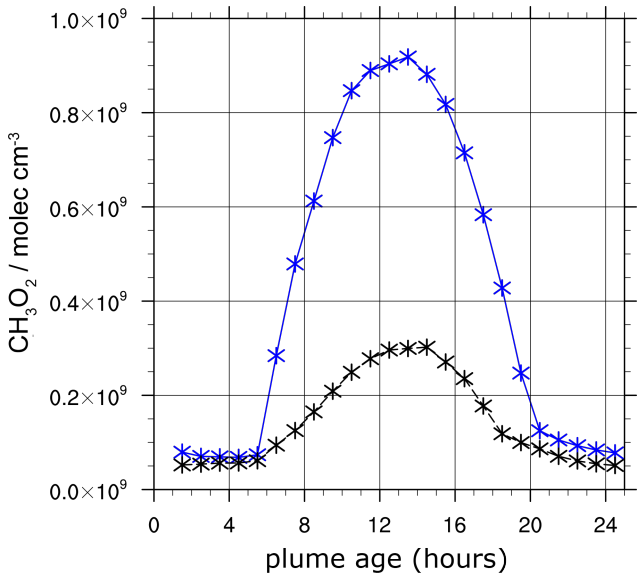

Figure 6.9: Average concentration of CH_3O_2 within the plume as it ages, for plume emitted between 2012-07-31 23:00:00 and 2012-08-01 00:00:00 (blue) and the mixing ratio in the equivalent model output of the plume-free run (black).

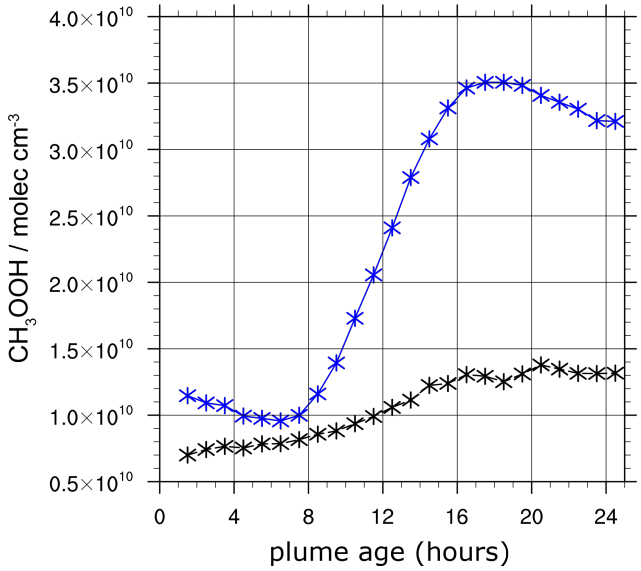

Figure 6.10: Average concentration of CH_3OOH within the plume as it ages, for plume emitted between 2012-07-31 23:00:00 and 2012-08-01 00:00:00 (blue) and the mixing ratio in the equivalent model output of the plume-free run (black).

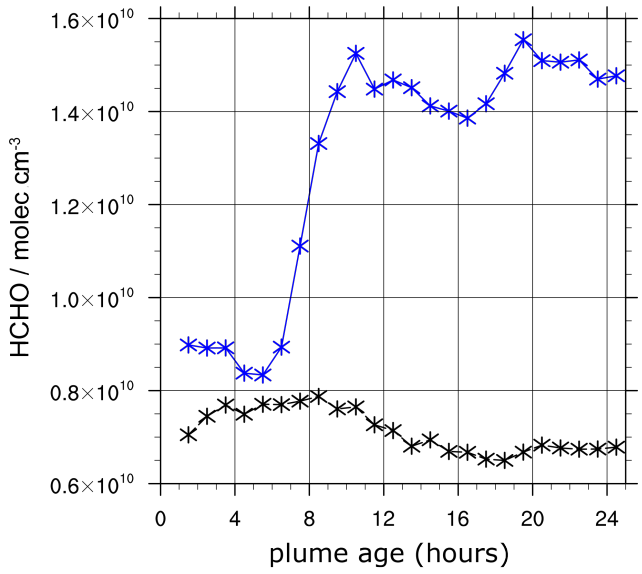

Figure 6.11: Average concentration of HCHO within the plume as it ages, for plume emitted between 2012-07-31 23:00:00 and 2012-08-01 00:00:00 (blue) and the mixing ratio in the equivalent model output of the plume-free run (black).

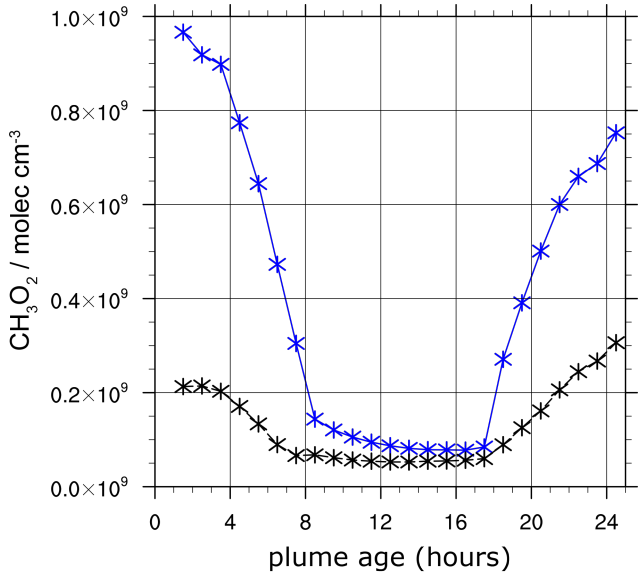

Figure 6.12: Average concentration of CH_3O_2 within the plume as it ages, for plume emitted between 2012-07-31 11:00:00 and 2012-07-31 12:00:00 (blue) and the mixing ratio in the equivalent model output of the plume-free run (black).

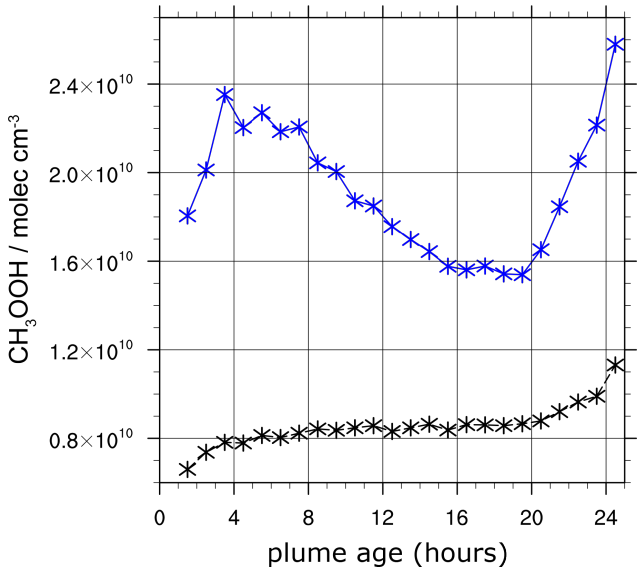

Figure 6.13: Average concentration of CH_3OOH within the plume as it ages, for plume emitted between 2012-07-31 11:00:00 and 2012-07-31 12:00:00 (blue) and the mixing ratio in the equivalent model output of the plume-free run (black).

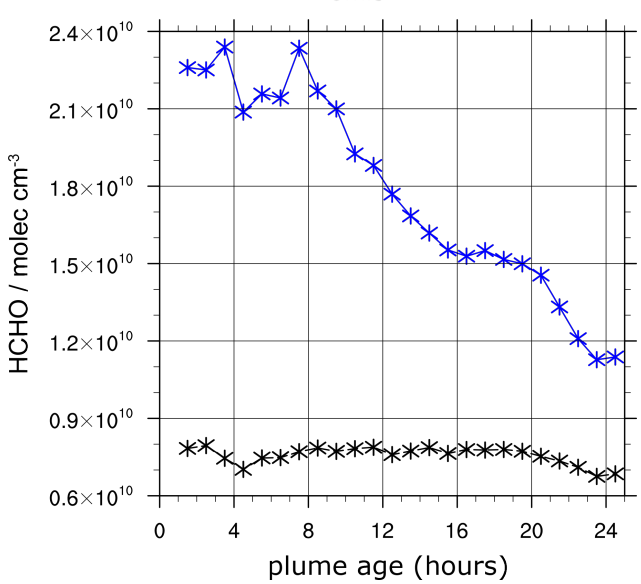

Figure 6.14: Average concentration of HCHO within the plume as it ages, for plume emitted between 2012-07-31 11:00:00 and 2012-07-31 12:00:00 (blue) and the mixing ratio in the equivalent model output of the plume-free run (black).

In the few hours shortly after emission there is a moderate elevation in the modelled concentrations of CH_3OOH and HCHO within the plume. This modelled phenomena occurs because of reactions between volcanic OH and HCl which produce Cl radicals. Because this reaction is incorrectly modelled to be approximately 5 times too fast, no robust conclusions can be drawn from this phenomena in the models.

The model output shows that a large in-plume increase in organics does not occur until dawn when photochemistry begins to occur. Comparison of the equivalent daytime plume and night time plume model output in Figures 6.9–6.14 shows that, qualitatively and quantitatively, the daytime in-plume increase of these species' concentrations is similar in both cases.

6.4 Aerosol

In Section 5.5 I discuss the two processes by which the plume increases the aerosol loading (and therefore the aerosol surface area available for heterogeneous reactions): primary aerosol is emitted directly from the volcano, and secondary sulphate aerosol forms within the plume from the oxidation of SO_2. The first of these processes is time-of-day independent, however the secondary aerosol formation requires OH.

Figure 6.15 shows the average aerosol surface area concentration within the night time emitted plume (blue) and in the equivalent model output from the plume-free run. Figure 6.16 shows, for a plume emitted during the night, the difference in aerosol surface area concentration within the plume compared to the plume-free model run as a ratio of the inert tracer. For approximately the first 9 hours of the plume, the aerosol surface area concentration as a ratio of the tracer is elevated and fairly stable. This means that the surface area increase is happening at the point of emission, and that no major in-plume processes other than dispersion perturb this stability.

This initial elevation of approximately 3×10^{-19} cm^2 per molecule of the inert tracer can be party attributed to the primary aerosol emissions of the volcano. However, as shown in Table 5.1, the volcano's effective emission ratio of surface area to the inert tracer[1] is $1.7 \times 10^{-19} cm^2.molec^{-1}$, meaning that only about half of this night time elevation in aerosol surface area can be attributed to these primary emissions.

[1]The modelled emission flux of the inert tracer is identical to the emission flux of SO_2

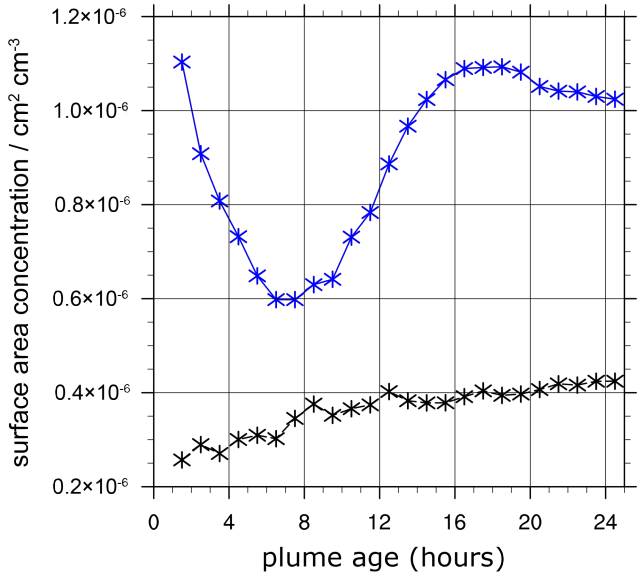

Figure 6.15: Differences in the average in-plume surface area concentration to the equivalent model output from the plume-free run, for plume emitted between 2012-07-31 23:00:00 and 2012-08-01 00:00:00 as it ages.

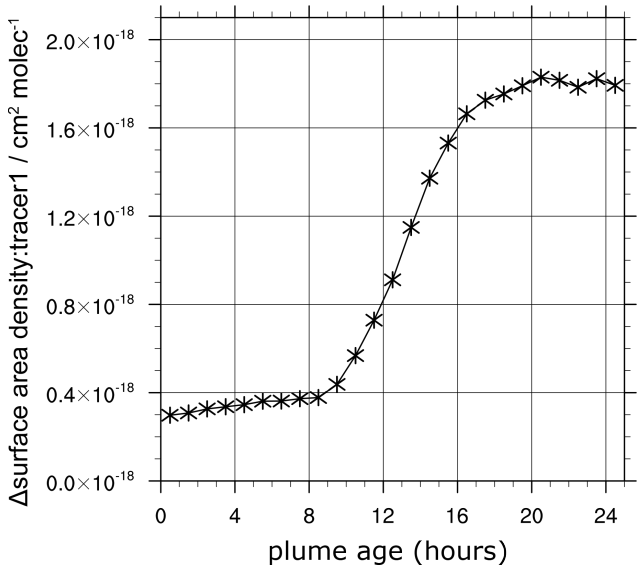

Figure 6.16: Differences in the average in-plume surface area concentration to the equivalent model output from the plume-free run, as a ratio of the inert tracer, for plume emitted between 2012-07-31 23:00:00 and 2012-08-01 00:00:00 as it ages.

The other half is formed from the oxidation of SO_2 by the OH directly emitted by the volcano. This can be identified by the tracer species tracer5P, which is modelled to be produced as a by-product of Reaction R39 (see Section 5.1). In the night time-emitted plume before sunrise, the modelled ratio of tracer5P to that of tracer1 is stable, at about 1.5×10^{-3}. The modelled emission ratio of OH to that of the inert tracer is 3.9×10^{-3} — these values therefore

suggest that slightly less than half of the OH reacts with SO_2. The rest is modelled to react with HCl, a proportion that is elevated due to the incorrect rate of the modelled OH + HCl reaction (see Appendix C). Without this error, the proportion of OH that reacts with SO_2 would be greater.

This "pseudo-primary" aerosol generation will occur in daytime emissions as well, but the effect is easier to identify in this night time model output.

The other notable feature of Figure 6.15 is that aerosol surface area is created within the plume during the day (the same process as identified in Section 5.5), however this rise is does not appear to become significant until several hours after dawn.

During the daytime the generation rate of secondary aerosol is limited by the OH concentration, which varies with sunlight. The OH concentration in the background atmosphere, although non-zero after dawn, builds slowly. This means that the rate of in-plume aerosol formation will also build slowly. Thus it takes time for the secondary aerosol formation to become significant.

Despite this, as shown in Figure 6.15, the primary, "pseudo-primary", and secondary aerosol is sufficient for the overall aerosol surface area concentration to be substantially increased within the plume above background levels for the entire 24-hour period plotted. The primary and "pseudo-primary" aerosol concentration decreases as the plume disperses over the night. Aerosol surface area density reaches a minimum shortly after sunrise after which secondary aerosol creation effects become significant enough to compensate for this plume dispersal and cause a net increase in plume aerosol surface area concentration. For plume emitted earlier in the night, which has longer to disperse before secondary aerosol formation begins, this minimum would be at a level nearer to the background concentration.

In conclusion, within a night-time emitted plume the aerosol surface area concentration is elevated. This is attributable to primary and "pseudo-primary" aerosol during the night and for some hours after sunrise, and then transitioning to a secondary aerosol-dominated situation. Despite the different form of the aerosol trends over time compared to the daytime plume case investigated in Section 5.5, it remains the case that the aerosol surface area density during the day is significantly elevated above background levels.

6.5 Bromine chemistry

As shown in Section 5.6, for a plume emitted during the day, sunset marks a halt in the active bromine cycling as almost all the bromine within the plume accumulates as BrCl. On sunrise the active bromine chemistry cycling resumes.

Figure 6.17, shows the bromine partitioning for a night time-emitted plume.

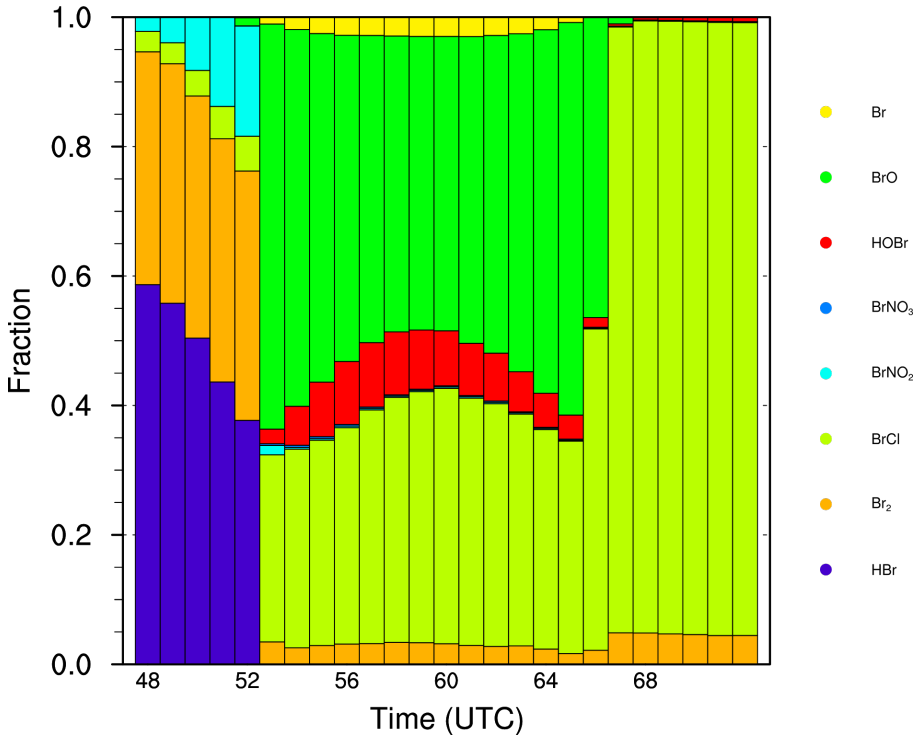

Figure 6.17: Average in-plume modelled distribution of bromine between the different forms plotted versus plume age, for plume emitted between 2012-07-31 23:00:00 and 2012-08-01 00:00:00.

I identify three different regimes in the chemical evolution depicted in Figure 6.17:

1. In the early plume, the plume is dominated by HBr, with a smaller fraction of Br_2 and an even lesser fraction of BrCl. As the night progresses, the HBr is slowly converted to $BrNO_2$.

2. Upon sunrise, the bromine chemistry almost immediately partitions in the same manner as observed for the daytime-emitted plume.

3. Upon sunset the bromine partitioning is the same (BrCl-dominated) as was observed during after sunset for the daytime-emitted plume.

6.5.1 Night time bromine chemistry of a night time-emitted plume

The bromine in the modelled volcanic emissions is, by volume, approximately 75% HBr and 25% Br, with other components being negligible. In the daytime-emitted plume discussed in Section 5.6, the heterogeneous chemistry is sufficiently fast to render HBr a very short-lived species, being completely eliminated from the plume. However for the night time emitted plume, HBr is stable with only a slow transfer to $BrNO_2$ reducing the proportion of bromine present as this species.

Immediately after emission, the modelled Br emitted from the volcano is highly unstable, and is very quickly converted to other forms, predominately Br_2. In addition, Reaction R60 occurs during this process and also converts a molecule of HBr to Br_2, resulting in the bromine fraction present as Br_2 after this process has finished being more than the initial proportion of Br in the emission.

As the night progresses there is a slow conversion of HBr to $BrNO_2$ via Reaction R62 reaction which occurs upon aerosol surfaces.

6.5.2 Post-sunrise bromine chemistry of a night time-emitted plume

These phenomena may be interesting of themselves, however they are of lesser importance when considering the plume after sunrise. On sunrise the bromine in these night time species is all rapidly subsumed into the active bromine cycling.

The daytime bromine partitioning in this plume is essentially identical to the long-term daytime partitioning identified in Section 5.6. Figure 6.17 shows clearly the moderate variation in the bromine partitioning with sunlight intensity, with a pattern that is symmetrical around noon. This variation is the same as discussed in Section 5.6.

Despite that there is little secondary volcanic aerosol shortly after sunrise, the available aerosol surface area is evidently sufficient for the reactive bromine cycling to occur without a significant limitation in the heterogeneous step.

The chemical regime that begins at sunset is essentially the same as that

which occurs within the daytime-emitted plume.

6.6 Ozone chemistry

Figures 6.18 and 6.19 show the average destruction of O_3 within a night time-emitted plume as it ages, in absolute terms and as a ratio of the inert tracer respectively.

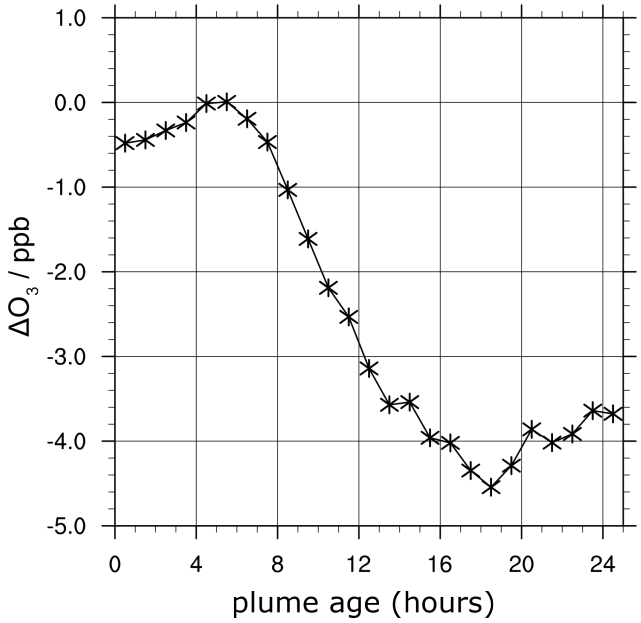

Figure 6.18: Differences in the average in-plume ozone concentration to the equivalent model output from the plume-free run for plume emitted between 2012-07-31 23:00:00 and 2012-08-01 00:00:00 as it ages.

The re-equilibration of the volcanic emissions results in a small depletion of O_3 immediately after emission, however the magnitude of this is negligible. As is shown in Figure 6.19, substantial O_3 depletion does not occur until sunrise. Upon sunrise, bromine cycling occurs. The associated O_3 destruction occurs, as a ratio of the inert tracer, at a similar rate to that observed for the day time-emitted plume, ceasing at sunset.

The night time net ozone creation caused by the plume's suppression of NO_x (see Section 5.7.2) does not occur within the night time-emitted plume's first night, as the NO_x suppression requires sunlight. By the time of the second night, the plume is too disperse for this effect to be significant. This means that the net O_3 depletion after 24 hours of plume evolution is actually slightly greater for the modelled night time-emitted plume as it is for the daytime-emitted plume

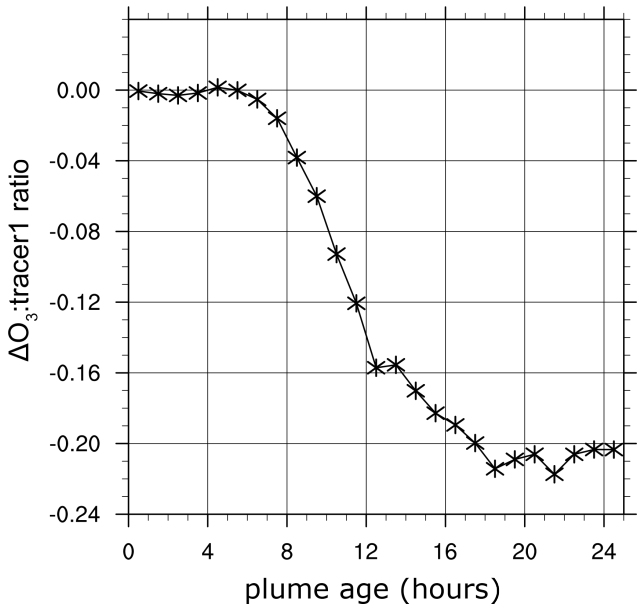

Figure 6.19: Differences in the average in-plume ozone concentration to the equivalent model output from the plume-free run, as a ratio of the inert tracer, for plume emitted between 2012-07-31 23:00:00 and 2012-08-01 00:00:00 as it ages.

(c.f. Figures 5.31 and 6.19), although the difference is small.

6.7 Conclusions

Although there are some phenomena that only occur in volcanic plumes that have not seen daylight, the chemical evolution of a night time-emitted plume during the day is essentially the same as that of a plume emitted during the daytime.

This may be a useful phenomenon if the results of this investigation were to be used to generate a parametrisation for representing the chemistry of volcanic plumes in a large scale model. This result would simplify such as task as when considering plume effects during the daytime, it does not appear to be necessary to differentiate between plume emitted at different points of the diurnal cycle.

Chapter 7

Volcanic intensity study

In Chapters 5 and 6, I investigate the modelled plume chemistry relating to 60 kg SO_2 s^{-1} volcanic emission (with lesser fluxes of aerosol and other volatiles). This is representative of strong but not atypical passive degassing behaviour of Mount Etna.

However volcanic emissions can vary over several orders of magnitude, and in this chapter I present results from model runs where the volcanic intensity is increased by 1 and 2 orders of magnitude compared to the base case. Apart from this change, no other alterations were made to the model setup. This has been done to maximise the ease of comparing the output with the base case.

Although the emission magnitudes modelled approach the magnitudes of explosive volcanic eruptions, these model runs are not applicable representations of such eruptions — such simulations would need to represent various aspects of explosive volcanic eruptions that have not been incorporated into these model runs, such as the vertical structure created by explosive thrust, differences (compared to the degassing case) of the emissions' chemical and aerosol composition, the aerosol microphysics in an extremely high aerosol loading environment, and extremes of temperature within the early plume. This exercise is intended to investigate how the plume chemistry identified in the previous chapters changes with increased intensity, identify upper emission-intensity limits to the validity of the results of the previous chapters, and to provide a starting reference point for dedicated investigations into the chemistry of larger eruptions.

This chapter also discusses variations in chemistry between the core of a plume, where volcanic gases are concentrated, and the edge of a plume were

they are more dilute.

7.1 Run details

This Chapter compares the model output also discussed in Chapter 5, with runs where all volcanic emissions (gas and aerosol emissions) are 10 and 100 times greater than in the base case. All other aspects of the model setup were unchanged.

Table 7.1: Volcanic intensity runs

Run number	Volcanic SO_2 emissions kg s^{-1} flux	Volcanic bromine emissions kg s^{-1}
I	60	0.045
II	600	0.45
III	6000	4.5

In this Chapter I will refer to the runs by Roman numerals, as tabulated in Table 7.1. Run **I** is the base case, as discussed in the previous chapters.

In all runs, the modelled flux of the inert tracer is set to be equal to that of the flux of SO_2.

7.2 Linear effects

For SO_2 a species which is directly emitted by the plume and is perturbed little by plume chemistry (see Section 5.1), its concentrations within the plume are proportionate to the magnitude of the emission. This is shown in Figure 7.1 which shows that the in-plume ratio of SO_2 to that of inert tracer is consistent between the three runs.

This occurs because the increase in intensity does not substantially change the removal of SO_2 from the plume. The rates of dry deposition processes are linear with the concentration of the deposited species (Wesely, 1989) and therefore the relative importance of this process is equal in each modelled case.

Chemical losses of SO_2, are discussed in Section 7.5 and indicate that the increase in intensity does increase the extent to which HO_x is depleted in the plume, which reduces the chemical loss rate. However as this loss is slow for even the run **I** case, this change is of negligible importance.

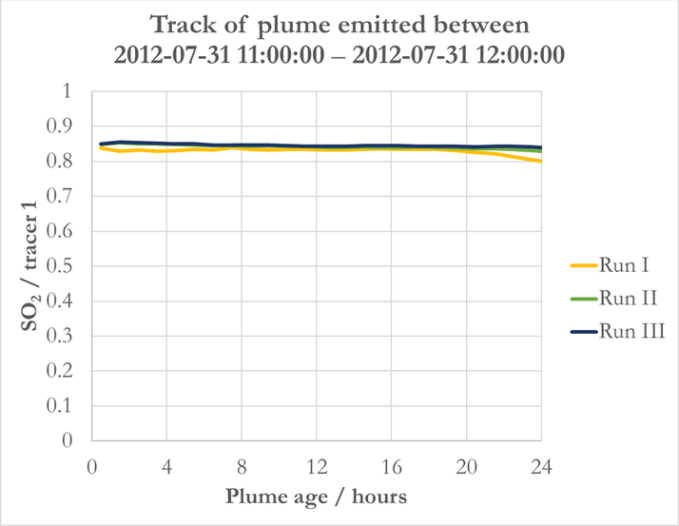

Figure 7.1: Average in-plume ratio of SO_2 to the inert tracer for plume emitted between 2012-07-31 11:00:00 and 2012-07-31 12:00:00 as it ages for the **I**, **II**, and **III** model runs.

Figure 7.2 shows that the same linear concentration—emission intensity relationship holds for HCl, the concentration of this species within the plume is in proportion to the intensity of emission.

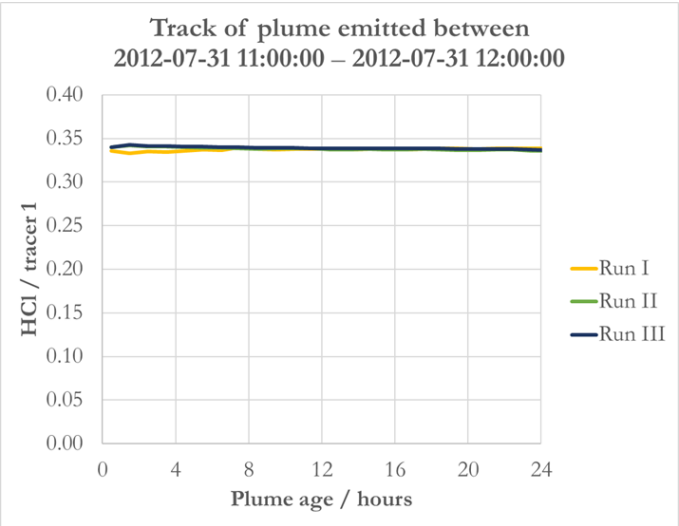

Figure 7.2: Average in-plume ratio of HCl to the inert tracer for plume emitted between 2012-07-31 11:00:00 and 2012-07-31 12:00:00 as it ages for the **I**, **II**, and **III** model runs.

7.3 Total depletion of NO_x

In Section 5.3, I show that in the run **I** situation, the modelled NO_x within the plume is moderately depleted compared to the background, a phenomenon

caused by bromine chemistry. Figures 7.3–7.5 show the relative impact of the modelled plumes, in comparison to the plume-free run, on NO_x mixing ratios downwind of the volcano.

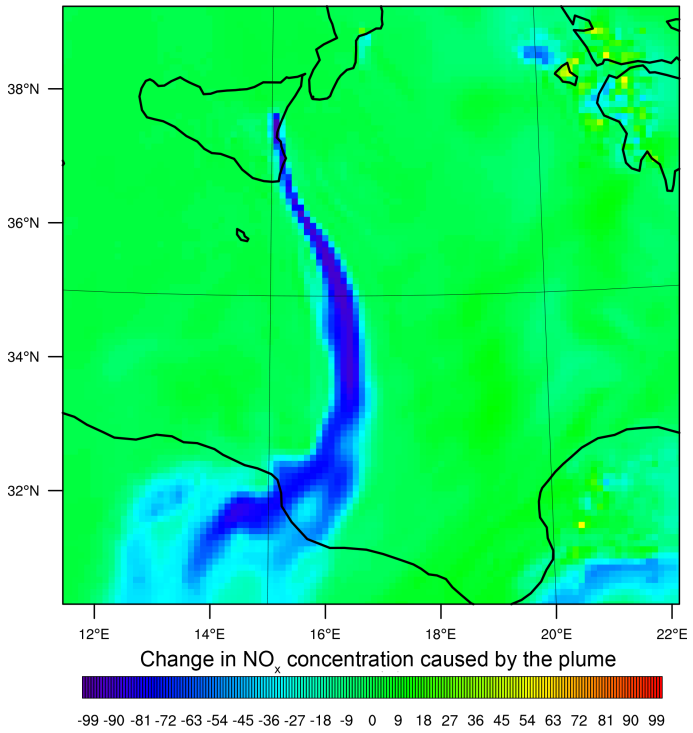

Figure 7.3: Relative difference in concentration of NO_x between model run **I** and the plume-free run. Negative values indicate a depletion caused by the plume. Plot shows a cross section of the model output at 3 km altitude at 2012-08-01 12:00:00.

In run **I** (Figure 7.3) the magnitude of the NO_x depletion varies between the plume core, where it is nearly 100%, and the plume edges where it is more moderate. The plume which is sufficiently old to have reached Africa is sufficiently dispersed such that there is no well-defined core.

In runs **II** and **III** the plume effect is stronger, with total depletion of NO_x within its core. The area of effect widens with plume intensity; as the magnitude of emission increases between these runs, areas which were previously part of the plume edge become part of the plume core.

A feature visible in Figure 7.5 is a region within the core of the plume where NO_x depletion appears not to occur. Although it looks like a region "missed" by the plume due to wind dynamics, this is actually the core of the plume. This phenomenon occurs because of the modelled suspension of bromine cycling in the very intense plume (see Section 7.8) which results in the non-occurrence of the NO_x-depleting effects discussed in Section 5.3.

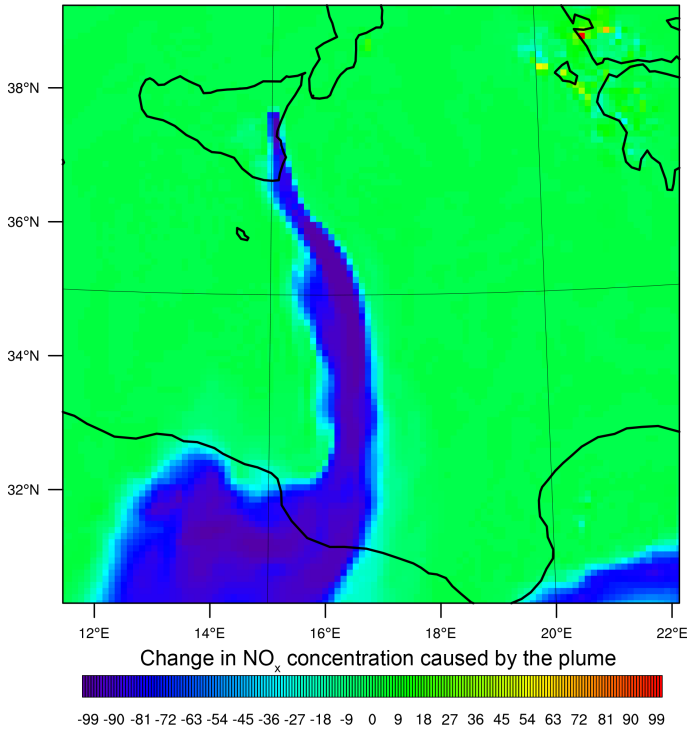

Figure 7.4: Relative difference in concentration of NO_x between model run **II** and the plume-free run. Negative values indicate a depletion caused by the plume. Plot shows a cross section of the model output at 3 km altitude at 2012-08-01 12:00:00.

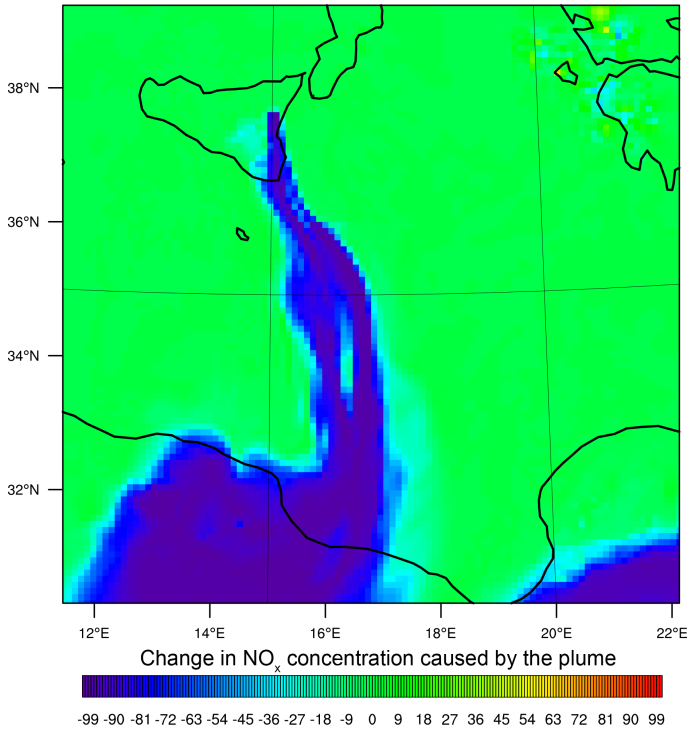

Figure 7.5: Relative difference in concentration of NO_x between model run **III** and the plume-free run. Negative values indicate a depletion caused by the plume. Plot shows a cross section of the model output at 3 km altitude at 2012-08-01 12:00:00.

7.4 Total depletion of ozone

In the base case (run **I**), O_3 is depleted within the plume (Section 5.7). This loss was a few 10s of % in the first hour of the plume, and a few % thereafter. This loss slightly perturbed the generation of OH radicals within the daytime plume, however this effect is not as significant as other chemical effects. The O_3 depletion is caused by bromine chemistry.

Figures 7.6–7.8 show the O_3 mixing ratio in a horizontal cross-section that contains the plume (3 km altitude) for runs **I**, **II**, and **III**.

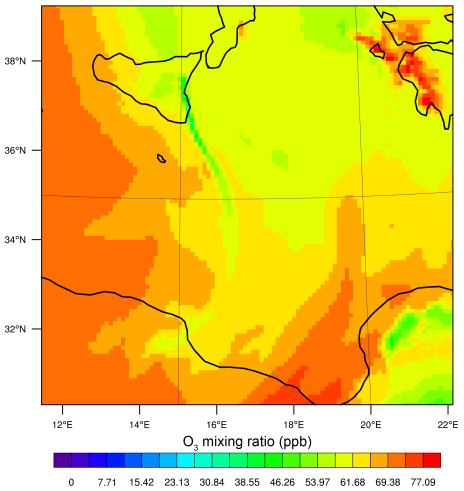

Figure 7.6: O_3 mixing ratio in model run **I**. Plot shows a cross section of the model output at 3 km altitude at 2012-08-01 12:00:00.

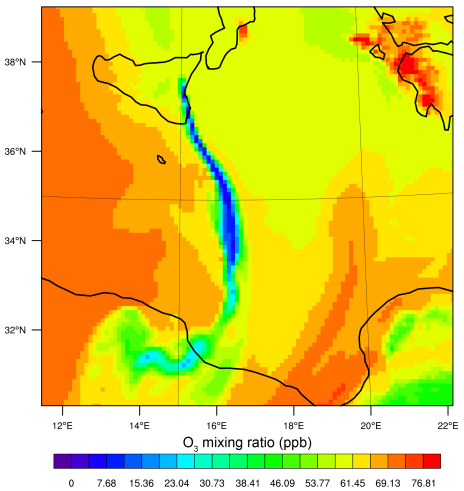

Figure 7.7: O_3 mixing ratio in model run **II**. Plot shows a cross section of the model output at 3 km altitude at 2012-08-01 12:00:00.

At the scale of these figures, the in-plume O_3 depletion in case **I** is barely

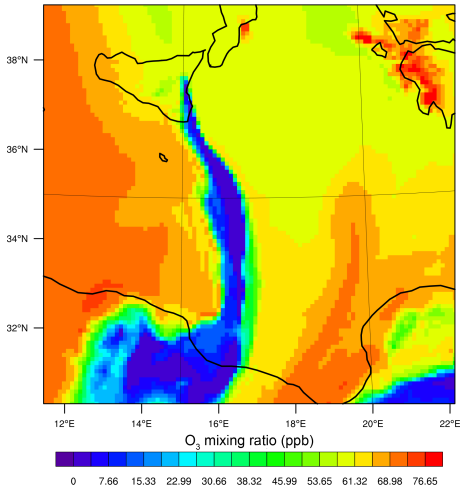

Figure 7.8: O_3 mixing ratio in model run **III**. Plot shows a cross section of the model output at 3 km altitude at 2012-08-01 12:00:00.

noticeable, being a thin area of moderate-to-low depletion running south from the volcano, producing an effect visible in this Figure for a few 100 km. As shown by the analyses in Section 5.7, the O_3-depleting effect does not cease at this point, however the dispersal is such that the net effect at any given point is a few ppb at most.

In run **II**, the O_3 depletion is stronger and the area of effect is larger (a similar phenomena to that seen for the NO_x depletion). It is easier to see in this figure the variation between the core of the plume and the edges, with the core having stronger depletion.

In run **III** the effect is, again, more intense and has a broader area of effect. Notable in this case is that there is a core of the plume where the O_3 depletion reaches totality.

In general terms, there is more O_3 depletion when the magnitude of emission is greater. O_3 loss is caused by bromine chemistry, therefore increased bromine emissions from the volcano cause increased O_3 loss.

In Section 5.7.2 I calculate the "efficiency" of bromine's destruction of O_3 for the base (run **I**) case. On average, over a 24-hour period, the modelled average O_3 destruction rate is 3×10^{-6} molecules O_3 per molecule of the inert tracer per second, which equates to a destruction rate of 5×10^{-3} molecules O_3 per atoms of volcanic bromine per second.

In Figure 7.9 I extend this analysis (as performed to create Figure 5.31) to runs **II** and **III**.

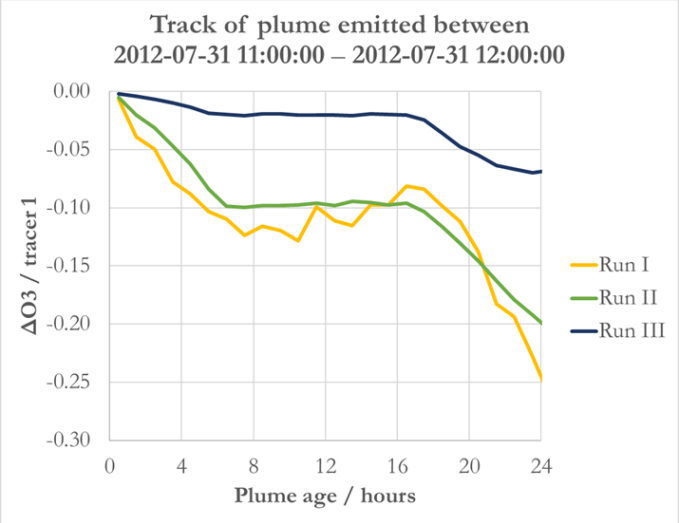

Figure 7.9: Average in-plume ratio of ΔO_3 (difference compared to the plume-free run, negative values indicting depletion caused by the plume) to the inert tracer for plume emitted between 2012-07-31 11:00:00 and 2012-07-31 12:00:00 as it ages for the **I**, **II**, and **III** model runs.

The night time increase in the ratio seen in run **I** (discussed in Section 5.7) is less significant in runs **II** and **III**, as this effect does not scale linearly with plume intensity. Other than this, the evolution of the ΔO_3:inert tracer ratio is similar in runs **I** and **II**, with a moderate loss of efficiency. Thus means that the modelled O_3 loss is moderately less than 10 times greater in run **II**.

This loss of efficiency is more pronounced in run **III**, where the total destruction of O_3 as a ratio of the inert tracer is substantially less than the other two runs. Below I list three explanations for this phenomenon. These are not alternative theories or competing effects, but rather three different ways of describing a negative feedback effect:

1. The complete destruction of O_3 in the core of the plume (Figure 7.8) limits the O_3 destruction, as it cannot be greater than 100%. The total rate is therefore limited by the rate of entrainment of O_3 from outside of the plume.

2. The O_3 destruction potential of much of the plume's bromine is "wasted" by being in locations where there is no further O_3 to deplete.

3. O_3 is necessary for bromine cycling to occur, therefore the complete destruction of O_3 halts the bromine cycling.

The bromine chemistry in these intense plumes is examined further in Section

7.8. From the model results discussed here, it can be inferred that a linear relationship of total O_3 loss to emission intensity approximately holds up to a high intensity level (modelled to be approximately a few 100 kg SO_2/s given the emission ratios used in these runs). Above this, a saturation effect limits the efficiency of the plume's O_3 destruction.

7.5 Depletion of HO_x

In section 5.2, I discuss the effect the plume has on the mixing ratios of OH and HO_2. Both are depleted within the plume.

Intensifying the emissions has a fairly straightforward effect on OH concentrations. In the case I the plume creates a narrow volume where OH is totally or near-totally eliminated, in the more intense plumes this volume is broader. Figures 7.10–7.12 show the OH concentrations for runs **I–III** in a horizontal cross-section of the model output. It should be noted here that the bug (Appendix C) means the plume OH-destructive effect is overestimated by the model, and these Figures should be interpreted qualitatively only.

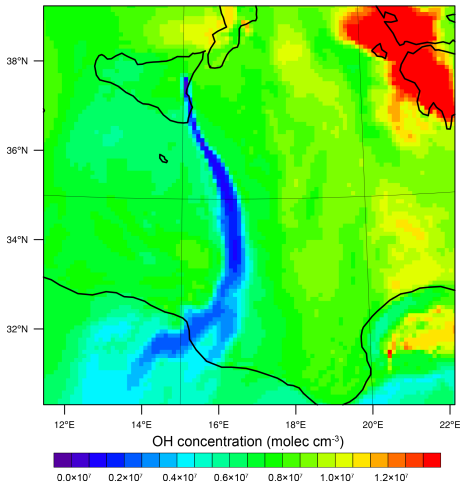

Figure 7.10: OH mixing ratio in model run **I**. Plot shows a cross section of the model output at 3 km altitude at 2012-08-01 12:00:00.

A more complicated phenomenon is seen for HO_2. Cross-sections of concentrations of HO_2 are shown in Figures 7.13–7.15.

Although the HO_2 loss, does become more substantial with greater emissions, the intensification of this effect is far less than the intensification of the emissions. Table 7.2 reports average modelled HO_2 concentrations for the

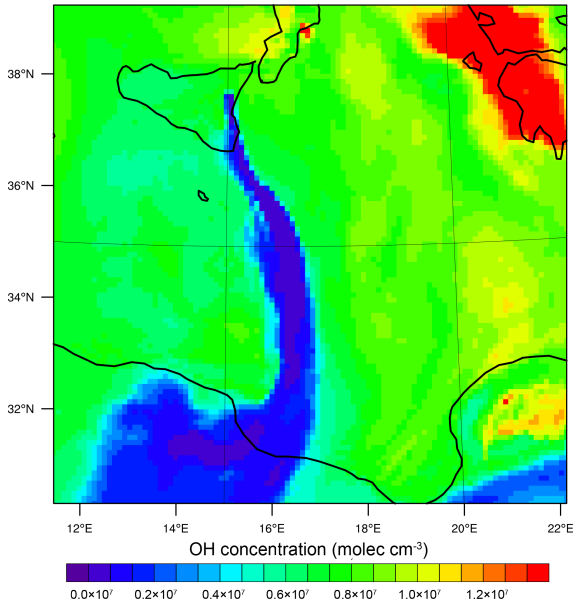

Figure 7.11: OH mixing ratio in model run **II**. Plot shows a cross section of the model output at 3 km altitude at 2012-08-01 12:00:00.

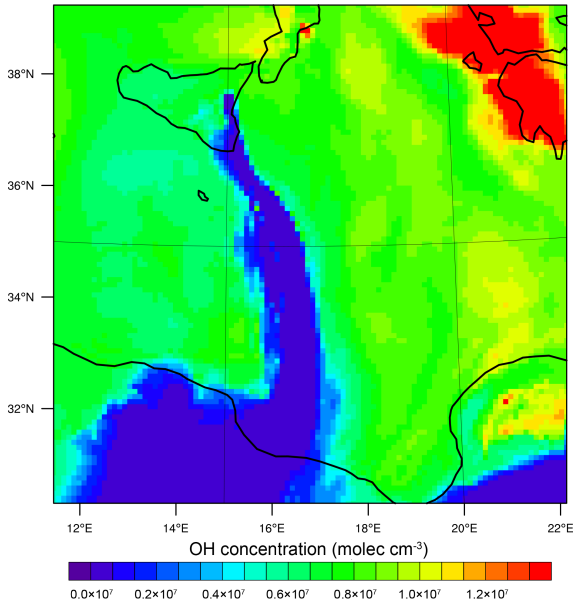

Figure 7.12: OH mixing ratio in model run **III**. Plot shows a cross section of the model output at 3 km altitude at 2012-08-01 12:00:00.

plume aged 1.5–2.5 hours in runs **I**–**III**. The $HO_2 + BrO$ reaction (Reaction R50 is the main destruction pathway of HO_2 in each case, and the k_{eff} of this reaction is reported.

The perturbation of the bromine cycling (see Section 7.8) means that despite the total amount of bromine emitted by the model volcano varies by orders of magnitude between these three runs, the concentration of BrO within the

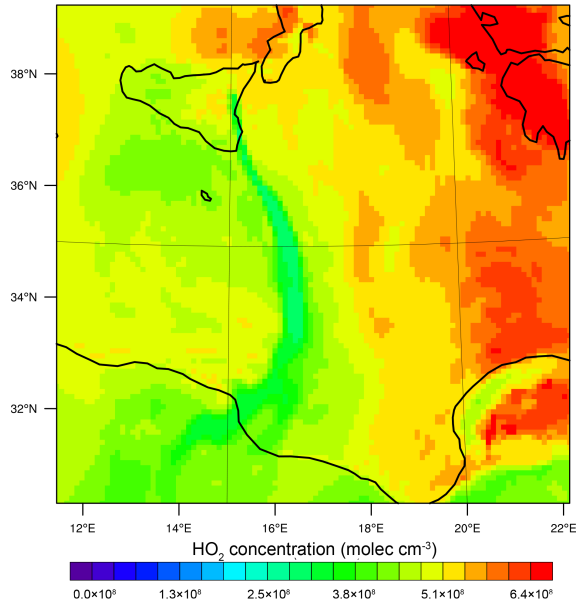

Figure 7.13: HO_2 mixing ratio in model run **I**. Plot shows a cross section of the model output at 3 km altitude at 2012-08-01 12:00:00.

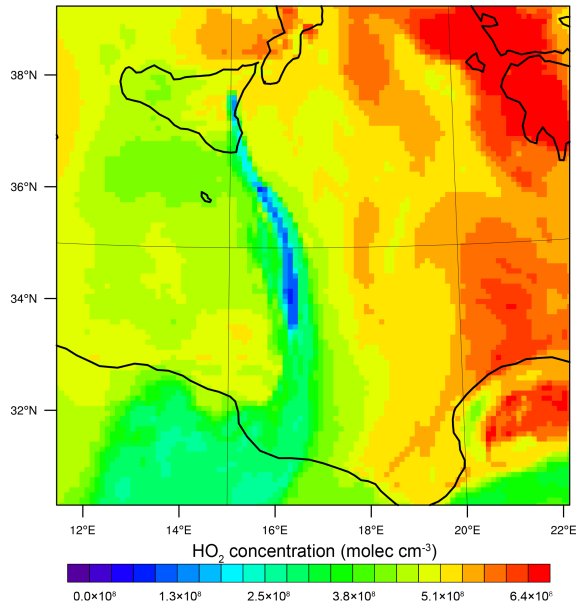

Figure 7.14: HO_2 mixing ratio in model run **II**. Plot shows a cross section of the model output at 3 km altitude at 2012-08-01 12:00:00.

evolved plume (and therefore the rate of the primary HO_2 loss reaction) varies by a much lesser amount.

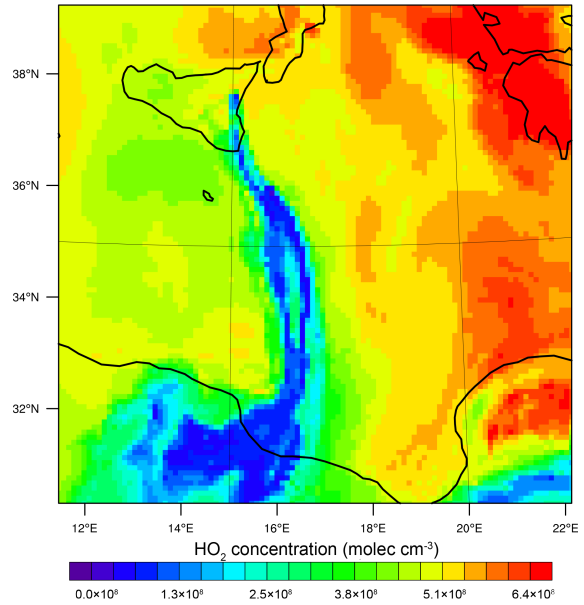

Figure 7.15: HO_2 mixing ratio in model run **III**. Plot shows a cross section of the model output at 3 km altitude at 2012-08-01 12:00:00.

Table 7.2: HO_2 concentrations and effective loss rates (with respect to reaction with BrO) for plume aged 1.5–2.5 hours at 2012-07-31 12:00:00

Run	$[HO_2]$ / molec cm^{-3}	BrO + HO_2 reaction k_{eff} / molec cm^{-3} s^{-1}
I	3.6×10^8	2.3×10^{-2}
II	2.4×10^8	4.1×10^{-2}
III	1.7×10^8	4.7×10^{-2}

7.6 Aerosol

In Section 5.5, I discuss the aerosol within the plume for the base case. At the point of emission, primary aerosol results in a an elevated aerosol surface area concentration (As discussed in Section 6.4, some of this aerosol is "pseudo-primary", being formed from volcanogenic OH immediately after emission from the vent. As the plume disperses, the concentration of this aerosol declines, however this is compensated for by the formation of secondary aerosol within the plume. The total aerosol surface area within the plume (from primary, secondary, and background aerosol) is sufficient that the heterogeneous part of the bromine cycling are not rate-limiting.

Figure 7.16 shows the average aerosol surface area of volcanic origin[1] for an ageing plume in the model output from runs **I–III**.

[1]The surface area of background aerosol, value taken from the equivalent model output in the plume-free run, has been excluded.

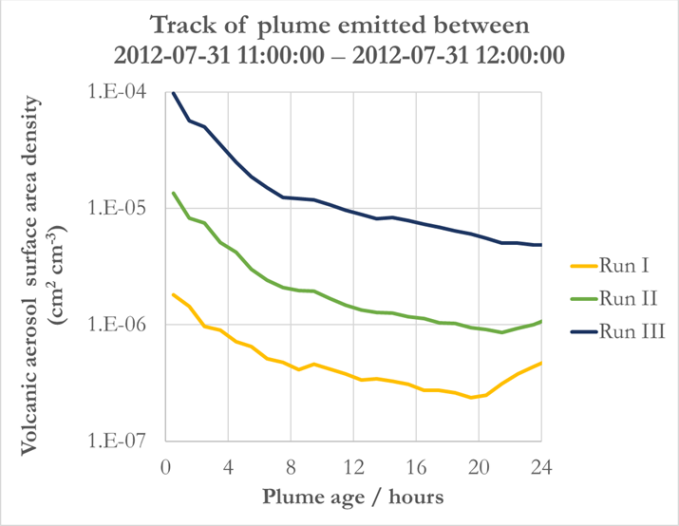

Figure 7.16: Average in-plume volcanic aerosol surface area density for plume emitted between 2012-07-31 11:00:00 and 2012-07-31 12:00:00 as it ages for the **I**, **II**, and **III** model runs.

The surface area from volcanogenic aerosol is substantially greater in the more intense runs. In the early plume this variation is close to being linear with emissions intensity, however the difference diminishes for more evolved plume. While the primary aerosol emissions are explicitly set to vary by orders of magnitude between the three model runs, the rate of secondary aerosol formation does not vary linearly. This can be more clearly seen in Figure 7.17, which shows the values plotted in Figure 7.16 as ratios of the inert tracer.

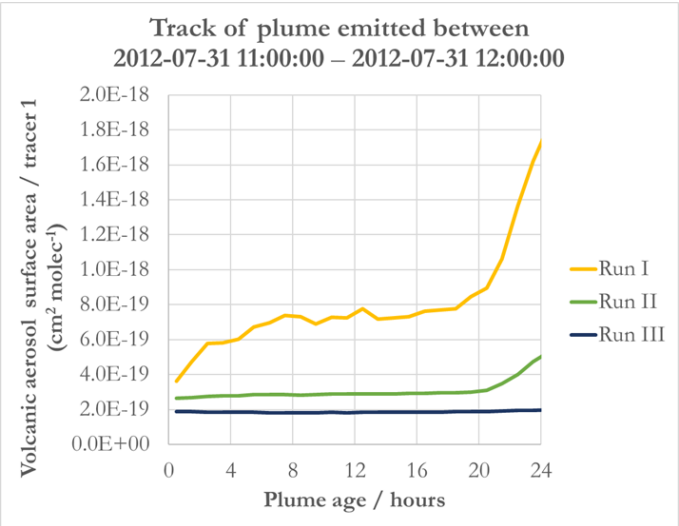

Figure 7.17: Average in-plume ratio of volcanic aerosol surface area to the inert tracer for plume emitted between 2012-07-31 11:00:00 and 2012-07-31 12:00:00 as it ages for the **I**, **II**, and **III** model runs.

As discussed in Section 5.5, an increase in the aerosol surface area to inert tracer ratio is an indication of secondary aerosol formation. Figure 7.17 shows that although the modelled emissions of SO_2 vary by orders of magnitude between the three runs, the secondary aerosol formation rate has varied in the same manner. The cause of this is the depletion of OH in the plume (see Section 7.5), which prevents the oxidation of SO_2 to H_2SO_4.

While secondary aerosol is the dominant form in the evolved plume in the run **I** case, for the more intense plume the aerosol is dominated by primary aerosol, as this is emitted in greater quantities and the secondary aerosol formation is suppressed.

7.7 Organic activation

In Section 5.4, I discuss the phenomenon of chlorine radicals released within the plume producing active organic chemistry. This radical is generated primarily by the photolysis of BrCl (Reaction R46), however the bug (see Appendix C) has caused the generation from HCl (Reaction R40 to be overestimated. Due to this error, the determinations made in this Section should be considered qualitatively only.

These Cl radicals react with CH_4, producing CH_3O_2, which degrades further, eventually forming CO. The CH_3O_2 produced is important, as it provides an alternative pathway for the conversion of BrO to HOBr.

Figures 7.18, 7.19, and 7.20 show the mixing ratio of CH_3O_2, CH_3OOH, and HCHO within the three modelled plumes as they age.

The relationship between the mixing ratios of these species and the intensity of the volcanic emissions is complex. In the following paragraphs I summarise the key points for these major species:

CH_3O_2 CH_3O_2 is increased above background levels in each case, due to phenomena discussed in Section 5.4. However the increased intensity of the modelled plume results in a *decrease* of the mixing ratio within the plume. This occurs because of a change in the halogen-dominated balance of sources and sinks of CH_3O_2 in the more intense plumes.

With OH even more suppressed in the more intense plumes than the default case (see Section 7.5), the principal source of Cl radicals within the plume is

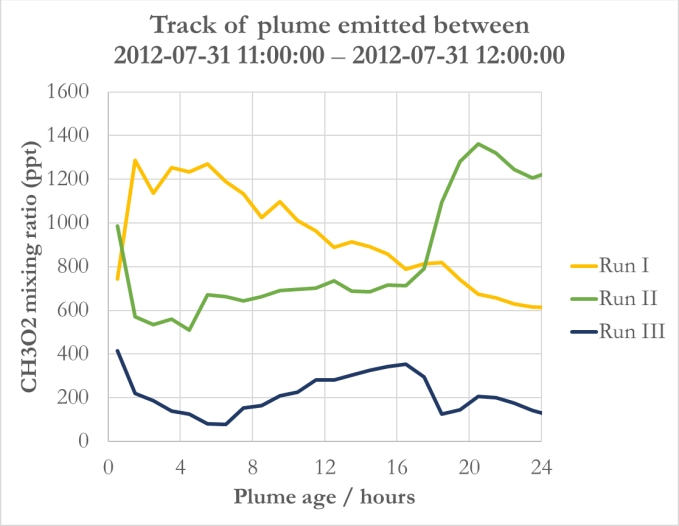

Figure 7.18: Average in-plume mixing ratio of CH_3O_2 for plume emitted between 2012-07-31 11:00:00 and 2012-07-31 12:00:00 as it ages for the **I**, **II**, and **III** model runs.

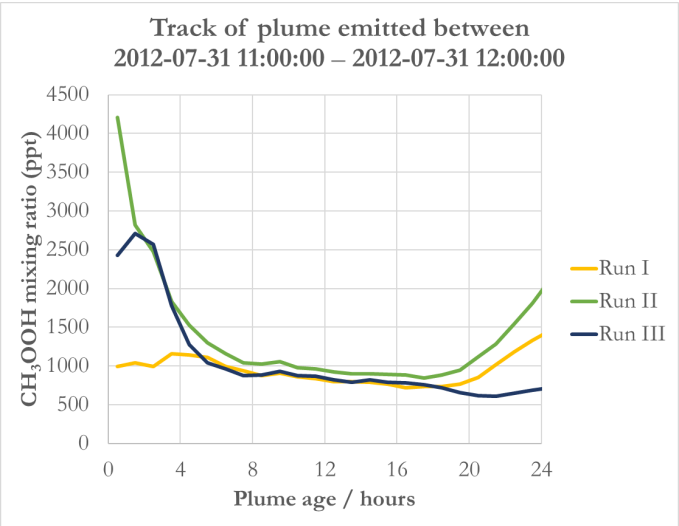

Figure 7.19: Average in-plume mixing ratio of CH_3OOH for plume emitted between 2012-07-31 11:00:00 and 2012-07-31 12:00:00 as it ages for the **I**, **II**, and **III** model runs.

photolysis of BrCl which is created in HCl-mediated bromine chemistry. The principle sink of CH_3O_2 in these intense plumes is reaction with BrO.

As discussed in Section 7.8, the bromine cycling in runs **II** and **III** is predominately HBr-mediated; Br_2 is formed instead of BrCl. This means that with more intense emissions the balance between reactive chlorine formation and reactive bromine formation shifts towards the latter, decreasing the concentration of CH_3O_2 within the plume.

For run **II**, after sunrise the modelled bromine cycling is HCl mediated, and

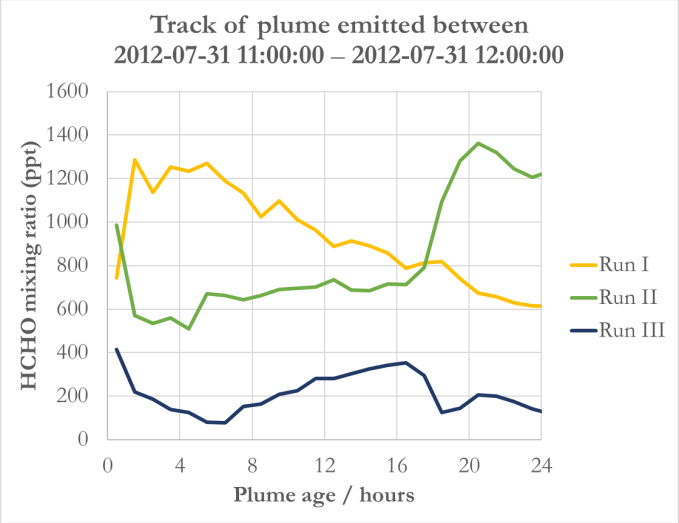

Figure 7.20: Average in-plume mixing ratio of HCHO for plume emitted between 2012-07-31 11:00:00 and 2012-07-31 12:00:00 as it ages for the **I**, **II**, and **III** model runs.

consequently the CH_3O_2 is boosted more in run **II** than run **I**, as the plume is more intense.

CH_3OOH The greater depletion of OH in the more intense plumes (see Section 7.5) effectively closes a major loss pathway of CH_3OOH. Without this loss, CH_3OOH concentrations are greater within the more intense plume.

HCHO As discussed in Section 5.4, the modelled in-plume HCHO concentration is increased above background levels in the run **I** case. The in-plume HCHO mixing ratio is lesser within the more intense plumes, to the extent that in the run **III** case the in-plume mixing ratio is less than the background ratio (approximately 400 ppt).

The cause of this is the variation in the amount of Br in these modelled plumes, which vary the rates of losses of HCHO to the

$$HCHO + Br \longrightarrow CO + HBr + HO_2 \qquad \text{(R63)}$$

reaction. The more intense plumes have greater concentrations of Br radicals (see Section 7.8).

The effect of the emissions on the in-plume organic chemistry is very much non-linear. The chemical evolution of the more intense plumes is qualitatively different to that of the run **I** case discussed in Section 5.4, resulting in a much

smaller impact than would be inferred by scaling up the impact of the run **I** case.

The run **II** case shows run **I**-like behaviour after sunrise (and several hours of dispersion), which suggests that intense plume eventually "reverts" to the chemical regime identified in Chapter 5, this phenomena is discussed in more detail below.

The organic chemistry is controlled by the halogen chemistry of the plume.

7.8 Bromine cycling

In the base case, although HBr is the dominant emission species, it is very quickly eliminated from the plume. Within an hour from emission, a stable cycling regime establishes itself. Bromine is continuously cycled during daylight, with $HOBr + HCl$ being the main heterogeneous reaction pathway. The rate of the cycling is dependant upon the actinic flux. At sunset, the cycling ceases and bromine almost entirely partitions to BrCl. The cycling resumes upon sunrise. The modelled BrO/SO_2 ratios within the plume were in the range of experimental observations. The bromine cycling in the base case is discussed in Section 5.6.

In this section I discuss the bromine cycling that occurs in runs **II** and **III**. As reported in Table 7.1, the volcanic emissions of bromine within these runs each have the same ratio to those of SO_2.

In Subsection 7.8.1 I discuss the bromine chemistry of the plume in aggregate, in Subsection 7.8.2 I discuss "lateral" variations in the chemistry of the plume (differences between the edge and core of the plume).

7.8.1 Overall plume effects

Figures 7.21–7.23 show how bromine is distributed between its different forms in these model runs.

There is a substantial, qualitative difference in how bromine partitions between these runs. Figure 7.21 is identical to Figure 5.19, and the bromine chemistry in this case is discussed in Section 5.6.

While in the base-case (run **I**), HBr is exhausted in plume within a few

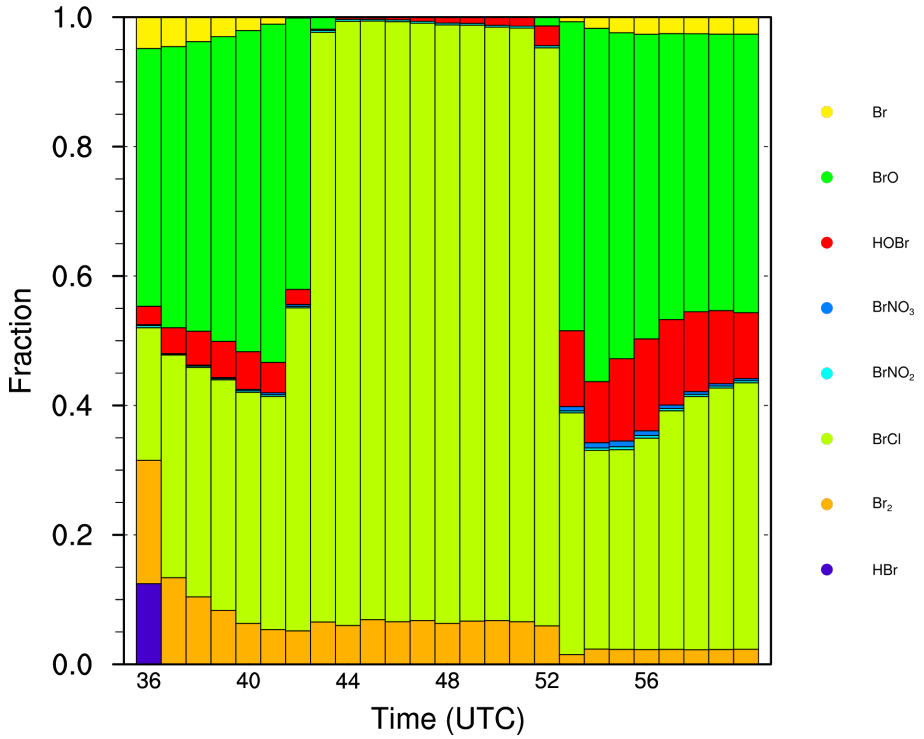

Figure 7.21: Run **I**: Average in-plume modelled distribution of bromine between the different forms plotted versus time, for plume emitted between 2012-07-31 11:00:00 and 2012-07-31 12:00:00.

Table 7.3: Weighted average values relating to 3–4 hour old plume at 2012-07-31 15:00:00 in output of model runs **I**, **II**, and **III**

Run	Br_y concentration	Bromine conversion rates / molec cm^{-3} s^{-1}			% heterogeneous cycling
	molec cm^{-3}	BrO $\longrightarrow$ HOBr	Br $\longrightarrow$ HBr	BrO + BrO $\longrightarrow$ Br or Br_2[a]	via HBr
I	9.8×10^8	4.2×10^6	8.9×10^5	1.9×10^6	22
II	9.3×10^9	9.6×10^6	1.2×10^7	2.4×10^7	98
III	9.7×10^{10}	5.8×10^6	6.9×10^6	3.0×10^7	99

[a] Values are total rates of bromine atom flux through this reaction.

minutes from release, in run **II** the depletion of HBr is, in relative terms, much slower, taking hours to complete. In the plume considered in Figure 7.22, this depletion of HBr is incomplete by sunset. Similar to the case as described in Section 6.5, there is little significant bromine chemistry during the night — there is a small conversion of HBr to $BrNO_2$ (Reaction R62), however this is suppressed by the NO_x depletion within the plume (see Section 7.3). On sunrise the last of this HBr is consumed.

Table 7.3 considers the modelled plume aged 3–4 hours at 2012-07-31 15:00:00 from each of the runs (i.e. that represented by the fourth column in Figures 7.21–7.23). The average concentration of Br_y is reported for context.

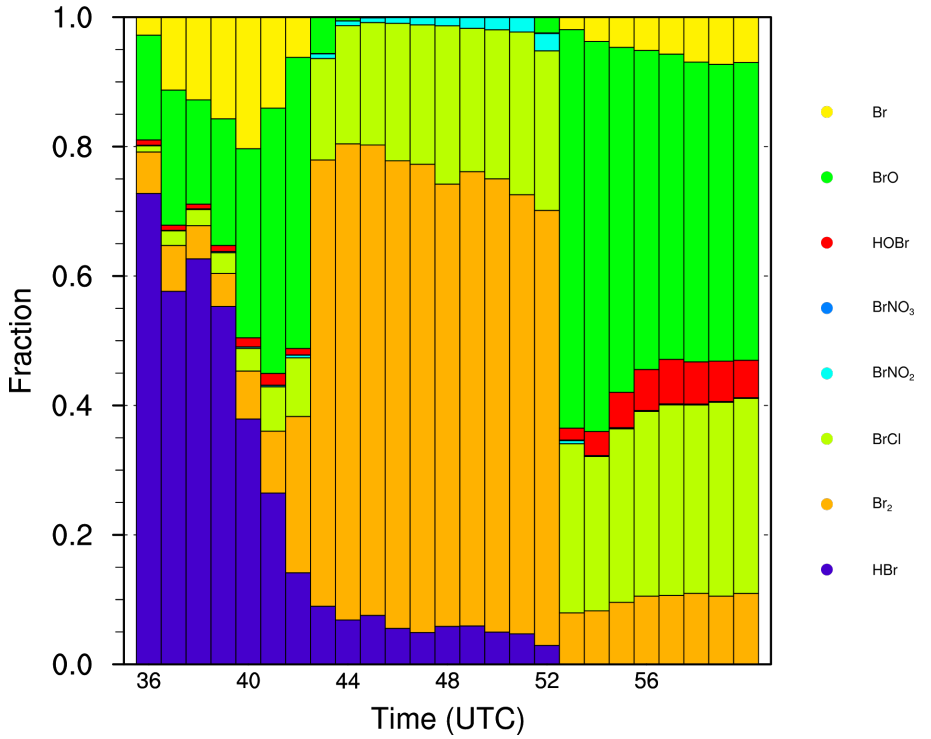

Figure 7.22: Run **II**: Average in-plume modelled distribution of bromine between the different forms plotted versus time, for plume emitted between 2012-07-31 11:00:00 and 2012-07-31 12:00:00.

7.8.1.1 Dominance of HBr pathway

While in run **I**, daytime bromine plume chemistry in the plume which is older than 1 hour was a stable state dominated by heterogeneous reactions with HCl, the persistence of HBr in these more intense runs within the plume means that the cycling is dominated instead by HBr. Table 7.3 considers the modelled plume aged 3–4 hours at 2012-07-31 15:00:00 from each of the runs (i.e. that represented the forth column in Figures 7.21–7.23). Table 7.3 shows that in runs **II** and **III**, most heterogeneous cycling of bromine proceeds via Reaction R60 (HBr + HOBr, as opposed to the Reaction R59 (HCl + HOBr)).

This also manifests in the species in which the reactive (non-HBr) bromine accumulates at night. In run **I**, where heterogeneous cycling is HCl dominated, the reactive bromine predominantly partitions to BrCl upon sunset. In these more intense plumes (**II**, **III**), Br_2 dominates.

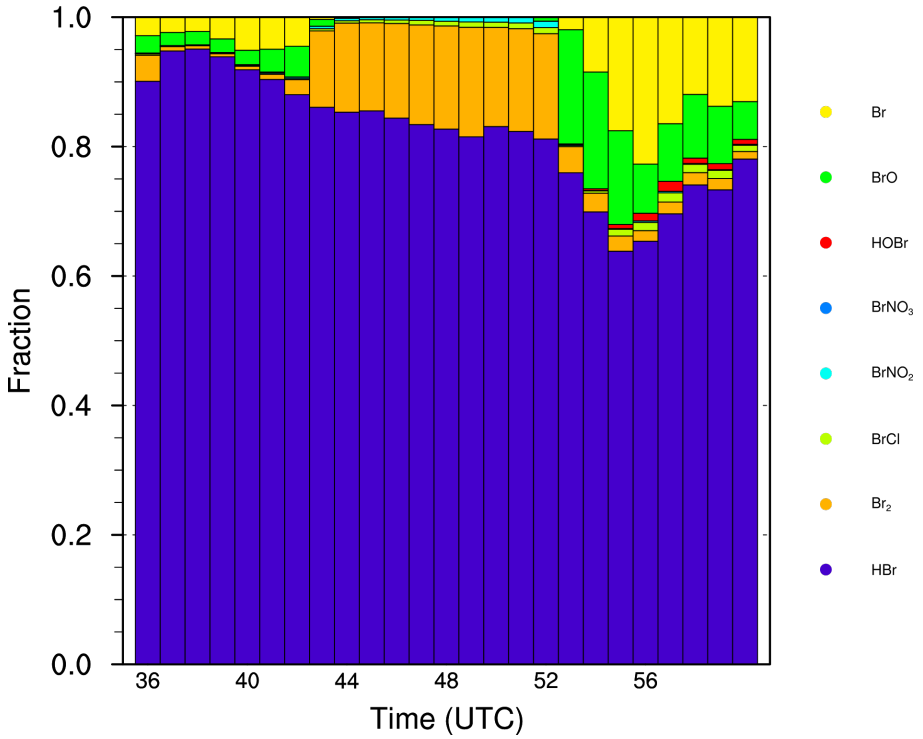

Figure 7.23: Run **III**: Average in-plume modelled distribution of bromine between the different forms plotted versus time, for plume emitted between 2012-07-31 11:00:00 and 2012-07-31 12:00:00.

7.8.1.2 Limitation of cycling speed

As HOBr is rapidly consumed in all runs (evidenced by the fact it does not accumulate within the plume), the total rate of BrO $\longrightarrow$ HOBr conversion via HO_2 (Reaction R41) or CH_3O_2 (Reaction R51) is a measure of the rate of "main path" bromine cycling. Despite the concentration of Br_y varying by orders of magnitude between the runs, the average rate of cycling of this bromine varies little; the rate in run **II** is only double that of run **I**, and the rate calculated from the model output of run **III** is less than that from run **II**. Although the bromine explosion is generally considered to be auto-catalytic, this model output suggests that for intense plumes there are negative feedbacks.

In run **I** HBr was very short lived within the plume and, in the evolved plume, constituted a negligible proportion of the total plume bromine. In runs **II** and **III**, HBr is a considerable proportion of the plume's bromine, which in these cases can be considered a less reactive form. The cycling, as measured by the rate of the BrO $\longrightarrow$ HOBr conversion, is slower when there is less bromine in these reactive forms.

In Figure 7.22 it can be seen that it takes several hours for the HBr to be

consumed. Each HOBr + HBr reaction converts one HBr molecule to reactive forms. Were this a one-way process, comparing the values of the HOBr formation reaction and the in-plume concentrations of Br_y in Table 7.3 would imply that this conversion process would be complete in a few hours (order of 10^3 seconds in run **II**, order of 10^4 seconds in run **III**). However inspection of Figures 7.22–7.23 show that this is not the case, release of bromine from HBr is much slower, and in some instances the net conversion is *from* reactive forms *to* HBr — notably the proportion of the plume bromine as HBr in the early plume in case **III** is greater than the proportion of volcanic emissions as HBr.

The cause of this is the conversion of bromine from Br to HBr, predominately in Reaction R55. In the intense plume, the rates at which reactive bromine is converted to HBr is similar to the rate of HBr's release via HOBr. The net effect of this is a slow conversion of reactive bromine to HBr or even the reverse process. This reversal is most clearly evident in the case of run **III** after sunrise.

The rate of the Br $\longrightarrow$ HBr conversion is high in the intense plumes because a large proportion of the reactive bromine is present as Br radicals.

Compared to run **I**, in the more intense plumes the modelled concentration of both HO_2 and CH_3O_2 is less (see Sections 7.5 and 7.7). This slows the conversion of BrO to HOBr.

Additionally, the rates of these reactions are ameliorated by the perturbation of the Br $\longleftrightarrow$ BrO equilibrium in the intense plumes. In cases **II** and **III**, the in-plume ratio of Br to BrO is much greater than in case **I**. This phenomenon is a result of the depletion of O_3 within the plume, which decreases the rate of Reaction R52.

In these models of intense plumes the bromine cycling exhibits negative feedback that limits the cycling and the release of bromine from HBr. In particular, the bromine cycling is limited by the depletion of O_3.

7.8.1.3 Importance of BrO + BrO reaction for bromine depletion

Although the average rate of heterogeneous cycling within these three model plumes is roughly similar, as discussed in Section 7.4 the amount of ozone loss varies substantially. The magnitude of the ozone loss isn't linear with plume intensity, which is primarily due to it reaching totality in the centre of the plume (especially in the run **III** case), however there is a strong positive correlation. In the more intense runs, the ozone depletion can be considered to be decoupled

from the rate of bromine cycling.

Excluding bypass reactions (as discussed in Section 5.7.1), the number of O_3 molecules destroyed per cycle in HBr-dominated cycling depends on the rate of HBr reformation, with a theoretical maximum of 2 molecules destroyed per cycle if no HBr reformation occurs. In the snapshots of runs **II** and **III** cases listed in Table 7.3, the rate of HBr formation roughly equals the cycling rate, which would yield an O_3 destruction efficiency of approximately 1 per cycle, the same as HCl-dominated cycling.

The substantial O_3 depletion in the intense plumes is primarily due to the following cycle:

$$BrO + BrO \longrightarrow 2\,Br + O_2 \tag{R64}$$

$$2\,(\,Br + O_3 \longrightarrow BrO + O_2) \tag{R65}$$

Reaction R65 can also form Br_2, which photolyses to 2Br.

This cycle destroys one O_3 molecule per bromine atom that cycles through it. In Section 5.7.1 I discuss how, in the base case, this reaction is only significant in the early, concentrated plume. In these cases with greater emissions the concentration of the plume is greater, resulting in this reaction remaining significant for a greater duration.

Comparing the rates of bromine processing through the main cycling and Reaction R65 from Table 7.3 allows the O_3-destruction caused by the plume to be attributed to these two mechanisms. This can be considered a "multiplier effect", a value describing the average number of times a bromine atom passes through the above cycle, destroying a molecule of O_3, before being recycled via HOBr. From snapshots of the model outputs tabulated in Table 7.3 this value is calculated to be 0.5, 2.5, and 5.2 for runs **I**, **II**, and **III** respectively.

In intense plumes this phenomena causes O_3 concentrations to be low within the plume (and effectively zero in its core), despite the negative feedbacks that limit the heterogeneous cycling.

7.8.1.4 Reversion to fully-reactive cycling state

In run **III** the majority of the plume bromine remains as HBr for the entire period tracked in Figure 7.23. However in run **II** (Figure 7.22) after sunrise HBr

is absent from the plume and the bromine partitioning is similar to that seen in the >1 hour old plume of case **I** — after consumption of HBr reservoir the chemistry "reverts" to this state. Although qualitatively similar, there are a few small differences in how this bromine partitions.

- Because there is significantly less O_3 in the post-sunrise plume **II** than in the equivalent model output from case **I**, the Br/BrO ratio is greater. Although it remains a small fraction of total plume bromine, in relative terms the fraction of Br_y as Br is substantially greater.
- Because of the increased Br fraction in case **II** compared to case **I**, HBr formation is more significant. The fraction of HBr in the post-sunrise run **II** plume is negligible, this HBr is rapidly consumed by the heterogeneous Reaction R60. Whereas in the run **I** case, Reaction R59 (involving HCl) was dominant, in the run **II** case the importance of the two reactions are more similar, resulting in the formation of significant reservoirs of both BrCl and Br_2.
- As discussed in Section 7.6, the aerosol surface area concentration is greater within the more intense plume. This has the effect of reducing the steady-state fraction of Br_y as HOBr, the greater surface area meaning it is more rapidly consumed by heterogeneous reactions and the steady-state concentration is reduced. This fraction is approximately half that in the equivalent run **I** output. As the HOBr fraction is small in both cases, this change has little impact on the overall chemistry.

Overall, despite these small differences, this chemistry is similar to the long-term daytime chemistry identified in Chapter 5. The BrO/Br_y ratio is also similar, around 50%.

7.8.1.5 BrO/SO_2 ratios

The most common bromine-related measurements relating to volcanic plumes are spectroscopic measurements of BrO. One of the potential uses of modelling studies such as this investigation is to allow for such measurements to be used to make estimations of total plume bromine content.

As discussed in Section 5.6.2, in the base case for plume greater than 1 hour old, the modelled BrO/Br_y ratio is relatively invariant with plume age. As a first approximation, an assumption that 50% of plume bromine is present as

BrO would be reasonably accurate for all times of day for which a spectroscopic measurement is likely to be made. The variation in this ratio with actinic flux (time of day) is relatively minor, and could possibly be accounted for in calculations if predictions or measurements of actinic flux are known.

For the more intense modelled plumes, the large and sustained fractions of Br_y as HBr mean that such an assumption is no longer valid. The bulk BrO/Br_y ratio will depend upon both the size of the HBr reservoir remaining at the time of interest, and the partitioning of the non-HBr bromine. Estimating these in a real case would be a non-trivial exercise, and would likely require making many assumptions. In practice, it would be necessary to be confident that the plume was in a low-HBr state before transforming a BrO measurement into an estimation of total Br_y.

The compositions and mixing ratios discussed thus far in this Chapter have been weighted averages of the entire plume (weighted by the concentration of the inert tracer, see Section 4.2.4). As discussed in Section 7.8.2, in these cases there is a significant difference between the chemistry of the plume's core and its edges.

7.8.2 Edge and core effects

The model output presented above show that the modelled chemistry varies significantly with (large) variations in the intensity of the plume, I have investigated this by comparing modelled plumes emitted from sources of varying strength and looking at their "bulk" properties.

Because of the nature of plume dispersion, plumes do not have well-defined edges — a single plume will have a concentrated core and a lesser concentration of the volcanic gases at its edges.

Figure 7.24 is a figure from (Bobrowski et al., 2007) which show the results from an observational approach to tackling this question. Through analysis of spectroscopic observations of a volcanic plume, the BrO/SO_2 ratio is determined to be lesser within the core than in the edges. The authors attribute this to reduced O_3 levels within the core of the plume.

In this subsection I discuss how, with a strong emission source, a single plume can exhibit significantly different halogen chemistry in different parts of the plume. The model output from run **II** is used to illustrate this phenomenon, as it clearly shows different chemical regimes occurring simultaneously.

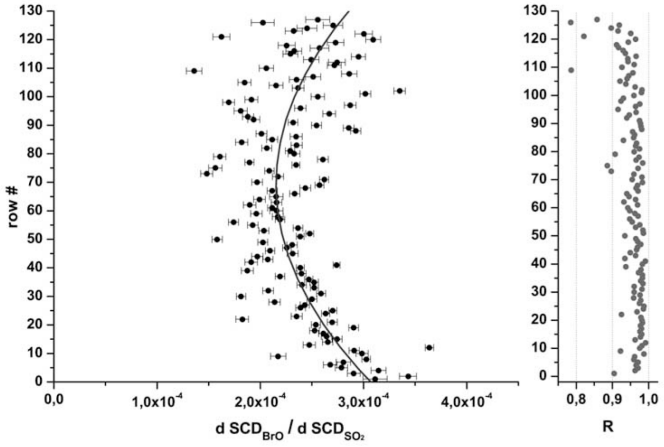

Figure 7.24: Figure 5 from Bobrowski et al. (2007) showing BrO/SO_2 ratios in the plume of Mount Etna. MAX-DOAS observations were analysed to yield a vertical profile of the ratio. The line-of-best-fit shows a slight decline in the ratio in the middle of the plume is reported. The right-hand chart shows the R values for the fit of BrO to SO_2 measurements for each data point.

Figures 7.25–7.29 plot model output relating to horizontal cross sections of the case **II** modelled plume, each showing differences between the core and edge regions.

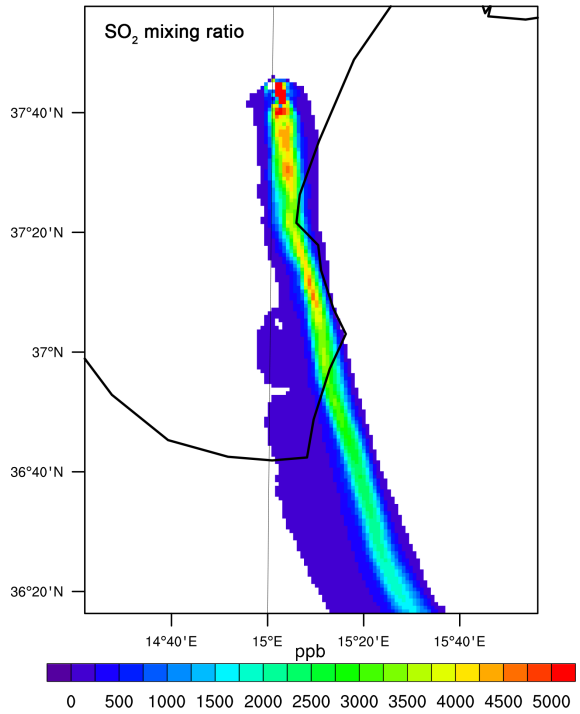

Figure 7.25: SO_2 mixing ratios in a horizontal cross section of the run **II** model output corresponding to 2012-08-01 12:00:00 and an altitude of 3000 mASL.

SO_2 Figure 7.25 shows SO_2 mixing ratios in the cross-section. SO_2 is a simple tracer of the plume; this Figure shows the plume's concentrated core, more dilute edges, and the smooth transition between them.

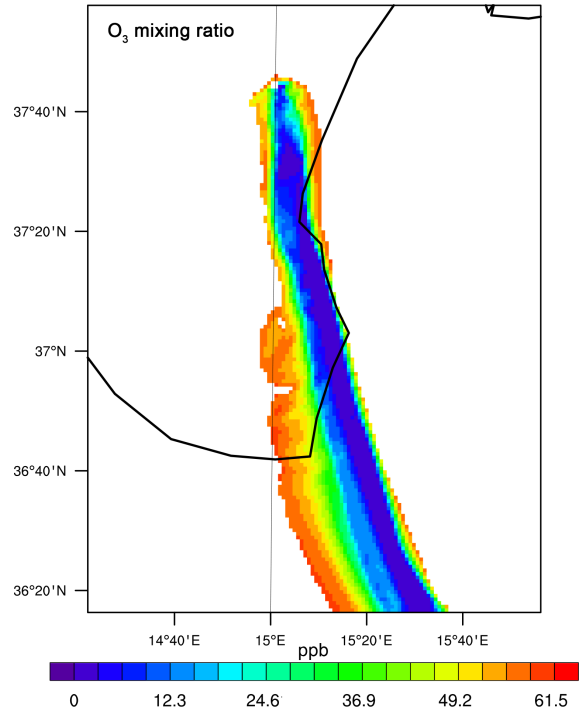

Figure 7.26: O_3 mixing ratios in a horizontal cross section of the run **II** model output corresponding to 2012-08-01 12:00:00 and an altitude of 3000 mASL.

O_3 As shown in Figure 7.26, O_3 depletion is greatest in the plume core. There is a core region, a few km across, where O_3 is almost totally depleted by bromine chemistry. Outside of this region the plume depletes O_3 to a lesser extent. The transition between the total depletion of O_3 that occurs in the plume core and the unperturbed air outside of the plume is gradual. This is caused by a variation in the strength of the O_3-destructive chemistry with plume intensity (as discussed in Section 7.4 above), and physical mixing of plume and background air.

HBr Figure 7.27 shows the fraction of Br_y that is present as HBr within the plume. HBr is a negligible fraction of plume bromine, except in a narrow core region of the plume. Comparing this to Figure 7.26, it can be seen that this core region is coincident with the region of near-total O_3 depletion. HBr is only persistent within regions of the plume where O_3 loss is sufficient to halt bromine cycling.

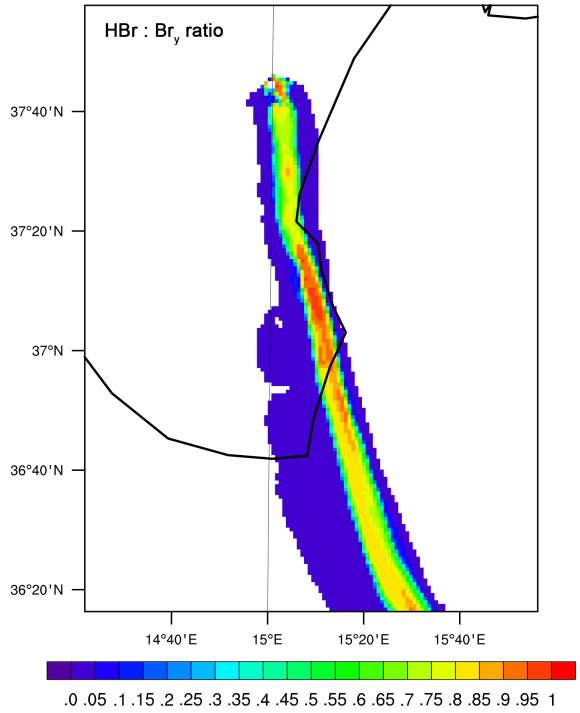

Figure 7.27: HBr/Br$_y$ ratios in a horizontal cross section of the run **II** model output corresponding to 2012-08-01 12:00:00 and an altitude of 3000 mASL.

Br$_2$ and BrCl Figures 7.28 and 7.29 show, respectively, the fractions of Br$_y$ present as Br$_2$ and BrCl within the plume. These species are created by the heterogeneous cycling reactions; Br$_2$ indicates that bromine is being cycled via the HOBr + HBr reaction, and BrCl indicates that bromine is being cycled via the HOBr + HCl reaction.

In the core of the plume, where O_3 is fully depleted, neither Br$_2$ or BrCl constitutes a significant fraction of Br$_y$. In this region, the lack of O_3 prevents bromine cycling.

Outside of this region bromine cycling occurs. BrCl is formed via heterogeneous chemistry; at the time of the model output depicted in Figure 7.29 the BrCl/Br$_y$ ratio in at the plume edges is similar to that which occurs throughout the run **I** model plume.

The Br$_2$/Br$_y$ ratio (Figure 7.28) is greatest in the parts of the plume just outside the core region. It is in this region that there is sufficient O_3 for cycling to occur, and sufficient HBr (either formed from Reaction R55 or mixed in from the core region) for Reaction R60 to generate significant amounts of Br$_2$. Further towards the edges of the plume, the Br$_2$ fraction is less, as a greater proportion of the heterogeneous cycling in these parts of the plume are HCl reactions.

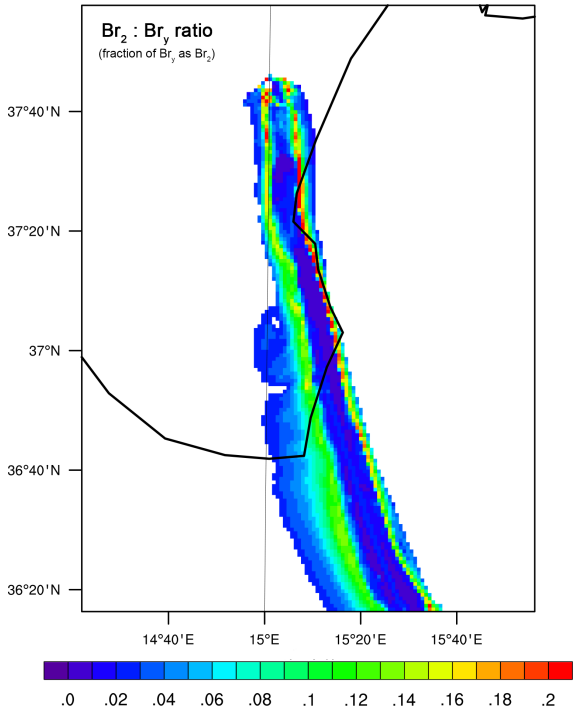

Figure 7.28: Br_2/Br_y ratios in a horizontal cross section of the run **II** model output corresponding to 2012-08-01 12:00:00 and an altitude of 3000 mASL. (Value is fraction of Br_y as Br_2, and accounts for there being two Br atoms per Br_2 molecule)

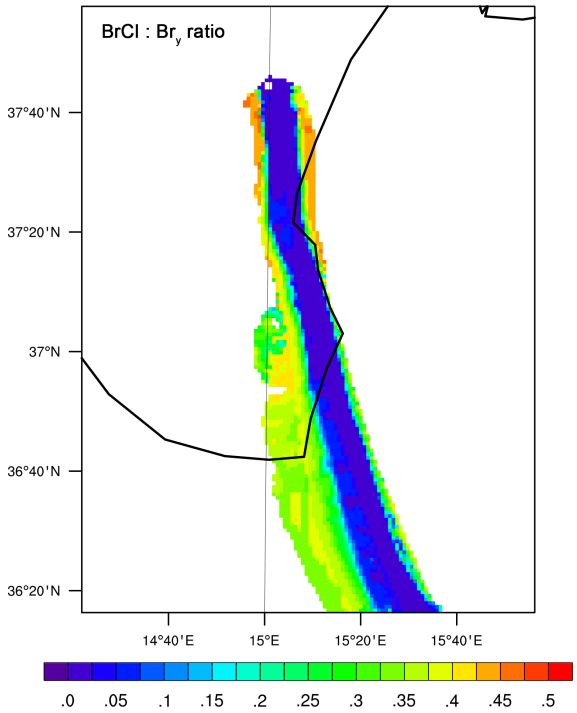

Figure 7.29: $BrCl/Br_y$ ratios in a horizontal cross section of the run **II** model output corresponding to 2012-08-01 12:00:00 and an altitude of 3000 mASL.

7.9 Conclusions of this section

In this Section I have shown how variations in the intensity of emissions cause changes within the plume's chemistry. Variations in intensity cause changes in the phenomena discussed in Chapter 5.

In terms of in-plume SO_2 and HCl concentrations (the species with the two greatest emission fluxes from the modelled volcano), this variation is simply linear with intensity of emission.

For phenomena where the volcanic plume chemistry depletes a species present in the background atmosphere (NO_x, O_3, OH) an increased intensity of emission is found to result in regions where complete depletion of these species occurs. The model output shows that in more intense plumes, the $BrO + BrO$ reaction becomes more important in terms of O_3 loss.

In these more intense modelled plumes, the depletion of OH limits the formation of secondary aerosol. However, the aerosol surface area density remains sufficient for efficient heterogeneous cycling of bromine; the aerosol in these cases is dominated by primary rather than secondary aerosol.

The halogen chemistry is more complex. Whereas in Section 5.6.3 I identified a single chemical regime that describes the bromine cycling in >1 hour-old plume in the base case, for these more intense plumes the model shows three different chemical regimes.

- **Core regime: bromine cycling limited** Where O_3 is near-completely depleted, the bromine cycling is very slow. In this regime, a significant fraction of Br_y exists as HBr.
- **Dilute regime: HCl cycling** This is "regime 3" as discussed in Section 5.6. It is dominated by the $HCl + HOBr \longrightarrow BrCl + H_2O$ heterogeneous reaction. This regime is characterised by a negligible HBr/Br_y ratio, and the predominant photolysable reservoir of bromine being BrCl.
- **Intermediate regime: HBr cycling** Between the core and dilute regimes is an intermediate case. In this case there is sufficient O_3 present for the bromine cycling to occur, but also the $HBr + HOBr \longrightarrow Br_2 + H_2O$ reaction is a significant part of the cycling. This occurs in regions where O_3 concentrations are greatly depleted (but not nil), which facilitates the formation of HBr from Br. This is a regime that is characterised by the

HBr/Br_y ratio being either nil or rapidly declining, and the Br_2 reservoir being comparable to or larger than that of BrCl.

In the base case discussed in Chapter 5, the entire daytime plume >1 hour old would be in the dilute regime. However for the more intense model plumes discussed in this Chapter, these three regimes can exist simultaneously, with the core regime occurring in the O_3-depleted core of the plume, the dilute regime occurring at the edges, and the intermediate regime between these regions. Inspection of the model output shows that while the transition between the dilute and intermediate regions is gradual, the transition between the intermediate and core regions is sharp, with a definite transition in the space of a few km.

Over time, with dispersal of the plume, the dilute regime becomes dominant.

The plume's reactive organic chemistry, which interacts with the halogen chemistry system, is also highly non-linear. As BrCl is only formed in the edges of the intense plumes, the generation of Cl radicals from its photolysis, and therefore the subsequent reactive organic chemistry does not occur throughout the plume. In general, the amount of reactive organic chemistry is in the intense plumes is much smaller than would be inferred by scaling up the impact of the base case.

Chapter 8

Perturbation studies

In Chapter 5 I present results from the WRF-Chem model; the "base case" set up as described in Chapter 2. I discuss the phenomena that occur within the model plume, and, through exploitation of the "modeller's advantage", I explain the causes of these phenomena.

In this Chapter I also aim to understand further the processes that cause the chemical phenomena in the modelled plume. This Chapter however takes a different approach; here model output from various runs are presented, and in each run the model setup is in one aspect perturbed from the base case. Through comparisons of the model output from the perturbed and base model runs, I highlight the impact that different facets of the plume chemistry have on the overall system.

8.1 Heterogeneous chemistry variations

As discussed in Chapters 2 and 4, the heterogeneous chemistry rates are the least well constrained rates in the model's chemical mechanism, and the model's skill in simulating the aerosol surface area available for heterogeneous reactions within the volcanic plume is likely quite low. In addition to this, the model runs considered here represent a single case which tries to approximate the Etnean plume in the summer of 2012–before generalising the results to other volcanoes it needs to be considered that the aerosol content is likely to vary considerably between plumes.

As a result, the representation of the heterogeneous reactions within the bromine chemistry system are subject to a large amount of uncertainty. In this

section I test the model's sensitivity to variations in the heterogeneous chemistry.

8.1.1 Model amendments

For these runs I ran the model with uniform variations in all of the heterogeneous reaction rates in the reaction mechanism. This is effectively equivalent to varying the γ factor (see in Section 2.2.2.4). In terms of the chemistry, such variation in the rate constants are effectively equivalent uniform variations in the aerosol surface area concentration.

I ran the model in two different amended modes:

- **75% het:** With heterogeneous rate constants at 75% of the base case
- **150% het:** With heterogeneous rate constants at 150% of the base case

Apart from these amendments these model runs were identical to the base case. The base case can be considered to be a **100% het** run for the purposes of this section.

These amendments impact both in- and out-of-plume chemistry. As well as runs with the plume, equivalent plume-free runs were performed for each amendment. Where differences between with- and without-plume runs are discussed below, these differences are between runs with the same amendment.

8.1.2 Model results

Figure 8.1 shows the distribution of bromine within the plume in the three cases for a portion of the plume as it ages.

The differences between these output are negligible, showing that the perturbation has almost no effect on the bromine speciation.

Another way of examining the modelled halogen-related activity within the plume is by inspection of the O_3 destruction. Figure 8.2 follows the same approach as used in Figure 5.31, plotting the evolution of the plume's ΔO_3 (the difference in O_3 concentrations between a model run with the plume and the equivalent model output in a the plume-free run) to inert tracer ratio as it ages.

Again, the difference between these output are negligible.

It is evident from these results that these moderate perturbations in the heterogeneous rate constants do not significantly change the halogen chemistry

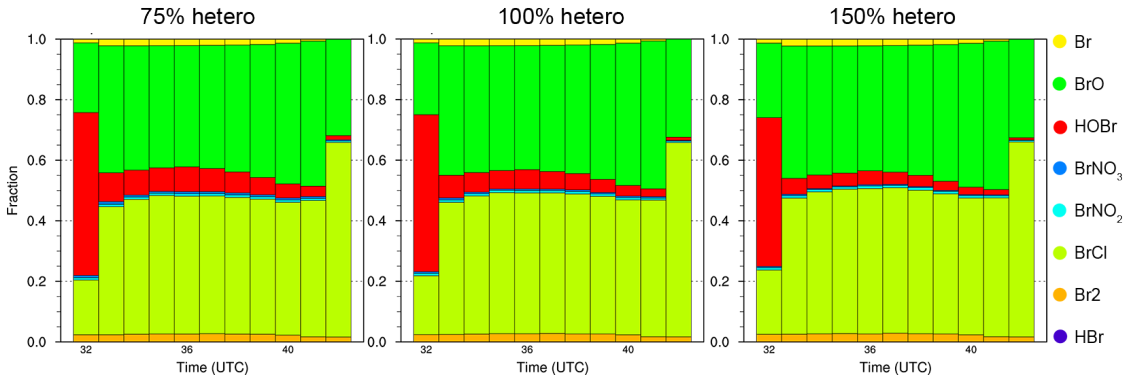

Figure 8.1: Modelled distribution of bromine between the different forms for plume emitted between 2012-07-31 07:00:00 and 2012-07-31 08:00:00. Model output shown for **75**, **100**, and **150% het** runs.

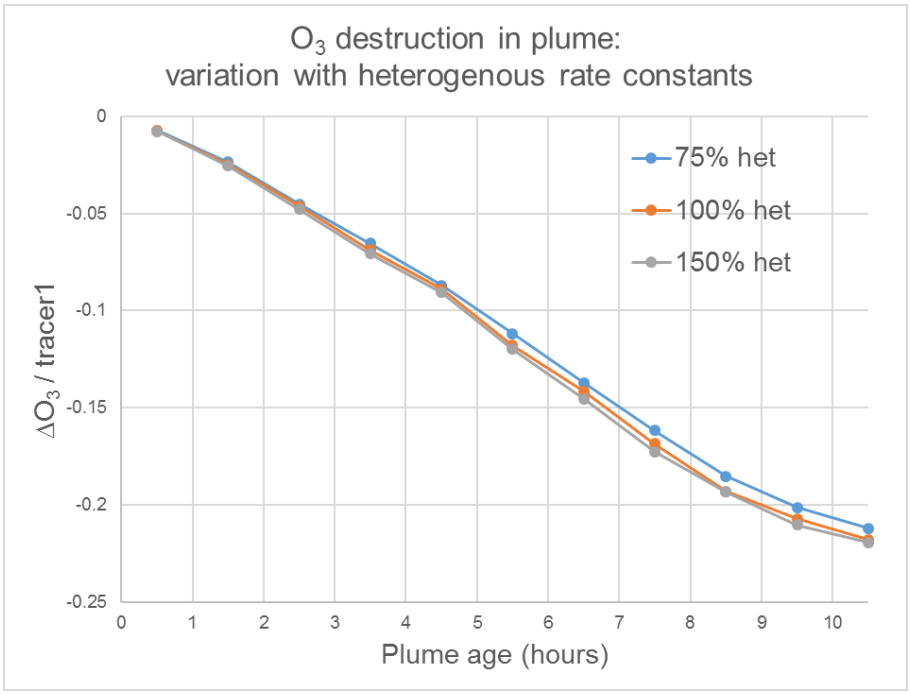

Figure 8.2: Modelled average absolute loss of O_3 in the plume (compared to the plume-free model run) as a ratio of the concentration of the inert tracer versus plume age for plume emitted between 2012-07-31 07:00:00 and 2012-07-31 08:00:00. Model output shown for **75**, **100**, and **150% het** runs.

of the plume. This shows that, in this modelled case, the heterogeneous step of the bromine cycling is not rate-limiting. This does not imply that the heterogeneous reactions are not necessary for rapid bromine cycling, rather that even when the rates are reduced to 75% of those in the base case the heterogeneous reactions occur sufficiently rapidly that the limitations of the overall cycling rate are imposed by other components of the cycling.

The representation of aerosol amounts, the associated surface area, and the rate constants of heterogeneous reactions within volcanic plumes, in the model are associated with a large amount of uncertainty, and are likely to be similarly uncertain in other numerical models. Additionally the amounts and nature of aerosol differs substantially between plumes. However, this result suggests that these factors may not be of significance to plume halogen chemistry. These results suggest that rates of heterogeneous reactions would need to be significantly slower than the estimates of this model in order to be rate-limiting. If the WRF model of this investigation's representation of heterogeneous rates is either approximately accurate or an underestimate, then such errors would not cause significant errors in the representation of bromine cycling.

8.2 Secondary aerosol variation

In Section 5.5 I discuss how, in the base case model output, although the model produces significant amounts of aerosol directly (primary aerosol), after a few hours of plume dispersal it is *secondary* aerosol (condensable species formed by gas-phase chemical reactions) that is the dominant form of aerosol within the plume, providing the majority of the surface area upon which the heterogeneous reactions of the bromine cycling occur. The principle reaction which forms secondary aerosol within the plume is Reaction R39 ($SO_2 + OH \longrightarrow H_2SO_4$), as the predominant fate of H_2SO_4 is the formation of sulphate aerosol.

In this exercise I investigate the importance of this reaction by running the model with Reaction R39 removed from the chemical mechanism, and compare this output with the base case. This also has the secondary effect of eliminating one of the in-plume depletion pathways of OH.

8.2.1 Model amendments

The model has been run with Reaction R39 removed from the chemical mechanism. All other model parameters remain identical to those for the base case run.

8.2.2 Model results

Figure 8.3 shows the difference in the distribution of bromine between the base case and this amended model run.

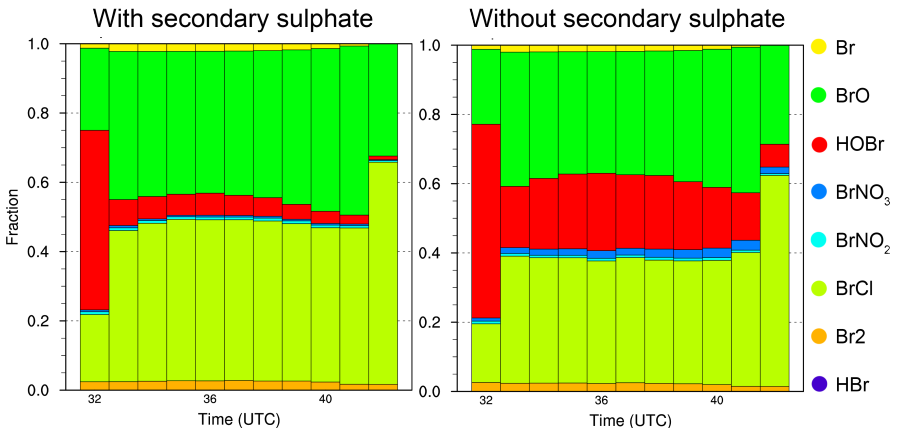

Figure 8.3: Modelled distribution of bromine between the different forms for plume emitted between 2012-07-31 07:00:00 and 2012-07-31 08:00:00. Model output shown for base model run and run without secondary sulphate aerosol formation.

The removal of the secondary sulphate formation pathway results in a greater accumulation of HOBr within the plume, with daytime HOBr fractions being of the order of 15-20% in the amended case, compared to approximately a third of that in the base case. Without secondary aerosol formation, the in-plume aerosol surface area density is reduced and the rates of the heterogeneous reactions of the bromine cycling will also fall. This change however does not prevent cycling from occurring — the other reactive bromine species are still present in slightly smaller quantities.

The subsequent reduction in the overall rate of bromine cycling is moderate. Figure 8.4 shows that the O_3 destruction is lesser in the model run without secondary aerosol — a result of bromine atoms spending more time per cycle as HOBr — however this difference is small.

Although secondary aerosol contributes the majority of the aerosol surface area in the base case, this result suggests that its production within the plume may not be necessary for bromine cycling. In this model run, the surface area provided by other aerosol was sufficient to facilitate bromine cycling at only a slightly reduced rate.

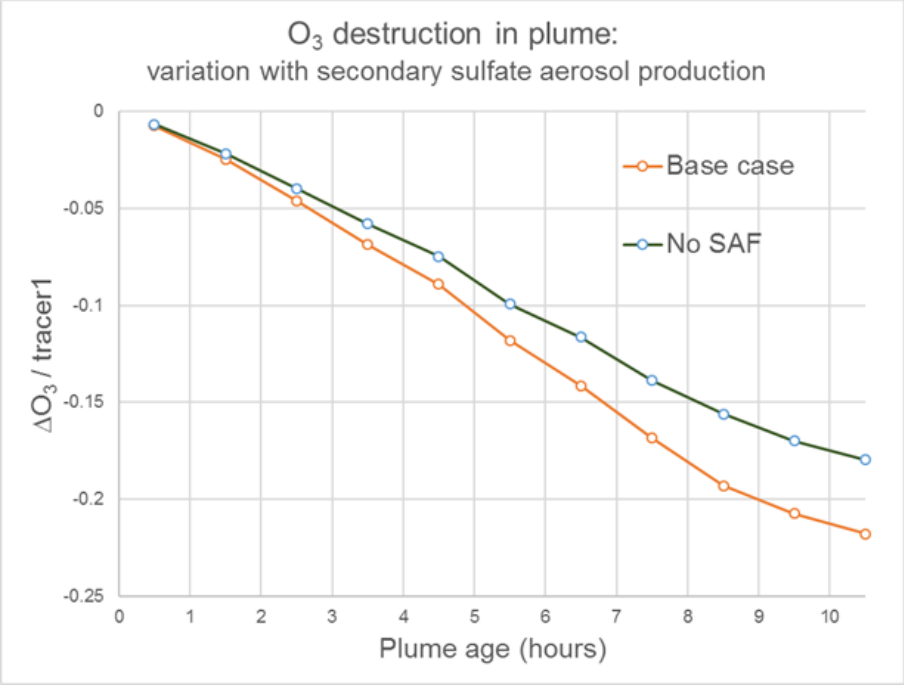

Figure 8.4: Modelled average absolute loss of O_3 in the plume (compared to the plume-free model run) as a ratio of the concentration of the inert tracer versus plume age for plume emitted between 2012-07-31 07:00:00 and 2012-07-31 08:00:00. Model output shown for base model run and run without secondary sulphate aerosol formation.

8.3 Conclusions of this Chapter

These results highlight that the plume chemistry is not sensitive to moderate changes in the availability of aerosol surface area. Heterogeneous reactions are necessary for the bromine cycling, however there is sufficient aerosol surface area even when secondary aerosol formation does not occur.

The model's representation of aerosol and the rates of heterogeneous reactions are associated with a large amount of uncertainty. The results of this section suggest that even if a correction altered the concentration of aerosol or the heterogeneous reaction rates by a substantial amount (up to the magnitude of the perturbations discussed in this Chapter), the model output regarding the gas-phase chemistry would not be significantly altered.

Chapter 9

Conclusions

In this chapter I summarise the findings of the previous Chapters, and discuss how the work of this investigation could be advanced.

9.1 Proof of concept

This investigation has shown that it is possible to incorporate a representation of plumes from passively degassing volcanoes into a 3D coupled meteorology and chemistry model.

Additionally, the field campaign (Chapter 3) has demonstrated how early-plume measurements can be used to assess in-plume chemistry.

9.1.1 Development of the model

This subsection gives a brief overview of the modifications made to the model in order to facilitate this investigation. These are discussed in much more detail in Chapter 2.

I have developed the capability in the *PREPCHEM* utility for the user to ascribe continuous emissions for a specific point in space, and also to choose the chemical composition of these emissions.

Additionally, a representation of halogen chemistry has been added to the CBMZ chemical mechanism — this is necessary for this investigation as the volcanic phenomena of primary interest involve halogen-containing gases. As with all chemical mechanisms in WRF-Chem, it has been necessary to use a

reduced halogen chemistry mechanism in order for modelling to be viable with the available computational resources.

The addition of these species to WRF-Chem has necessitated various changes to chemistry-related routines. These changes mean that the new modelling system treats these halogen species like other chemical tracers, being capable of representing their emission, deposition, transport, and reactions.

Previous studies have shown that heterogeneous reactions are important components of the "bromine explosion" mechanism which has been identified in volcanic plumes. It was therefore necessary to include such reactions in the mechanism. However, unlike gas-phase reactions and photolysis reactions, calculation of heterogeneous rates was not a capability of WRF-Chem in the unmodified version.

WRF-Chem does include a representation of aerosols of various types and several size bins. We added a routine to calculate the total surface area (per volume) of this aerosol. The rates of heterogeneous reactions were calculated to be proportional to the predicted collision rate of molecules of the reactants with aerosol particles. There are several potential problems with this approach (which are discussed below), however it does allow for calculation of these rates using the pre-existing framework of WRF-Chem's treatment of aerosol.

In combination, the point-source emissions utility and the addition of halogen chemistry to the model's chemical mechanism allow for this version of WRF-Chem to be used as a model of the chemistry of volcanic plumes. Specifically, for this investigation WRF-Chem was set up to model a passively-degassing episode of Mount Etna, during the summer of 2012.

9.1.2 Assessment of model skill

In Chapter 4, I compare the model output to various external data in order to determine its skill in relation to the task of this investigation. This model was not intended to replicate precisely the meteorological/atmospheric chemistry situation at a particular location and time, rather it needed to simulate a *representative* situation which allowed general conclusions about the plume chemistry to be made. In practice, this meant that I attempted to replicate the summer 2012 situation at Mount Etna as much as possible, but did not consider small differences from observational data, or the fact that for much of the model output there exists no observational data suitable for verification,

to be insurmountable problems. In this Section, I use the term "adequate" to describe the model passing this criterion.

Overall such data are sparse, with fewer observations of chemistry than for meteorology.

9.1.2.1 Meteorology

WRF-Chem appears to replicate approximately the meteorological situation of the time and location modelled, although it appears not be able to replicate some observations of extremely dry conditions. Clouds and precipitation events are almost entirely absent from the modelled area in this time period, and therefore this assessment did not evaluate the model's skill in regard to this. I conclude in Section 4.3.5 that, with regard to meteorology, the model appears to have sufficient skill for the purposes of this investigation.

9.1.2.2 Background chemistry

With less observational data available, the equivalent validation for the model's non-volcanic chemistry and aerosol is inherently more uncertain. Observations are only available for a small number of species. I have assessed the skill the model has with regard to these observable species. It is necessary to assume that, without observations to the contrary, the model is adequate in skill with regard to unobserved species relevant to this investigation. Observations from the field campaign and aircraft campaign (outside of the plume) cover, spatially and temporally, a small range, though these are in the primary area of interest to this investigation. The model output is compared with a reanalysis product, which is itself partially formed by modelling.

In Section 4.4 I conclude that the modelled gas-phase chemistry appears to be free from major anomalies, which suggests that the model is simulating a chemistry background that is adequate for this investigation. However on examination of the modelled aerosol, I found a "cloud" of very high aerosol content over Sicily in the first day of model output. There is insufficient data to determine whether this represents an error in modelling, or a natural phenomenon that is being well-represented. However in either case it is an anomaly, and, as the intention is to model an environment representative of typical conditions, I have chosen not to assess output which may be perturbed by this anomaly. The first 24 hours of model output therefore are considered

"spin-up time". The representation of aerosol is one of the least certain aspects of the model.

9.1.2.3 Volcanic phenomena

Section 4.5 assesses the skill of the model in representing the chemistry and dispersion of the volcanic plume.

The model shows a dispersion of the plume which approximately matches that observed via aircraft observations.

With regards to chemistry, the modelled volcanic plume demonstrates the two main phenomena that have been observed in volcanic plumes: elevated concentrations of BrO, and depletion of O_3.

- The magnitude of the modelled column ratios of BrO to SO_2 (the latter being used as an assumed inert tracer of the plume intensity) are within the range of "typical" observations from volcanoes (and Mount Etna specifically). The modelled variation of this ratio with distance from the source, and variations between the plume core and edges, shows a similar trend to that deduced from observational studies.
- The magnitude of O_3 depletion, both in absolute terms and in terms of the ratio of the O_3 loss to SO_2 mixing ratios, can be determined from both the model output and aircraft observations. These datasets show a high degree of agreement, both quantitatively and qualitatively.

Although many aspects of the plume chemistry (such as bromine species other than BrO) are not directly observable, the apparent high skill the model shows with regards to the observable phenomena suggests that WRF-Chem is successfully modelling the main chemical processes within the plume, and lends confidence to conclusions drawn from the model output regarding unobservable phenomena.

9.1.2.4 Overall

With a few caveats, the model appears to show adequate skill with regards to simulating the environs of the Mount Etna plume, and shows good agreement with observations regarding phenomena within the plume. These results

suggest that, after applying a spin-up time, the developed system is capable of producing output useful for the task of this investigation.

9.1.3 Demonstration of early-plume analysis method

The field campaign described in Chapter 3 is not wholly novel, the measurement approach used was developed from a previous campaign discussed in Vance et al. (2010). What is new however is the analysis which is done on this data, which allows for a more quantitative assessment of the ozone-destructive chemistry (yielding an estimate of the rate of destruction) than any other similar study.

This quantification was performed with relatively inexpensive equipment, and gives insight into plume halogen chemistry without observing it directly. The approach could be used for other ground-based volcano-monitoring field campaigns.

9.2 Field campaign and MISTRA modelling results

The results of Chapter 3 show that the plume of Mount Etna causes significant O_3 destruction within a few minutes of emission. The results suggest that, at the time of measurement, the plume of Mount Etna destroyed O_3 at a rate of approximately 10^{-4} molecules of O_3 per molecules of the inert tracer SO_2 per second. This occurred despite the air being very dry on one day of the measurement period, suggesting that the heterogeneous processes required for the O_3-destructive halogen chemistry are still able to occur at very low relative humidities.

Elevated levels of BrO were observed in this plume (in a more aged portion than the main measurements). This phenomenon, which has been observed in many other plumes, indicates that reactive bromine chemistry is occurring within this plume.

The 1D MISTRA model was used to model the first hour of the plume with a variety of settings regarding NO_x and heterogeneous chemistry. Some volcanic volatile measurements were used to determine the initial conditions for this modelling.

When no volcanic NO_x emissions are modelled there is reasonable agreement

between the MISTRA model output and the observations – both show O_3 loss in the early plume. Inspection of the model output shows that, when heterogeneous chemistry is active, the bromine explosion occurs, converting HBr to more reactive forms of bromine and destroying ozone. The model output shows that reactive bromine generated in the initial high-temperature "effective source region" is sufficient to produce O_3 depletion in the early plume without heterogeneous chemistry, however without continual heterogeneous chemistry the O_3 and BrO signal dissipate.

When the model was run with volcanic NO_x emissions, this had the effect of delaying the active bromine chemistry, as bromine was "tied up" in relatively unreactive nitrogen-containing forms. These results did not match the early plume O_3 observations, suggesting that the plume emissions may contain little or no NO_x

9.3 Main modelling results

In Chapter 5 I report results from the model when it is run in the "base case", the model set up designed to represent "typical" passive degassing behaviour of Mount Etna. These results include extensions of the "observable phenomena" (discussed in Section 9.1.2.3) beyond the temporal and spatial range of observations, as well as model output that relates to species that are difficult or impossible to directly observe. I exploit the "modeller's advantage" (see section 1.4.1) and use various techniques to evaluate the model output, including the use of "artificial" tracers.

The phenomena identified cover a range of chemical systems. The model output shows connections between these systems. Several of these effects can be broadly categorised as destruction of oxidants within the plume.

Several of these phenomena have been identified in previous modelling studies. However, where possible, I have tried to advance upon these by presenting my results in a high level of detail and being quantitative (where appropriate).

9.3.1 Sulphur chemistry

The model output shows that the depletion of oxidants (specifically, in this case, OH) in the plume greatly increases the lifetime of SO_2 with respect to gas-phase chemical loss. Because OH is nearly completely eliminated within the core of the plume, the instantaneous chemical lifetime of SO_2 during the day is extended from 10s of hours to what is essentially an indefinite length of time.

In observation studies SO_2 is often considered to be an effectively inert tracer of volcanic plumes. This strengthens the case for using SO_2 measurements in such a fashion.

It is likely that as the plume dissipates this effect also dissipates and the SO_2 lifetime with respect to OH oxidation reverts to normal. As also discussed in later sections, the outputs of this investigation are not sufficient to determine at what point "plume chemistry" ceases. Therefore this investigation is only sufficient to estimate a lower bound on the magnitude of this effect: for the base case run modelled, in terms of SO_2 amounts, the chemical loss of SO_2 via OH oxidation is negligible for *at least* the first day of plume transport.

This investigation also has not addressed other forms of SO_2 loss, specifically cloud chemistry (a $SO_2 + H_2O_2$ reaction in clouds is known to be a significant SO_2 sink (Husain et al., 2000)) and wet deposition. Neither of these processes are relevant to the Summer 2012 Mount Etna case modelled, however it does mean that this result is not necessarily applicable to plumes which intersect clouds or precipitation, or cases where volcanic H_2O emissions generate a sustained cloud.

9.3.2 HO_x chemistry

As discussed above, OH levels are greatly reduced within the plume. In Section 5.2 I show that, additionally, HO_2 levels are reduced by plume chemistry, although, in relative terms, this depletion is not as substantial as that for OH.

By evaluating various reaction rates, I identify the causes of this depletion. HO_x is destroyed within the plume due to reactions with reactive halogens. The remaining HO_x is more strongly partitioned to HO_2 due to Reaction R39. Comparison of the loss/production rates of OH and HO_2 with the rates of interconversion suggests that in the plume, these two species can be considered decoupled.

This loss of oxidative capacity is far stronger than the relative loss of O_3. This shows that in-plume O_3 concentrations, while interesting, cannot be considered a useful measure of the oxidative capacity within such plumes.

9.3.3 Reactive nitrogen

The model results discussed in Chapter 5 are from runs that do not include emissions of NO_x from the volcano — the effects discussed in Section 5.3 refer to perturbations of NO_x in the modelled background. The background free troposphere into which the plume is emitted is modelled to be quite clean, the effects discussed here relate to a modelled redistribution of only a few ppt of NO_x.

Concentrations of NO_x are substantially reduced within the modelled plume, this is modelled to be converted to HNO_3. The main pathway in the normal atmosphere for NO_2 to HNO_3 conversion is reaction with OH, this pathway is almost completely cut off in the plume due to the depletion of OH. Instead in the plume the main such pathway is through reaction with BrO (forming $BrNO_3$ as an intermediate). In this regard, the increased BrO within the plume more than compensates for the OH depletion.

The HNO_3 mixing ratios within the plume are boosted, both by the above process, and by the revolatisation of nitrate from aerosol. The plume contains high concentrations of acid (HCl directly emitted by the volcano and H_2SO_4 produced from SO_2 oxidation). These acids displace HNO_3 from aerosol particles, transferring it into the gas phase.

Elevated concentrations of HNO_3 have been measured in the plumes of various volcanoes. These are often considered evidence of NO_x emissions from vents (formed when N_2 and O_2 in background air are exposed to high temperatures. A set of direct NO measurements also exist, but this is a smaller dataset all measured by the same potentially unreliable method). However the kinetics of such a process cannot be easily resolved with current theory. The results here do not present a simple answer to this conflict.

These results demonstrate how the reactive bromine of volcanic plumes might facilitate the rapid conversion of volcanogenic NO_x to nitrate.

Both HNO_3 revolatisation from aerosol and NO_x-to-nitrate conversion via bromine chemistry are ways in which volcanic plumes could perturb reactive nitrogen chemistry without there being direct NO_x or nitrate emissions from

the volcano. Interpretations of measurements of reactive nitrogen in volcanic plumes would need to account for both these effects.

9.3.4 Chlorine–organic chemistry

The modelled volcano is a strong source of HCl. This is, comparatively, a very stable form of chlorine. However WRF-Chem models significant generation of Cl radicals via the photolysis of BrCl, a species generated by the bromine cycling when HCl is involved in the heterogeneous step (Reaction R59).

This generation does not effectively destroy HCl, as HCl is rapidly reformed after generation of the Cl radical.

The predominant fate of these Cl radicals in the model is reaction with alkanes, principally CH_4. This triggers alkane degradation pathways, which ultimately terminate in CO_2. These pathways are the same as those triggered by OH-oxidation in the normal atmosphere, however this oxidation is much more rapid (and more than compensates for the OH depletion) as is evidenced by the elevated levels of oxygenated organic species, intermediates in the degradation process, within the model plume.

The in-plume degradation mechanism of CH_4 is similar to that of the normal OH-triggered mechanism, but with some perturbations. In the plume, OH degradation reactions are much slower due to the depletion discussed above, whilst reactions which involve bromine (which are of negligible importance outside of the plume) become significant pathways.

HCHO is a spectroscopically detectable substance, with signatures in the ultraviolet. Bobrowski (2005) reports HCHO measurements within volcanic plumes. The mechanism identified within this investigation may help explain these observations.

To my knowledge, no published study has previously identified this phenomenon as a possible HCHO source in volcanic plumes (the possibility of Cl-induced CH_4 degradation is briefly mentioned in Gliß et al. (2015)).

9.3.5 Aerosol within the plume

Before beginning this summary, it is necessary to mention that, as discussed in Section 9.1.2, model output relating to aerosol comes with a high degree of

uncertainty. The primary aerosol emission of the volcano in the model, both in terms of total mass and size distribution, is based upon in-situ measurements from the field campaign (Appendix B). These varied significantly over the period of measurement, and the extrapolation from these data in order to cover all of the size bins of the model introduces more uncertainly into the estimate.

I differentiate between three different types of aerosol in the model plume:

- Primary aerosol, the direct particulate emissions from the volcano
- Secondary aerosol, aerosol generated within the plume from the gas phase, predominately sulphate generated from the oxidation of SO_2. This oxidation only occurs during daylight.
- "Pseudo-primary" aerosol (see Section 6.4), secondary aerosol that forms immediately after emission from the vent. This aerosol is formed by the oxidation of SO_2 by volcanogenic OH.

I find that aerosol levels are high in all of the modelled plume. Initially, this is predominantly due to primary aerosol. As the plume disperses this primary aerosol concentration decreases, however the aerosol concentrations remain high due to the formation of secondary aerosol within the plume. Once the plume is a few hours old, secondary aerosol is the dominant form of aerosol.

For eruptions that occur during the night the secondary aerosol formation does not occur until sunrise. In these cases the additional "pseudo-primary" aerosol formed at source becomes significant in determining the aerosol levels within the night-time plume.

Because of secondary aerosol formation, the modelled aerosol surface area within the plume is enough that the bromine cycling is not limited by the availability of aerosol.

9.3.6 Bromine chemistry

The model results show that active bromine cycling occurs within plume. The model reproduces the frequently observed phenomena of elevated BrO in vertical columns intersecting the plume, as well as in-plume O_3 destruction. The quiescent degassing plume modelled causes moderate O_3 destruction within the plume, but does not eliminate it.

I inspect the modelled bromine chemistry in the first hour of the plume in detail.

The model results show HBr being very short-lived within the plume and being eliminated within the first few minutes. The initial bromine chemistry creates a reservoir of Br_2. Over a time scale of order 10s of minutes, this reservoir is replaced by BrCl. Once this BrCl reservoir has formed, the bromine chemistry — thought still active — settles into a steady state for the duration of daylight. In this state, all of the plume bromine can be considered to be part of the cycling.

I found that the high levels of aerosol surface area within the plume (as discussed in Section 9.3.5), mean that the modelled bromine cycling is not limited by the rate of the heterogeneous reaction. I also find volcanic HCl to be necessary for the continued bromine cycling — with HBr exhausted in the plume the predominant heterogeneous reaction is via HCl (Reaction R59).

In regard to the conversion of BrO to HOBr the in-plume formation of CH_3O_2 (see Section 9.3.4) compensates for the loss of HO_2.

In this state, with abundant aerosol surface area, abundant HCl, and only moderate O_3 destruction, the rate of the cycling of the bromine explosion is limited by the actinic flux.

Because both the production and loss of BrO are dependant upon photolysis rates, the proportion of the plume bromine that exists as BrO in the steady state is largely invariant with the time of day at which the plume is observed. In these model results, this proportion is roughly 50%. The consistency of this result in the evolved plume, and its invariance with time of day and plume dispersal, lend weight to the idea of using spectroscopic observations of BrO to measure and quantify bromine emissions from volcanoes.

The bromine cycling ceases at night-time, but resumes upon sunrise. My modelling, which is limited to approximately one day of plume evolution, has not found a point at which chemical or physical phenomenon stop bromine cycling occurring during the daytime.

9.3.7 Ozone chemistry

The bromine cycling destroys O_3. The plume of the modelled passively degassing volcano has O_3 depletions of order 10s of % in the early plume, and a few % after this. Because the bromine cycling is driven by sunlight, O_3 losses

are more rapid around local noon.

In aggregate over the diurnal cycle, the O_3 destruction caused by the volcano in the model is approximately 5×10^{-3} molecules O_3 per atoms of bromine per second.

9.4 Volcanic emissions at night

Because the plume chemistry is highly dependant on sunlight, in Chapter 6 I investigated plumes that are emitted during darkness.

In general, most of the phenomena discussed previously also occur in such plumes — when emission occurs during the night these phenomena are delayed until sunrise. Night-time emission does not prevent these phenomena from occurring or significantly alter their nature.

9.5 Variations in volcanic intensity

In Chapter 7 I evaluate model output from runs where the intensity of the volcanic output is 10 and 100 times greater than in the base run. The intention of this was to identify chemical phenomena that might occur in more intense plumes. These runs are not however intended to represent accurately more intense eruptions of Mount Etna, which would likely be significantly different in physical structure and chemical composition.

As well as bulk effects, in this chapter I evaluated modelled differences between the core and edges of plumes.

I found that in the core of intense plumes, depletions caused by plume chemistry become total eliminations. In particular bromine chemistry eliminates almost all of the O_3 and the chemistry becomes O_3 limited. In the absence of O_3, the bromine cycling does not occur and HBr is the dominant form of bromine. This is a distinct chemical regime from that identified in the "base case" plume. In the $10\times$ intensity case this O_3 limitation does end after sufficient plume dispersion, "reverting" to the chemistry of the base case.

At the edges of the modelled intense plume are regions where the plume intensity is similar to that in the core of the "base case" plumes and the plume chemistry in these regions is similar.

Between these two regimes, I identify a thin intermediate region. Here bromine cycling is able to occur, and there is significant HBr present. This results in $HOBr + HBr \longrightarrow Br_2 + H_2O$ being the dominant heterogeneous reaction in this region.

The distinction between O_3-limited and non-O_3 limited chemical regimes may be an explanation for the plumes identified by Hörmann et al. (2013) where SO_2 and BrO columns did not correlate.

9.6 Perturbation studies

In Chapter 8 I consider model output from runs with alterations to the model's representation of aerosol and heterogeneous chemistry. I ran the model with the rates of the heterogeneous reactions increased and with them decreased. I also ran the model with secondary aerosol formation turned off. I find that the model's bromine chemistry is insensitive to these alterations, confirming an inference made in Chapter 5 that the heterogeneous recycling of bromine, though necessary for the bromine cycling to occur, does not appear to be the rate-limiting step of the cycling.

9.7 Summary discussion

9.7.1 Synthesis of field campaign, *MISTRA* modelling and WRF-Chem approaches

This document has presented three different approaches for studying the plume; the field measurements and *MISTRA* modelling discussed in Chapter 3, and the WRF-Chem modelling deployed in the other Chapters. These approaches are complimentary for our understanding of the chemistry of the plume.

In Chapter 4 various observational results have been compared to model output as part of the assessment of the model skill. Observational results of aerosol amounts have been used to determine the modelled aerosol emissions (see Appendix B). That the *MISTRA* modelling with volcanic NO_x emissions poorly reproduced the ground-based observations was one of the reasons it was decided not to include volcanic NO_x emissions in WRF-Chem. Observations were also used to determine the dilution factors used in *MITRA*.

The three approaches generally cover different time scales — the ground-based field campaign measurements cover the first few minutes of plume evolution, the MISTRA modelling extends this out to approximately an hour, whilst the WRF-Chem modelling covers 10s of hours.

All three approaches show O_3 being continually depleted by the plume chemistry during daylight, and the quantifications of the rates of these processes from the different methods yield similar results. *MISTRA* and WRF-Chem output can be inspected to analyse "directly" the chemical processes occurring (as the concentrations of all modelled species in the modelled space and time can be reported by the models and the rates of reactions calculated). From these it can be seen that O_3 depletion and the formation of BrO within the plume are due to the bromine explosion.

It should be noted that there are significant differences between *MISTRA* and WRF-Chem output, likely due to O_3 limitation in *MISTA*. The WRF-Chem results actually show closer agreement with published results from a different 1D model, *Plumechem* (Roberts et al., 2014a). This is discussed in Section 5.8.

9.7.2 Plume timeline overview

An instructive summary of the results of this document is to outline the major phenomena which I have observed or modelled occurring within in the plume in chronological order.

- Immediately upon emission, some high-energy species created by the high temperatures of the effective source region react rapidly. Any OH emitted by the volcano reacts rapidly with SO_2, producing "pseudo-primary" sulphate aerosol.
  While most bromine is emitted as HBr, a minority is emitted as Br. This reactive Br quickly re-equilibrates to other reactive bromine forms. The bromine explosion is therefore active from the very earliest plume, though it is retarded by its own destruction of O_3.

- Over the first few minutes, background air containing O_3 is entrained into the plume. The bromine explosion accelerates, destroying O_3 and converting the remaining HBr into reactive bromine forms.
  Sulphur and bromine chemistry eliminate HO_x (especially OH) in this entrained air. This occurs throughout the plume, though the effect

weakens with dilution. OH is consumed in reaction with SO_2, which creates secondary sulphate aerosol.

- After a few minutes have elapsed, all of the HBr in the plume is consumed–all of the bromine is in "reactive" forms. However the bromine cycling (and associated O_3 destruction) continues, as HCl begins to replace HBr in the heterogeneous cycling step.
  BrCl becomes the dominant photolysible reservoir (replacing Br_2). A secondary consequence of this is that Cl radicals are produced through photolysis. These radicals oxidise alkanes (principally CH_4) from the entrained air, causing elevated levels of oxidised organics.

- After approximately half an hour, the plume reaches a stable state. The cycling continues, maintained by abundant volcanogenic HCl and aerosol — the levels of the latter are sustained due to continual sulphate production in the plume. O_3 is destroyed in the plume, but the O_3 depletion effect is small, only a few %, not fast enough for the cycling to be O_3 limited. O_3 levels are maintained by entrainment of background air. Overall, the rate of the bromine cycling is limited by the actinic flux.
  In this stable state, BrO constitutes approximately half of plume bromine. The plume slightly perturbs the low levels of NO_y in the clean free tropospheric air. NO_x is suppressed as it is converted to HNO_3 by bromine chemistry. HNO_3 is boosted both by this process and because sulphate pushes out nitrate from background aerosol.

- Over the next few hours this stability is maintained, with only a gradual change introduced by the change in actinic flux over the course of the day. Eventually plume dispersal outpaces secondary aerosol formation, however my modelling has not observed any time in the first couple of days of plume evolution where the heterogeneous reaction step is rate-limiting for the bromine cycling.

- On sunset the bromine cycling stops, and little significant plume chemistry occurs. These processes resume on sunrise.

- The scope of this investigation was limited to the first couple of hours of plume evolution. Any further stages (including the point where plume chemistry ceases to be significant) have not been identified.

9.7.3 Applicability to other volcanoes and scaling up

This investigation has concerned Mount Etna with passive degassing activity. However the investigation is intended to further understanding of similar plumes in a general sense, rather than just specifically this one from Etna.

Volcanoes and their plumes will differ, however observations seem to suggest that BrO is nearly always present in plumes. This investigation has shown that the ozone-destructive bromine cycling occurs during daytime when bromine, aerosol, and hydrochloric acid are all present — and Etna is not exceptional in any of these regards. Thus I would not expect a qualitative difference in phenomena to occur for a different passively degassing volcano.

As discussed in Chapter 7, the crude intensification of the modelled plume performed in that investigation cannot be assumed to be a reliable model of a higher-magnitude volcanic eruption. However it does provide some insight into how a more intense eruption may be qualitatively different from the case discussed in Chapter 5; most notably having large volumes where the chemistry is O_3 limited.

Additionally, as seen in Chapter 7, intense plumes will disperse over time. In Chapter 7 the chemistry of these modelled plumes after dispersion came to resemble that of the "base case" plume. If this happens in real cases (which seems likely), then the results of this investigation could be relevant to more dispersed plumes from intense eruptions.

It should be noted that for large eruptions which put material into the stratosphere the results of this investigation would not be relevant, as stratospheric chemistry is substantially different to tropospheric chemistry.

This investigation has considered a plume which enters a clean, free-tropospheric environment and NO_x chemistry was largely irrelevant for the overall chemistry of this plume. Were a plume to enter a more polluted environment (containing more NO_x), the chemistry may be different. In the *MISTRA* study in Section 3.4 it was seen that, where NO_x is present in the plume, the formation of nitrogen-containing bromine species retards the cycling. This is an unknown factor, however most terrestrial volcanoes are remote and this is unlikely to be significant for many.

Though spatially widespread, the absolute O_3 depletion in the evolved plume of the base case is small, only a few ppb. This is within the general level of variation expected in free tropospheric O_3.

As this investigation has not determined at what age of plume the phenomena identified cease (or cease to be distinct from the background) it is not possible to put an upper limit on this impact of an eruption. It may be the case that these effects sometimes continue until bromine is removed from the atmosphere by physical processes, in which case this duration could vary substantially between eruptions. Because of this, it is not useful to try and scale up the results of this investigation to quantify the overall impact of all volcanoes or estimate the net effect of one volcano over time.

9.8 Further work

In this section I outline a few possible ways in which the work of this investigation could be advanced.

Although the results of this investigation are intended to apply to passive degassing volcanic plumes in general, I have exclusively focussed on Mount Etna. The model should, with only minor amendments, be able to simulate eruptions from other volcanoes and investigate whether to what extend variations in background chemistry and emission height have upon the phenomena identified.

In general, there are a large number of parameters in the model setup which could be altered. For example the modelling study Roberts et al. (2014b) used the *PlumeChem* model to explore part of this *parameter space* — specifically they investigate sensitivity to aerosol loading, air:magmatic gas ratios in the high temperature effective source region, bromine content of the emissions, and dispersion parameters. Some of the most obvious extensions to the work of this investigation involve exploring this parameter space. However WRF-Chem is less suited to such a task than 1D models with lower computational requirements. A sensible strategy for a future study would be to use a 1D model initially to explore the parameter space, and then to use WRF-Chem to produce detailed output for a few settings of interest.

The modelling in Section 3.4 showed differing results from MISTRA for volcanic emissions that did and did not contain NO_x. It would be informative to see whether similar phenomena occurred in WRF-Chem.

All of the modelling in this investigation has been on plumes that intersect neither precipitation nor clouds. WRF-Chem, with its in-built meteorological

calculations, would be well suited to modelling the impact of such intersections on the plume chemistry. Wet deposition of soluble species and aerosol would be phenomena seen in such runs. Before doing such an investigation, it would probably be necessary to add the reaction of SO_2 and H_2O_2 that is known to occur in clouds (Husain et al., 2000).

The community's understanding of halogen chemistry is continually evolving, and any future study should consider incorporating developments which have occurred since this model was built. For example, a future iteration of this WRF-Chem model could incorporate Roberts et al. (2014b)'s developments regarding bromine-nitrogen chemistry, and Roberts et al. (2014a)'s developments regarding uptake of HOBr onto particles.

In general, any model can always be improved, and this version of WRF-Chem is no different. In particular, the underlying version of WRF used in this investigation is 3.4.1., whereas the most recent version of WRF is version 3.7.1.. Recreating this model system in a new version of WRF would be a non-trivial task, but would allow an investigation to benefit from the improvements made to WRF in the last few years.

The computational resources available to researchers are continually expanding, and these allow more detailed and extensive models to be employed. An investigation with access to greater resources than were available to me may be in a position to, for example, use a more complex reaction mechanism, a higher spatial resolution, or a larger model domain.

In this investigation the plume travels outside of the model area after a little over a day. The chemical phenomena within the plume are still ongoing at this point, and thus this investigation is only able to place a lower limit on the duration of these phenomena. Employing a larger model domain may allow an investigation to estimate this duration, and therefore quantify the total effect of volcanic emissions on regional chemistry.

This investigation has not focussed on chlorine oxides. A small dataset of observations of chlorine oxides at volcanoes exists, this dataset is much smaller than the equivalent BrO dataset. Although the model mechanism contained several reactions which form and interchange such species, in the runs almost all Cl atoms produced react with alkanes to reform HCl. Further studies could investigate this, and see if/how the observations and model output could be resolved.

This investigation has focussed on passive degassing volcanic events. The

chemistry of more intense plumes is also of interest. Modelling these with skill could potentially be done with WRF-Chem, but would require a more sophisticated approach than the investigations of Chapter 7. Such investigations would need to consider the shape of eruption columns caused by the thrust of large eruptions, as well as other physical and chemical factors.

This investigation has used WRF-Chem, however other 3D models exist. Adapting such a model to perform a similar task to this investigation would be a sizeable task, but may be useful if a model has advantages that WRF-Chem does not.

The approach used in this investigation would be too computationally expensive to be directly imported into a global model. However it may be possible to determine from regional modelling such as that done in this investigation a methodology for parametrising the impacts of volcanoes on atmospheric chemistry within a global model.

Lastly, the results of this investigation may inform the design of future observational studies. Observations from ground- or aircraft-based campaigns may be able to evaluate whether some of the phenomena observed in the model output do occur in real volcanic plumes. In particular, elevated levels of HCHO within the plume, as predicted by the model, may be spectroscopically detectable, therefore allowing this model prediction to be verified (or otherwise). It may be possible to find such signals, or their absence, in data acquired in previous campaigns that were looking for oxidised halogens.

Appendix A

Derivation of tracer ratio method

At various points in this investigation I use the ratio of the change of a species' concentration caused by the plume to the concentration of a plume tracer species as a measure of chemical change. In Chapter 3 this tracer is SO_2, which is assumed to be effectively inert and negligible in the background in comparison to within the plume. When analysing WRF-Chem model output I use "tracer1", a tracer species which is modelled to be only produced by the volcano, and is absolutely inert within the model.

In this Appendix I prove, mathematically, that this approach is valid.

The following is a proof that $\Delta A \ / \ \Delta B$ cannot be changed by physical plume mixing processes, and thus any change observed in the ratio is the result of chemical change only.

Starting with a generic plume dispersal equation for a change in concentration due to mixing (von Glasow et al., 2003),

$$\begin{aligned}\left.\frac{\mathrm{d}c}{\mathrm{d}t}\right|_{\mathrm{mix}} &= -\frac{1}{A_{\mathrm{p}}}\frac{A_{\mathrm{p}}}{\mathrm{d}t}(c - c_{\mathrm{bg}}) \\ &= -\omega(c - c_{\mathrm{bg}}),\end{aligned}$$

where A_{p} is the cross-sectional area of the plume, $\omega = \omega(t)$ is the mixing parameter, c and c_{bg} are the concentration of the species in the plume and the background air, respectively.
Discretising,

$$\left.\frac{\delta c}{\delta t}\right|_{\mathrm{mix}} = -\omega(c - c_{\mathrm{bg}}).$$

Let c_i be the concentration of the species at time t_i:

$$c_2 = c_1 + \frac{\delta c}{\delta t}\delta t = c_1 - \omega(c_1 - c_{\mathrm{bg}})\delta t.$$

We define

$$\Delta c_i = c_i - c_{\mathrm{bg}}.$$

Therefore,

$$\begin{aligned}\Delta c_2 &= c_1 - \omega(c_1 - c_{\mathrm{bg}})\delta t - c_{\mathrm{bg}} \\ &= \Delta c_1 - \Delta c_1 \omega \delta t = \Delta c_1(1 - \omega\delta t).\end{aligned}$$

Taking the ratio of gas A and gas B,

$$\frac{\Delta c_2^{\mathrm{A}}}{\Delta c_2^{\mathrm{B}}} = \frac{\Delta c_1^{\mathrm{A}}(1 - \omega\delta t)}{\Delta c_1^{\mathrm{B}}(1 - \omega\delta t)} = \frac{\Delta c_1^{\mathrm{A}}}{\Delta c_1^{\mathrm{B}}}.$$

If the concentration of B is negligible outside of the plume is negligible in comparison to within the plume (i.e. $B_{\mathrm{bg}} \approx 0$) then $\Delta B = B$ and $\Delta A/\Delta B = \Delta A/B$.
Therefore,

$$\frac{\Delta A_{,1}}{B_{,1}} = \frac{\Delta A_{,2}}{B_{,2}}$$

Therefore, if no chemical change in A or B occurs between time 1 and time 2, the ratio remains unchanged. If B can be considered chemically inert, then $\Delta A/B$ can be used as a measure of the chemical change of A.

For example, in Chapter 3 $\Delta O_3/SO_2$ is used as a measure of the chemical depletion of ozone of within the plume as SO_2 outside of the plume is negligible compared to within it, and SO_2 can be considered effectively inert over the distances considered.

Appendix B

Primary aerosol input

The attribution statement of Section 3.0.5 also applies to this Appendix

In this appendix I show how I have derived the magnitude and size distribution of the primary aerosol emissions used within WRF-Chem using observational data made on Mount Etna during the field campaign described in Chapter 3.

This exercise requires various assumptions and extrapolations from a small set of data. Oner of the reasons for presenting this exercise as an appendix rather than in the main body of this document is to emphasise that this investigation is not a rigorous study of the volcanic aerosol. Rather, this exercise is an attempt to obtain a "best guess" for this necessary input from the available data.

B.1 Task

In the modelling of this investigation, I have used a chemical scheme which incorporates the the MOSAIC 8-bins aerosol scheme (Zaveri et al., 2008). This divides aerosol of a given type into eight bins by size; these are tabulated in Table B.1.

In this exercise, I produce estimates for the aerosol mass flux from the volcano as a ratio of the SO_2 emissions, and also estimate the size distribution of this aerosol in terms of the MOSAIC size bins. These estimates are used as inputs in the model runs.

The aerosol scheme used also distinguishes aerosol by chemical composition as well as size. There is no data available from the field campaign from which

Table B.1: Size bins used in the MOSAIC 8-bins aerosol scheme

Bin Number	Diameter range / μm
1	0.04–0.08
2	0.08–0.16
3	0.16–0.31
4	0.31–0.63
5	0.63–1.25
6	1.25–2.5
7	2.5–5
8	5–10

such an estimate could be derived. Instead results from the literature were used for this purpose, this is discussed in Section 2.2.3.2.

B.2 Available data

This exercise uses data measured at site "d1-28". This site was not used in the analysis of Chapter 3 as it did not have an associated upwind site, however it is useful for this exercise as it measured a plume which, on the basis of visual observations, was a mixture of plume emitted by all active vents. An optical particle counter was deployed for a period of slightly over 2 hours. SO_2 data was also collected at this site.

This optical particle counter records aerosol counts, in units of counts per m^3, for six different aerosol size bins, tabulated in Table B.2.

Table B.2: Aersol size buns used by the optical particle counter

Bin Number	Diameter range / μ m
1	0.3–0.5
2	0.5–1
3	1–3
4	3–5
5	5–10
6	>10

It is assumed that because the measurements were taken within a few hundred metres of the vents that negligible secondary aerosol formation had occurred while the plume was transported from vents to the measurement sites, and therefore the measurements can be considered representative of primary aerosol. This assumption does not consider the "pseudo-primary" aerosol

discussed in Section 6.4.

The SO_2 measurements are discussed in Chapter 3. Average SO_2 mixing ratios for each measurement site were calculated.

Because the SO_2 measurements were mixing ratios and the aerosol measurements were concentrations, it was necessary to use a value of air density to convert between these units. From inspection of the pressure and temperature measurements made in the field campaign, a value of 29.6 moles m^{-3}, approximately two-thirds standard sea-level air density, was determined.

B.3 Analysis

Apart from MOSAIC bin 8 and observation bin 5, the two sets of bins do not exactly match. Additionally MOSAIC bins 1–3 correspond to smaller aerosol than is possible to measure with the optical particle counter. Therefore, in order to estimate the populations of the MOSAIC bins, it is necessary to both interpolate and extrapolate from the observational data.

For each observational bin, an average of the number density for each site was calculated. Using the mid-points of each observation bin as a representative diameter, these were then fitted to a power-law distribution (see section 7.1.9 of Seinfeld and Pandis, 2006). Number density estimates for each bin were interpolated/extrapolated from this fit using the mid-points of the MOSAIC bins as representative diameters.

These number density estimates were then converted to estimates of the aerosol mass/SO_2 mass ratio by assuming spherical particles at the representative diameters for each bin, an aerosol density of 1800 kg m^{-3}, the SO_2 measurements for each site, and the air density.

Although the distribution and overall aerosol/SO_2 ratio varies significantly between the different sites, especially those relating to different vents, it is necessary to have a single set of values for the model input. Therefore, for each bin, the average aerosol/SO_2 mass ratio for all sites is calculated. These values, tabulated in Table B.3, are used for the model input.

Table B.3: Modelled primary aerosol emissions

MOSAIC bin Number	Diameter range / μm	Aerosol/SO_2 ratio
1	0.04–0.08	3.8×10^{-3}
2	0.08–0.16	3.4×10^{-3}
3	0.16–0.31	3.0×10^{-3}
4	0.31–0.63	2.9×10^{-3}
5	0.63–1.25	3.8×10^{-3}
6	1.25–2.5	11.9×10^{-3}
7	2.5 –5	8.6×10^{-3}
8	5 –10	5.3×10^{-3}
Overall ratio		42.6×10^{-3}

Appendix C

Bug in WRF-Chem set-up

Between the time when this thesis was initially submitted and the viva examination, Dr. Alba Badia, who is using this modified WRF-Chem model in a successor investigation into oceanic halogen emissions, identified a bug in the set-up of the chlorine chemistry. This bug will have been present in all the model runs discussed in this document.

Given the timing of this discovery, it was not viable to re-do all of the modelling for this thesis, though any further publications resulting from this work will present only results from the corrected model.

The impact of this bug is discussed below — the magnitude of the impact varying between different chemical systems. To accounting for this error, when doing the post-viva corrections some conclusions based upon the model output have been redacted as they are not robust, while for others I have added caveats.

The bug impacts 16 gas-phase chemical reactions. The E_a coefficient for these reactions were incorrectly entered as $-E_a$, causing the calculated rates to be incorrect.

This bug does not impact heterogeneous reactions or photolysis reactions—thus the calculation of the direct impact of chlorine on the bromine cycle (through BrCl's heterogeneous formation and photolytic destruction) are not impacted by this bug.

Methane oxidation and chlorine oxide chemistry The error in the calculation of the $Cl + CH_4$ reaction causes the determined rate to be extremely fast, about 4000 times greater than it should be. CH_4 is present throughout the atmosphere, both within and outside of the plume. Cl atom radicals are calculated to

have a negligible lifetime in the atmosphere, existing for only a fraction of a second before reacting with CH_4 — Cl radicals' lifetime, with respect to reaction without the bug is of the order of 0.2 seconds, with the bug this reduces to approximately $50\mu s$. This has the effect of "switching off" oxidised chlorine chemistry as effectively no Cl atoms react in the chlorine oxide forming reactions. Thus the bug in the $Cl + CH_4$ reaction makes the bugs in the other Cl and chlorine oxide reactions moot.

While, even without the bug, the very short lifetime of Cl radicals means that a substantial reservoir of Cl itself would not be expected to build up. However some chlorine oxide (ClO_x) species are longer-lived. An offline calculation of the expected correct rates of these reactions finds that the fate of Cl atoms should be approximately 20% being consumed by reactions with alkanes, forming HCl, whilst approximately 80% would react with O_3, forming ClO (other reactions are negligible). Photolysis or other outputs from chlorine oxide chemistry would eventually reform Cl, whereupon again approximately 20% would be "lost" to $Cl + CH_4$.

Over time a steady state would emerge where the formation of reactive chlorine (from BrCl or from HCl) was matched by the loss (formation of HCl). A reservoir of chlorine oxides would build up in this case.

With the bug, this Cl formation-equals-destruction state is achieved immediately rather than after a reservoir build-up time. With or without the bug, the modelled formation of oxidised organics from $Cl + CH_4$ would eventually be limited by the rate of Cl formation, though the bug has omitted a prior reservoir build-up step of unknown duration.

The bug means the model effectively does not do chlorine oxide chemistry, and no conclusions about this system can be drawn from the model. Therefore this document makes no attempt to address observations of OClO in volcanic plumes.

This bug may have caused some chlorine oxide cycling-related O_3 destruction to have been omitted. This is an error of unknown magnitude, however, as discussed in 1.1.5.5, a review of the literature shows that chlorine chemistry is not expected to cause O_3 loss of a similar magnitude to that of bromine chemistry.

$HCl + OH$ reaction The other significant effect of this bug is that the rate of the $HCl + OH$ reaction is greatly overestimated, by approximately a factor of 5.

This does not have a significant effect on HCl concentrations. Despite this bug HCl is significantly in excess throughout the plume.

This bug will have overestimated the OH suppression the plume causes. The phenomenon of OH suppression is still predicted to occur, as sulphur and bromine chemistry are HO_x destructive. However in the bug-impacted plume chemistry, the HCl reaction was responsible for approximately 60% of the OH loss reactions.

Lastly, this bug will have caused an overestimation of the formation of Cl atoms. Were this bug to be corrected, there would be fewer Cl atoms produced. However, Cl radicals would not become unimportant to the modelled chemistry, because substantial Cl is produced from photolysis of BrCl. Photolysis of BrCl is calculated correctly in the model. Approximately half of the Cl production in the bug-affected model runs comes from this photolysis reaction. Without the bug this photolysis would be the dominant Cl-production pathway. Thus, to a rough approximation, were the bug to be corrected the modelled Cl production rate would be approximately halved.

Appendix D

Chemical mechanism

This appendix lists all of the species and reactions that are included in the *uea01_hg3* mechanism and are processed by KPP (see Section 2.2.2).

D.1 Species

The *uea01_hg3* mechanism considers many gas phase chemical species. For the most part, an entity in this mechanism refers to a specific molecule. However, for larger organics, there is not a direct equivalence between these modelled entities and individual molecules—*uea01_hg3* is a development of the *CBMZ_MOSAIC_8bins* scheme (Zaveri and Peters, 1999; Zaveri et al., 2008) which employs a lumped-structure mechanism for dealing with such species.

Table D.1 lists every chemical species included in the mechanism. The left column lists the names by which these species are known in KPP. For some species the meanings of these names are not immediately clear, and as such the right column gives a full description of each species. Artificial tracers are not included in this list.

Some species are listed as "Species representing a class of organic aerosol in gas-phase mechanism". These are "artificial" tracers that allow for interaction between the CBMZ gas-phase chemistry and the MOSAIC aerosol chemistry.

Table D.1: Species in the chemical mechanism

KPP name	Description
H2SO4	sulfuric acid
HNO3	nitric acid

HCl	hydrochloric acid
NH3	ammonia
NO	nitric oxide
NO2	nitrogen dioxide
NO3	nitrate radical
N2O5	nitrogen pentoxide
HONO	nitrous acid
HNO4	pernitric acid
O3	ozone
O1D	oxygen atom singlet D
O3P	oxygen atom triplet P
OH	hydroxyl radical
HO2	hydroperoxyl radical
H2O2	hydrogen peroxide
BR	bromine atom
BR2	bromine molecule
BRO	bromine oxide
HBR	hydrogen bromide
HOBR	hypobromous acid
BRNO2	bromine nitrite
BRNO3	bromine nitrate
HG	mercury atom
HGBR	mercury bromide radicals
HGBR2	mercury (II) bromide
CL	chlorine atom
CLO	chlorine monoxide
OCLO	chlorine dioxide
CL2	chlorine dimer
CLNO2	nitryl chloride
CLNO3	chlorine nitrate
HOCL	hypochlorous acid
BRCL	bromine monochloride
HGCL	mercury chloride radical
HGCL2	mercury (II) chloride
CH4	methane
CO	carbon monoxide
SO2	sulfur dioxide
C2H6	ethane

CH3O2	methylperoxy radical
ETHP	ethylperoxy radical
HCHO	formaldehyde
CH3OH	methanol
ANOL	ethanol
CH3OOH	methyl hydrogen peroxide
ETHOOH	ethyl hydrogen peroxide
ALD2	acetaldehyde
HCOOH	formic acid
RCOOH	higher organic acids
C2O3	peroxyacyl radical
PAN	peroxyacyl nitrate
PAR	paraffin carbon
AONE	acetone
MGLY	methylglyoxal
ETH	ethene
OLET	terminal olefin carbons
OLEI	internal olefin carbons
TOL	toluene
XYL	xylene
CRES	cresol and higher molecular weight phenols
TO2	toluene-OH adduct
CRO	methylphenoxy radical
OPEN	high molecular weight aromatic ox. frag
ONIT	organic nitrate
ROOH	higher organic peroxide
RO2	alkylperoxy radical
ANO2	acetylmethylperoxy radical
NAP	nitratoalkyl peroxy radicals
XO2	NO to NO_2 operator
XPAR	PAR removal operator
ISOP	isoprene
ISOPRD	lumped intermediate species
ISOPP	lumped peroxyradical of isoprene
ISOPN	NO_3-isoprene adduct
ISOPO2	lumped peroxyradical of isoprene
ARO1	Species representing a class of organic aerosol in gas-phase mechanism
ARO2	Species representing a class of organic aerosol in gas-phase mechanism

ALK1	Species representing a class of organic aerosol in gas-phase mechanism
OLE1	Species representing a class of organic aerosol in gas-phase mechanism
API1	Species representing a class of organic aerosol in gas-phase mechanism
API2	Species representing a class of organic aerosol in gas-phase mechanism
LIM1	Species representing a class of organic aerosol in gas-phase mechanism
LIM2	Species representing a class of organic aerosol in gas-phase mechanism
API	alpha-pinene
LIM	limonene

D.2 Reactions

The following tables list the photolysis- gas- and heterogeneous-phase reactions that are included in *uea01_ hg3*. The listing below used the KPP names for species as listed in Table D.1. The reaction numbers are arbitrary and are included here for the readers convenience. These do not match the sequentially-assigned reaction numbers for chemical reactions mentioned in the main text of this document.

As discussed in Section 1.4, this is a simplified version of the known chemistry of the atmosphere, using every known reaction in WRF-Chem would not be viable. Not all reactions stoichiometrically balance. Some reactions listed are representations of several reactions, for example the listed $SO_2 + OH \longrightarrow H_2SO_4 + HO_2$ reaction does not stoichiometrically balance because it is a simplified version of a short series of reactions. Also, production of non-modelled species such as O_2 are not listed.

"hv" refers to a photon of light, indicating a photolysis reaction.

Table D.2: Photolysis reactions

No.	Reaction
1	NO2 + hv → NO + O3P
2	NO3 + hv → .89 NO2 + .89 O3P + .11 NO
3	HONO + hv → OH + NO
4	HNO3 + hv → OH + NO2
5	HNO4 + hv → HO2 + NO2
6	N2O5 + hv → NO2 + NO3
7	O3 + hv → O3P
8	O3 + hv → O1D

9	H2O2 + hv → 2 OH
10	HCHO + hv → 2 HO2 + CO
11	HCHO + hv → CO
12	CH3OOH + hv → HCHO + HO2 + OH
13	ETHOOH + hv → ALD2 + HO2 + OH
14	ALD2 + hv → CH3O2 + HO2 + CO
15	AONE + hv → C2O3 + CH3O2
16	MGLY + hv → C2O3 + CO + HO2
17	OPEN + hv → C2O3 + CO + HO2
18	ROOH + hv → OH + 0.4 XO2 + 0.74 AONE + 0.3 ALD2 + 0.1 ETHP + 0.9 HO2 + 1.98 XPAR
19	ONIT + hv → NO2 + 0.41 XO2 + 0.74 AONE + 0.3 ALD2 + 0.1 ETHP + 0.9 HO2 + 1.98 XPAR
20	ISOPRD + hv → 0.97 C2O3 + 0.33 HO2 + 0.33 CO + 0.7 CH3O2 + 0.2 HCHO + 0.07 ALD2 + 0.03 AONE
21	BRO + hv → BR + O3
22	BR2 + hv → 2 BR
23	HBR + hv → BR
24	HOBR + hv → BR + OH
25	BRNO2 + hv → BR + NO2
26	BRNO3 + hv → BR + NO3
27	OCLO + hv → O3 + CLO
28	CL2 + hv → 2 CL
29	HOCL + hv → CL + OH
30	CLNO2 + hv → CL + NO2
31	CLNO3 + hv → CL + NO3
32	BRCL + hv → BR + CL

Table D.3: Other gas-phase reactions

No.	Reaction
33	O1D + M → O3P
34	O1D + H2O → 2 OH
35	O3P + M → O3
36	O3P + O3 → 2 O2
37	O3P + NO2 → NO
38	O3P + NO2 → NO3
39	O3P + NO → NO2

```
40  O3 + NO → NO2
41  O3 + NO2 → NO3
42  O3 + OH → HO2
43  O3 + HO2 → OH
44  OH + M → HO2 + H2O
45  OH + NO → HONO
46  OH + NO2 → HNO3
47  OH + NO3 → HO2 + NO2
48  OH + HONO → NO2
49  OH + HNO3 → NO3
50  OH + HNO4 → NO2
51  OH + HO2 → H2O
52  OH + H2O2 → HO2
53  HO2 + HO2 → H2O2
54  HO2 + HO2 + H2O → H2O2
55  HO2 + NO → OH + NO2
56  HO2 + NO2 → HNO4
57  HO2 + NO2 → HONO
58  HNO4 → HO2 + NO2
59  NO3 + NO → NO2 + NO2
60  NO3 + NO2 → NO + NO2
61  NO3 + NO2 → N2O5
62  NO3 + NO3 → 2 NO2
63  NO3 + HO2 → 0.3 HNO3 + 0.7 NO2 + 0.7 OH
64  N2O5 + H2O → 2 HNO3
65  N2O5 → NO3 + NO2
66  CO + OH → HO2
67  SO2 + OH → H2SO4 + HO2
68  OH + CH4 → CH3O2
69  C2H6 + OH → ETHP
70  PAR + OH → RO2 + .012 ALK1
71  HCHO + OH → HO2 + CO
72  HCHO + NO3 → HNO3 + HO2 + CO
73  ALD2 + OH → C2O3
74  ALD2 + NO3 → C2O3 + HNO3
75  AONE + OH → ANO2
76  MGLY + OH → XO2 + C2O3
77  MGLY + NO3 → HNO3 + C2O3 + CO
```

78	ETH + O3 → HCHO + 0.22 HO2 + 0.12 OH + 0.24 CO + 0.52 HCOOH
79	ETH + OH → XO2 + 1.56 HCHO + HO2 + 0.22 ALD2
80	OLET + O3 → 0.57 HCHO + 0.47 ALD2 + 0.33 OH + .26 HO2 +0.07 CH3O2 + 0.06 ETHP + 0.03 RO2 + 0.13 C2O3 + 0.04 MGLY + 0.03 CH3OH + 0.06 CH4 + 0.01 C2H6 + 0.31 CO + 0.22 HCOOH + 0.09 RCOOH + 1.06 XPAR + 0.008 OLE1
81	OLEI + O3 → 1.03 ALD2 + 0.07 AONE + 0.6 OH + 0.22 HO2 + 0.1 CH3O2 + 0.05 ETHP + 0.09 RO2 + 0.11 ANO2 + 0.19 C2O3 + 0.07 MGLY + 0.04 CH3OH + 0.08 CH4 + 0.01 C2H6 + 0.3 CO + 0.16 RCOOH + 2.26 XPAR + 0.008 OLE1
82	OLET + OH → XO2 + HO2 + HCHO + ALD2 + XPAR + 0.008 OLE1
83	OLEI + OH → XO2 + HO2 + 0.23 AONE + 1.77 ALD2 + 2.23 XPAR + 0.008 OLE1
84	OLET + NO3 → NAP + 0.008 OLE1
85	OLEI + NO3 → NAP + 0.008 OLE1
86	TOL + OH → 0.08 XO2 + 0.12 CRES + 0.2 HO2 + 0.8 TO2 + 0.039 ARO1 + 0.108 ARO2
87	XYL + OH → 0.5 XO2 + 0.55 HO2 + 0.05 CRES + 0.8 MGLY + 1.1 PAR + 0.45 TO2 + 0.039 ARO1 + 0.108 ARO2
88	TO2 + NO → 0.95 NO2 + 0.95 OPEN + 0.95 HO2 + 0.05 ONIT
89	CRES + OH → 0.4 CRO + 0.6 XO2 + 0.6 HO2 + 0.3 OPEN + 0.039 ARO1 + 0.108 ARO2
90	CRES + NO3 → CRO + HNO3 + 0.039 ARO1 + 0.108 ARO2
91	CRO + NO2 → ONIT
92	OPEN + OH → XO2 + C2O3 + 2 CO + 2 HO2 + HCHO
93	OPEN + O3 → 0.03 ALD2 + 0.62 C2O3 + 0.7 HCHO + 0.69 CO + 0.08 OH + 0.03 XO2 + 0.76 HO2 + 0.2 MGLY
94	ISOP + OH → ISOPP + 0.08 XO2
95	ISOP + O3 → 0.6 HCHO + 0.65 ISOPRD + 0.27 OH + 0.07 CO + 0.39 RCOOH + 0.07 HO2 + 0.15 ALD2 + 0.2 XO2 + 0.2 C2O3
96	ISOP + NO3 → ISOPN
97	ISOPRD + OH → 0.5 C2O3 + 0.5 ISOPO2 + 0.2 XO2
98	ISOPRD + O3 → 0.27 OH + 0.1 HO2 + 0.11 C2O3 + 0.07 XO2 + 0.05 CH3O2 + 0.16 CO + 0.15 HCHO + 0.02 ALD2 + 0.09 AONE + 0.85 MGLY + 0.46 RCOOH
99	ISOPRD + NO3 → 0.07 C2O3 + 0.07 HNO3 + 0.64 CO + 0.28 HCHO + 0.93 ONIT + 0.28 ALD2 + 0.93 HO2 + 0.93 XO2 + 1.86 PAR

```
100 ISOPP + NO → 0.09 ONIT + 0.91 NO2 + 0.91 HO2 + 0.63 HCHO +
    0.91 ISOPRD + 0.18 PAR
101 ISOPN + NO → 1.2 NO2 + 0.8 ONIT + 0.8 ALD2 + 0.8 HO2 + 0.2
    ISOPRD + 1.6 PAR
102 ISOPO2 + NO → NO2 + HO2 + 0.59 CO + 0.55 ALD2 + 0.25 HCHO
    + 0.34 MGLY + 0.63 AONE
103 ISOPP + HO2 → ROOH
104 ISOPN + HO2 → ONIT + 2 PAR
105 ISOPO2 + HO2 → ROOH
106 CH3OOH + OH → 0.7 CH3O2 + 0.3 HCHO + 0.3 OH
107 ETHOOH + OH → 0.7 ETHP + 0.3 ALD2 + 0.3 OH
108 ROOH + OH → 0.77 RO2 + 0.19 MGLY + 0.04 ALD2 + 0.23 OH +
    0.42 XPAR
109 ONIT + OH → NAP
110 C2O3 + NO2 → PAN
111 PAN → C2O3 + NO2
112 CH3OH + OH → HCHO + HO2
113 CH3O2 + NO → HCHO + HO2 + NO2
114 ETHP + NO → ALD2 + HO2 + NO2
115 RO2 + NO → .16 ONIT + .84 NO2 + .34 XO2 + .62 AONE + .25
    ALD2 + .08 ETHP + .76 HO2 + 1.68 XPAR
116 C2O3 + NO → NO2 + CH3O2
117 ANO2 + NO → NO2 + C2O3 + HCHO
118 NAP + NO → 1.5 NO2 + .5 HCHO + .5 ALD2 + .5 ONIT + .5 HO2
    + XPAR
119 XO2 + NO → NO2
120 CH3O2 + NO3 → HCHO + HO2 + NO2
121 ETHP + NO3 → ALD2 + HO2 + NO2
122 RO2 + NO3 → NO2 + .4 XO2 + .74 AONE + .3 ALD2 + .1 ETHP +
    .9 HO2 + 1.98 XPAR
123 C2O3 + NO3 → NO2 + CH3O2
124 ANO2 + NO3 → NO2 + C2O3 + HCHO
125 NAP + NO3 → 1.5 NO2 + .5 HCHO + .5 ALD2 + .5 ONIT + .5 HO2
    + XPAR
126 XO2 + NO3 → NO2
127 CH3O2 + HO2 → CH3OOH
128 ETHP + HO2 → ETHOOH
129 RO2 + HO2 → ROOH
```

```
130 C2O3 + HO2 → .4 RCOOH + .4 O3
131 ANO2 + HO2 → ROOH
132 NAP + HO2 → ONIT
133 XO2 + HO2 → PROD
134 ANOL + OH → ALD2 + HO2
135 PAR + XPAR → PROD
136 CH3O2 → .66 HCHO + .32 HO2 + .34 CH3OH
137 ETHP → .8 ALD2 + .6 HO2 + .2 C2H6
138 RO2 → .24 XO2 + .21 ALD2 + .57 AONE + .06 ETHP + .54 HO2 +
    1.25 XPAR
139 C2O3 → CH3O2
140 ANO2 → .7 C2O3 + .7 HCHO + .15 MGLY + .15 AONE
141 NAP → .5 NO2 + .5 HCHO + .5 ALD2 + .5 ONIT + XPAR
142 ISOPP → ISOPRD
143 ISOPN → ALD2 + ONIT + 2 PAR
144 ISOPO2 → .5 ALD2 + .5 AONE
145 XO2 → PROD
146 BR + O3 → BRO
147 BR + HO2 → HBR
148 BR + HCHO → HBR + CO + HO2
149 BR + CH3OOH → CH3O2 + HBR
150 BRO + HO2 → HOBR
151 BRO + CH3O2 → 0.72HOBR + 0.28 BR + 0.28 HO2 + HCHO
152 BRO + NO → BR + NO2
153 BRO + NO2 → BRNO3
154 BRO + BRO → 1.62 BR + 0.19 BR2
155 HBR + OH → BR + H2O
156 BR + NO2 → BRNO2
157 BRNO3 → BRO + NO2
158 HG + BR → HGBR
159 HGBR → HG + BR
160 HGBR + BR → HGBR2
161 HG + BR2 → HGBR2
162 HGBR + HGBR → HG + HGBR2
163 HGBR2 + SO2 → BR + HG + SO2
164 HGBR2 → HG
165 API + OH → .0064 API1 + .055 API2
166 API + NO3 → .0 API1 + .0 API2
```

167	API + O3 → .022 API1 + .19 API2
168	LIM + OH → .037 LIM1 + .056 LIM2
169	LIM + NO3 → .0 LIM1 + .0 LIM2
170	LIM + O3 → .13 LIM1 + .19 LIM2
171	OH → Br (see Section 2.2.2.3)
172	CL + O3 → CLO
173	CL + HO2 → 0.8 HCL + 0.2 CLO + 0.2 OH
174	CL + H2O2 → HCL + HO2
175	CL + RO2 → 0.5 CLO + 0.5 HCHO + 0.5 HO2 + 0.5 HCl + 0.5 CO
176	CL + CH4 → HCl + CH3O2
177	CL + C2H6 → HCl + RO2
178	CL + HCHO → HCL + HO2 + CO
179	CL + CLNO3 → CL2 + NO3
180	CLO + HO2 → HOCL
181	CLO + CH3O2 → CL + HCHO + HO2
182	CLO + NO → Cl + NO2
183	CLO + NO2 → ClNO3
184	CLO + CLO → CL2
185	CLO + CLO → OCLO + CL
186	HCL + OH → H2O + CL
187	CLNO2 + OH → HOCL + NO2
188	CLNO3 + OH → 0.5 CLO + 0.5 HNO3 + 0.5 HOCL + 0.5 NO3
189	BRO + CLO → 0.93 BR + 0.5 OCLO + 0.43 CL + 0.07 BRCL
190	HG + CL → HGCL
191	HG + HCL → HGCL + HO2
192	HG + CL2 → HGCL2
193	HGCL + CL → HGCL2
194	HGCL + HGCL → HGCL2 + HG
195	HGCL2 + SO2 → HG + CL2 + SO2

Table D.4: Heterogeneous reactions

No.	Reaction
196	N2O5 → 2 HNO3
197	N2O5 + HCL → ClNO2 + HNO3
198	N2O5 + HBr → BrNO2 + HNO3
199	CLNO3 → HOCL + HNO3
200	CLNO3 + HCL → CL2 + HNO3

201	CLNO3 + HBR → BRCL + HNO3
202	BRNO3 → HOBR + HNO3
203	BRNO3 → HOBR
204	BRNO3 + HCL → BRCL + HNO3
205	BRNO3 + HBR → BR2 + HNO3
206	HOBR + HBR → BR2
207	HOBR + HCL → BRCL
208	HOCL + HBR → BRCL
209	HGCL2 → HG + CL2
210	HGBR2 → HG + BR2

References

Aiuppa, A., Federico, C., Franco, A., Giudice, G., Gurrieri, S., Inguaggiato, S., Liuzzo, M., McGonigle, A. J. S., and Valenza, M. Emission of bromine and iodine from mount etna volcano. *Geochemistry Geophysics Geosystems*, 6: Q08008, 2005a. doi: 10.1029/2005gc000965.

Aiuppa, A., Inguaggiato, S., McGonigle, A., O'Dwyer, M., Oppenheimer, C., Padgett, M., Rouwet, D., and Valenza, M. H_2S fluxes from Mt. Etna, Stromboli, and Vulcano (Italy) and implications for the sulfur budget at volcanoes. *Geochimica et Cosmochimica Acta*, 69(7):1861–1871, 2005b. doi: 10.1016/j.gca.2004.09.018.

Aiuppa, A., Franco, A., von Glasow, R., Allen, A. G., D'Alessandro, W., Mather, T. A., Pyle, D. M., and Valenza, M. The tropospheric processing of acidic gases and hydrogen sulphide in volcanic gas plumes as inferred from field and model investigations. *Atmospheric Chemistry and Physics*, 7(5):1441–1450, 2007. doi: 10.5194/acp-7-1441-2007.

Aiuppa, A., Shinohara, H., Tamburello, G., Giudice, G., Liuzzo, M., and Moretti, R. Hydrogen in the gas plume of an open-vent volcano, Mount Etna, Italy. *Journal of Geophysical Research-Solid Earth*, 116, 2011. doi: 10.1029/2011jb008461.

Aiuppa, A., Giudice, G., Liuzzo, M., Tamburello, G., Allard, P., Calabrese, S., Chaplygin, I., McGonigle, A. J. S., and Taran, Y. First volatile inventory for gorely volcano, kamchatka. *Geophysical Research Letters*, 39:L06307, 2012. doi: 10.1029/2012gl051177.

Allen, A. G., Baxter, P. J., and Ottley, C. J. Gas and particle emissions from Soufriere Hills Volcano, Montserrat, West Indies: characterization and health hazard assessment. *Bulletin of Volcanology*, 62(1):8–19, 2000. doi: 10.1007/s004450050287.

Allen, A. G., Oppenheimer, C., Ferm, M., Baxter, P. J., Horrocks, L. A., Galle, B., McGonigle, A. J. S., and Duffell, H. J. Primary sulfate aerosol and associated emissions from Masaya Volcano, Nicaragua. *Journal of Geophysical Research: Atmospheres*, 107(D23):ACH 5–1–ACH 5–8, 2002. doi: 10.1029/2002JD002120.

Ammann, M., Cox, R. A., Crowley, J. N., Jenkin, M. E., Mellouki, A., Rossi, M. J., Troe, J., and Wallington, T. J. Evaluated kinetic and photochemical data

for atmospheric chemistry: Volume VI - heterogeneous reactions with liquid substrates. *Atmospheric Chemistry and Physics*, 13(16):8045–8228, 2013. doi: 10.5194/acp-13-8045-2013.

Atkinson, R., Baulch, D. L., Cox, R. A., Crowley, J. N., Hampson, R. F., Hynes, R. G., Jenkin, M. E., Rossi, M. J., and Troe, J. Evaluated kinetic and photochemical data for atmospheric chemistry Volume I - gas phase reactions of O_x, HO_x, NO_x and SO_x species. *Atmospheric Chemistry and Physics*, 4(6): 1461–1738, 2004. doi: 10.5194/acp-4-1461-2004.

Atkinson, R., Baulch, D. L., Cox, R. A., Crowley, J. N., Hampson, R. F., Hynes, R. G., Jenkin, M. E., Rossi, M. J., Troe, J., and Subcommittee, I. Evaluated kinetic and photochemical data for atmospheric chemistry: Volume II - gas phase reactions of organic species. *Atmospheric Chemistry and Physics*, 6(11): 3625–4055, 2006. doi: 10.5194/acp-6-3625-2006.

Atkinson, R., Baulch, D. L., Cox, R. A., Crowley, J. N., Hampson, R. F., Hynes, R. G., Jenkin, M. E., Rossi, M. J., and Troe, J. Evaluated kinetic and photochemical data for atmospheric chemistry: Volume III - gas phase reactions of inorganic halogens. *Atmospheric Chemistry and Physics*, 7(4): 981–1191, 2007. doi: 10.5194/acp-7-981-2007.

Atkinson, R., Baulch, D. L., Cox, R. A., Crowley, J. N., Hampson, R. F., Hynes, R. G., Jenkin, M. E., Rossi, M. J., Troe, J., and Wallington, T. J. Evaluated kinetic and photochemical data for atmospheric chemistry: Volume IV - gas phase reactions of organic halogen species. *Atmospheric Chemistry and Physics*, 8(15):4141–4496, 2008. doi: 10.5194/acp-8-4141-2008.

Bagnato, E., Aiuppa, A., Parello, F., Calabrese, S., D'Alessandro, W., T.A., M., McGonigle, A., Pyle, D., and Wängberg, I. Degassing of gaseous (elemental and reactive) and particulate mercury from mount etna volcano (southern italy). *Atmospheric Environment*, 41(35):7377–7388, 2007. doi: 10.1016/j.atmosenv.2007.05.060.

Bandy, A. R., Maroulis, P. J., Wilner, L. A., and Torres, A. L. Estimates of the fluxes of NO, SO_2, H_2S, CS_2 and OCS from mt st. helens deduced from in situ plume concentration measurements. *Geophysical Research Letters*, 9(9): 1097–1100, 1982. doi: 10.1029/GL009i009p01097.

Bey, I., Jacob, D. J., Yantosca, R. M., Logan, J. A., Field, B. D., Fiore, A. M., Li, Q., Liu, H. Y., Mickley, L. J., and Schultz, M. G. Global modeling of tropospheric chemistry with assimilated meteorology: Model description and evaluation. *Journal of Geophysical Research: Atmospheres*, 106(D19):23073–23095, 2001. doi: 10.1029/2001JD000807.

Bobrowski, N. and Giuffrida, G. Bromine monoxide / sulphur dioxide ratios in relation to volcanological observations at Mt. Etna 2006 –2009. *Solid Earth*, 3 (2):433–445, 2012. doi: 10.5194/se-3-433-2012.

Bobrowski, N. and Platt, U. SO_2/BrO ratios studied in five volcanic plumes. *Journal of Volcanology and Geothermal Research*, 166(3-4):147–160, 2007. doi: 10.1016/j.jvolgeores.2007.07.003.

Bobrowski, N., Hönninger, G., Galle, B., and Platt, U. Detection of bromine monoxide in a volcanic plume. *Nature*, 423(6937):273–276, 2003. doi: 10.1038/nature01625.

Bobrowski, N., von Glasow, R., Aiuppa, A., Inguaggiato, S., Louban, I., Ibrahim, O. W., and Platt, U. Reactive halogen chemistry in volcanic plumes. *Journal of Geophysical Research-Atmospheres*, 112(D6), 2007. doi: 10.1029/2006jd007206.

Bobrowski, N., von Glasow, R., Giuffrida, G. B., Tedesco, D., Aiuppa, A., Yalire, M., Arellano, S., Johansson, M., and Galle, B. Gas emission strength and evolution of the molar ratio of BrO/SO_2 in the plume of Nyiragongo in comparison to Etna. *Journal of Geophysical Research: Atmospheres*, 120(1):277–291, 2015. doi: 10.1002/2013JD021069. 2013JD021069.

Bobrowski, N. *Volcanic gas studies by multi axis differential optical absorption spectroscopy*. PhD thesis, University of Heidelberg, 2005.

Boichu, M., Oppenheimer, C., Roberts, T. J., Tsanev, V., and Kyle, P. R. On bromine, nitrogen oxides and ozone depletion in the tropospheric plume of Erebus volcano (Antarctica). *Atmospheric Environment*, 45(23):3856–3866, 2011. doi: 10.1016/j.atmosenv.2011.03.027.

Bureau, H., Keppler, H., and Métrich, N. Volcanic degassing of bromine and iodine: experimental fluid/melt partitioning data and applications to stratospheric chemistry. *Earth and Planetary Science Letters*, 183(1–2):51–60, 2000. doi: http://dx.doi.org/10.1016/S0012-821X(00)00258-2.

Cantrell, C. A. Technical note: Review of methods for linear least-squares fitting of data and application to atmospheric chemistry problems. *Atmospheric Chemistry and Physics*, 8(17):5477–5487, 2008. doi: 10.5194/acp-8-5477-2008.

Crowley, J. N., Ammann, M., Cox, R. A., Hynes, R. G., Jenkin, M. E., Mellouki, A., Rossi, M. J., Troe, J., and Wallington, T. J. Evaluated kinetic and photochemical data for atmospheric chemistry: Volume V - heterogeneous reactions on solid substrates. *Atmospheric Chemistry and Physics*, 10(18):9059–9223, 2010. doi: 10.5194/acp-10-9059-2010.

Damian, V., Sandu, A., Damian, M., Potra, F., and Carmichael, G. R. The kinetic preprocessor KPP—a software environment for solving chemical kinetics. *Computers and Chemical Engineering*, 26(11):1567 – 1579, 2002. doi: 10.1016/S0098-1354(02)00128-X.

Delmelle, P., Delfosse, T., and Delvaux, B. Sulfate, chloride and fluoride retention in andosols exposed to volcanic acid emissions. *Environmental Pollution*, 126(3):445–457, 2003. ISSN 0269-7491. doi: 10.1016/s0269-7491(03)00196-9.

Donovan, A., Tsanev, V., Oppenheimer, C., and Edmonds, M. Reactive halogens (BrO and OClO) detected in the plume of Soufrière Hills Volcano during an eruption hiatus. *Geochemistry, Geophysics, Geosystems*, 15(8):3346–3363, 2014. doi: 10.1002/2014GC005419.

EPA, U. *Laboratory study to explore potential interferences to air quality monitors*. Research Triangle Park, N.C. : U.S. Environmental Protection Agency, Office of Air Quality Planning and Standards, 1999.

Fickert, S., Adams, J. W., and Crowley, J. N. Activation of Br_2 and BrCl via uptake of HOBr onto aqueous salt solutions. *Journal of Geophysical Research: Atmospheres*, 104(D19):23719–23727, 1999. doi: 10.1029/1999JD900359.

Freitas, S. R., Longo, K. M., Alonso, M. F., Pirre, M., Marecal, V., Grell, G., Stockler, R., Mello, R. F., and Sánchez Gácita, M. PREP-CHEM-SRC – 1.0: a preprocessor of trace gas and aerosol emission fields for regional and global atmospheric chemistry models. *Geoscientific Model Development*, 4(2):419–433, 2011. doi: 10.5194/gmd-4-419-2011.

General, S., Bobrowski, N., Pöhler, D., Weber, K., Fischer, C., and Platt, U. Airborne I-DOAS measurements at Mt. Etna: BrO and OClO evolution in the plume. *Journal of Volcanology and Geothermal Research*, 300:175–186, 2015. doi: 10.1016/j.jvolgeores.2014.05.012.

Gerlach, T. M. Volcanic sources of tropospheric ozone-depleting trace gases. *Geochemistry Geophysics Geosystems*, 5:Q09007, 2004. doi: 10.1029/2004gc000747.

Gerlach, T. Volcanic versus anthropogenic carbon dioxide. *Eos, Transactions American Geophysical Union*, 92(24):201–202, 2011. doi: 10.1029/2011EO240001.

Gliß, J., Bobrowski, N., Vogel, L., Pöhler, D., and Platt, U. OClO and BrO observations in the volcanic plume of Mt. Etna—implications on the chemistry of chlorine and bromine species in volcanic plumes. *Atmospheric Chemistry and Physics*, 15(10):5659–5681, 2015. doi: 10.5194/acp-15-5659-2015.

Guenther, A., Karl, T., Harley, P., Wiedinmyer, C., Palmer, P. I., and Geron, C. Estimates of global terrestrial isoprene emissions using MEGAN (Model of Emissions of Gases and Aerosols from Nature). *Atmospheric Chemistry and Physics*, 6(11):3181–3210, 2006. doi: 10.5194/acp-6-3181-2006.

Halmer, M., Schmincke, H., and Graf, H. The annual volcanic gas input into the atmosphere, in particular into the stratosphere: a global data set for the past 100 years. *Journal of Volcanology and Geothermal Research*, 115(3–4):511 – 528, 2002. doi: 10.1016/S0377-0273(01)00318-3.

Hobbs, P. V., Tuell, J. P., Hegg, D. A., Radke, L. F., and Eltgroth, M. W. Particles and gases in the emissions from the 1980-1981 volcanic-eruptions of Mt St-Helens. *Journal of Geophysical Research-Oceans and Atmospheres*, 87(Nc13): 1062–1086, 1982. doi: 10.1029/JC087iC13p11062.

Hobbs, P. V., Radke, L. F., Lyons, J. H., Ferek, R. J., Coffman, D. J., and Casadevall, T. J. Airborne measurements of particle and gas emissions from the 1990 volcanic eruptions of Mount Redoubt. *Journal of Geophysical Research-Atmospheres*, 96(D10):18735–18752, 1991. doi: 10.1029/91JD01635.

Hörmann, C., Sihler, H., Bobrowski, N., Beirle, S., Penning de Vries, M., Platt, U., and Wagner, T. Systematic investigation of bromine monoxide in volcanic plumes from space by using the GOME-2 instrument. *Atmos. Chem. Phys.*, 13 (9):4749–4781, 2013. doi: 10.5194/acp-13-4749-2013.

Hubler, G., Montzka, D. D., Norton, R. B., Murphy, P. C., Fehsenfeld, F. C., Liu, S. C., Ridley, B. A., Walega, J. G., Atlas, E., Grahek, F. E., Heidt, L. E., Merrill, J., Huebert, B. J., and Bodhaine, B. A. Total reactive oxidized nitrogen (NO_y) in the remote Pacific troposphere and its correlation with O_3 and CO - Mauna-Loa-Observatory Photochemistry Experiment 1988. *Journal of Geophysical Research-Atmospheres*, 97(D10):10427–10447, 1992. doi: 10.1029/91JD03112.

Huebert, B., Vitousek, P., Sutton, J., Elias, T., Heath, J., Coeppicus, S., Howell, S., and Blomquist, B. Volcano fixes nitrogen into plant-available forms. *Biogeochemistry*, 47(1):111–118, 1999. doi: 10.1023/A:1006276011055.

Husain, L., Rattigan, O. V., Dutkiewicz, V., Das, M., Judd, C. D., Khan, A. R., Richter, R., Balasubramanian, R., Swami, K., and Walcek, C. J. Case studies of the $SO_2 + H_2O_2$ reaction in clouds. *Journal of Geophysical Research: Atmospheres*, 105(D8):9831–9841, 2000. doi: 10.1029/1999JD901177.

Inness, A., Baier, F., Benedetti, A., Bouarar, I., Chabrillat, S., Clark, H., Clerbaux, C., Coheur, P., Engelen, R. J., Errera, Q., Flemming, J., George, M., Granier, C., Hadji-Lazaro, J., Huijnen, V., Hurtmans, D., Jones, L., Kaiser, J. W., Kapsomenakis, J., Lefever, K., Leitão, J., Razinger, M., Richter, A., Schultz, M. G., Simmons, A. J., Suttie, M., Stein, O., Thépaut, J.-N., Thouret, V., Vrekoussis, M., Zerefos, C., and the MACC team. The MACC reanalysis: an 8 yr data set of atmospheric composition. *Atmospheric Chemistry and Physics*, 13 (8):4073–4109, 2013. doi: 10.5194/acp-13-4073-2013.

Jacob, D. *Introduction to atmospheric chemistry*. Princeton University Press, 1999. ISBN 0691001855.

Jacobson, M. Z. *Fundamentals of Atmospheric Modeling*. Cambridge University Press, Second edition, 2005. ISBN 9781139165389.

Jiménez, P. A. and Dudhia, J. Improving the representation of resolved and unresolved topographic effects on surface wind in the WRF model. *Journal of Applied Meteorology and Climatology*, 51:300–316, 2012. doi: 10.1175/JAMC-D-11-084.1.

JRC & PBL. Emission Database for Global Atmospheric Research (EDGAR), release version 4.1., 2010. URL http://edgar.jrc.ec.europa.eu.

Kärcher, B. Aviation-produced aerosols and contrails. *Surveys in Geophysics*, 20 (2):113–167, 1999. doi: 10.1023/A:1006600107117.

Kaschka, T. Chemical modelling of volcanic plumes. Master's thesis, Universitity of Heidelberg, 2007.

Keeler, J. and Wothers, P. *Why chemical reactions happen*. Oxford University Press, 2003. ISBN 0199249733.

Kelly, P. J., Kern, C., Roberts, T. J., Lopez, T., Werner, C., and Aiuppa, A. Rapid chemical evolution of tropospheric volcanic emissions from Redoubt Volcano, Alaska, based on observations of ozone and halogen-containing gases. *Journal of Volcanology and Geothermal Research*, 259:317–333, 2013. doi: 10.1016/j.jvolgeores.2012.04.023.

Kern, C., Sihler, H., Vogel, L., Rivera, C., Herrera, M., and Platt, U. Halogen oxide measurements at Masaya Volcano, Nicaragua using active long path differential optical absorption spectroscopy. *Bulletin of Volcanology*, 71(6): 659–670, 2009. doi: 10.1007/s00445-008-0252-8.

Lee, C., Kim, Y. J., Tanimoto, H., Bobrowski, N., Platt, U., Mori, T., Yamamoto, K., and Hong, C. S. High ClO and ozone depletion observed in the plume of Sakurajima volcano, Japan. *Geophysical Research Letters*, 32(21), 2005. doi: 10.1029/2005gl023785.

Louban, I., Bobrowski, N., Rouwet, D., Inguaggiato, S., and Platt, U. Imaging DOAS for volcanological applications. *Bulletin of Volcanology*, 71(7):753–765, 2009. doi: 10.1007/s00445-008-0262-6.

Macintyre, H. L. and Evans, M. J. Sensitivity of a global model to the uptake of N_2O_5 by tropospheric aerosol. *Atmospheric Chemistry and Physics*, 10(15): 7409–7414, 2010. doi: 10.5194/acp-10-7409-2010.

Martin, R. S., Mather, T. A., and Pyle, D. M. High-temperature mixtures of magmatic and atmospheric gases. *Geochem. Geophys. Geosyst.*, 7:Q04006, 2006. doi: 10.1029/2005GC001186.

Martin, R. S., Roberts, T. J., Mather, T. A., and Pyle, D. M. The implications of H_2S and H_2 kinetic stability in high-t mixtures of magmatic and atmospheric gases for the production of oxidized trace species (e.g., BrO and NO_x). *Chemical Geology*, 263(1-4):143–150, 2009. doi: 10.1016/j.chemgeo.2008.12.028.

Martin, R. S., Ilyinskaya, E., and Oppenheimer, C. The enigma of reactive nitrogen in volcanic emissions. *Geochimica et Cosmochimica Acta*, 95:93–105, 2012. doi: 10.1016/j.gca.2012.07.027.

Martin, S. T., Schlenker, J. C., Malinowski, A., Hung, H.-M., and Rudich, Y. Crystallization of atmospheric sulfate-nitrate-ammonium particles. *Geophysical Research Letters*, 30(21), 2003. doi: 10.1029/2003GL017930.

Mather, T. A., Pyle, D. M., and Allen, A. G. Volcanic source for fixed nitrogen in the early earth's atmosphere. *Geology*, 32(10):905–908, 2004a. doi: 10.1130/G20679.1.

Mather, T., Allen, A., Davison, B., Pyle, D., Oppenheimer, C., and McGonigle, A. Nitric acid from volcanoes. *Earth and Planetary Science Letters*, 218(1–2):17–30, 2004b. doi: 10.1016/S0012-821X(03)00640-X.

McGonigle, A. J. S., Delmelle, P., Oppenheimer, C., Tsanev, V. I., Delfosse, T., Williams-Jones, G., Horton, K., and Mather, T. A. SO_2 depletion in tropospheric volcanic plumes. *Geophysical Research Letters*, 31(13):L13201, 2004. doi: 10.1029/2004gl019990.

Myhre, G., Shindell, D., Bréon, F.-M., Collins, W., Fuglestvedt, J., Huang, J., Koch, D., Lamarque, J.-F., Lee, D., Mendoza, B., Nakajima, T., Robock, A., Stephens, G., Takemura, T., and Zhang, H. Anthropogenic and natural radiative forcing. In Stocker, T., Qin, D., Plattner, G.-K., Tignor, M., Allen, S., Boschung, J., Nauels, A., Xia, Y., Bex, V., and Midgley, P., editors, *Climate Change 2013: The Physical Science Basis. Contribution of Working Group I to the Fifth Assessment Report of the Intergovernmental Panel on Climate Change*. Cambridge University Press, 2013. doi: 10.1017/CBO9781107415324.018.

Nakicenovic, N., Alcamo, J., Davis, G., Vries, B. D., Fenhann, J., Gaffin, S., Gregory, K., Griibler, A., Jung, T. Y., Kram, T., Lebre, E., Rovere, L., Michaelis, L., Mori, S., Morita, T., Smith, S., Swart, R., Rooijen, S. V., Victor, N., and Dadi, Z. Emissions scenarios, 2000.

NCEP. NCEP FNL operational model global tropospheric analyses, continuing from July 1999, 2000.

NEI. 2011 national emissions inventory, version 2 technical support document, 2011.

Neri, M., Casu, F., Acocella, V., Solaro, G., Pepe, S., Barardino, P., Sansosti, E., Caltabiano, T., Lundgren, P., and Lanari, R. Deformation and eruptions at Mt. Etna (Italy): a lesson from 15 years of observations. *Geophysical Research Letters*, 36:L02309, 2009. doi: 10.1029/2008GL036151.

Oppenheimer, C., Kyle, P. R., Tsanev, V. I., McGonigle, A. J. S., Mather, T. A., and Sweeney, D. Mt. Erebus, the largest point source of NO2 in Antarctica. *Atmospheric Environment*, 39(32):6000–6006, 2005. doi: 10.1016/j.atmosenv.2005.06.036.

Oppenheimer, C., Tsanev, V. I., Braban, C. F., Cox, R. A., Adams, J. W., Aiuppa, A., Bobrowski, N., Delmelle, P., Barclay, J., and McGonigle, A. J. S. BrO formation in volcanic plumes. *Geochimica et Cosmochimica Acta*, 70(12):2935–2941, 2006. doi: 10.1016/j.gca.2006.04.001.

Oppenheimer, C., Kyle, P., Eisele, F., Crawford, J., Huey, G., Tanner, D., Kim, S., Mauldin, L., Blake, D., Beyersdorf, A., Buhr, M., and Davis, D.

Atmospheric chemistry of an Antarctic volcanic plume. *Journal of Geophysical Research-Atmospheres*, 115, 2010. doi: 10.1029/2009jd011910.

Parrella, J. P., Jacob, D. J., Liang, Q., Zhang, Y., Mickley, L. J., Miller, B., Evans, M. J., Yang, X., Pyle, J. A., Theys, N., and Van Roozendael, M. Tropospheric bromine chemistry: implications for present and pre-industrial ozone and mercury. *Atmospheric Chemistry and Physics*, 12(15):6723–6740, 2012. doi: 10.5194/acp-12-6723-2012.

Pierce, R. B., Schaack, T., Al-Saadi, J. A., Fairlie, T. D., Kittaka, C., Lingenfelser, G., Natarajan, M., Olson, J., Soja, A., Zapotocny, T., Lenzen, A., Stobie, J., Johnson, D., Avery, M. A., Sachse, G. W., Thompson, A., Cohen, R., Dibb, J. E., Crawford, J., Rault, D., Martin, R., Szykman, J., and Fishman, J. Chemical data assimilation estimates of continental U.S. ozone and nitrogen budgets during the Intercontinental Chemical Transport Experiment—North America. *Journal of Geophysical Research: Atmospheres*, 112(D12):D12S21, 2007. doi: 10.1029/2006JD007722.

Pyle, D. M. and Mather, T. A. The importance of volcanic emissions for the global atmospheric mercury cycle. *Atmospheric Environment*, 37(36):5115 – 5124, 2003. doi: 10.1016/j.atmosenv.2003.07.011.

Riedel, K. and Lassey, K. Detergent of the atmosphere. *Water & Atmosphere*, 16, 2008.

Roberts, T. J., Braban, C. F., Martin, R. S., Oppenheimer, C., Adams, J. W., Cox, R. A., Jones, R. L., and Griffiths, P. T. Modelling reactive halogen formation and ozone depletion in volcanic plumes. *Chemical Geology*, 263(1-4):151–163, 2009. doi: 10.1016/j.chemgeo.2008.11.012.

Roberts, T. J., Jourdain, L., Griffiths, P. T., and Pirre, M. Re-evaluating the reactive uptake of HOBr in the troposphere with implications for the marine boundary layer and volcanic plumes. *Atmospheric Chemistry and Physics*, 14 (20):11185–11199, 2014a. doi: 10.5194/acp-14-11185-2014.

Roberts, T. J., Martin, R. S., and Jourdain, L. Reactive bromine chemistry in Mt. Etna's volcanic plume: the influence of total Br, high temperature processing, aerosol loading and plume-air mixing. *Atmospheric Chemistry and Physics*, 14: 11201–11219, 2014b. doi: 10.5194/acp-14-11201-2014.

Roine, A. *HSC chemistry 6.1.* Outotec, 2007.

Saiz-Lopez, A. and von Glasow, R. Reactive halogen chemistry in the troposphere. *Chemical Society Reviews*, 41(19):6448–6472, 2012. doi: 10.1039/c2cs35208g.

Salerno, G., Burton, M., Oppenheimer, C., Caltabiano, T., Randazzo, D., Bruno, N., and Longo, V. Three-years of SO_2 flux measurements of Mt. Etna using an automated UV scanner array: Comparison with conventional traverses and uncertainties in flux retrieval. *Journal of Volcanology and Geothermal Research*, 183:76–83, 2009. doi: 10.1016/j.jvolgeores.2009.02.013.

Sander, R., Keene, W. C., Pszenny, A. A. P., Arimoto, R., Ayers, G. P., Baboukas, E., Cainey, J. M., Crutzen, P. J., Duce, R. A., Hönninger, G., Huebert, B. J., Maenhaut, W., Mihalopoulos, N., Turekian, V. C., and Van Dingenen, R. Inorganic bromine in the marine boundary layer: a critical review. *Atmospheric Chemistry and Physics*, 3(5):1301–1336, 2003. doi: 10.5194/acp-3-1301-2003.

Sander, R. Compilation of Henry's law constants for inorganic and organic species of potential importance in environmental chemistry, 1999. URL http://www.henrys-law.org/.

Sander, S. P., Abbatt, J., Barker, J. R., Burkholder, J. B., Friedl, R. R., Golden, D. M., Huie, R. E., Kolb, C. E., Kurylo, M. J., Moortgat, G. K., Orkin, V. L., and Wine, P. H. Chemical kinetics and photochemical data for use in atmospheric studies, evaluation No. 17, JPL publication 10-6, 2011.

Sawyer, G. M., Salerno, G. G., Le Blond, J. S., Martin, R. S., Spampinato, L., Roberts, T. J., Mather, T. A., Witt, M. L. I., Tsanev, V. I., and Oppenheimer, C. Gas and aerosol emissions from Villarrica volcano, Chile. *Journal of Volcanology and Geothermal Research*, 203(1-2):62–75, 2011. doi: 10.1016/j.jvolgeores.2011.04.003.

Schell, B., Ackermann, I. J., Hass, H., Binkowski, F. S., and Ebel, A. Modeling the formation of secondary organic aerosol within a comprehensive air quality model system. *Journal of Geophysical Research: Atmospheres*, 106(D22):28275–28293, 2001. ISSN 2156-2202. doi: 10.1029/2001JD000384.

Schumann, U., Weinzierl, B., Reitebuch, O., Schlager, H., Minikin, A., Forster, C., Baumann, R., Sailer, T., Graf, K., Mannstein, H., Voigt, C., Rahm, S., Simmet, R., Scheibe, M., Lichtenstern, M., Stock, P., Ruba, H., Schauble, D., Tafferner, A., Rautenhaus, M., Gerz, T., Ziereis, H., Krautstrunk, M., Mallaun, C., Gayet, J. F., Lieke, K., Kandler, K., Ebert, M., Weinbruch, S., Stohl, A., Gasteiger, J., Gross, S., Freudenthaler, V., Wiegner, M., Ansmann, A., Tesche, M., Olafsson, H., and Sturm, K. Airborne observations of the Eyjafjalla volcano ash cloud over Europe during air space closure in April and May 2010. *Atmospheric Chemistry and Physics*, 11(5):2245–2279, 2011. doi: 10.5194/acp-11-2245-2011.

Seinfeld, J. H. and Pandis, S. N. *Atmospheric Chemistry and Physics*. John Wiley & Sons, New York, Chichester, Weinheim, 2006. ISBN 978-0-471-72018-8.

Shallcross, D. E., Leather, K. E., Bacak, A., Xiao, P., Lee, E. P. F., Ng, M., Mok, D. K. W., Dyke, J. M., Hossaini, R., Chipperfield, M. P., Khan, M. A. H., and Percival, C. J. Reaction between CH_3O_2 and BrO radicals: A new source of upper troposphere lower stratosphere hydroxyl radicals. *The Journal of Physical Chemistry A*, 119(19):4618–4632, 2015. doi: 10.1021/jp5108203.

Simpson, W. R., von Glasow, R., Riedel, K., Anderson, P., Ariya, P., Bottenheim, J., Burrows, J., Carpenter, L. J., Friess, U., Goodsite, M. E., Heard, D., Hutterli, M., Jacobi, H. W., Kaleschke, L., Neff, B., Plane, J., Platt, U., Richter, A., Roscoe, H., Sander, R., Shepson, P., Sodeau, J., Steffen, A., Wagner, T., and Wolff, E.

Halogens and their role in polar boundary-layer ozone depletion. *Atmospheric Chemistry and Physics*, 7(16):4375–4418, 2007. doi: 10.5194/acp-7-4375-2007.

Skamarock, W. C., Klemp, J. B., Dudhia, J., Gill, D., Barker, D. M., Duda, M. G., Huang, X., Wang, W., and Powers, J. G. A description of the Advanced Research WRF version 3. NCAR Tech. Technical report, Note NCAR/TN-475+STR, 2008.

Stutz, J. and Platt, U. Numerical analysis and estimation of the statistical error of differential optical absorption spectroscopy measurements with least-squares methods. *Applied Optics*, 35(30):6041–6053, 1996. doi: 10.1364/ao.35.006041.

Surl, L., Donohoue, D., Aiuppa, A., Bobrowski, N., and von Glasow, R. Quantification of the depletion of ozone in the plume of Mount Etna. *Atmospheric Chemistry and Physics*, 15(5):2613–2628, 2015. doi: 10.5194/acp-15-2613-2015.

Theys, N., De Smedt, I., Van Roozendael, M., Froidevaux, L., Clarisse, L., and Hendrick, F. First satellite detection of volcanic OClO after the eruption of Puyehue-Cordón Caulle. *Geophysical Research Letters*, 41(2):667–672, 2014. doi: 10.1002/2013GL058416.

Tiesi, A., Villani, M., D'Isidoro, M., Prata, A., Maurizi, A., and Tampieri, F. Estimation of dispersion coefficient in the troposphere from satellite images of volcanic plumes: Application to Mt. Etna, Italy. *Atmospheric Environment*, 40(4):628 – 638, 2006. doi: 10.1016/j.atmosenv.2005.09.079.

UCAR. *User's Guide for the Advanced Research WRF (ARW) Modeling System Version 3.4*.

van Roozendael, M. and Fayt, C. *WinDOAS 2.1 Software User Manual*. BIRA-IASB, 2001.

Vance, A., McGonigle, A. J. S., Aiuppa, A., Stith, J. L., Turnbull, K., and von Glasow, R. Ozone depletion in tropospheric volcanic plumes. *Geophysical Research Letters*, 37(22):L22802, 2010. doi: 10.1029/2010GL044997.

Vogt, R., Crutzen, P. J., and Sander, R. A mechanism for halogen release from sea-salt aerosol in the remote marine boundary layer. *Nature*, 383(6598): 327–330, 1996. doi: 10.1038/383327a0.

von Glasow, R. Atmospheric chemistry in volcanic plumes. *Proceedings of the National Academy of Sciences of the United States of America*, 107(15):6594–6599, 2010. doi: 10.1073/pnas.0913164107.

von Glasow, R. and Crutzen, P. J. *Tropospheric Halogen Chemistry*, volume 4, page 66. 2007.

von Glasow, R., Lawrence, M. G., Sander, R., and Crutzen, P. J. Modeling the chemical effects of ship exhaust in the cloud-free marine boundary layer. *Atmospheric Chemistry and Physics*, 3:233–250, 2003. doi: 10.5194/acp-3-233-2003.

von Glasow, R., von Kuhlmann, R., Lawrence, M. G., Platt, U., and Crutzen, P. J. Impact of reactive bromine chemistry in the troposphere. *Atmospheric Chemistry and Physics*, 4(11/12):2481–2497, 2004. doi: 10.5194/acp-4-2481-2004.

von Glasow, R., Sander, R., Bott, A., and Crutzen, P. J. Modeling halogen chemistry in the marine boundary layer 1. Cloud-free MBL. *Journal of Geophysical Research: Atmospheres*, 107(D17):ACH 9–1–ACH 9–16, 2002. doi: 10.1029/2001JD000942.

von Glasow, R., Bobrowski, N., and Kern, C. The effects of volcanic eruptions on atmospheric chemistry. *Chemical Geology*, 263(1-4):131–142, 2009. doi: 10.1016/j.chemgeo.2008.08.020.

Warner, T. T. Quality assurance in atmospheric modeling. *Bulletin of the American Meteorological Society*, 92:1601–1610, 2011. doi: 10.1175/BAMS-D-11-00054.1.

Watson, I. M. and Oppenheimer, C. Particle size distributions of Mount Etna's aerosol plume constrained by sun photometry. *Journal of Geophysical Research: Atmospheres*, 105(D8):9823–9829, 2000. doi: 10.1029/2000JD900042.

Weast, R. C. *CRC Handbook of Chemistry and Physics 1st Student Edition*. Boca Raton, FL CRC Press, Inc, 1988.

Weinheimer, A. J. Chemical methods: chemiluminescence, chemical amplification, electrochemistry, and derivatization. Blackwell Publishing, 2006.

Wennberg, P. Atmospheric chemistry - bromine explosion. *Nature*, 397(6717): 299, 1999. doi: 10.1038/16805.

Wesely, M. Parameterization of surface resistances to gaseous dry deposition in regional-scale numerical models. *Atmospheric Environment (1969)*, 23(6): 1293–1304, 1989. doi: 10.1016/0004-6981(89)90153-4.

Wild, O., Zhu, X., and Prather, M. J. Fast-J: Accurate simulation of in-and below-cloud photolysis in tropospheric chemical models. *Journal of Atmospheric Chemistry*, 37(3):245–282, 2000. doi: 10.1023/A:1006415919030.

Wittmer, J., Bobrowski, N., Liotta, M., Giuffrida, G., Calabrese, S., and U., P. Active alkaline traps to determine acidic-gas ratios in volcanic plumes: sampling technique and analytical methods. *Geochem. Geophys. Geosyst*, 2014. doi: 10.1002/2013GC005133.

Zaveri, R. A. and Peters, L. K. A new lumped structure photochemical mechanism for large-scale applications. *Journal of Geophysical Research: Atmospheres*, 104(D23):30387–30415, 1999. doi: 10.1029/1999JD900876.

Zaveri, R. A., Easter, R. C., Fast, J. D., and Peters, L. K. Model for Simulating Aerosol Interactions and Chemistry (MOSAIC). *Journal of Geophysical Research: Atmospheres*, 113(D13), 2008. doi: 10.1029/2007JD008782.

Zeldovich, J. The oxidation of nitrogen in combustion and explosions. *Acta Physicochim*, 21(4):577–628, 1946.